Synthetic and Computational Studies of Group 3 and Group 4 imido and hydrazido compounds

Simona Mellino



Thesis submitted to the University of Oxford for the degree of
Doctor of Philosophy, April 2017.

The work described in this Thesis was carried out in the Chemistry Research Laboratory, University of Oxford from October 2014 to April 2017 under the supervision of Professor Philip Mountford. All work is my own unless stated to the contrary, and has not previously been submitted for any degree at this or any other university.

Simona Mellino

Simona Mellino

April 2017

Abstract

Simona Mellino Hilary 2017

Jesus College D.Phil. Thesis

This Thesis describes the synthesis and reactivity of titanium-nitrogen multiply bonded compounds. Mechanistic and bonding studies on titanium imido, hydrazido and borylimido complexes as well as on a novel scandium borylimide recently reported in our research group were described.

Chapter 1 provides an introduction to Group 4 and Group 3 metal-nitrogen multiply bonded compounds including synthesis, bonding and reactivity of titanium imido, hydrazido, alkylidene hydrazido and borylimido complexes, (L)Ti=NR, (L)Ti=NNR_2, (L)Ti=$NNCR_2$ and (L)Ti=NBR_2.

Chapter 2 describes the reactions of the hydrazido compound Ti($N_2^{iPr}N^{Me}$)($NNPh_2$)(py) with the Si–H and B–H bonds of silanes and boranes and with H_2. The nature and mechanism of these reactions were investigated both computationally and experimentally.

Chapter 3 explores a series of new reactions and unprecedented transformations of organic boranes and silanes with titanium half-sandwich compounds. In addition, detailed mechanistic work, using DFT calculations, was performed to understand the chemistry behind these reactions.

Chapter 4 describes the bonding and reactivity of novel borylimido compounds. The systematic approach recently implemented in our research group to synthesise new titanium borylimido compounds, is described. A full computational study of the bonding of compounds with sandwich and half-sandwich structures is explained in detail.

Chapter 5 explores the experimental attempts to isolate the first scandium borylimido complex performed in our group. DFT and QTAIM and detailed mechanistic study are presented.

Chapter 6 contains experimental details, characterising data and DFT energies and coordinates of the optimized structures for the chemistry presented in Chapters Tw-Five.

CD Appendix contains CIF files for all new crystallographically characterised complexes and XYZ files for all the DFT optimized structures.

Acknowledgements

First, I must extend my sincere gratitude to Prof. Philip Mountford for giving me the opportunity to study at Oxford University and for supporting me during these years and to Dr. Eric Clot for helping me.

I want to thank all the people in Mountford Group for helping me and making my DPhil more enjoyable. In particular, I would like to thank Karen Gamero, for being the best friend ever – I love you! I would like to thank Dr Laura Stevenson for her knowledge about titanium chemistry and Dr Insun Yu for all of her advice, her hard work for the lab and her personal support – I really appreciate it. Thanks go to all the people working on the "hydrazide-borylimide project", Bowen, Martin, Ben and Archie.

Thanks also go to Dr Nick Rees for maintenance of the NMR facilities, and Dr Amber Thompson and Prof. Richard Cooper for assistance with X-ray crystallography, as well as to all of the support staff of the CRL. The "personal acknowledgments" will be in Italian.

A Me stessa, per avercela fatta, inevitabilmente da sola, ancora una volta. A mia Nonna, per essere stata madre, guida, e ispirazione di vita. Alla mia famiglia per avermi supportato e sopportato. A mia sorella Chiara e a mia Mamma, per i loro consigli e per la loro comprensione. Al mio cucciolo d'uomo per essere la Donna forte che è, per farmi battere il cuore e commuovere ogni volta che la vedo sorridere; avrò cura di te per sempre. Alla mia migliore amica, Luisa, per avermi insegnato cosa significa amare incondizionatamente. A tutte le persone che mi hanno accompagnato in questi anni, Giancarlo, Anna, Stefano, Lorenzo, Clarissa, Nino, Fiorella e Erminia. Alle due persone che mi hanno incoraggiato a non mollare, se sono qui ora è anche grazie a voi, Caterina e Giovanni. A te che hai reso gli ultimi tre mesi meno difficili e più felici. A te, Carmen, per la tua pazienza e per esserci, sempre e per sempre. Infine a te, che nove anni fa mi hai preso per mano e mi hai salvato la vita.

Contents

	Declaration	i
	Abstract	ii
	Acknowledgements	iii
	Contents	iv
	Abbreviations	viii
	Notes	xiii

Chapter 1 Introduction

1.1	General introduction	1
1.2	The imido ligand	2
1.3	Group 4 imido complexes	3
1.3.1	Titanium imido complexes	3
1.3.2	Zirconium and hafnium imido complexes	5
1.3.3	Structural features	7
1.3.4	Stoichiometric reactions	8
1.3.5	Catalytic hydroamination	11
1.4	Scandium imido complexes	12
1.5	The hydrazido ligand	15
1.6	Group 4 hydrazido complexes	16
1.6.1	Titanium hydrazido complexes	16
1.6.2	Zirconium and hafnium hydrazido complexes	18
1.6.3	Structural features	19
1.6.4	Stoichiometric reactions involving the $M=N_{im}$ bond	20
1.6.5	Stoichiometric reactions involving $N_{\alpha}–N_{\beta}$ bond cleavage	22
1.6.6	Catalytic reactions	25
1.7	Group 4 alkylidene hydrazide complexes	27
1.8	Titanium borylimido complexes	29
1.9	Summary and objectives	31
1.10	References	31

Chapter 2 Titanium N_2N-supported hydrazido complexes: experimental results and mechanistic DFT studies

2.1	Overview	42
2.2	Introduction	42
2.3	Reaction of Ti($N_2^{iPr}N^{Me}$)($NNPh_2$)(py) (**1.70**) with silanes	44
2.4	DFT mechanism of the reaction of Ti($N_2^{iPr}N^{Me}$)($NNPh_2$)(py) (**1.70**) with $PhSiH_3$	46
2.5	DFT Mechanism of the reaction of Ti($N_2^{iPr}N^{Me}$)($NNPh_2$)(py) (**1.70**) with boranes	50
2.6	Reaction of Ti($N_2^{iPr}N^{Me}$)($NNPh_2$)(py) (**1.70**) with H_2	58
2.7	Reaction and attempted DFT Mechanism of Ti($N_2^{iPr}N^{Me}$){N(H)SiH_2Ph}(NPh_2) (**1.71**) with silanes	59
2.8	Conclusions	64
2.9	References	65

Chapter 3 Reactivity studies of titanium imido, hydrazido and alkylidene hydrazido complexes with B-H bonds of boranes: experimental and computational studies

3.1	Overview	69
3.2	Introduction	69
3.3	Selection of titanium complexes and boranes	72
3.4	Reactions of imido complexes Ti=NR with boranes	74
3.5	Computational studies of Cp*Ti{$MeC(N^iPr_2)_2$}(NTol) (**3.1**)	81
3.6	Reactions of Cp*Ti{$MeC(N^iPr_2)_2$}($NNCPh_2$) (**1.40**) with boranes	84
3.7	Computational studies on Cp*Ti{$MeC(N^iPr_2)_2$}($NNCPh_2$) (**1.40**)	90
3.8	Reactions of Cp*Ti{$MeC(N^iPr_2)_2$}($NNMe_2$) (**1.39**) and Cp*Ti{$MeC(N^iPr_2)_2$}($NNPh_2$) (**1.38**) with boranes	93
3.8.1	Reactions with $HB(C_6F_5)_2$ and HBPin: experimental and computational results	94
3.8.2	Reactions with 9-BBN	99
3.8.3	Studies of the formation of Cp*Ti{$MeC(N^iPr_2)_2$}(NBC_8H_{14}) (**1**)	104
3.9	Other reactions	118

3.10 Conclusion and Outlook 118
3.11 References 119

Chapter 4 Sandwich and half-sandwich titanium borylimides: synthesis, bonding and reactivity

4.1 Overview 124
4.2 Introduction 124
4.3 Synthesis of new titanium borylimido compounds 126
4.3.1 Synthesis of $Ti\{NB(NAr'CH)_2\}Cl_2(NHMe_2)_2$ (**4.1**) 127
4.3.2 Synthesis of titanium borylimido complexes with sandwich and half-sandwich structures 129
4.4 Computational studies of bonding in half-sandwich borylimides 132
4.4.1 Molecular Orbital Analysis of half- sandwich complexes 133
4.4.2 Bond dissociation energies, QTAIM and NBO calculations of half-sandwich compounds 143
4.4.3 Exchange energetics and relationship between the N-H and Ti-N BDEs 158
4.5 Molecular Orbital Analysis of metallocene complexes 164
4.6 Experimental and computational studies of reactivity: reactions with CO_2, CS_2, iso(thio)cyanates and TolCHO 170
4.7 Conclusions 181
4.8 References 182

Chapter 5 Novel Scandium alkyl- and boryl- imides: DFT studies on small molecule reactivity

5.1 Overview 186
5.2 Introduction 186
5.3 Synthesis and characterization of the scandium borylamido complex, $(L^1)Sc(Me)\{NHB(NAr'CH)_2\}$ (**5.1**) 187
5.4 Reactivity studies of $(L^1)Sc(Me)\{NHB(NAr'CH)_2\}$ (**5.1**): thermolysis reaction and trapping of a transient borylimido complex with alkynes 189
5.5 Computational studies of the thermolysis reactions of 197

$(L^1)Sc(Me)\{NHB(NAr'CH)_2\}$ (**5.1**)
5.6 Conclusions 212
5.7 References 213

Chapter 6 Experimental details and characterising data

6.1 General methods and implemenation 217
6.2 Literature preparations 217
6.3 X-ray data collection and processing parameters 218
6.4 Experimental details and characterising data for Chapter Two 218
6.5 References 231

Chapter 7 Computational details

7.1 Density Functional Theory (DFT) 241
7.2 Basis set 243
7.3 Dispersion interactions 244
7.4 Solvation models 245
7.5 Natural bond orbitals (NBO) analysis 247
7.6 Quantum theory of atoms in molecules (QTAIM) 248
7.7 Frequency calculations in Gaussian 249
7.8 Pseudopotentials and relativistic effects 250
7.9 General Computational methodology 251
7.10 Chapter Two 252
7.10.1 Reactions of $Ti(N_2{}^{iPr}N^{Me})(NNPh_2)(py)$ (**1.70**) with $PhSiH_3$ 252
7.10.2 Reactions of $Ti(N_2{}^{iPr}N^{Me)})(NNPh_2)(py)$ (**1.70**) with boranes and H_2 253
7.11 Chapter Three 258
7.12 Chapter Four 263
7.13 Chapter Five 269
7.14 References 275

Appendix 278

CD Appendix

Abbreviations

General

Å	Ångstrom
atm	atmosphere(s)
Avg.	average
ca	*circa*, about
cf.	*confer*, compared to
CSD	Cambridge Structural Database
^{o}	degrees
^{o}C	degrees Celsius
d	day(s)
e	elementary charge
Fac	facially coordinating
g	grams
h	hour(s)
η	hapticity
K	Kelvin
kcal mol^{-1}	kilocalorie(s) per mole
M	molarity, mol dm^{-3}
mbar	millibar(s)
Mer	Meridonally coordinating
min	minute(s)
mL	millilitre(s)
mmol	millimole(s)
MOCVD	Metal-Organic Chemical Vapour Deposition
RDS	rate determining step
RT	room temperature
s	second(s)
μ	bridging
μmol	micromole(s)
vs	versus

Chemical

9-BBN	9-borabicyclo[3.3.1]nonane
Ar	aryl group
Ar'	2,6-$C_6H_3{}^iPr_2$
Ar^F	C_6F_5
bipy	2,2'-bipyridine
^{n}Bu	*n*-butyl
Cat	1,2-$O_2C_2Me_4$
cent	ring centroid
Cp	C_5H_5
Cp*	C_5Me_5
Cp'	C_5H_4Me
Cy	Cyclohexyl
DMAP	4-dimethylaminopyridine
E	generic chalcogen atom
EIE	equilibrium isotope effect
Et	Ethyl
H_2Me_4taa	tetramethyl dibenzotetraaza[14]annulene
H-hpp	1,3,4,6,7,8-hexaydro-2*H*-pyrimido[1,2-*a*]pyrimidine
IDipp	*N*,*N*'-bis(2,6-diisopropylphenyl)imidazol-2-ylidene
^{i}Pr	*iso*-propyl
KIE	kinetic isotope effect(s)
L	a supporting ligand (set)
Me	methyl
$Me_3[6]aneN_3$	1,3,5-trimethyltriazacyclohexane
$Me_3[9]aneN_3$	1,4,7-trimethyltriazacyclononane
Mes	2,4,6-$C_6H_2Me_3$
N_2NN'	$(2\text{-}C_5H_4N)CH_2N(CH_2CH_2NSiMe_3)_2$
N_2N^R	generic diamide-amine ligand
N_2N^{py}	$MeC(2\text{-}C_5H_4N)(CH_2NSiMe_3)_2$
$N_2{}^{SiMe_3}N^{Me}$	$MeN(CH_2CH_2NSiMe_3)_2$
$N_2{}^{ArF}N^{Me}$	$MeN(CH_2CH_2NAr^F)_2$
N_2N^{Me,C_3}	$MeN(CH_2CH_2CH_2NSiMe_3)_2$
$N_2N^{SiMe_3}$	$Me_3SiN(CH_2CH_2NSiMe_3)_2$

$N_2^{iPr}N^{Me}$	$MeN(CH_2CH_2N^iPr)_2$
$N_2^{TBS}N^{py}$	$MeC(2\text{-}C_5H_4N)\{CH_2N(Si^tBuMe_2)\}_2$
$N_2^{TFAP}N^{py}$	$MeC(2\text{-}C_5H_4N)\{CH_2NH(2\text{-}C_6F_4NMe_2)\}_2$
$N_2^{3,5\text{-}Xyl}N^{py}$	$MeC(2\text{-}C_5H_4N)\{CH_2NH(3,5\text{-}C_6H_3Me_2)\}_2$
$N^{3,5\text{-}Xyl}N^{pyr}$	2-(3,5-dimethylphenylamino)pyrrolinato
$N_2^{pyr}N^{Me}$	*N*,*N*-di(pyrrolyl-α-methyl)-*N*-methylamine
$N_2^{SiMe3}O$	$O\text{-}(CH_2CH_2NSiMe_3)_2$
$N_2^{Ar}O$	$O\text{-}(2\text{-}C_6H_4NSiMe_3)_2$
$N^{pyr}N^{Me_2}$	$Me_2NCH_2(2\text{-}NC_4H_3)$
Ph	phenyl
Pin	2,3-dimethyl-2,3-butanediol
PNP	$N\{2\text{-}P^iPr_2\text{-}4\text{-}C_6H_3Me\}_2$
py	pyridine
py'	4-pyrrolidinopyridine
R	generic aryl or alkyl
^{t}Bu	*tert*-butyl
Tex	*Tert*-hexyl
THF	tetrahydrofuran
TMEDA	N,N,N',N'-tetramethylethylenediamine
Tol	$4\text{-}C_6H_4Me$
$Tp^{tBu,Me}$	tris(3-methyl-5-*tert*-butylpyrazolyl)borate
TTP	*meso*-tetra-*p*-tolylporphyrinato dianion
X	generic anionic ligand
Xyl	$2,6\text{-}C_6H_3Me_2$
ZPE	zero point energy
‡	transition state or activation parameter

Calculations

BCP	bond critical point
BDE	bond dissociation
DFT	density functional theory
δ	delocalisation index
ε	ellipticity
G	kinetic energy density

H	energy density
HOMO	highest occupied molecular orbital
k	bond force constant
LUMO	lowest unoccupied molecular orbital
MO	molecular orbital
NBO	natural bonding orbital
NLMO	natural localised molecular orbital
TS	transition state
ρ	electron density
Q	charge
QTAIM	Quantum Theory of Atoms in Molecules
V	potential energy density
$\nabla^2\rho$	electron density Laplacian

Mass Spectrometry

EI	electron impact
FI	field impact
HR	high-resolution
m/z	mass to charge ratio
MS	mass spectrometry

Nuclear Magnetic Resonance Spectroscopy

$^{13}C\{^1H\}$	proton-decoupled ^{13}C
$^{11}B\{^1H\}$	proton-decoupled ^{11}B
$^{19}F\{^1H\}$	proton-decoupled ^{19}F
app.	apparent
br.	broad
COSY	correlation spectrocopy
d	doublet
HMBC	heteronuclear multiple-bond correlation
HSQC	heteronuclear single quantum correlation
Hz	Hertz
i	*ipso*

J	coupling constant
m	*meta*
m	multiplet
MHz	Megahertz
NMR	nuclear magnetic resonance
NOE	nuclear Overhauser effect
o	*ortho*
p	*para*
ppm	parts per million
q	quartet
HOESY	2D Heteronuclear nuclear Overhauser effect spectroscopy
s	singlet
sept.	septet
t	triplet
VT	variable temperature
δ	chemical shift in ppm

Infrared Spectroscopy

br.	broad
IR	infrared
cm^{-1}	wavenumber
m	medium
s	strong
w	weak
ν	frequency

Notes

Literature compounds described in this Thesis are numbered **1.x**, **2.x**, **3.x**, **4.x**, **5.x** according to the Chapter in which they first occur. The new compounds described in this Thesis are numbered **1** – **14**. Density functional theory (DFT) calculated compounds are clearly stated in the text.

X-ray crystallography data was collected, solved and refined by the Author with the help and guidance of Prof. Philip Mountford. Molecular drawings were produced by Prof. Philip Mountford.

DFT calculations were performed in collaboration with Prof. Philip Mountford of the University of Oxford and with Dr Eric Clot of Université Montpellier, France.

1.1 General introduction

Over the past four decades, in part because of their relevance to the catalytic reduction of dinitrogen to ammonia, research into metal-nitrogen multiple bonds has been developed. Intermediates proposed in the fixation of dinitrogen and of particular relevance to our research group are the transition-metal nitrogen multiple bond, and in particular the hydrazido complexes, (L)M=NNR$_2$ (R = alkyl or aryl). To date many practical applications of both ligands have been reported, namely a wide range of stoichiometric and catalytic reactions as well as industrial applications. These include the stoichiometric and catalytic reduction of dinitrogen,[1–6] carbodiimide metathesis,[7] olefin polymerisation,[8–12] MOCVD (Metal-Organic Chemical Vapour Deposition)[9,13,14] and new C-N bond forming reactions including hydroamination and hydrohydrazination (N-H bond addition across the C=C or C≡C bonds of alkenes, alkynes, allenes and carbodiimides).[15–27]

This Thesis describes the novel reactivity of Group 4 titanium imido, hydrazido(2-) and alkylidene hydrazido(2-) complexes toward E-H bond activation reactions (where E = H, B or Si) with silanes and boranes. A rationale bonding and reactivity analysis of titanium and scandium complexes containing the related borylimido functionalities, (L)M=NBR$_2$, performed by means of DFT calculations is also reported. Parts of this work have been published.[28] The computational studies on the reactivity of monomeric hydrazido(2-) complexes of titanium with different supporting ligands, namely diamide-amine supporting ligands and a Cp*-amidinate supporting ligands is described in Chapter Two and Chapter Three. A rational route to synthetize novel borylimido compounds along with computational studies on the bonding features and the reactivity of these complexes is described in Chapter Four. Following the experimental results on the formation of the first rare earth metal borylimide, namely of scandium, recently reported in our research group, Chapter 5 will focus on the computational studies performed to understand the bonding and reactivity. This Chapter introduces the chemistry of Group 4 imido, hydrazido(2-) and alkylidene hydrazido(2-) complexes and of Group 3 imido complexes. The bonding of these different complexes is also described. Finally, an overview of the novel borylimido chemistry is presented.

1.2 The imido ligand

Transition metal complexes containing terminal imido ligands have been known since the late 1950s. The imido ligand can either function as a spectator ligand or as an active site leading to a wide range of reactivity. In the past years, several reviews have been published.[29–33] A description of the binding mode of the imido ligand along with bonding features of Group 4 and Group 3 metal imides will be described in this Chapter and compared to the parent hydrazido, alkylidene hydrazido and borylimido compounds.

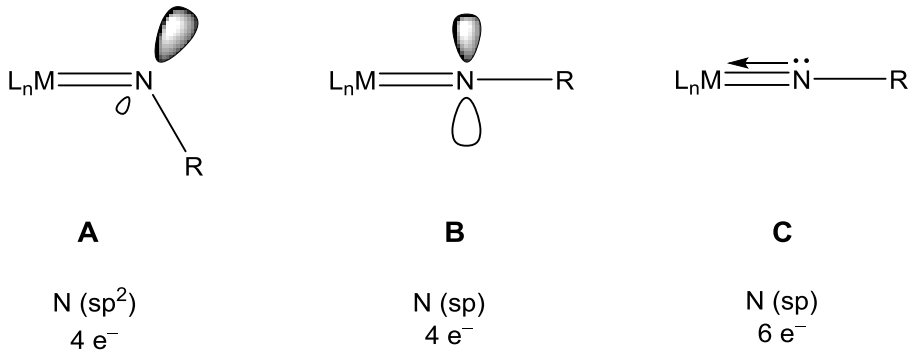

Figure 1.1. Bonding modes of the terminal imido ligand, along with orbital hybridisation of the N atom, and the valence electron count of the ligand.[31]

A dianionic imido ligand is considered to be bound to a transition metal with one σ-bond and either one or two π-interactions, depending on the nature of the metal to which is bound.[31] Structure A of Figure 1.1 shows a bent M–N–R linkage with an sp^2-hybridised nitrogen atom which gives an M=N double bond ($\sigma^2\pi^2$). The nitrogen lone pair resides in an sp^2 orbital. This bonding situation is rare; and more common for later transition metals such as molybdenum and tungsten.[34,35] The second binding mode, features an sp hybridisation at nitrogen meaning that the lone pair resides in a pure p orbital (Structure B, Figure 1.1), and a formal M=N double bond ($\sigma^2\pi^2$). To some extent, this situation arises in complexes where the lone pair cannot effectively donate to the metal centre due to a lack of acceptor orbitals of suitable symmetry or energetic match. For example, in so-called π-loaded imido complexes, such as $Cp_2Ti(N^tBu)(py)$, what appears to be a twenty valence electron count is rationalised by considering that competition of the imido π-components against the π-donor orbitals of the Cp ligands prevents full donation of the lone pair to the metal.[36] In the vast majority of imido complexes, donation of the lone pair to the metal centre is effective, which gives rise to Structure C (Figure 1.1). Here, a

formal triple bond ($\sigma^2\pi^4$) is formed, in which the imido dianion now acts as a six electron donor. Throughout this Thesis, the imido linkage is drawn as a double bond for simplicity to highlight the dianionic nature of the ligand.

1.3 Group 4 imido complexes

1.3.1 Titanium imido complexes

The first structurally authenticated terminal imido titanium compound reported by Roesky in 1990, $Ti\{NP(S)Ph_2\}Cl_2(py)_3$, was synthesised from the reaction of $TiCl_4$ with $Ph_2P(S)NSiMe_3$ and Me_3SiCl.[37] Alternative methods of synthesising imido compounds include the oxidation of Ti (+2) species[38,39] and reaction of compounds of the type $(L)TiCl_2$ with two equivalents of MNHR (M = Li or K).[40]

A more general route was published within our reseach group in 1994, which employed the development of the titanium imido synthon $Ti(N^tBu)Cl_2(py)_3$ (**1.1**, Scheme 1.1), from $TiCl_4$, $^tBuNH_2$ and pyridine[41] which served as entry points to a large number of variously-substituted titanium imido compounds (Scheme 1.2) through both salt metathesis and neutral ligand exchange protocols.[33,36,40,42–45] Arylimido complexes of the type $Ti(NAr)Cl_2(py)_3$ (**1.2**, Examples of Ar = Xyl (2,6-$C_6H_3Me_2$), Tol (4-C_6H_4Me) and Ph, Scheme 1.2) were also obtained by arylamine/tert-butylimide exchange reactions with **1.1**.[33,41,42,46] Unfortunately, in this case, the analogous reactions of $TiCl_4$ with a selection of anilines and pyridine were unsuccessful.

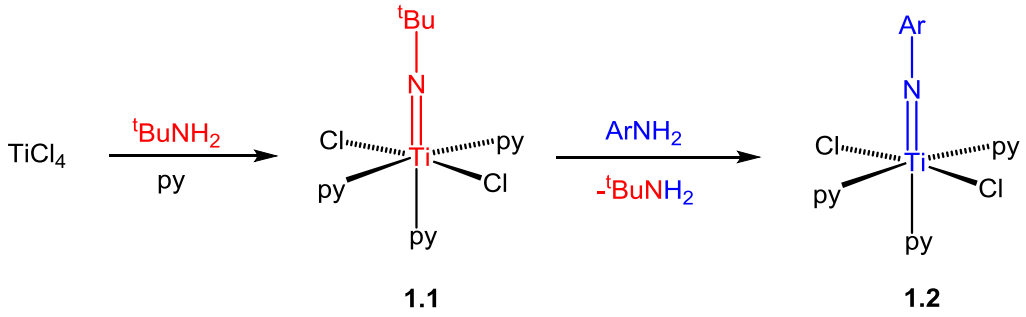

1.1 **1.2**

Scheme 1.1. Synthesis of complexes of the type $Ti(NR)Cl_2(py)_3$ (R = ^{t}Bu (**1.1**) or aryl (**1.2**)).[41]

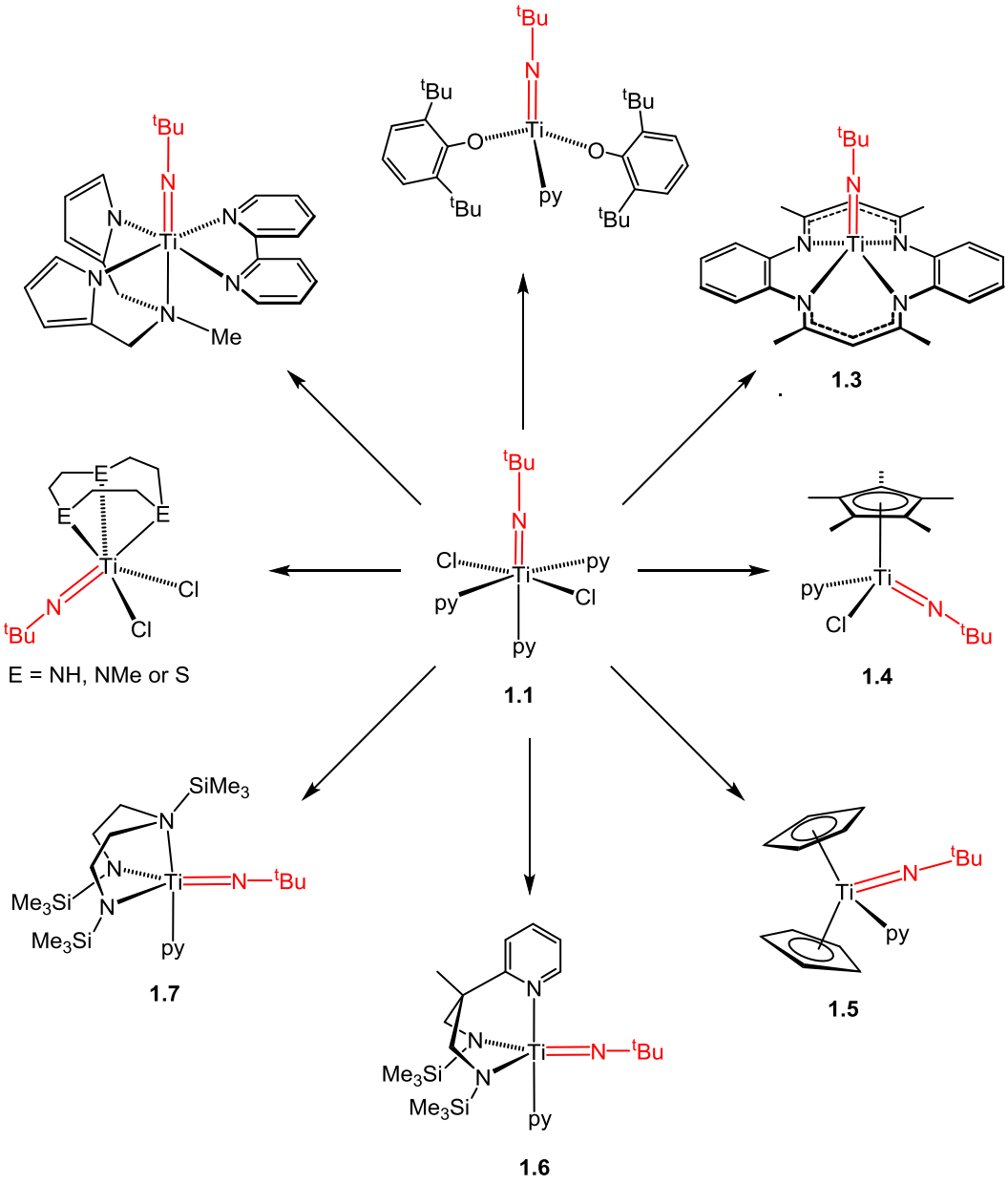

Scheme 1.2. Examples of titanium *tert*-butylimido complexes synthesised from $Ti(N^tBu)Cl_2(py)_3$ (**1.1**).[33,36,40,42–45]

In many cases, it was reported that the aniline/*tert*-butylimide exchange reaction could be carried out subsequent to the incorporation of the desired supporting ligand set. For example, reaction of the tetraazamacrocycle-supported *tert*-butylimido complex $Ti(N^tBu)(Me_4taa)$ (**1.3**, H_2Me_4taa = tetramethyl dibenzotetraaza[14]-annulene) with a range of anilines (H_2NAr; Ar = Ph, Tol, Xyl, 4-$C_6H_4NO_2$ and 4-$C_6H_4NMe_2$) yielded the corresponding arylimido compounds cleanly.[44,45] Similarly, the half-sandwich *tert*-butylimide **1.4** also forms a range of complexes of the type $Cp^*Ti(NAr)Cl(py)$ (Ar = Ar', 2,6-$C_6H_3Br_2$, 2-$C_6H_4{}^tBu$, 2-$C_6H_4{}^iPr$) upon reaction with the respective aniline.[47]

The compound $Ti(NMe_2)_2Cl_2$ has also proved to be a useful synthetic entry point into titanium imido compounds, in particular those with neutral, N_3-tridentate supporting ligands. This starting material is prepared through a simple redistribution reaction between $TiCl_4$ and $Ti(NMe_2)_4$,[48] and yields a wide range of imido complexes of the type $Ti(NR)Cl_2(NHMe_2)_2$ (R = alkyl (**1.8**) or aryl (**1.9**)) upon protonolysis with the respective alkylamine or aniline (Scheme 1.3).[49]

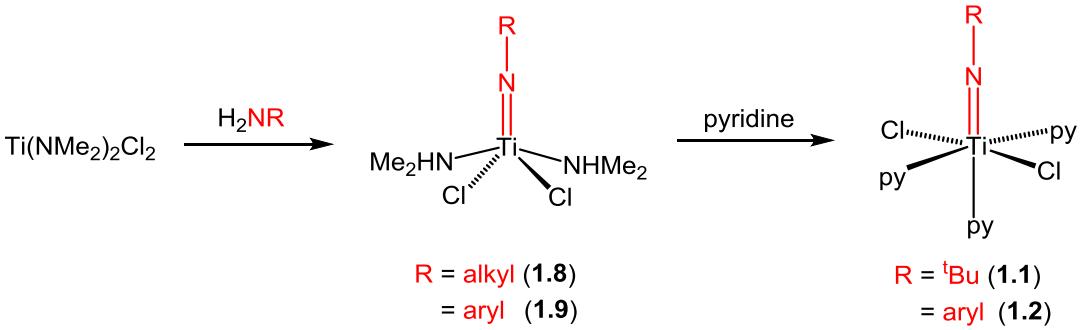

Scheme 1.3. Synthesis of $Ti(NR)Cl_2(NHMe_2)_2$ (R = alkyl (**1.8**) or aryl (**1.9**)), and reactions with pyridine.[49]

Subsequent ligand displacement reactions with neutral ligands then produced the respective dichloride imido compounds. For example, reaction with $Me_3[9]aneN_3$ (1,4,7-trimethyltriazacyclononane) yields the compounds $Ti(NR)Cl_2(Me_3[9]aneN_3)$ (R = alkyl (**1.10**) or aryl (**1.11**)).[8] In some cases the previously described tris(pyridine) imido compounds **1.1** and **1.2** could be synthesised from **1.8** and **1.9** following reaction in neat pyridine. This synthetic method allowed access to some previously unknown imido synthons and also produced the first titanium compound to contain a chiral imido ligand, namely $Ti\{N\text{-}(S)\text{-}(-)\text{-}CH(Me)Ph\}Cl_2(py)_3$.[50] The trans influence of the imido ligand in compounds of the type **1.1** and **1.2** results in a longer Ti–Npyridine bond distance for the trans pyridine ligand. This results in a relatively labile pyridine ligand which can be removed under reduced pressure to form the chloride-bridged dimers $Ti_2(NR)_2Cl_2(\mu\text{-}Cl)(py)_4$ (R = alkyl or aryl).[51] The trans influence reflects the effect on the ground state of the molecule, in particular on bond lengths and stability of ground state complexes. The trans effect instead reflects the labilization (rate of substitution) of a ligand trans to another.

1.3.2 Zirconium and hafnium imido complexes

The first Group 4 examples reported by Bergman in 1988 were the family of complexes, [$Cp_2Zr(NR)$] (R = ^{t}Bu (**1.12**), Xyl (**1.13**) or 4-$C_6H_4{}^t$Bu (**1.14**)).[52] These transient complexes were synthesised from thermolysis of the corresponding amido compounds $Cp_2Zr(NHR)(R')$ (R' = alkyl) and spontaneously dimerised to give dimeric complexes of the general type $Cp_4Zr_2(\mu\text{-}NR)_2$ (R = ^{t}Bu, **1.12**). However, if the thermolysis was performed in THF the monomeric terminal imido species, $Cp_2Zr(N^tBu)(THF)$ (**1.15**) could be isolated. Dimeric zirconium and hafnium complexes containing bridging imido ligands had been previously observed by Nugent and Harlow in 1979 from the reaction of $M(NMe_2)_4$ (M = Zr or Hf) with H_2N^tBu.[52] The larger radius of zirconium and hafnium compared to titanium renders the synthesis of monomeric terminal imido compounds more difficult, as more steric protection is required at the reactive metal–nitrogen multiple bond. The same thermolytic method used to synthesise **1.15** was later used by Bergman and co-workers to prepare a mixed-sandwich complex, $Cp^*CpZr(N^tBu)(THF)$.[53]

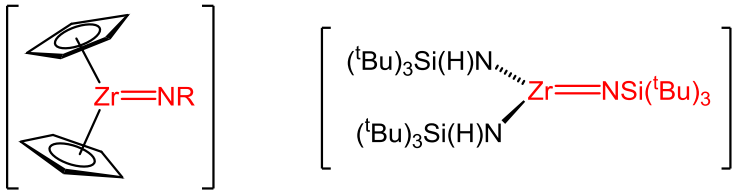

R = ^{t}Bu (**1.12**)
Xyl (**1.13**)
4-$C_6H_4{}^t$Bu (**1.14**)

1.16

Figure 1.2. Early examples of transient zirconium imido complexes.[51,54]

The transient imide [$Zr(NSi^tBu_3)(HNSi^tBu_3)_2$] (**1.16**, Figure 1.2) was similarly prepared by Wolczanski and co-workers using a thermolysis procedure. Subsequent trapping with THF produced the isolable compound $Zr(NSi^tBu_3)(NHSi^tBu_3)_2(THF)$.[55] In 1992, Wigley and co-workers reported the preparation of a zirconium analogue of the titanium synthons $Ti(NAr)Cl_2(py)_3$ (**1.2**), namely $Zr(NAr')Cl_2(py)_3$ (**1.17**), from the reaction of $ZrCl_4(THF)_2$ with LiNAr', Me_3SiCl and pyridine.[54] They were, however, unable to extend this result to a wider range of alkyl- or arylimido functionalities. In the absence of pyridine, the compound $Zr(NAr')Cl_2(THF)_2$ was formed, and later crystallographic characterisation by Mountford and co-workers showed that this was a dimeric species containing bridging imido ligands.[56] The analogous hafnium compound $Hf(NAr')Cl_2(THF)_2$ was also reported

by Wigley's research group.[57] Protonolysis methodologies based on the reactions of $Zr(CH_2SiMe_3)_2Cl_2(Et_2O)_2$ and $Zr(NMe_2)_2Cl_2(THF)_2$ with a range of primary alkylamines and anilines were later found to provide general entry points to dimeric zirconium imido dichloride compounds in our research group.[49] However, addition of pyridine to such compounds did not result in monomeric compounds and the addition of lithiated ligands was not successful.

Compound **1.17** was shown by to be a precursor to other zirconium imido complexes, namely the dimeric compounds $[(\eta^8\text{-}C_8H_8)Zr(\mu\text{-}NAr')]_2$ and $[Cp'ZrCl(\mu\text{-}NAr')]_2$ (Cp' = $\eta^5\text{-}C_5H_4Me$).[56] Our research group later used complex **1.17** for the synthesis of a number of further 2,6-diisopropylphenylimido complexes.[57,58] Zirconium and hafnium imido compounds can also be synthesised from dichloride precursors. For example, reaction of the macrocycle-supported dichloride compounds $(TTP)MCl_2$ (M = Zr or Hf, TTP = *meso*-tetra-*p*-tolylporphyrinato dianion) with two equivalents of LiNHAr' produced M(NAr')(TTP) (M = Zr (**1.18**) or Hf).[59] Once isolated, these compounds react with amines to yield bis(amido) compounds. Our research group also reported the synthesis of the imido compound $Zr(N_2NN')(N^tBu)(py)$ (N_2NN' = $(2\text{-}C_5H_4N)CH_2N(CH_2CH_2NSiMe_3)_2$) from the dichloride precursor $Zr(N_2NN')Cl_2$ and $LiCH_2SiMe_3$, H_2N^tBu and pyridine.[60] Again, addition of a primary amine resulted in the formation of a bis(amido) compound.

1.3.3 Structural features

In recent years, several studies detailing both experimental and computational studies into the geometric and electronic structures of titanium compounds have emerged. All the compounds mentioned are monomeric with a formal $\sigma^2\pi^4$ metal-nitrogen triple bond as reported in Section 1.2. For the following compounds, $Ti(NR)Cl_2(py)_3$ (R = alkyl (**1.1**) or aryl (**1.2**)), $Ti(NR)(NHMe_2)_2Cl_2$ (R = alkyl (**1.8**) or aryl (**1.9**)) and $Ti(NR)(Me_3[9]aneN_3)Cl_2$ (R = alkyl (**1.10**) or aryl (**1.11**)), short Ti–N bond lengths (range 1.672(2) – 1.7420(13) Å) and linear Ti–N–R bond angles (range 164.46(17) – 180 ^{o}) are indicative of such a triple bond.[41,49,61,62] In general, the alkylimido compounds have shorter Ti–N bonds in comparison to their arylimido counterparts (avg. Ti–NR bond length R = alkyl, 1.690(1) Å and R = aryl 1.7183(7) Å). A clear example of this is found in the series of compounds $Ti(NR)(NHMe_2)_2Cl_2$ (R = ^{i}Pr (**1.8a**), Ph (**1.9a**), C_6F_5 (**1.9b**), 2,3,5,6-C_6HCl_4 (**1.9c**), 2-$C_5H_4CF_3$ (**1.9d**) and 2-$C_6H_4{}^t$Bu (**1.9e**))[108] and the series of

compounds Ti(NR)(Me_3[9]ane)Cl_2 (R = ^{t}Bu (**1.10a**), Xyl (**1.11a**), Ar′ (**1.11b**), Ph (**1.11c**), and C_6F_5 (**1.11d**))[62] where the Ti–N bonds lengths increased in the order R = alkyl < aryl < electron-withdrawing aryl. The Ti–N bond lengthening effect of the electron-withdrawing substituent was also observed in the following series of compounds, Ti(NR)$Cl_2(py)_3$ (R = ^{t}Bu (**1.1**), 4-C_6H_4Me (**1.2a**) and 4-$C_6H_4NO_2$ (**1.2b**)). Compound **1.2b** was found to have a much longer bond length than **1.1** and **1.2a** (1.722(3) *vs.* 1.705(3) and 1.705(4) Å).[41] For this latter series of compounds the higher coordination number and *trans* influence of the pyridine ligand generally result in a longer Ti–N bond distance.

In 2011, a DFT study was carried out in order to better understand the structure and bonding of a range of cyclopentadienyl-amidinate supported imido and hydrazido compounds.[63] The model system CpTi{$MeC(NMe)_2$}(NR) (R = alkyl, aryl or NR_2) was employed and it was found that the Ti=N bond length was significantly shorter when R = Me compared to R = Ph (1.688 *vs*. 1.709 Å) consistent with the experimental results discussed above. When R = Ph, donation from the Ti=N π orbital can occur into the π* orbital of the phenyl ring. Donation from the π orbital of the phenyl ring into the π* orbital of Ti=N can also occur, both effects lead to a longer Ti=N bond.

As mentioned previously, the *trans* effect of the imido ligand can result in loss of the *trans*-pyridine ligand under vacuum and formation of chloride bridged dimers. In 1999 a computational study investigating this *trans* influence in compounds of the type Ti(NR)$Cl_2(py)_3$ (R = alkyl (**1.1**) or aryl (**1.2**)) was published.[64] which employed model compounds of the type Ti(NR)$Cl_2(NH_3)_3$ (R = ^{t}Bu, Ph, 4-$C_6H_4NO_2$). It was reported that, although the *trans*-pyridine ligands are longer than the *cis*-pyridine ligands in all cases (in agreement with experimental results), the difference in the *trans* and *cis* Ti–N bond distances does not vary as the R group is varied.

1.3.4 Stoichiometric reactions

The main point of interest for Group 4 imido compounds is their reactivity at the unsaturated M=NR linkage. The majority of Group 4 imido reaction chemistry involves [2+2] cycloaddition reactions of unsaturated substates at the imido bond. However, some examples involving C–H activation have also been reported. Bergman's zirconium imide $Cp_2Zr(N^tBu)(THF)$ (**1.15**) displays extensive reaction chemistry with various substrates, some examples are shown in Scheme 1.4.[51,65–68]

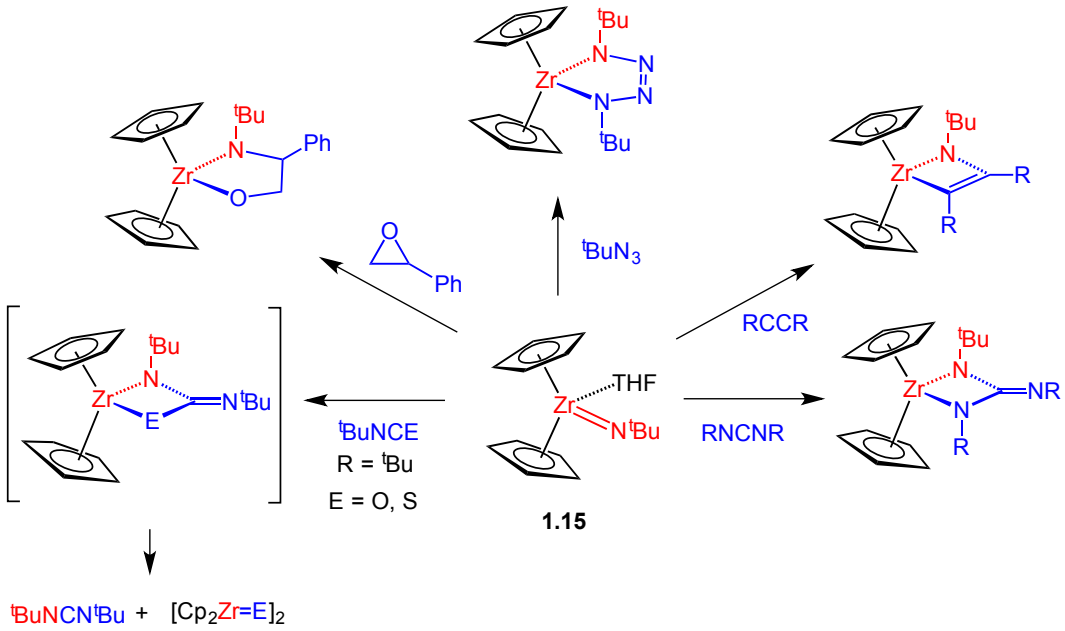

Scheme 1.4. Selected reactions of the zironocene imido compound $Cp_2Zr(N^tBu)(THF)$ (**1.14**).

Many of the reactions of **1.15** were found to be reversible and some reaction products exist in equilibrium with the starting materials. Examples involving the reaction with alkynes, alkenes and allenes in some cases lead to hydroamination of the organic substrates, *vide infra*.

The diamide-amine supported complex $Ti(N_2N^{py})(N^tBu)(py)$ (**1.19**, N_2N^{py} = $MeC(2\text{-}C_5H_4N)(CH_2NSiMe_3)_2$) exhibits a particularly rich reaction chemistry and selected transformations are outlined in Scheme 1.5.[40,42,69–75] Reaction of **1.19** with terminal alkynes yielded azatitanocyclobutene compounds of the type **1.20**, whereas reaction with internal alkynes or allenes lead to the formation of titanaazetidines **1.21**. Interestingly reaction with isocyanates resulted in insertion into the N_{amide}–Si bond to yield **1.22** containing an intact imido ligand.

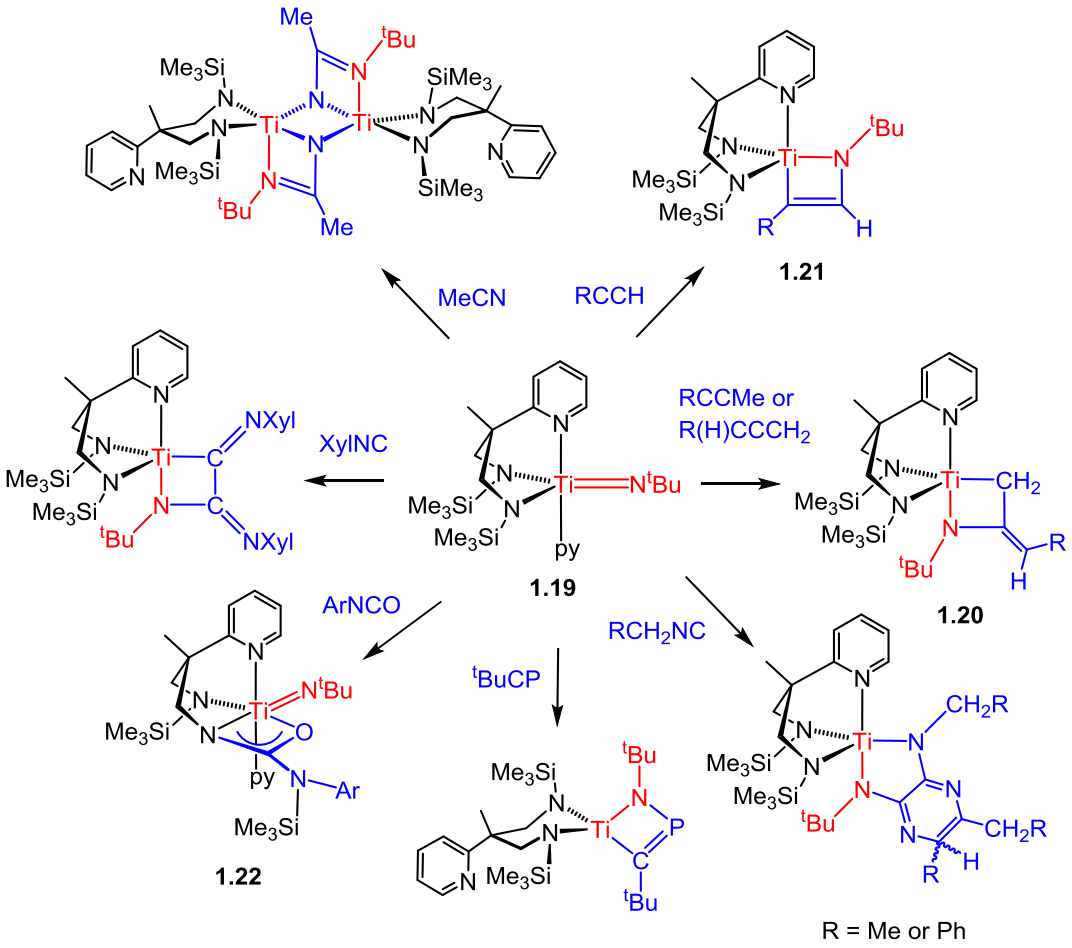

Scheme 1.5. Selected reactions of Ti(N_2N^{py})(N^tBu)(py) (**1.19**).

In 2009, Gade and co-workers published the synthesis of the cyclopentadienyl-amidinate compounds Cp*Ti($N^{Xyl}N$)(NAr) (Ar = Xyl (**1.23**) or 2,4,6-$C_6H_2Me_3$ (Mes) (**1.24**), $N^{Xyl}N$ = 2-(3,5-dimethylphenylamino)pyrrolinato) and Cp*Ti($N^{Xyl}N$)(N^tBu)($^tBuNH_2$) (**1.25**), and their reactivity with terminal alkynes. The arylimido compounds **1.23** and **1.24** produced azatitanocyclobutene compounds following cycloaddition reactions, whereas the alkylimido compound **1.25** underwent a C–H activation reaction of the terminal alkyne to yield the acetylide-amide compound Cp*Ti($N^{Xyl}N$)(HN^tBu)(CCAr).[76]

Several other compounds display reactivity with organic molecules. For example, reaction of Zr(NAr′)(TTP) (**1.18**) with isocyanates proceeds *via* a cycloaddition reaction followed by isomerisation and a subsequent extrusion reaction to generate carbodiimides.[59] The comparable compounds Ti(NAr)(Me_4taa) (**1.3**, Ar = Ph, Tol, Xyl, 4-$C_6H_4NO_2$ or 4-$C_6H_4NMe_2$) gave an alternative reaction yielding the κ^2 N,N-bound ureate complexes Ti{N(Ar)C(O)N(Ar)}(Me_4taa) which were stable to extrusion and in some cases reversible.[43]

Titanium imido complexes have been shown to be capable of activating H–H and S–H bonds. The compound (η^5-C_5H_3-1,3-$SiMe_3$)$_2$Ti(NPh) and its homologues add H_2 in a 1,2 fashion across the imido bond yielding hydride-amide compounds.[39] The compound $Cp_2Ti(N^tBu)(py)$ reacts with MeSH to yield $Cp_2Ti(SMe)_2$ and with SH_2 to yield the dimer $Cp_2Ti(\mu\text{-}S)_2TiCp_2$ or the monomer $Cp_2Ti(SH)_2$.[77] The corresponding reaction of $Ti(N^tBu)(Me_4taa)$ with H_2S gave the terminal sulfide compound $Ti(Me_4taa)(S)$.[43]

Another interesting reaction of particular relevance for this Thesis, is the reaction of the cyclopentadienyl-amidinate supported compound $Cp^*Ti\{MeC(N^iPr)_2\}(NTol)$ with $PhSiH_2X$ (X = Cl or Br), which gave cleavage of the silicon-halogen bond to yield silylamido-chloride complexes which were unstable in solution.[78]

1.3.5 Catalytic hydroamination

Hydroamination is the addition of an N–H bond across an unsaturated C–C bond and is an atom-economical method for the efficient formation of new C–N bonds. Group 4 metals have been widely studied as such catalysts and through a series of mechanistic studies three mechanisms have been established.[17,18,79–88] The most commonly found mechanism, the "imide route" proceeds through a [2+2] cycloaddition reaction at the M=NR bond. Protonolysis with an equivalent of amine then occurs to regenerate the imido catalyst and release the organic amine-alkene which then undergoes tautomerisation to yield the more stable imine isomer (Scheme 1.6).[89–93] Some examples are discussed below.

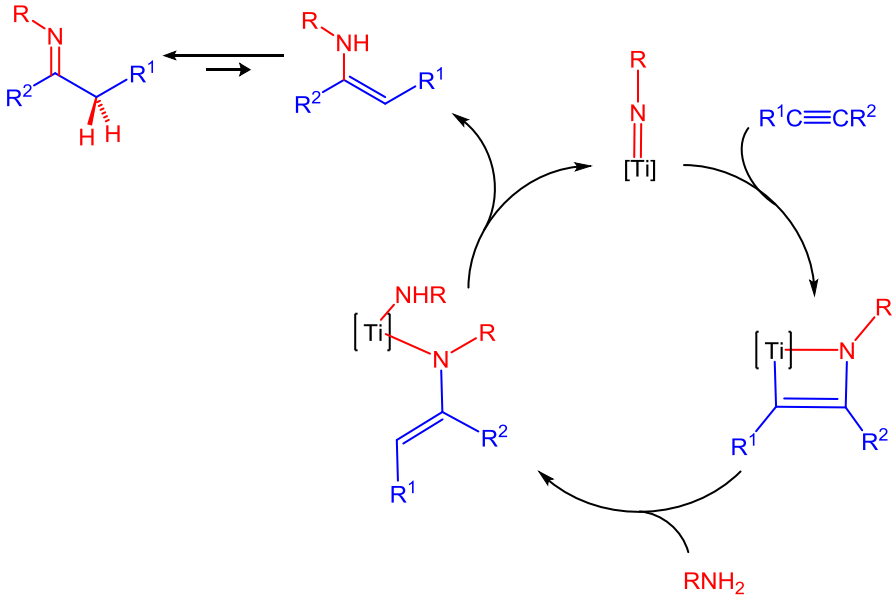

Scheme 1.6. General hydroamination catalytic cycle.

The titanium complexes Cp*Ti($N^{Xyl}N$)(NXyl) (**1.23**) and Cp*Ti($N^{Xyl}N$)(N^tBu)($^tBuNH_2$) (**1.25**) catalyse the hydroamination of both terminal and internal alkynes at 5 mol% catalyst loading however, long reaction times and high temperatures are required (24 h, 105 ^oC).[76] The parent compound Cp*Ti($N^{Xyl}N$)Me_2 (**1.26**), from which both **1.23** and **1.25** are synthesised was also found to be an active catalyst (the imido species are generated *in situ*). Both compounds were also shown to catalyse intramolecular hydroamination reactions. Several other titanium catalysts have been reported including $Cp_2Ti(\eta^2$-$Me_3SiC_2SiMe_3)$,[83] $Ti(NMe_2)_2$(dpma) (dpma = *N,N*-di(pyrrolyl-α-methyl)-*N*-methylamine),[19] and $Ti(NMe_2)_4$.[94] All three of which are proposed to proceed *via* an imido intermediate synthesised *in situ*. Examples of zirconium and hafnium hydroamination catalysts include Bergman's zirconium complex $Cp_2Zr(NHXyl)_2$[90] and Trate's hafnium complex (CCC^{Bu}-NHC)Hf(NMe_2)I_2 (CCC^{Bu}-NHC = 2-(1,3-bis(N-butylimidazol-2-ylidene)-phenylene).[95]

1.4 Scandium imido complexes

Generally speaking, terminal imido complexes of rare earth metals are much more scarce in comparison to their Group 4 counterparts and synthetic and reactivity studies have been performed the last seven years.[96] Prior to this, the field was limited to the isolation of dimeric complexes or higher-nuclearity clusters which contained bridging imido ligands, as the putative first-formed monomeric complexes had a tendency to form these more stable structures, especially for the larger lanthanides and yttrium.[97–109] For example, treatment of the lanthanide naphthalide complexes Ln($C_{10}H_8$)$(THF)_3$ (Ln = Yb, Sm) with azobenzene resulted in formation of the tetranuclear complexes Ln(μ-η^2:η^2-$N_2Ph_2)_4(\mu_3$-NPh$)_2(THF)_x$, which contain two phenylimido ligands that bridge three metal centres each, capping the tetranuclear core.[101,110] The four-electron reduction of an azobenzene unit to form the two imido ligands is accompanied by oxidation of the four metal centres from Ln(II) to Ln(III).

A number of complexes containing an $Ln_2(\mu_2$-$NR)_2$ core have also been reported.[104–106] For example, treatment of Yb(NHAr')$_4${Na(THF)} with 2 or 4 equiv. ^nBuLi yields the mixed amido-imido complex {(Ar'N)(Ar'NH)Yb(μ-NAr')$\}_2${[Li(THF)][Na(THF)]$\}_2$ (**1.27**, Figure 1.3) or the related imido complex {$(Ar'N)_2$Yb(μ-NAr')$\}_2${$[Li_2$(THF)][Na(THF)]$\}_2$, respectively, which both incorporate an $Yb_2(\mu_2$-$NAr')_2$ core.[104] Hessen and co-workers then extended this chemistry to a scandium system; reaction of the 2,3-dimethylbutadiene complex {η^5,η^1-

$C_5H_4(CH_2)_2NMe_2\}Sc(C_6H_{10})$ with PhCN gave the complex $[\{\eta^5,\eta^1\text{-}C_5H_4(CH_2)_2NMe_2\}Sc\{\mu_2\text{-}NC(Ph)C_6H_{10}\}]_2$ (**1.28**, Figure 1.3) *via* insertion of the nitrile into an Sc–C bond and attack of the other methylene group of the diene to force a cyclisation.[106] Rapid dimerisation of the three-coordinate imido complex then results in the dimeric **1.28**.

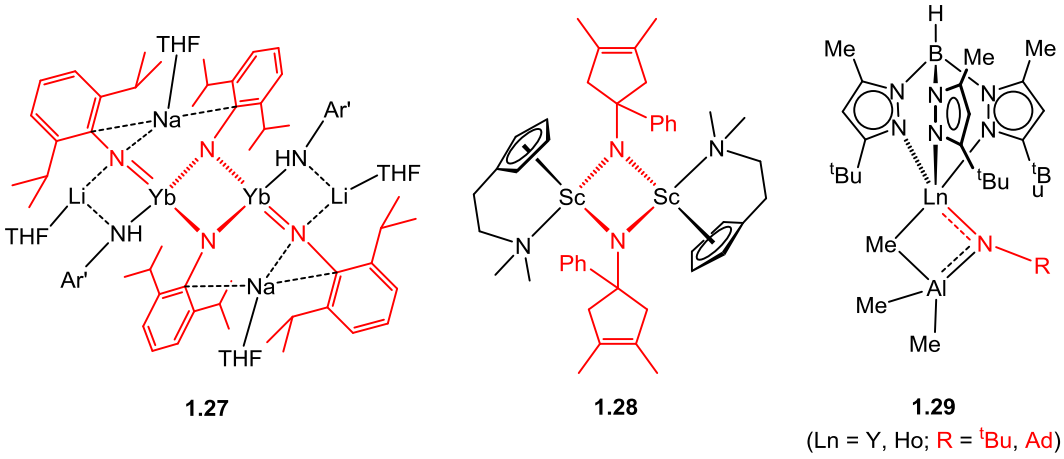

1.27 **1.28** **1.29**

(Ln = Y, Ho; R = ^{t}Bu, Ad)

Figure 1.3. Examples of rare earth complexes containing bridging and Lewis acid-supported imido ligands.[104,106,111]

Related μ^2-imido motifs have also been described in Lewis acid-stabilised imido complexes, a number of which have been prepared in recent years by Anwander and co-workers.[98,101,111–115] For example, reaction of $(Tp^{tBu,Me})LnMe(AlMe_4)$ (Ln = Y, Ho; $Tp^{tBu,Me}$ = tris(3-methyl-5-*tert*-butylpyrazolyl)borate) with H_2N^tBu or H_2NAd (Ad = adamantyl) produced the respective monomeric complex $(Tp^{tBu,Me})Ln\{(\mu_2\text{-}Me)AlMe_2\}(\mu_2\text{-}NR)$ (**1.29**, R = ^{t}Bu, Figure 1.3).[107] In the attempt to obtain the first terminal imido comple of scandium, Mindiola and co-workers synthetized the Lewis acid-stabilised complex $(PNP)Sc\{(\mu_2\text{-}Me)AlMe_2\}(\mu_2\text{-}NAr')$ (PNP = $N\{2\text{-}P^iPr_2\text{-}4\text{-}C_6H_3Me\}_2$) from (PNP)Sc(Me)(NHAr') and $AlMe_3$,[114] and subsequently added pyridine to remove the supporting $AlMe_3$. Unfortunately, the reaction gave the undesired C–H bond activation of pyridine to yield the pyridyl complex $(PNP)Sc(NHAr')(\eta^2\text{-}NC_5H_4)$. The same product was also obtained from reaction of (PNP)Sc(Me)(NHAr') directly with pyridine, and mechanistic studies showed that this proceeds *via* a transient imido complex (PNP)Sc(NAr')(py) which rapidly undergoes intramolecular C–H bond activation.

The first isolable terminal imido complex was reported by Chen and co-workers in 2010.[116] This was achieved using DMAP as a very strong external base, in combination

with the introduction of a new bulky β-diketiminate (NacNac)-type supporting ligand with a pendant NMe_2 donor; heating of $(L^1)Sc(Me)(NHAr')$ (**1.30**, L^1 = $(Ar')NC(Me)CHC(Me)NCH_2CH_2NMe_2$) in the presence of DMAP gave the terminal imido complex $(L^1)Sc(NAr')(DMAP)$ (**1.31**, Scheme 1.7). The short $Sc–N_{im}$ distance (1.881(5) Å) and near-linear $Sc–N_{im}–C$ angle (169.6(5)°) in **1.31** are consistent with a triple bond, as described for Group 4 imides above. DFT calculations also indicated the presence of two orthogonal π bonds and the $\sigma^2\pi^4$ nature of the triple bond.[116]

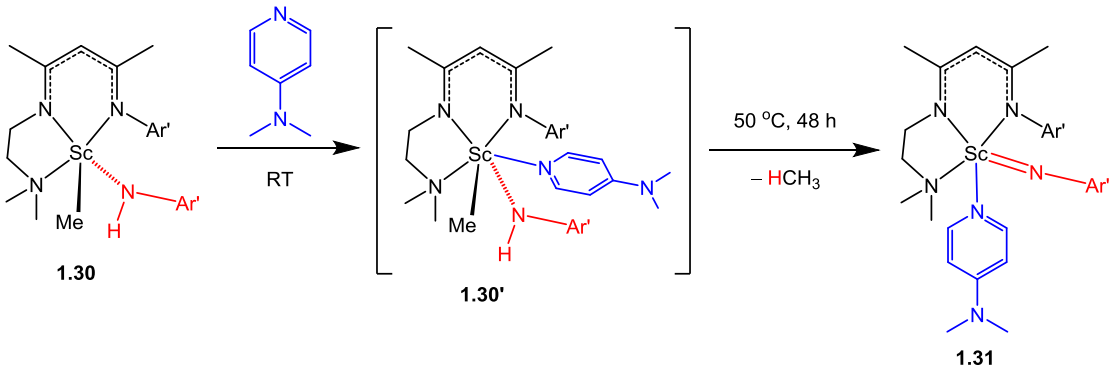

Scheme 1.7. Synthesis of $(L^1)Sc(NAr')(DMAP)$ (**1.31**).[116]

After having initial problems separating the by-product DMAP from the products of reactions of **1.31**,[117] Chen and co-workers later found that DMAP could be abstracted from this complex using 9-BBN (9-borabicyclo[3.3.1]nonane), or an alkyl derivative, to produce a base-free imide $(L^1)Sc(NAr')$ (**1.31'**) that could then undergo reactions with added substrates, some examples of which are highlighted here (Scheme 1.8).[117] Addition of 9-BBN and MeCCPh to **1.31** at RT produced the first reported azascandacyclobutene $(L^1)Sc\{N(Ar')C(Me)C(Ph)\}$ (**1.32**) *via* [2+2] cycloaddition of the alkyne at the metal–nitrogen multiple bond. Complex **1.31** reacts with 9-BBN and the terminal alkenes $H_2C=C(H)R$ (R = ^{t}Bu, ^{n}Pr) to form the *trans*-alkenyl complexes $(L^1)Sc(NHAr')\{C(H)=C(H)R\}$ (**1.33**) *via* C–H bond activation at the terminal methylene group of the alkene. When **1.31'** was generated from **1.31** with the addition of $^t BuCH_2CH_2BC_8H_{14}$, and heated at 50 °C without the addition of another reagent, a "tuck-in" complex (**1.34**, Scheme 1.8) was formed *via* C–H bond activation of a supporting ligand isopropyl group at the metal–nitrogen bond in a 1,2-fashion, which regenerates a protonated anilido ligand. Interestingly, addition of THF to **1.31'** results in the THF-coordinated imide $(L^1)Sc(NAr')(THF)$ (**1.35**) as an isolable complex.

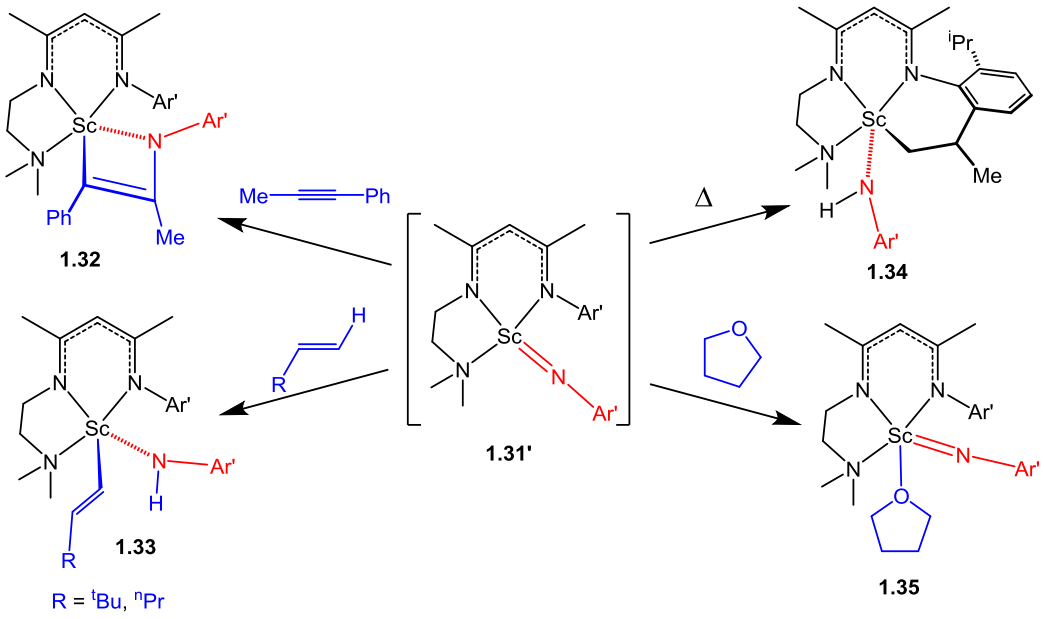

Scheme 1.8. Reactions of the *in situ*-generated imide (L^1)Sc(NAr') (**1.31'**).[117]

1.5 The hydrazido ligand

Until relatively recently, transition metal hydrazido ($L_nM{=}NNR_2$) chemistry at the Group 4 metals was very poorly developed. This is in considerable contrast to the situation for the related imido complexes reported in Section 1.4. A bonding description is explained in this Section and the synthesis and reactivity of Group 4 hydrazido complexes will be discussed in Section 1.7. Hydrazido ligands may bind to transition metal centres through several coordination modes, as reported previously for the imido ligands.[19] One of the defining features is the formal charge on the hydrazido fragment and the other one is the hapticity with respect to the metal centre. Depending on the presence and identity of the substituents at N_α, the formal charge can be −1 or −2. The hapticity with respect to the metal centre can be η^1- or η^2- depending on whether it binds to the metal centre through one or both nitrogen atoms of the ligand. Finally, the ligand can be terminal, bound to one metal, or bridging between to two metal centres, denoted by μ_2.[19] Several potential bonding modes observed for the hydrazido ligand are illustrated in Figure 1.4. From this point onwards, hydrazido(2-) mentioned in this Thesis refers to η^1-hydrazido(2-) of the general type (L)Ti=NNR_2 (where R = alkyl, aryl or mixed alkyl/aryl), and where other bonding modes are reported they are clearly labelled. The nitrogen atoms are described as $M{=}N_\alpha{-}N_\beta R_2$ in all cases.

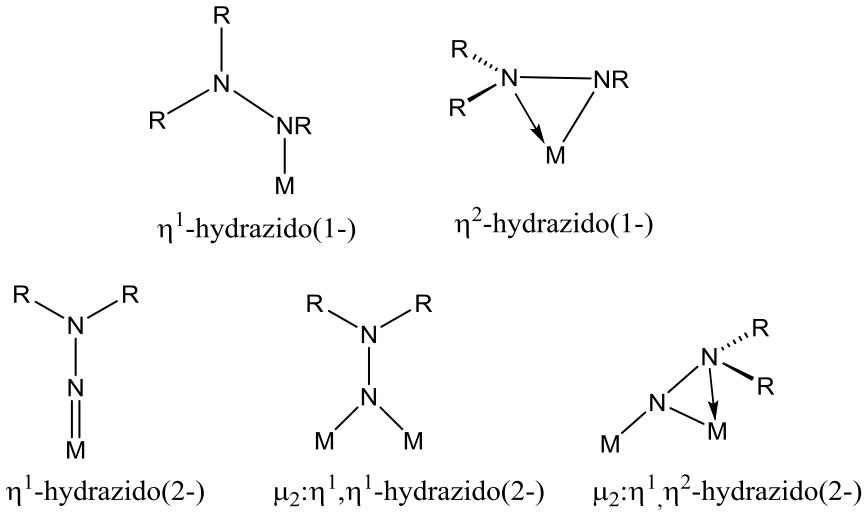

Figure 1.4. A selection of the bonding modes of the hydrazido ligand.

1.6 Group 4 hydrazido complexes

1.6.1 Titanium hydrazido complexes

Although the first monomeric η^1-titanium hydrazide(2-) complex, $Cp_2Ti\{NN(SiMe_3)_2\}$, was synthesised by Wiberg in 1978, *via* the reaction of Cp_2TiCl_2 and $N_2(SiMe_3)_2$, the compound was never structurally characterised.[65] It was not until 2004 that the first structurally authenticated monomeric η^1-titanium hydrazide(2-) complex was synthesised, namely $Ti(NNMe_2)(^tBu\text{-bpy})(dpma)$ (dpma = *N,N*-di(pyrrolyl-α-methyl)-*N*-methylamine, ^tBu-bpy = 4,4'-di-*tert*-butyl-2,2'-bipyridine) by Odom *et al.* in 2004.[19]

In 2005, the diphenylhydrazide starting material $Ti(NNPh_2)Cl_2(py)_3$ (**1.36**) was reported.[118,119] This allowed access to a wide range of hydrazide complexes following reaction with the desired lithiated or protonated ligand. Compound **1.36** was synthesised from $Ti(N^tBu)Cl_2(py)_3$ and Ph_2NNH_2, in a *tert*-butylimide/hydrazine exchange reaction. Examples of various supporting ligand sets used to synthesise η^1-hydrazido(2-) complexes are given in Figure 1.5.[119–121]

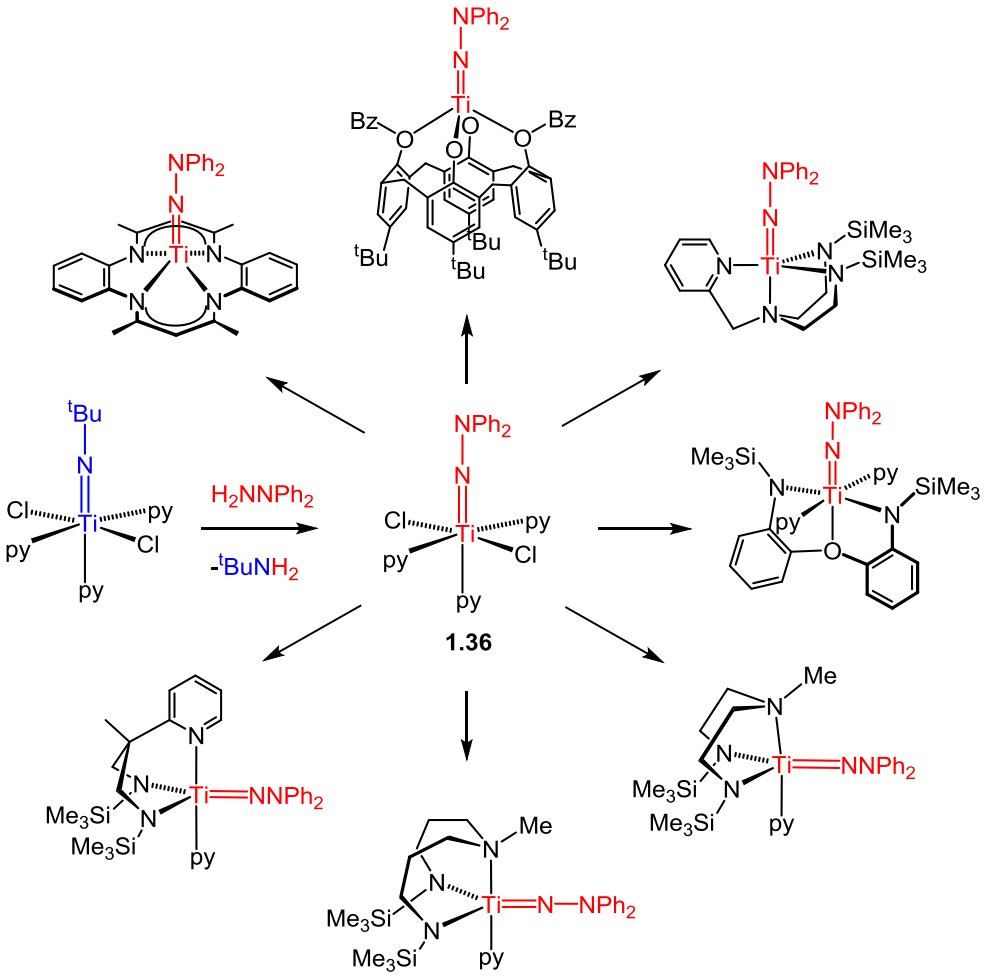

Figure 1.5. Examples of various titanium diphenyl hydrazide complexes synthesised from $Ti(NNPh_2)Cl_2(py)_3$ (**1.36**).

The Cp*-amidinate supported hydrazide systems were found to be particularly interesting. The hydrazide and alkylidene hydrazide complexes $Cp^*Ti\{MeC(N^iPr_2)_2\}(NNR_2)$ (R_2 = Ph_2 (**1.38**) or Me_2 (**1.39**); R = CPh_2 (**1.40**)) were synthesised from the imido complex $Cp^*Ti\{MeC(N^iPr)_2\}(N^tBu)$ (**1.37**) via an exchange reaction with hydrazine or hydrazone (Equation 1.1).[75,122] and all four yielded a wide range of reaction products.

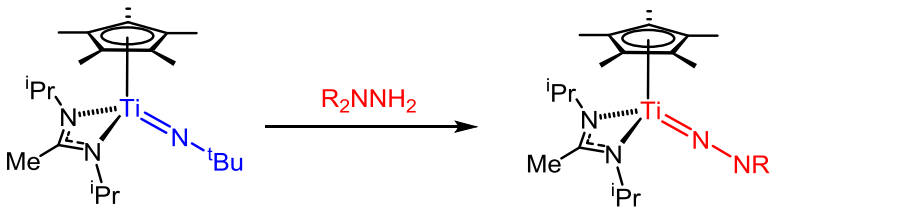

1.37 R = Ph_2 (**1.38**), Me_2 (**1.39**) or CPh_2 (**1.40**)

Equation 1.1

1.6.2 Zirconium and hafnium hydrazido complexes

The first monomeric terminal hydrazido complex of zirconium was reported by Bergman and co-workers in 1991.[123] $Cp_2Zr(NNPh_2)$ (**1.41**) was observed to be a transient complex obtained from thermolysis of $Cp_2Zr(NHNPh_2)(CH_2CH_2{}^tBu)$, which then rapidly dimerises in solution to form a complex with bridging hydrazido ligands. When prepared in the presence of DMAP, however, the isolable hydrazide $Cp_2Zr(NNPh_2)$(DMAP) (**1.42**) was successfully formed.

The diamide-pyridine-supported hydrazide $Zr(N_2{}^{TBS}N^{py})(NNPh_2)$(py) (**1.43**, $N_2{}^{TBS}N^{py}$ = $MeC(2\text{-}C_5H_4N)(CH_2NSiMe_2{}^tBu)_2$) was prepared by Gade and co-workers in 2007 through reaction of $Zr(N_2{}^{TBS}N^{py})Cl_2$ with $LiNHNPh_2$, then dehydrohalogenation with $LiN(SiMe_3)_2$.[124] In 2008, the same method was used to prepare the first hafnium hydrazido compound $Hf(N_2{}^{TBS}N^{py})(NNPh_2)$(py) (**1.44**).[125] Unfortunately, no zirconium or hafnium hydrazido synthon, to which a wide range of supporting ligands can be added, has been successfully prepared. This has meant that a desired supporting ligand is usually added to the metal prior to addition of the hydrazido ligand. For example, $Zr(NMe_2)_4$ has proved to be a useful starting material, and addition of the protioligand $H_2N_2{}^{3,5\text{-}Xyl}N^{py}$ ($MeC(2\text{-}C_5H_4N)(CH_2N(H)\text{-}3,5\text{-}C_6H_3Me_2)_2$) yields the bis(amido) compound $Zr(N_2{}^{3,5\text{-}Xyl}N^{py})(NMe_2)_2$. A second protonolysis reaction can then be carried out with two cyclic hydrazines H_2NNR_2 in the presence of DMAP to yield the hydrazido compounds $Zr(N_2{}^{3,5\text{-}Xyl}N^{py})(NNR_2)(DMAP)_2$ (R = C_9H_{10} (**1.45**, Figure 1.6) or $C_{12}H_8$).[126] Interestingly, reaction of the protioligand $H_2N_2{}^{ArF}N^{py}$ ($MeC(2\text{-}C_5H_4N)(CH_2N(H)Ar^F)_2$), which bears electron-withdrawing aryl substituents on the N_{amide} atoms, with $Zr(NMe_2)_2$ at 90 °C resulted in the formation of the difluoride compound $Zr(N_2{}^{TFAP}N^{py})F_2$ (**1.46**, $N_2{}^{TFAP}N^{py}$ = $MeC(2\text{-}C_5H_4N)\{CH_2N(2\text{-}C_6F_4NMe_2)\}_2$).[127] Compound **1.46** is formed from the exchange of one of the *ortho*-fluorine substituents on both aryl rings with a dimethylamido group originating from $Zr(NMe_2)_4$. However, it was still possible to obtain a hydrazido

compound, $Zr(N_2^{TFAP}N^{py})(NNPh_2)$, from **1.46** *via* reaction with $LiNHNPh_2$ and then $LiN(SiMe_3)_2$.

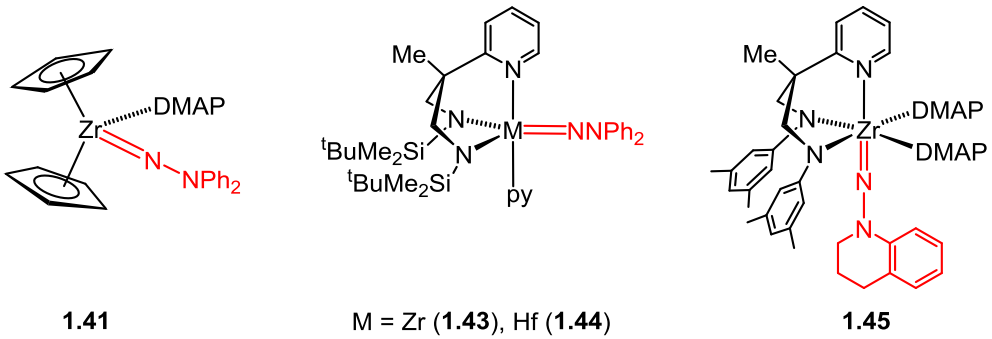

1.41 M = Zr (**1.43**), Hf (**1.44**) **1.45**

Figure 1.6. Examples of zirconium and hafnium hydrazido complexes.[123–127]

1.6.3 Structural features

To date there have several studies detailing the structure of titanium hydrazido compounds and in particular into the effect of N_β substituents on the geometry of titanium hydrazide complexes.[26,63,128,129] For example, in the cyclopentadienyl-amidinate supported hydrazide complexes, $Cp^*Ti\{MeC(N^iPr)_2\}(NNR_1R_2)$ (**1.38, 1.39, 1.47**),[63] the N_β substituents were varied from dialkyl to diaryl ($R_1 = R_2 =$ Ph (**1.38**) or Me (**1.39**); $R_1 =$ Me, $R_2 =$ Ph (**1.47**)) and all three compounds structurally characterised. In all cases, the respective short and long $Ti{=}N_\alpha$ (1.723(2) – 1.734(2) Å) and N_α–N_β (1.369(2) – 1.386(2) Å) bond lengths and linear Ti–N_α–N_β bond angles (159.5(1) – 166.3(2) °) are all consistent with formally Ti≡N triple bonds and N–N single bonds. The ligands are therefore formal η^1-hydrazido(2-) ligands, as given in Figure 1.5. However, with aryl substituents the N_β appears planar, consistent with sp^2 hybridisation, from lone pair delocalisation into at least one phenyl ring (the dimethyl hydrazido complex, **1.39**, possesses a pyramidal N_β as expected). In all three cases there is donation of the N_β lone pair into the $Ti{=}N_\alpha$ π^* antibonding orbital, resulting in a longer $Ti{=}N_\alpha$ bond. The Ti=N bond length increases in the order **1.39** (NMe_2) < **1.47** (NMePh) ≈ **1.38** (NPh_2). Accordingly, DFT calculations performed on simplified models of the compounds $Cp^*Ti\{MeC(N^iPr)_2\}(NNR_1R_2)$ showed that on forcing N_β to be planar in the case of **1.39** the $Ti{=}N_\alpha$ bond lengthened by 0.011 Å. The DFT calculated $Ti{=}N_\alpha$–R bond lengths were therefore found to increase in the order R = NPh_2 < NMePh < NMe_2 (planar N_β) in line with increasing basicity of N_β. The relative bond lengths of $Ti{=}N_\alpha$ and N_α–N_β are also related, with the shortest $Ti{=}N_\alpha$ bond found with the longest N_α-N_β bond, and *vice versa*.

DFT calculations were also carried out on alkyl and arylimido compounds for comparison as fully explained in Section 1.3.3. Hydrazide complexes, in general, show longer Ti=N_α bonds than alkyl imide complexes, as expected based on $N_\beta RR'$ lone pair donation lengthening the Ti=N_α bond. On the other hand, the Ti=N_α bond lengths of aryl imide complexes lie in between dialkyl and diaryl hydrazide complexes. This is a consequence of the π accepting nature of the phenyl ring leading to Ti=N_α π orbital to phenyl π* orbital and phenyl π orbital to Ti=N_α π* orbital interactions as described above.[63,130] To conclude, the Ti=N_α bond lengths of hydrazide and imide complexes supported by cyclopentadienyl-amidinate ligands are found to increase in the order Ti=N_α–R, R = Me < NMe_2 < Ph < NPh_2 ≈ NMePh < NMe_2 (planar N_β).

1.6.4 Stoichiometric reactions involving the M=N_{im} bond

Group 4 hydrazido compounds exhibit a variety of reactivity with small molecules, and reaction at the M=N_{im} multiple bond *via* a [2+2] cycloaddition, as in Group 4 imides, is a common first step. In many cases the products of this initial cycloaddition can be isolated and characterised, and then undergo further reaction. These secondary reactions can include insertion of a second substrate into the now single M–N_{im} bond or extrusion of a new organic compound.

The first examples of isolable compounds resulting from [2+2] cycloaddition reactions of a titanium hydrazido compound were the reactions of the macrocycle-supported complex Ti($NNPh_2$)(Me_4taa) with CO_2 or TolNCO. However, neither metallacyclic product was structurally authenticated.[44] The sandwich compound Cp_2Ti($NNPh_2$)(py) (**1.48**) underwent a [2+2] cycloaddition reaction with ^{t}BuCP to give one of the first examples of a structurally authenticated cycloaddition product for any metal hydrazide, as well as the first reported reactivity of a hydrazido compound with a phosphaalkyne.[131]

The stoichiometric reactions of the cyclopentadienyl-amidinate-supported hydrazido compounds Cp*Ti{MeC(N^iPr)$_2$}(NNR_2) (R = Me (**1.39**) or Ph (**1.38**)) have been successful and are particularly relevant for the work described in this Thesis. With CE_2 (E = O or S), [2+2] cycloaddition reactions occurred, initially yielding the carbamate-type compounds **1.49** and **1.50** (Scheme 1.9). When E = O, a second insertion occurred into the now single Ti–N_{im} bond resulting in "double insertion" complexes of the type **1.51**.[63] Reactions of **1.38** and **1.39** with isocyanates gave different reaction outcomes. The reaction of the diphenylhydrazido compound **1.38** yielded isolable cycloaddition products

with both alkyl and aryl isocyanates, whereas the dimethylhydrazido analogue **1.39** reacted with Ar'NCO and ^{t}BuNCO to give the oxo-bridged dimer [Cp*Ti{MeC(N^{i}Pr)$_2$}(μ-O)]$_2$ (**1.52**), and the organic compounds ^{t}BuNCNNMe$_2$ (**1.53**) and cyclic N(Me)$_2$NC(NAr')N(Ar')C(O) (**1.54**) respectively, following extrusion from the inherently unstable cycloaddition intermediates (Scheme 1.9).[122] Interestingly, reaction of **1.39** with two equivalents of TolNCO gave Cp*Ti{MeC(N^{i}Pr)$_2$}{OC(NNMe$_2$)N(Tol)C(NTol)O} (**1.55**) following the same cycloaddition-extrusion pathway as with Ar'NCO and ^{t}BuNCO. However, in this case, rapid cycloaddition of the extruded organic fragment to Ti=O (instead of dimerisation) formed Cp*Ti{MeC(N^{i}Pr)$_2$}{N(Tol)C(NNMe$_2$)O} (not observed), which then reacts with a second equivalent of TolNCO to give **1.55**. Investigation of the reactions of Cp*Ti{MeC(N^{i}Pr)$_2$}(NNMe$_2$) (**1.39**) with silanes, recently reported in our research group, showed the 1,2-addition of Si-H and Si-X bonds across Ti=N$_\alpha$, affording complexes of the type Cp*Ti{MeC(N^{i}Pr)$_2$}(X){N(NMe$_2$)SiH$_2$Ph} (e.g. X = Cl (**1.56**), Scheme 1.9).[78,132] Coordination of N$_\beta$ to titanium is also seen on reaction with [Et$_3$NH][BPh$_4$], forming [Cp*Ti{MeC(N^{i}Pr)$_2$}{η^2-N(H)NMe$_2$}][BPh$_4$] (**1.57**, Scheme 1.9), confirmed by structural analysis.[78] Though reaction with the triethylammonium salt gave protonation at N$_\alpha$, reaction with alkylating agents MeI, CH$_2$PhBr and EtBr resulted in alkylation at N$_\beta$, yielding [Cp*Ti{MeC(N^{i}Pr)$_2$}(NNRMe$_2$)][X] (R = Me, X = I; R = CH$_2$PhBr r Et, X = Br). Computational studies performed on these reactions showed that the products formed by protonation at the N$_\alpha$ are thermodynamically preferred in all cases. This results established that the R-X addition reactions are under kinetic control.[129]

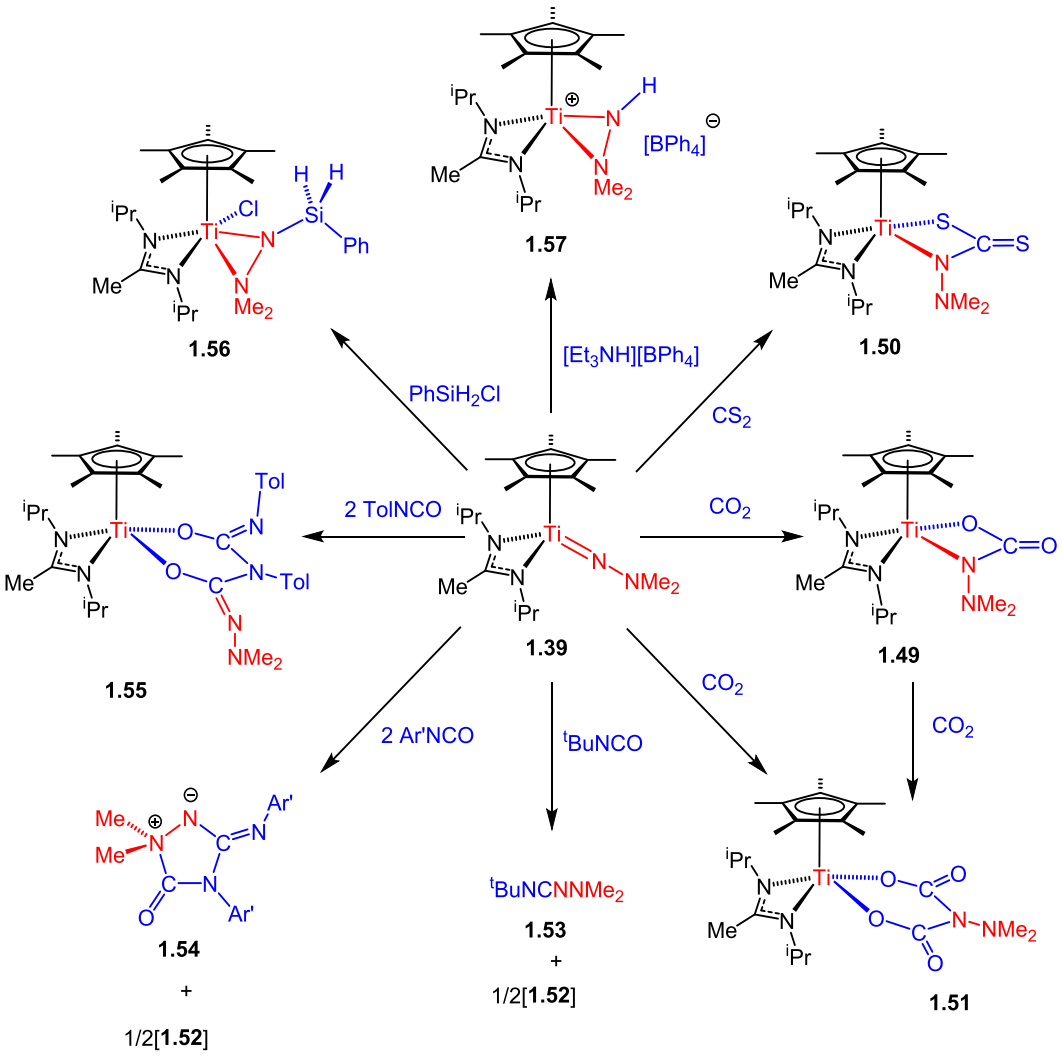

Scheme 1.9. Reactions of Cp*Ti{MeC(N^{i}Pr)$_2$}(NNR$_2$) (R = Me (**1.39**) or Ph (**1.38**) with unsaturated substrates.[63,78,129,132]

1.6.5 Stoichiometric reactions involving N_α–N_β bond cleavage

Group 4 hydrazido chemistry exhibits a wide range of processes involving reductive cleavage of the N_α–N_β bond by oxidisable substrates such as isonitriles, which are not possible in the analogues imido complexes. For example, the diamide-donor-supported compound Ti($N_2^{SiMe_3}N^{Me}$)(NNPh$_2$)(py) (**1.58**) reacts with one equivalent of XylNC to give the N_α–N_β bond cleavage product Ti($N_2^{SiMe_3}N^{Me}$)(NPh$_2$)(NCNXyl) (**1.59**, Figure 1.7).[133] DFT calculations indicated that loss of pyridine, then formation of an isonitrile adduct occur, prior to the formation of a three-membered intermediate which is supported by coordination of the N_β atom to the metal centre. From here, N_α–N_β bond cleavage is facile and results in formation of the final products.[133] An analogous isonitrile insertion reaction had previously been reported for the zirconium hydrazide

$Zr(N_2^{TBS}N^{py})(NNPh_2)(py)$ (**1.60**) and ^tBuNC,[127] and was later reported for the reaction of $Ti(N_2^{SiMe_3}O)(NNPh_2)(py)_2$ (**1.61**, $N_2^{SiMe_3}O$ = $O(CH_2CH_2NSiMe_3)_2$) with ^tBuNC.[134] Compound **1.61** also reacts with XylNC, consuming two equivalents of the substrate. The first equivalent results in N_α–N_β bond cleavage as above and the second equivalent reacts with one of the N–$SiMe_3$ ligand bonds yielding **1.62** (Figure 1.7). N_α–N_β bond cleavage is also observed in the reactions of complex **1.60** with propylene sulfide or Ph_3PSe, which form the dimeric compounds $\{Zr(N_2^{TBS}N^{py})(NPh_2)\}_2(\mu\text{-}N_2E)$ (E = S (**1.63**) or Se (**1.64**), Figure 1.7).[124] The hydrazido compound $Ti(N_2N^{Me})(NNPh_2)(py)$ reacts with internal alkynes to yield vinyl imido compounds of the type **1.65** (Figure 1.7). The alkyne has regiospecifically inserted into the N–N bond following a [2+2] cycloaddition reaction.[135]

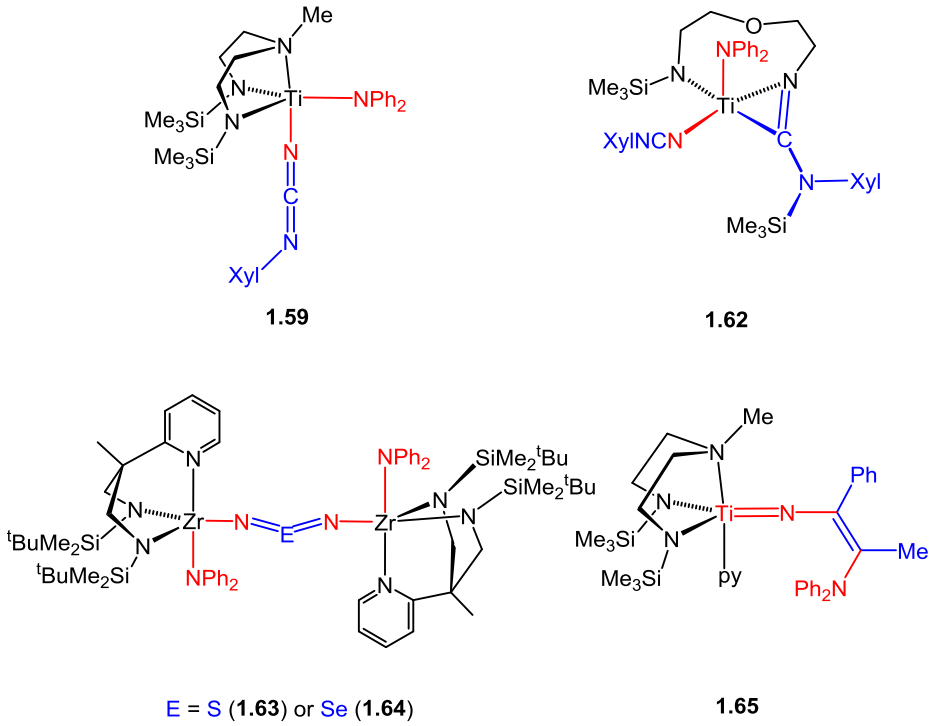

Figure 1.7. N_α–N_β bond cleavage products of Group 4 hydrazido compounds.[124,133,134,135]

These reactions with isonitriles are reminiscent of an early example of Group 4 hydrazido reactivity which was reported by Bergman and co-workers. The *in situ*-generated hydrazide $Cp_2Zr(NNPh_2)$ (**1.41**) undergoes N_α–N_β bond cleavage upon reaction with CO to form the mixed zirconium amide-isocyanate $Cp_2Zr(NCO)(NPh_2)$ (**1.66**, Scheme 1.10).[123] Compound **1.41**, also reacted with symmetrical internal alkynes RCCR (R = Et, Ph or Tol) to yield the complexes **1.67**, **1.68** and **1.69**, respectively (Scheme 1.10). These complexes contain seven-membered metallacycles formed from N_α–N_β bond cleavage followed by a C–H bond activation. Similar reactions with internal alkynes were reported

for the diamide-pyridine-supported **1.60**, for which the products were either seven-membered metallacycles as above or (in the case of MeCCMe) a vinylimido complex, $Zr(N_2{}^{TBS}N^{py})\{NC(Me)=C(Me)NPh_2\}$, which represents insertion of the alkyne into the N_α–N_β bond.[136]

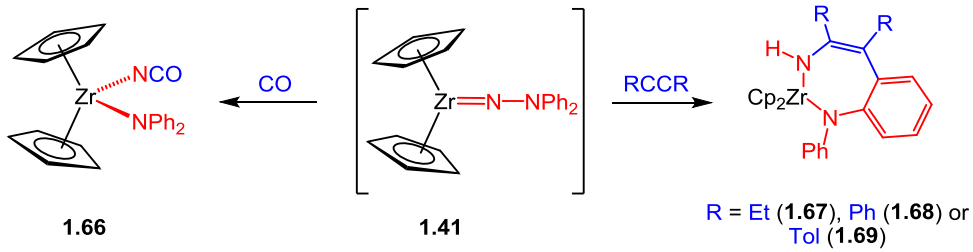

Scheme 1.10. Reactions of $Cp_2Zr(NNPh_2)$ (**1.41**) with CO and internal alkynes.[123]

Of particular relevance to this Thesis is the recently published work[28] on the reactivity of $Ti(N_2{}^{iPr}N)(NNPh_2)(py)$ (**1.70**) with silanes and boranes, which will be extensively explored in Chapter 2. Reaction of $Ti(N_2{}^{iPr}N)(NNPh_2)(py)$ (**1.70**) with $PhSiH_3$ gave quantitative conversion to $Ti(N_2{}^{iPr}N)\{N(H)SiH_2Ph\}(NPh_2)$ (**1.71**) which exists as two isomers, denoted *trans*-2 and *cis*-2 (Scheme 1.11). Reaction with Ph_2SiH_2 gave an analogous product, namely $Ti(N_2{}^{iPr}N)\{N(H)SiHPh_2\}(NPh_2)$ (**1.72**), which likewise exists as mixture of *trans* and *cis* isomers. In both cases, the complete cleavage of the N_α–N_β bond occurred, forming the new NPh_2 and $N(H)SiHPh_2$ ligands (each having an N atom in a formal –3 oxidation state compared to –2 in $Ti(N_2{}^{iPr}N)(NNPh_2)(py)$). Following this results, the reaction of **1.70** with 1 equiv. of 9-BBN dimer was reported to give conversion to the borylamide $Ti(N_2{}^{iPr}N)\{N(H)BC_8H_{14}\}(NPh_2)$ (**1.73**) together with $py{\cdot}HBC_8H_{14}$.

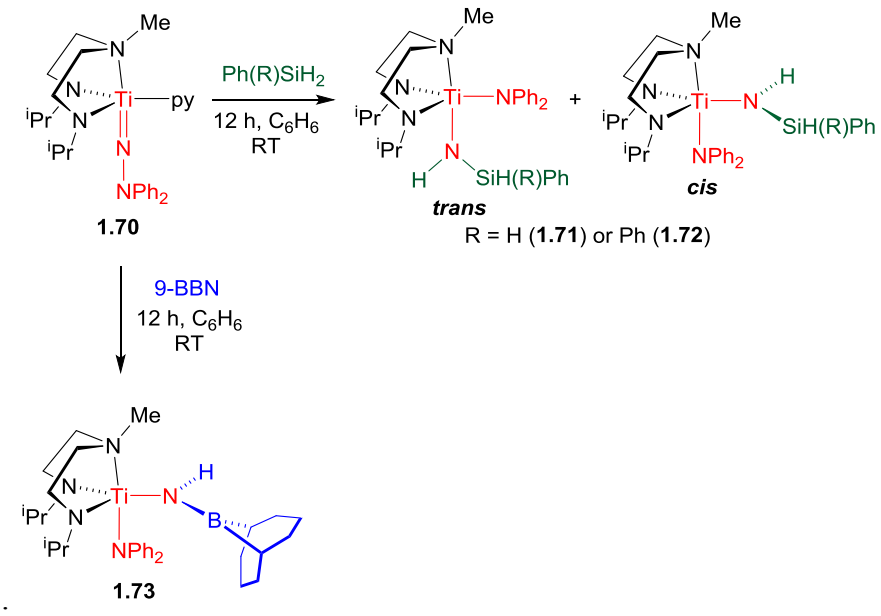

Scheme 1.11. Reactions of Ti($N_2^{iPr}N$)($NNPh_2$)(py) (**1.70**) with $PhSiH_3$, Ph_2SiH_2 and 9-BBN dimer.[28]

1.6.6 Catalytic reactions

Given the widespread use of Group 4 imido complexes as catalysts for the hydroamination of alkynes, described in Section 1.3.5, a large body of work has subsequently been built around analogous processes which may be catalysed by Group 4 hydrazido complexes. Firstly, a direct extension of hydroamination catalysis known as hydrohydrazination, in which the N–H bonds of an N,N-disubstituted hydrazine are added across an alkyne to form hydrazones, has received much attention, and several examples of Group 4 catalytic systems have been reported[19,21,25,26,80,83] Like hydroamination, hydrohydrazination is postulated to proceed through metallacycles of the type **1.74** (Figure 1.8) which can then undergo protonolysis of the Ti–C and Ti–N bonds upon addition of an equivalent of hydrazine to form hydrazones (**1.75**). This second step is proposed to proceed *via* a transient mixed bis(hydrazido(1–)) intermediate, in analogy to the mechanism for hydroamination shown in Scheme 1.5.

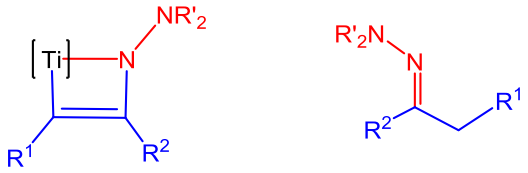

1.74 **1.75**

Figure 1.8. Metallacyclic intermediates of hydrohydrazination (**1.74**), and resulting hydrazones (**1.75**).

Such catalytic reactions have typically been found to require high temperatures (> 75 °C) and long reaction times (2 – 75 h), with harsher conditions being necessary for internal alkynes. In many cases, the active hydrazido catalyst is synthesised *in situ* from the corresponding diamide pre-catalyst (L)Ti(NMe_2)$_2$ upon introduction of the hydrazine.[2021,25,80] In 2011, Gade and co-workers reported that the cyclopentadienyl-amidinate-supported compounds Cp*Ti($N^{3,5\text{-Xyl}}N^{pyr}$)(NNRR')(L) (R = R' = Ph or Me; R = Ph, R' = Me; L = py, DMAP or H_2N^tBu) were capable of catalysing the hydrohydrazination of a range of alkynes with quantitative conversion taking place within 1 h at RT (at 5 mol% catalyst loading).[26] In some cases, further reactions of the hydrazones can take place to form other nitrogen-containing organic compounds. The formation of indoles,[19,21,22,80,83] pyrroles[80] and tryptamines[23] in this way have been reported, with these cyclisations usually requiring the addition of an external Lewis base such as $ZnCl_2$ for their successful catalysis.

Furthermore, an iminohydrazination reaction has been developed using the pre-catalysts **1.76** and **1.77** (Figure 1.9), where an alkyne, hydrazine and organic isocyanide are coupled in a single reaction to form a 1,3-iminohydrazone.[24,137] This process has since been developed further, and the precatalyst Ti(NMe_2)$_2$(pypyr)$_2$ (**1.78**, Hpypyr = 2-(2'-pyridyl)-3,5-dimethylpyrrole, Figure 1.9) can be used in the multicomponent coupling of alkynes, isonitriles and monosubstituted hydrazines to yield pyrroles in a single step, without the need for an external Lewis acid.[138]

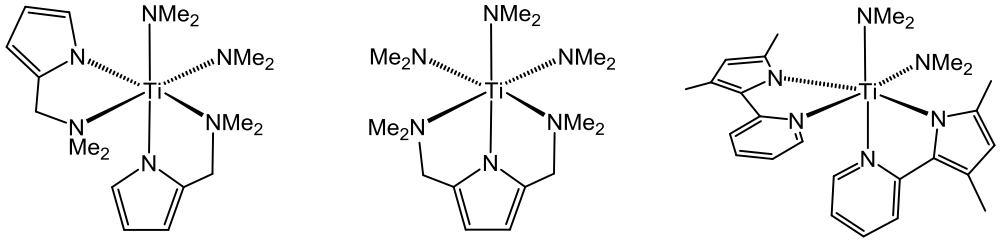

1.76 **1.77** **1.78**

Figure 1.9. Titanium pre-catalysts.

1.7 Group 4 alkylidene hydrazide complexes

Diazoalkane or hydrazonido complexes, which possess $N_\alpha N_\beta CR_2$ ligands, are significantly less well-developed then the parent imido and hydrazido compounds. Synthesis of these complexes normally involves the use of potentially explosive diazoalkanes, although azines, dinitrogen and hydrazones have also been used.[139] In 2013, our group used a *tert*-butylimide/hydrazone exchange methodology to synthetize $Cp^*Ti\{MeC(N^iPr)_2\}(NNCPh_2)$ (**1.40**).[122]

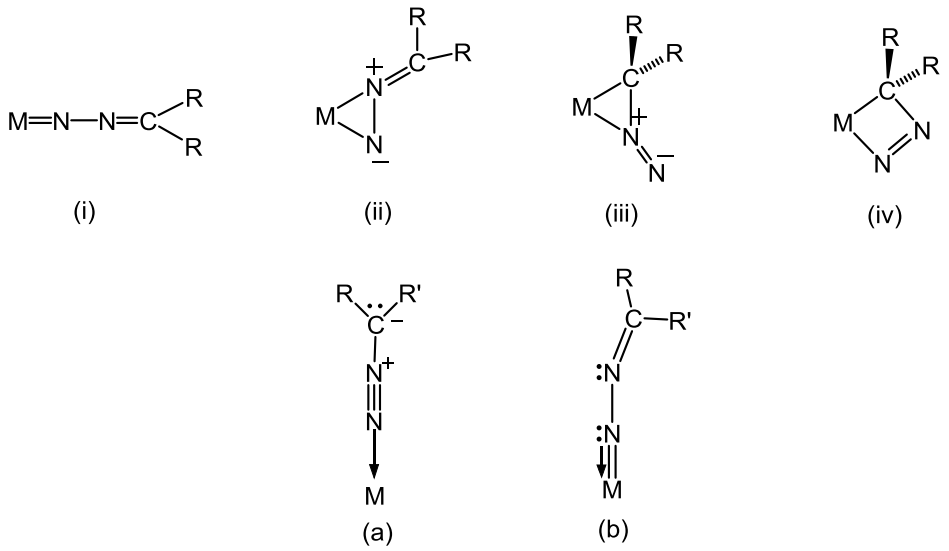

Figure 1.10. *(Top)* Possible bonding modes for an alkylidene hydrazido ligand coordinated to a metal. *(Bottom)* Various resonance forms for an alkylidene hydrazido ligand coordinated in a monomeric η^1-fashion.[140]

Like hydrazides, the addition of an $N_\beta CR_2$ moiety enables these ligands to coordinate through more than one binding mode, as depicted in Figure 1.10. Within the monomeric η^1 bonding mode ((i), Figure 1.10) there are two possible resonance forms, (a) and (b), with the % contribution of each identified through the M-N_α, N_α-N_β and N_β-C_α bond

distances and M-N_α-N_β and N_α-N_β-C_α bond angles.[140] Like the analogous hydrazide complexes, DFT analysis of the bonding in **1.40** showed destabilisation of the Ti=N_α π_v orbital by the N_β lone pair. Although both **1.40** and the dimethyl hydrazide complex **1.39** are stabilised by the pyramidal geometry around N_β, the extent of N_β lone pair donation is found to be much less significant in the case of **1.40**, consistent with the Ti=N_α-R bond length increasing in the order R = Me < Ph < $NCPh_2$ < NMe_2.

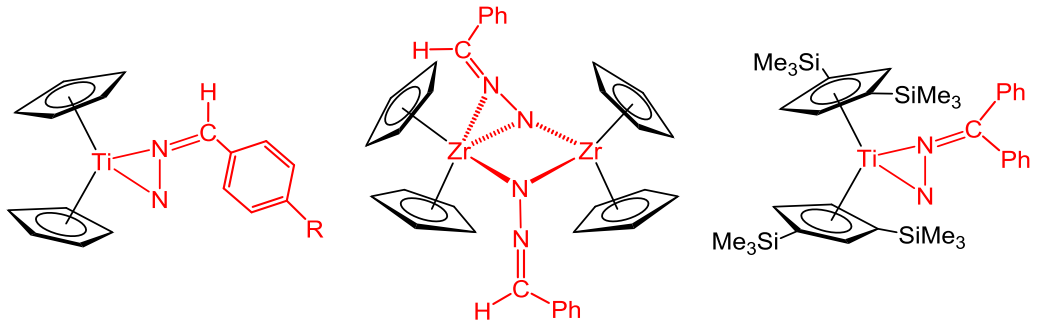

1.79 **1.80** **1.82**

Figure 1.11. Examples of Group 4 alkylidene hydrazido complexes.

Although η^1-alkylidene hydrazido ligands on titanium are rare, complexes which possess side-on bonding ligands, as shown in (ii), Figure 1.11, are more common. These include $Cp^*_2Ti\{\eta^2$-NNC(H)$SiMe_3\}$ and $Cp^*_2Ti\{\eta^2$-NNC(H)Ar} (**1.79**, Ar = Ph (**1.79a**), Tol (**1.79b**), 4-$C_6H_4CF_3$, 4-C_6H_4Cl and 4-$C_6H_4NMe_2$, Figure 1.11) synthesised by Bergman *et al.*[141,142] and $Cp^*CpTiCl\{N(H)NCPh_2\}$ and $Ti\{\eta^5$-$C_5H_4(SiMe_2$-η^1-$NNCPh_2)\}Cl_2$ synthesised by Cuenca *et al.*[143] Dimeric structures containing alkylidene hydrazide ligands, bonding in a similar fashion to η^2-hydrazido(2-) ligands, have also been observed, for example reaction of Cp_2ZrCl_2 with $Li_2NNC(H)Ph$ produced the zirconium dimer, $[Cp_2Zr]_2(\mu$-η^1:η^1-NNCHPh)(μ-η^2:η^1-NNCHPh) (**1.80**, Figure 1.11).[144]

To date only a few studies on the reactivity of these complexes have been reported. In 1998 Bergman reported the reaction of **1.79b** with CO which resulted in N_α–N_β bond cleavage forming $Cp^*_2Ti\{NC(H)Tol\}(NCO)$ (**1.81**, Figure 1.13),[142,141] reminiscent of $Cp_2Zr(NNPh_2)(DMAP)$ (**1.42**).[123] In contrast reaction of $\{\eta^5$-1,3-$C_5H_3(SiMe_3)_2\}_2Ti(\eta^2$-$NNCPh_2)$ (**1.82**, Figure 1.12) with CO yields the adduct $\{\eta^5$-1,3-$C_5H_3(SiMe_3)_2\}_2Ti(NNCPh_2)(CO)$ (**1.83**, Figure 1.12).[145] Adducts were also observed on addition of ^{t}BuNC and DMAP to **1.82** and **1.79a** yielding the η^1-alkylidene hydrazide complexes $Cp^*_2Ti\{NNC(H)Ph\}(^t$BuNC) and $\{\eta^5$-1,3-$C_5H_3(SiMe_3)_2\}_2Ti(NNCPh_2)$(DMAP), respectively.[39,142] Reaction of primary silanes with

$Cp^*Ti\{MeC(N^iPr)_2\}(NNCPh_2)$ (**1.40**) formed $Cp^*Ti\{MeC(N^iPr)_2\}$-$\{N(RSiH_2)N(CHPh_2)\}$[122] presumably *via* $Cp^*Ti\{MeC(N^iPr)_2\}$-$\{N(RSiH_2)N(CPh_2)\}(H)$ since reaction of **1.79b** with Ph_2SiH_2 or $PhSiH_3$ gave $Cp^*Ti\{N(SiHRPh)NC(H)Tol\}(H)$ (R = H or Ph (**1.84**), Figure 1.12) following Si-H bond addition across Ti-N.[146] Moreover, a comprehensive study into the reactivity of **1.40** highlighted similar reactivity to the hydrazide compounds depicted in Scheme 1.10, forming cycloaddition and "double insertion" products with heterocumulenes and alkynes, such as $Cp^*Ti\{MeC(N^iPr)_2\}\{SC(NNCPh_2)N(Tol)C(NTol)O\}$ (**1.85**) $Cp^*Ti\{MeC(N^iPr)_2\}\{N(NCPh_2)C(Ar^{F5})C(H)\}$ (**1.86**) and $Cp^*Ti\{MeC(N^iPr)_2\}\{N(NCPh_2)C(Ar^{F5})NC(Ar^{F5})N\}$ (**1.87**) following reaction with TolNCS and TolNCO, $Ar^{F5}CCH$ and $Ar^{F5}CN$, respectively (Figure 1.12).[147]

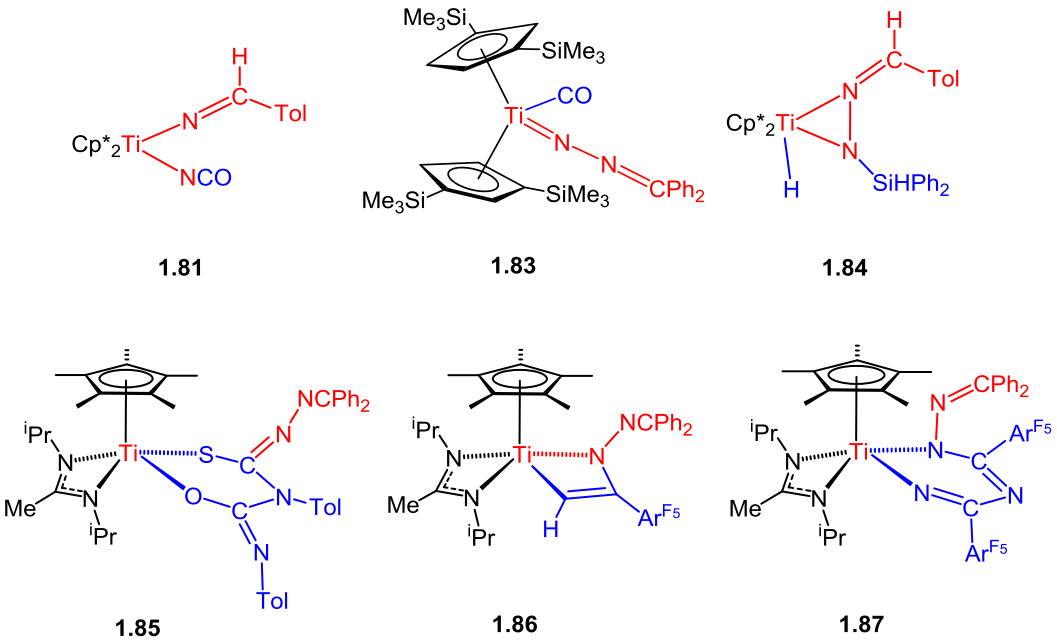

Figure 1.12. Reaction products from titanium alkylidene hydrazide complexes with small substrates.

1.8 Titanium borylimido complexes

The substitution of a BR_2 group at the N_{im} atom of a metal–nitrogen multiply bonded functional group forms a borylimido moiety. Transition metal complexes containing a terminal borylimido ligand have been studied recently, although no well-established synthetic routes are known. Moreover, there have been no reactivity studies with small molecules.

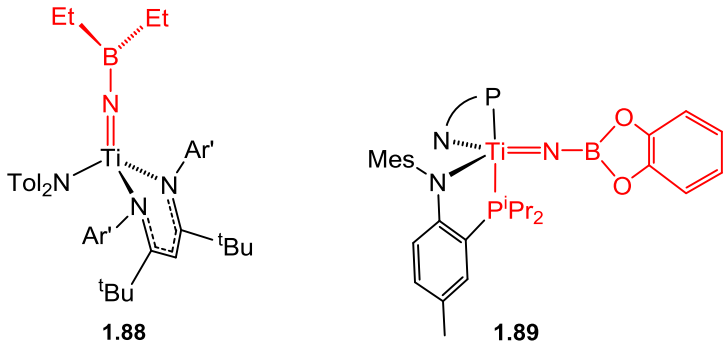

Figure 1.13. Previously reported titanium terminal borylimido complexes.[148,149]

The first report of a Group 4 complex containing a terminal borylimido ligand came from Mindiola and co-workers in 2014: (^{tBu}NacNac)Ti(NBEt$_2$)(NTol$_2$) (**1.88**, Figure 1.13) was prepared through a serendipitous reaction of the parent imido (terminal NH) compound with 2 equivalents of NaHBEt$_3$.[149] In 2017, the same research group reported the synthesis of a terminal borylimido complex, **1.89** obtained via salt methathesis reaction of the titanium salt, [μ_2-K(OEt$_2$)]$_2$[(PN)$_2$Ti=N]$_2$ (PN = N-(2-(diisopropylphosphino)-4-methylphenyl)-2,4,6-trimethylanilide) and ClBcat (cat = catechol).[148] Recently, our research group communicated the preparation of a terminal borylimido complex of titanium through the reaction of a diphenyl- or dimethylhydrazide (**1.38** or **1.39**, respectively) with 1 equivalent of 9-BBN dimer. The formation of Cp*Ti{MeC(N^{i}Pr)$_2$}(NBC$_8$H$_{14}$) (**1**) was accompanied by elimination of the respective diphenyl- or dimethylaminoborane and H$_2$ (Equation 1.2).[28] This reaction will be extensively explained in Chapter 3.

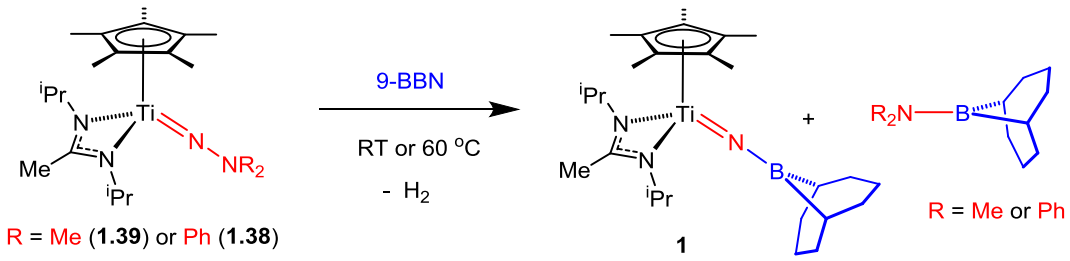

Equation 1.2.

More recently our research group developed a versatile synthetic routes to titanium borylimides, incorporating the bulky borylamine H$_2$NB(NAr'CH)$_2$ (where Ar' = Dipp) and taking inspiration from the synthetic methodologies reported for the titanium imido and hydrazido chemistry. In particular, compounds with sandwich (**1.90**) and half-sandwich (**1.91**) structures and with tridentate nitrogen-based supporting ligand (**1.92**)

were synthetized (Figure 1.14).[150] An extensive description of these reactions will be provided in Chapter 4.

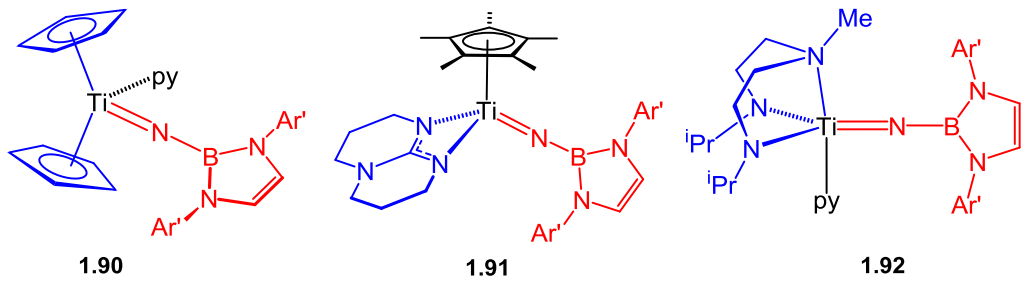

Figure 1.14. Examples of titanium terminal borylimido compounds recently reported in our research group.[150]

1.9 Summary and objectives

This Chapter has explored the well-established chemistry of Group 4 imido, hydrazido and alkylidene hydrazido complexes, including their synthesis, reactivity and structure, as well as practical applications in catalysis. The more recent evolution of rare earth imido chemistry has also been described. Finally, a survey of terminal borylimido complexes which are known across the transition metals has been described. One aim of this Thesis is to investigate the mechanism of the novel reactions of titanium hydrazido and alkylidene hydrazido compounds described in this Chapter with boranes and silanes. The reactivity of titanium borylimides with small molecules such as CO_2 and CS_2 has been recently explored in our research group as explained in Section 1.9. Thus, a second aim of this Thesis is to understand the bonding features and the reactivity of these novel titanium borylimido compounds[150] and to compare them with the analogues imide and hydrazide complexes. A third aim of this Thesis is to extend the mechanistic and bonding studies performed on the titanium half-sandwich imido, hydrazido and borylimido complexes to the scandium borylimides recently reported in our research group.[150]

1.10 References

1 J. Chatt, A. J. Pearman and R. L. Richards, *J. Chem. Soc. Dalton Trans.*, 1977, 2139–2142.

2 M. Hidai, *Coord. Chem. Rev.*, 1999, **185–186**, 99–108.

3 R. R. Schrock, *Angew. Chem. Int. Ed.*, 2008, **47**, 5512–5522.

4 R. R. Schrock, *Acc. Chem. Res.*, 2005, **38**, 955–962.

5 W. W. Weare, X. Dai, M. J. Byrnes, J. M. Chin, R. R. Schrock and P. Muller, *Proc. Natl. Acad. Sci.*, 2006, **103**, 17099–17106.

6 D. V Yandulov and R. R. Schrock, *Inorg. Chem.*, 2005, **44**, 1103–1117.

7 N. Hazari and P. Mountford, *Acc. Chem. Res.*, 2005, **38**, 839–849.

8 N. Adams, H. J. Arts, P. D. Bolton, D. Cowell, S. R. Dubberley, N. Friederichs, C. M. Grant, M. Kranenburg, A. J. Sealey, B. Wang, P. J. Wilson, A. R. Cowley, P. Mountford and M. Schröder, *Chem. Commun. (Camb).*, 2004, 434–435.

9 P. D. Bolton and P. Mountford, *Adv. Synth. Catal*, 2005, **347**, 355–366.

10 H. R. Bigmore, S. R. Dubberley, M. Kranenburg, S. C. Lawrence, A. J. Sealey, J. D. Selby, M. A. Zuideveld, A. R. Cowley and P. Mountford, *Chem. Commun.*, 2006, 436–438.

11 H. R. Bigmore, M. A. Zuideveld, A. M. Kowalczyk, A. R. Cowley, M. Kranenburg, E. J. L. McInnes and P. Mountford, *Inorg. Chem.*, 2006, **45**, 6411–6423.

12 P. J. Wilson, A. J. Blake, P. Mountford and M. Schroder, *Chem. Commun.*, 1998, 1007–1008.

13 C. H. Winter, P. H. Sheridan, T. S. Lewkebandara, M. J. Heeg and J. W. Proscia, *J. Am. Chem. Soc.*, 1992, **114**, 1095–1097.

14 T. S. Lewkebandara, P. H. Sheridan, M. J. Heeg, A. L. Rheingold and C. H. Winter, *Inorg. Chem.*, 1994, **33**, 5879–5889.

15 I. Bytschkov and S. Doye, *Eur. J. Org. Chem.*, 2003, **2003**, 935–946.

16 S. Doye, *Synlett*, 2004, 1653–1672.

17 A. V Lee and L. L. Schafer, *Eur. J. Inorg. Chem.*, 2007, 2243–2255.

18 T. E. Müller, K. C. Hultzsch, M. Yus, F. Foubelo and M. Tada, *Chem. Rev.*, 2008, **108**, 3795–3892.

19 Y. Li, J. Shi and A. L. Odom, *J. Am. Chem. Soc.*, 2004, **126**, 1794–1803.

20 J. S. Johnson and R. G. Bergman, *J. Am. Chem. Soc.*, 2001, **123**, 2923–2924.

21 C. Cao, Y. Shi and A. L. Odom, *Org. Lett.*, 2002, **4**, 2853–2856.

22 L. Ackermann and R. Born, *Tetrahedron Lett.*, 2004, **45**, 9541–9544.

23 V. Khedkar, A. Tillack, M. Michalik and M. Beller, *Tetrahedron Lett.*, 2004, **45**, 3123–3126.

24 S. Banerjee, Y. Shi, C. Cao and A. L. Odom, *J. Organomet. Chem.*, 2005, **690**, 5066–5077.

25 S. Banerjee, E. Barnea and A. L. Odom, *Organometallics*, 2008, **27**, 1005–1014.

26 K. Weitershaus, H. Wadepohl and L. H. Gade, *Organometallics*, 2009, **28**, 3381–3389.

27 M. D. Fryzuk, B. A. MacKay, S. A. Johnson and B. O. Patrick, *Angew. Chem. Int. Ed.*, 2002, **41**, 3709–3712.

28 L. Stevenson, S. Mellino, E. Clot and P. Mountford, *J. Am. Chem. Soc.*, 2015, **137**, 10140–10143.

29 W. A. Nugent and B. L. Haymore, *Coord. Chem. Rev.*, 1980, **31**, 123–175.

30 W. A. Nugent and J. M. Mayer, in *Metal-Ligand Multiple Bonds*, Wiley-Interscience, New York, 1988.

31 D. E. Wigley, in *Progress in Inorganic Chemistry*, ed. K. D. Karlin, Wiley-Interscience, New York, 1994, vol. 42, pp. 239–482.

32 M. H. Chisholm and I. P. Rothwell, in *Comprehensive Coordination Chemistry*, Pergamon Press, Oxford, 1987, vol. 2, pp. 161–184.

33 P. Mountford, *Chem. Commun.*, 1997, 2127–2134.

34 B. L. Haymore, E. A. Maatta and R. A. D. Wentworth, *J. Am. Chem. Soc.*, 1979, **101**, 2063–2068.

35 A. S. Batsanov, A. E. Goeta, J. A. K. Howard, A. K. Hughes, A. L. Johnson and K. Wade, *J. Chem. Soc. Dalton Trans.*, 2001, **8**, 1210–1217.

36 S. C. Dunn, P. Mountford and D. A. Robson, *J. Chem. Soc. Dalton Trans.*, 1997, **2**, 293–304.

37 H. W. Roesky, H. Voelker, M. Witt and M. Noltemeyer, *Angew. Chem. Int. Ed.*, 1990, **29**, 669–670.

38 R. Duchateau, A. J. Williams, S. Gambarotta and M. Y. Chiang, *Inorg. Chem.*, 1991, **30**, 4863–4866.

39 T. E. Hanna, I. Keresztes, E. Lobkovsky, W. H. Bernskoetter and P. J. Chirik, *Organometallics*, 2004, **23**, 3448–3458.

40 N. Hazari and P. Mountford, *Acc. Chem. Res.*, 2005, **38**, 839–849.

41 A. J. Blake, P. E. Collier, S. C. Dunn, W. Li, P. Mountford and O. V Shishkin, *J. Chem. Soc. Dalton Trans.*, 1997, 1549–1558.

42 L. H. Gade and P. Mountford, *Coord. Chem. Rev.*, 2001, **216–217**, 65–97.

43 D. Swallow, J. M. McInnes and P. Mountford, *J. Chem. Soc. Dalton Trans.*, 1998, 2253–2260.

44 A. J. Blake, J. M. McInnes, P. Mountford, G. I. Nikonov, D. Swallow and D. J. Watkin, *J. Chem. Soc. Dalton Trans.*, 1999, 379–392.

45 E. Müller, J. Müller, F. Olbrich, W. Brüser, W. Knapp, D. Abeln and F. T. Edelmann, *Eur. J. Inorg. Chem.*, 1998, 87–91.

46 S. C. Dunn, A. S. Batsanov and P. Mountford, *J. Chem. Soc. Chem. Commun.*, 1994, **724**, 2007–2008.

47 C. T. Owen, P. D. Bolton, A. R. Cowley and P. Mountford, *Organometallics*, 2007, **26**, 83–92.

48 M. Froneman, D. L. Cheney and T. A. Modro, *Phosphorus. Sulfur. Silicon Relat. Elem.*, 1990, **47**, 273–281.

49 N. Adams, H. R. Bigmore, T. L. Blundell, C. L. Boyd, S. R. Dubberley, A. J. Sealey, A. R. Cowley, M. E. G. Skinner and P. Mountford, *Inorg. Chem.*, 2005, **44**, 2882–2894.

50 C. Lorber, R. Choukroun and L. Vendier, *Eur. J. Inorg. Chem.*, 2006, 4503–4518.

51 P. J. Walsh, F. J. Hollander and R. G. Bergman, *J. Am. Chem. Soc.*, 1988, **110**, 8729–8731.

52 W. A. Nugent and R. L. Harlow, *Inorg. Chem.*, 1979, **18**, 2030–2032.

53 R. L. Zuckerman, S. W. Krska and R. G. Bergman, *J. Am. Chem. Soc.*, 2000, **122**, 751–761.

54 D. J. Arney, M. A. Bruck, S. R. Huber and D. E. Wigley, *Inorg. Chem.*, 1992, **31**, 3749–3755.

55 C. C. Cummins, S. M. Baxter and P. T. Wolczanski, *J. Am. Chem. Soc.*, 1988, **110**, 8731–8733.

56 S. R. Dubberley, S. Evans, C. L. Boyd and P. Mountford, *Dalton Trans.*, 2005, 1448–1458.

57 A. J. Blake, P. Mountford, G. I. Nikonov and D. Swallow, *Chem. Commun.*, 1996, 1835–1836.

58 A. J. Blake, P. E. Collier, L. H. Gade, P. Mountford, J. Lloyd, S. M. Pugh, M. Schubart, M. E. G. Skinner and D. J. M. Trösch, *Inorg. Chem.*, 2001, **40**, 870–877.

59 J. L. Thorman, I. A. Guzei, Young and L. K. Woo, *Inorg. Chem.*, 1999, **38**, 3814–3824.

60 M. E. G. Skinner, T. Toupance, D. A. Cowhig, B. R. Tyrrell and P. Mountford, *Organometallics*, 2005, **24**, 5586–5603.

61 N. Adams, H. J. Arts, P. D. Bolton, D. Cowell, S. R. Dubberley, N. Friederichs, C. M. Grant, M. Kranenburg, A. J. Sealey, B. Wang, P. J. Wilson, M. Zuideveld, A. J. Blake, M. Schröder and P. Mountford, *Organometallics*, 2006, **25**, 3888–3903.

62 A. E. Guiducci, C. L. Boyd and P. Mountford, *Organometallics*, 2006, **25**, 1167–1187.

63 P. J. Tiong, A. Nova, L. R. Groom, A. D. Schwarz, J. D. Selby, A. D. Schofield, E. Clot and P. Mountford, *Organometallics*, 2011, **30**, 1182–1201.

64 N. Kaltsoyannis and P. Mountford, *J. Chem. Soc., Dalton Trans.*, 1999, 781–789.

65 K. E. Meyer, P. J. Walsh and R. G. Bergman, *J. Am. Chem. Soc.*, 1995, **117**, 974–985.

66 S. Y. Lee and R. G. Bergman, *Tetrahedron*, 1995, **51**, 4255–4276.

67 S. Y. Lee and R. G. Bergman, *J. Am. Chem. Soc.*, 1995, **117**, 5877–5878.

68 S. A. Blum, V. A. Rivera, R. T. Ruck, F. E. Michael and R. G. Bergman, *Organometallics*, 2005, **24**, 1647–1659.

69 D. J. M. Trösch, P. E. Collier, A. Bashall, L. H. Gade, M. McPartlin, P. Mountford and S. Radojevic, *Organometallics*, 2001, **20**, 3308–3313.

70 B. D. Ward, A. Maisse-Francois, P. Mountford and L. H. Gade, *Chem. Commun.*

(Camb)., 2004, 704–705.

71 N. Vujkovic, J. L. Fillol, B. D. Ward, H. Wadepohl, P. Mountford and L. H. Gade, *Organometallics*, 2008, **27**, 2518–2528.

72 A. Bashall, P. E. Collier, L. H. Gade, M. McPartlin, P. Mountford and D. J. M. Trösch, *Chem. Commun.*, 1998, 2555–2556.

73 A. Bashall, P. E. Collier, L. H. Gade, M. McPartlin, P. Mountford, S. M. Pugh, S. Radojevic, M. Schubart, I. J. Scowen and D. J. M. Trösch, *Organometallics*, 2000, **19**, 4784–4794.

74 S. M. Pugh, D. J. M. Trösch, D. J. Wilson, A. Bashall, F. G. N. Cloke, L. H. Gade, P. B. Hitchcock, M. McPartlin, J. F. Nixon and P. Mountford, *Organometallics*, 2000, **19**, 3205–3210.

75 B. D. Ward, G. Orde, E. Clot, A. R. Cowley, L. H. Gade and P. Mountford, *Organometallics*, **24**, 2368–2385.

76 K. Weitershaus, B. D. Ward, R. Kubiak, C. Müller, H. Wadepohl, S. Doye and L. H. Gade, *Dalton Trans.*, 2009, 4586–4602.

77 P. Mountford, *J. Organomet. Chem.*, 1997, **528**, 15–18.

78 P. J. Tiong, A. Nova, A. D. Schwarz, J. D. Selby, E. Clot and P. Mountford, *Dalton Trans.*, 2012, **41**, 2277–2288.

79 A. P. Duncan and R. G. Bergman, *Chem. Rec.*, 2002, **2**, 431–445.

80 A. L. Odom, *Dalton Trans.*, 2005, 225–233.

81 S. Doye, *Synlett*, 2004, **2004**, 1653–1672.

82 K. C. Hultzsch, *Adv. Synth. Catal.*, 2005, **347**, 367–391.

83 A. Tillack, H. Jiao, I. G. Castro, C. G. Hartung and M. Beller, *Chem. - A Eur. J.*, 2004, **10**, 2409–2420.

84 B. F. Straub and R. G. Bergman, *Angew. Chem. Int. Ed.*, 2001, **40**, 4632–4635.

85 S. Tobisch, *Dalton Trans.*, 2006, **13**, 4277.

86 S. Tobisch, *Chem. - A Eur. J.*, 2007, **13**, 4884–4894.

87 C. Müller, R. Koch and S. Doye, *Chem. - A Eur. J.*, 2008, **14**, 10430–10436.

88 S. Tobisch, *Chem. - A Eur. J.*, 2008, **14**, 8590–8602.

89 J. S. Johnson and R. G. Bergman, *J. Am. Chem. Soc.*, 2001, **123**, 2923–2924.

90 P. J. Walsh, A. M. Baranger and R. G. Bergman, *J. Am. Chem. Soc.*, 1992, **114**, 1708–1719.

91 A. M. Baranger, P. J. Walsh and R. G. Bergman, *J. Am. Chem. Soc.*, 1993, **115**, 2753–2763.

92 F. Pohlki and S. Doye, *Angew. Chem.*, 2001, **113**, 2361–2364.

93 L. E. N. Allan, G. J. Clarkson, D. J. Fox, A. L. Gott and P. Scott, *J. Am. Chem. Soc.*, 2010, **132**, 15308–15320.

94 L. Ackermann, R. G. Bergman and R. N. Loy, *J. Am. Chem. Soc.*, 2003, **125**, 11956–11963.

95 J. Cho, T. K. Hollis, E. J. Valente and J. M. Trate, *J. Organomet. Chem.*, 2011, **696**, 373–377.

96 O. T. Summerscales and J. C. Gordon, *RSC Adv.*, 2013, **3**, 6682–6692.

97 G. R. Giesbrecht and J. C. Gordon, *Dalton Trans.*, 2004, 2387–2393.

98 D. Schädle, C. Schädle, K. W. Törnroos and R. Anwander, *Organometallics*, 2012, **31**, 5101–5107.

99 D. Schädle, C. Schädle, D. Schneider, C. Maichle-Mössmer and R. Anwander, *Organometallics*, 2015, **34**, 4994–5008.

100 K. D. Conroy, W. E. Piers and M. Parvez, *Organometallics*, 2009, **28**, 6228–6233.

101 A. A. Trifonov, M. N. Bochkarev, H. Schumann and J. Loebel, *Angew. Chem. Int. Ed.*, 1991, **30**, 1149–1151.

102 Z. Xie, S. Wang, Q. Yang and T. C. W. Mak, *Organometallics*, 1999, **18**, 1578–1579.

103 S. Wang, Q. Yang, T. C. W. Mak and Z. Xie, *Organometallics*, 1999, **18**, 5511–5517.

104 H. Chan, H. Li and Z. Xie, *Chem. Commun.*, 2002, 652–653.

105 J. C. Gordon, G. R. Giesbrecht, D. L. Clark, P. J. Hay, D. W. Keogh, R. Poli, B. L. Scott and J. G. Watkin, *Organometallics*, 2002, **21**, 4726–4734.

106 D. J. Beetstra, A. Meetsma, B. Hessen and J. H. Teuben, *Organometallics*, 2003, **22**, 4372–4374.

107 A. G. Avent, P. B. Hitchcock, A. V Khvostov, M. F. Lappert and A. V Protchenko, *Dalton Trans.*, 2004, 2272–2280.

108 D. Cui, M. Nishiura and Z. Hou, *Angew. Chem. Int. Ed.*, 2005, **44**, 959–962.

109 C.-L. Pan, W. Chen, S. Song, H. Zhang and X. Li, *Inorg. Chem.*, 2009, **48**, 6344–6346.

110 N. S. Emelyanova, M. N. Bochkarev, H. Schumann, J. Lebel and L. Esser, *Koord. Khim.*, 1994, **20**, 789–793.

111 D. Schädle, C. Maichle-Moessmer, C. Schädle and R. Anwander, *Chem. - A Eur. J.*, 2015, **21**, 662–670.

112 C. Schädle, D. Schädle, K. Eichele and R. Anwander, *Angew. Chem. Int. Ed.*, 2013, **52**, 13238–13242.

113 D. Schädle, M. Meermann-Zimmermann, C. Schädle, C. Maichle-Mössmer and R. Anwander, *Eur. J. Inorg. Chem.*, 2015, **2015**, 1334–1339.

114 J. Scott, F. Basuli, A. R. Fout, J. C. Huffman and D. J. Mindiola, *Angew. Chem. Int. Ed.*, 2008, **47**, 8502–8505.

115 D. Schädle, C. Maichle-Mössmer, K. Törnroos and R. Anwander, *Inorganics*, 2015, **3**, 500–510.

116 E. Lu, Y. Li and Y. Chen, *Chem. Commun.*, 2010, **46**, 4469–4471.

117 J. Chu, E. Lu, Z. Liu, Y. Chen, X. Leng and H. Song, *Angew. Chem. - Int. Ed.*, 2011, **50**, 7677–7680.

118 J. D. Selby, C. D. Manley, A. D. Schwarz, E. Clot and P. Mountford, *Organometallics*, 2008, **27**, 6479–6494.

119 T. B. Parsons, N. Hazari, A. R. Cowley, J. C. Green and P. Mountford, *Inorg. Chem.*, 2005, **44**, 8444.

120 B. D. Ward, G. Orde, E. Clot, A. R. Cowley, L. H. Gade and P. Mountford, *Organometallics*, 2004, **23**, 4444.

121 A. D. Schwarz, C. S. Onn and P. Mountford, *Angew. Chem. Int. Ed.*, 2012, **51**,

12298–12302.

122 P. J. Tiong, L. R. Groom, E. Clot and P. Mountford, *Chem. Eur. J.*, 2013, **19**, 4198–4216.

123 P. J. Walsh, M. J. Carney and R. G. Bergman, *J. Am. Chem. Soc.*, 1991, **113**, 6343–6345.

124 H. Herrmann, J. L. Fillol, H. Wadepohl and L. H. Gade, *Angew. Chem. Int. Ed.*, 2007, **46**, 8426–8430.

125 H. Herrmann, J. L. Fillol, T. Gehrmann, M. Enders, H. Wadepohl and L. H. Gade, *Chem. - A Eur. J.*, 2008, **14**, 8131–8146.

126 S. A. Scholl, H. Wadepohl and L. H. Gade, *Organometallics*, 2013, **32**, 937–940.

127 S. A. Scholl, G. T. Plundrich, H. Wadepohl and L. H. Gade, *Inorg. Chem.*, 2013, **52**, 10158–10166.

128 J. D. Selby, M. Feliz, A. D. Schwarz, E. Clot and P. Mountford, *Organometallics*, 2011, **30**, 2295–2307.

129 A. J. Clulow, J. D. Selby, M. G. Cushion, A. D. Schwarz and P. Mountford, *Inorg. Chem.*, 2008, **47**, 12049–12062.

130 A. D. Schwarz, A. Nova, E. Clot and P. Mountford, *Inorg. Chem.*, 2011, **50**, 12155–12171.

131 J. D. Selby, C. Schulten, A. D. Schwarz, A. Stasch, E. Clot, C. Jones and P. Mountford, *Chem. Commun.*, 2008, 5101–5103.

132 P. J. Tiong, A. Nova, E. Clot and P. Mountford, *Chem. Commun.*, 2011, **47**, 3147–3149.

133 A. D. Schofield, A. Nova, J. D. Selby, A. D. Schwarz, E. Clot and P. Mountford, *Chem. Eur. J.*, 2011, **17**, 265–285.

134 J. Unruangsri, H. Morgan, A. D. Schwarz, A. D. Schofield and P. Mountford, *Organometallics*, 2013, **32**, 3091–3107.

135 A. D. Schofield, A. Nova, J. D. Selby, C. D. Manley, A. D. Schwarz, E. Clot and P. Mountford, *J. Am. Chem. Soc.*, 2010, **132**, 10484–10497.

136 T. Gehrmann, S. A. Scholl, J. L. Fillol, H. Wadepohl and L. H. Gade, *Chem. Eur.*

J., 2012, **18**, 3925–3941.

137 S. Banerjee and A. L. Odom, *Organometallics*, 2006, **25**, 3099–3101.

138 A. A. Dissanayake and A. L. Odom, *Chem. Commun.*, 2012, **48**, 440–442.

139 M. Hidai and Y. Mizobe, *Chem. Rev.*, 1995, **95**, 1115–1133.

140 M. Dartiguenave, M. J. Menu, E. Deydier, D. Yves and H. Siebald, *Coord. Chem. Rev.*, 1998, **178**–**180**, 623–663.

141 A. W. Kaplan, J. L. Polse, R. A. Andersen and R. G. Bergman, *J. Am. Chem. Soc.*, 1998, **120**, 11649–11662.

142 J. L. Polse, A. W. Kaplan, R. A. Andersen and R. G. Bergman, *J. Am. Chem. Soc.*, 1998, **120**, 6316–6328.

143 T. Cuenca, V. Tabernero and E. Herdtweck, 2002, **663**.

144 G. M. Arvanltls, J. Jeffrey Schwartz and D. Van Engen, 1986, **5**, 2157–2159.

145 T. E. Hanna, E. Lobkovsky and P. J. Chirik, *Inorg. Chem.*, 2007, **46**, 2359–2361.

146 T. Gehrmann, J. L. Fillol, H. Wadepohl and L. H. Gade, *Organometallics*, 2012, **31**, 4504–4515.

147 T. Gehrmann, J. Lloret Fillol, S. A. Scholl, H. Wadepohl and L. H. Gade, *Angew. Chem. Int. Ed.*, 2011, **50**, 5757–5761.

148 L. N. Grant, B. Pinter, T. Kurogi, M. E. Carroll, G. Wu, B. C. Manor, P. J. Carroll and D. J. Mindiola, *Chem. Sci.*, 2017, **8**, 1209–1244.

149 R. Thompson, C. H. Chen, M. Pink, G. Wu and D. J. Mindiola, *J. Am. Chem. Soc.*, 2014, **136**, 8197.

150 B. Clough, DPhil Thesis, University of Oxford, 2016.

2.1 Overview

This Chapter describes the reactions of the hydrazido compound Ti($N_2^{iPr}N^{Me}$)($NNPh_2$)(py) (**1.70**) with the Si–H and B–H bonds of silanes and boranes and with H_2. The nature and mechanism of these reactions were investigated both computationally and experimentally.

The main experimental results are described, along with a full DFT mechanistic study. The onward reaction of one isolated silylamido reaction product with further equivalents of silanes is also studied. The experimental results have been performed by Dr. Laura Stevenson, former DPhil student in our group. Part of the reported work has been recently published.[1]

2.2 Introduction

Over the last 5-8 years Group 4 hydrazides of the type (L)M=NNR_2 have been studied in great detail. In particular, a variety of addition or insertion reactions of the Ti=Nα multiple bond with unsaturated substrates have been reported[2–17]. While there are some analogies with the corresponding better-established Group 4 imides, a distinctive aspect of the Group 4 hydrazido is the typical facile reductive cleavage of the Nα-Nβ bond that can also occur with substrates such as CO[2], isocyanides[6,14] and alkynes to form new N-element functional groups and/or organic products.[9,11,12] Several example of stoichiometric and catalytic reactions of titanium hydrazides have been reported in the Introduction.

Only one example of the reaction of Group 4 dialkylhydrazides with the Si-H bonds of silanes has been reported to date, namely the reversible 1,2-addition to the Ti=Nα multiple bond of Cp*Ti{$MeC(N^iPr)_2$}($NNMe_2$) (**1.39**) shown in Equation 2.1.[18] The corresponding diphenylhydrazide compound Cp*Ti{$MeC(N^iPr)_2$}($NNPh_2$) (**1.38**) showed no reactivity with silanes. The analogous cyclopentadienyl-amidinate supported compound Cp*Ti{$MeC(N^iPr)_2$}($NNCPh_2$) (**1.40**) undergoes the same Si-H bond activation reaction with both primary and secondary silanes to give Cp*Ti{$MeC(N^iPr)_2$}{N(R′RSiH)N($CHPh_2$)} (Equation 2.2).[19] Interestingly, none of these three compounds has been reacted with boranes, and neither of them reacted with H_2. This reactivity was explored in detail and will be discussed in the following chapters.

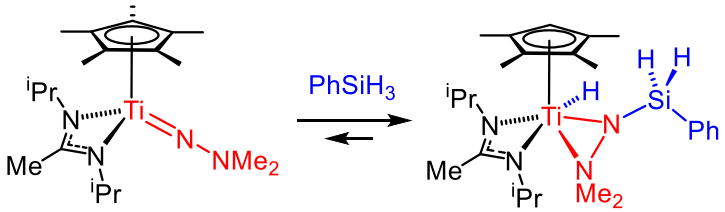

1.39

Equation 2.1

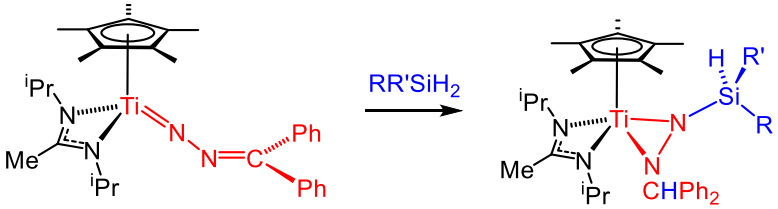

1.40

Equation 2.2

Of further relevance to the work described in this Chapter are the E–H bond activation, and in some cases N–N bond cleavage reactions, of early transition-metal-bound N_2 with the Si–H[20–22] and B–H[23–25] bonds of silanes and boranes, respectively. These proceed via bimetallic intermediates in all instances. The subsequent N–N bond breaking reactions (formally silyl- or borylimido ligands) are sometimes accompanied by ancillary ligand degradation (especially in the case of Group 5 borane reaction products) and are typically assisted (in Group 4) by addition of a reducing agent such as CO.

The unusual reactions of the diamide-amine-supported titanium hydrazides of the type $Ti(N_2N^{Me})(NNAr_2)(py)$ (Equation 2.3) with certain alkynes in which the rather sterically unencumbered ancilliary ligand allows access to new types of intermediate and mechanism in hydrohydrazination catalysis was recently reported in our group.[11,12] In this contribution, work within our group has begun to focus on reactions of this compound with selected silanes and boranes, leading to the reductive cleavage of the N_α–N_β bond and formation of silyl- and boryl-amido and imido species, along with N_α and N_β atom transfer. A full mechanistic study was performed in order to elucidate the reaction mechanism. In this chapter a full overview of the reactivity of $Ti(N_2^{iPr}N^{Me})(NNPh_2)(py)$ (**1.70**) will be described. In the following chapters the half-sandwich counterparts (**1.38**, **1.39** and **1.40**) will be explored in more detail. The systematic procedure to select the computational methodology will be explained in Chapter 7.

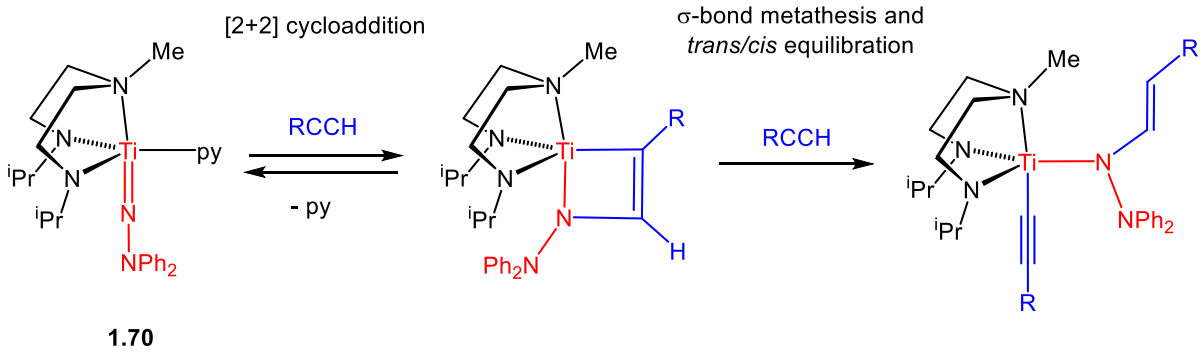

Equation 2.3

2.3 Reaction of Ti($N_2^{iPr}N^{Me}$)($NNPh_2$)(py) (1.70) with silanes

Ti($N_2^{iPr}N^{Me}$)($NNPh_2$)(py) (**1.70**) was reported to react with the following silanes: $BuSiH_3$, $PhSiH_3$ and Ph_2SiH_2 by Laura Stevenson. No reaction was observed with Mes_2SiH_2, Ph_3SiH or Et_3SiH, presumably because of the larger steric bulk. This paragraph will focus on reaction of **1.70** with $PhSiH_3$, for which a full computational study was performed. Experimentally, the reaction between **1.70** and $PhSiH_3$ proceeded at room temperature to give quantitative conversion to the diamide compound Ti($N_2^{iPr}N^{Me}$){N(H)SiH_2Ph}(NPh_2) (**1.71**), which exists as two isomers denoted ***trans*-1.71** and ***cis*-1.71** in a 40:60 ratio (*trans* and *cis* refer to the relative orientations of the -N(H)SiH_2Ph ligand and NMe donor, Equation 2.4).

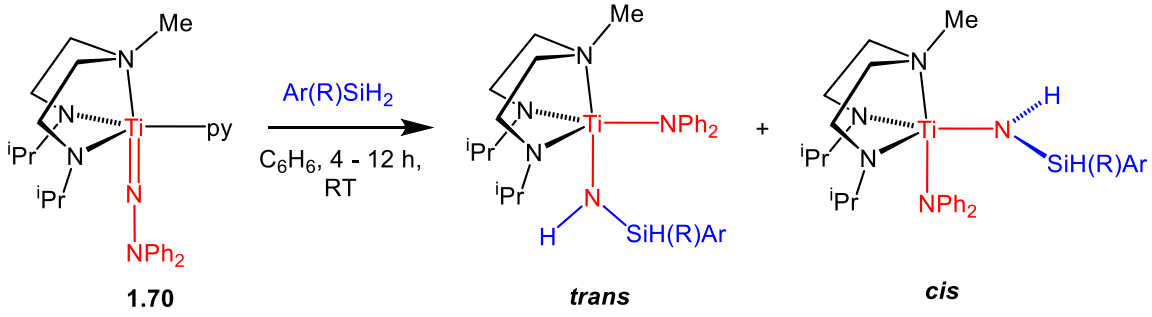

R = H, Ar = Ph (**1.71**), 3,5-$C_6H_3(CF_3)_2$ (**2.1**) or 4-C_6H_4OMe (**2.2**)

R = Ph, Ar = Ph (**1.72**)

Equation 2.4

To establish the kinetic/thermodynamic nature of the two products a series of experiments were performed. When followed by ^{1}H NMR spectroscopy in toluene-d_8 from -78 °C to 25 °C the reaction started to occur at *ca.* -10 °C, initially forming only ***trans*-1.71**, establishing this as the kinetic product. On warming to *ca.* 10 °C the *cis* isomer started to appear, and after several hours at room temperature the thermodynamic equilibrium was established. Similar isomerisations have been reported elsewhere with this type of

supporting ligand.[14] No exchange on the NMR timescale was observed at room temperature.

Reaction of $Ti(N_2^{iPr}N^{Me})(NNPh_2)(py)$ (**1.70**) also proceeds smoothly with the substituted primary aryl silanes 3,5-$C_6H_3(CF_3)_2SiH_3$ and 4-$C_6H_4OMeSiH_3$ to yield the analogous products $Ti(N_2^{iPr}N^{Me})\{N(H)SiH_2(3,5\text{-}C_6H_3(CF_3)_2)\}(NPh_2)$ (**2.1**) and $Ti(N_2^{iPr}N^{Me})\{N(H)SiH_2(4\text{-}C_6H_4OMe)\}(NPh_2)$ (**2.2**) (Equation 2.4).

Reaction with Ph_2SiH_2 gave the analogous reaction product, namely $Ti(N_2^{iPr}N^{Me})\{N(H)SiHPh_2\}(NPh_2)$ (**1.72**), which likewise exists as a mixture of *cis* and *trans* isomers (50:50 ratio).

The crystal structure of $Ti(N_2^{iPr}N^{Me})\{N(H)SiHPh_2\}(NPh_2)$ (**1.71**) is reported in Figure 2.1. Compound ***trans*-1.72** is a five-coordinate distorted trigonal bipyramidal complex with a N(1)-Ti(1)-N(3) angle of 168.24°. The diamide-amine ligand is bound facially occupying one axial and two equatorial sites. The reaction of **1.70** with Ph_2SiH_2 resulted in complete cleavage of the N_α–N_β bond and in the formation of the new NPh_2 and $N(H)SiHPh_2$ ligands. Each of the two ligands now has an N atom in a formal -3 oxidation state compared to -2 in **1.70** positioned *cis* and *trans*, respectively, to the NMe moiety of $N_2^{iPr}N^{Me}$. The Ti(1)-N(1) distance of 1.9307(9) Å is within the region expected for a titanium amide bond. The sum of the angles subtended at N(1) is *ca.* 360° indicating significant donation of the lone pair located on N(1) into titanium π-acceptor orbitals. The Ti(1)-N(2) bond distance is slightly longer (2.0115(9) Å), as expected for a secondary amide.

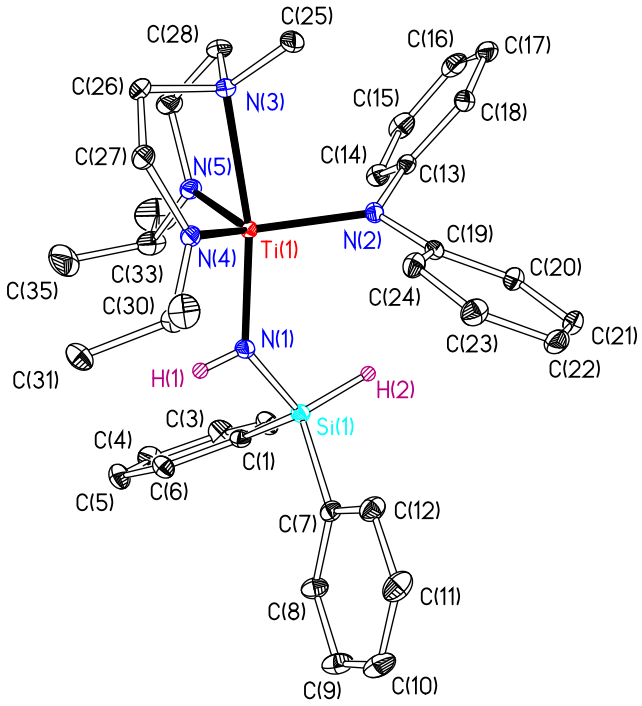

Figure 2.1. Displacement ellipsoid plot[26] (20% probability) of Ti($N_2^{iPr}N^{Me}$){N(H)SiHPh$_2$}(NPh$_2$) (***trans*-1.72**). Carbon-bound H atoms are omitted for clarity.

2.4 DFT mechanism of the reaction of Ti($N_2^{iPr}N^{Me}$)(NNPh$_2$)(py) (1.70) with PhSiH$_3$

The formation of the compounds Ti($N_2^{iPr}N^{Me}$){N(H)SiH(R)Ar}(NPh$_2$) (R = H, Ar = Ph (**1.71**), 3,5-$C_6H_3(CF_3)_2$ (**2.1**) or 4-C_6H_4OMe (**2.2**); R = Ph, Ar = Ph (**1.72**)) represents the first reductive cleavage of a hydrazide or related N–N bond by a silane at a single metal centre, with net insertion of the N_α atom of Ti($N_2^{iPr}N^{Me}$)(NNPh$_2$)(py) (**1.72**) into a silane Si–H bond. Further experiments and DFT calculations were carried out to elucidate the mechanism.

The full mechanism for the reaction of **1.70** with PhSiH$_3$ was calculated by DFT (Figure 2.2). An initial screening of a variety of DFT functionals and basis sets was performed, as described in Chapter 7. Earlier results were published using a def2-svp basis set for the optimization including dispersion corrections, followed by single point calculations with a def2-tzvp basis set for the SCRF solvent calculations.[1] The calculations have been performed again by using a def2-qzvpp basis set for the SCRF calculations.[27] All the calculations with H_2 and boranes were performed by using this new basis set. In this

paragraph only, results with both methodologies will be compared. As will be explained after, both basis sets gave comparable results.

DFT calculations found two related pathways for the formation of **1.71**, starting from the different isomers of **1.70** (with the $NNPh_2$ group *cis* or *trans* to NMe). All the Gibbs free energies are referenced to the isomer ***trans*-1.71** (0.0 kcal mol^{-1}). The lowest energy pathway leads to the experimentally observed kinetic product ***trans*-1.71** which may then isomerise readily to the thermodynamic equilibrium mixture of *cis* and *trans* isomers. As is well established for the reactions of many diamide-amine supported imido and hydrazido analogues of **1.70**, the reaction proceeds *via* loss of pyridine to form the four-coordinate **Int1** with has a relative Gibbs free energy of 19.7 kcal mol^{-1}. Note that, the barrier to dissociate pyridine cannot be easily evaluated, therefore the difference between the Gibbs free energy of **Int1** and ***cis*-1.70** + $PhSiH_3$ (namely 17.5 kcal mol^{-1}) can be used as the lowest point to estimate this barrier. Generally speaking, when performing a dissociation reaction the computed scan of the distance involved in the dative bond (elongation of the $Ti\text{-}N_{pyridine}$ bond in this case) is useful to evaluate the highest energy point on the potential energy surface. The 1,2-addition of Si–H to the $Ti{=}N_\alpha$ bond of **Int1** proceeds in a facile manner *via* **Int2** (relative G = 13.3 kcal mol^{-1}). The adduct **Int2** features the necessary interactions between Ti and H (1.873 Å) as well as donation of the lone pair situated on N_α into a σ* Si–H orbital resulting in a hypervalent Si atom, as suggested by a trigonal bipyramidal geometry at the Si atom. $PhSiH_3$ is however only weakly bound to the metal centre as confirmed by the Si–N distance (2.579 Å), a minimal lengthening of the $Ti{=}N_\alpha$ bond was observed (1.756 *vs.* 1.729 Å). As expected, the barrier to cleave the Si-H bond and simultaneously coordinate N_β to Ti to yield the silylhydrazido-hydride species **Int3** is quite low. **Int3** is the analogous species found in the reactions of $Cp^*Ti\{MeC(N^iPr)_2\}(NNMe_2)$ (**1.39**) with silanes. DFT studies on this system found that β-NMe_2 played a key role in these reactions providing stabilisation from both a kinetic and thermodynamic point of view.[18] The presence of the N_β group is indeed a key element to differentiate the reactivity of the imido and the hydrazido Group 4 compounds. The barrier from this species, namely irreversible hydride transfer to N_α and a highly exergonic reductive N_α–N_β bond cleavage, to give the final product at -58.7 kcal mol^{-1} is readily accessible ($\Delta G^\ddagger$ = 17.3 kcal mol^{-1}). The alternative pathway starting from the *trans* isomer of **1.70**, is almost identical, but the final transition state (analogous to **TS2**) has $\Delta G^\ddagger$ = 22.6 kcal mol^{-1} and is therefore not competitive. As previously

reported an isomerization between the *cis* and the *trans* isomer is expected to occur easily to form the most abundant isomer, namely *trans*-**1.71**.

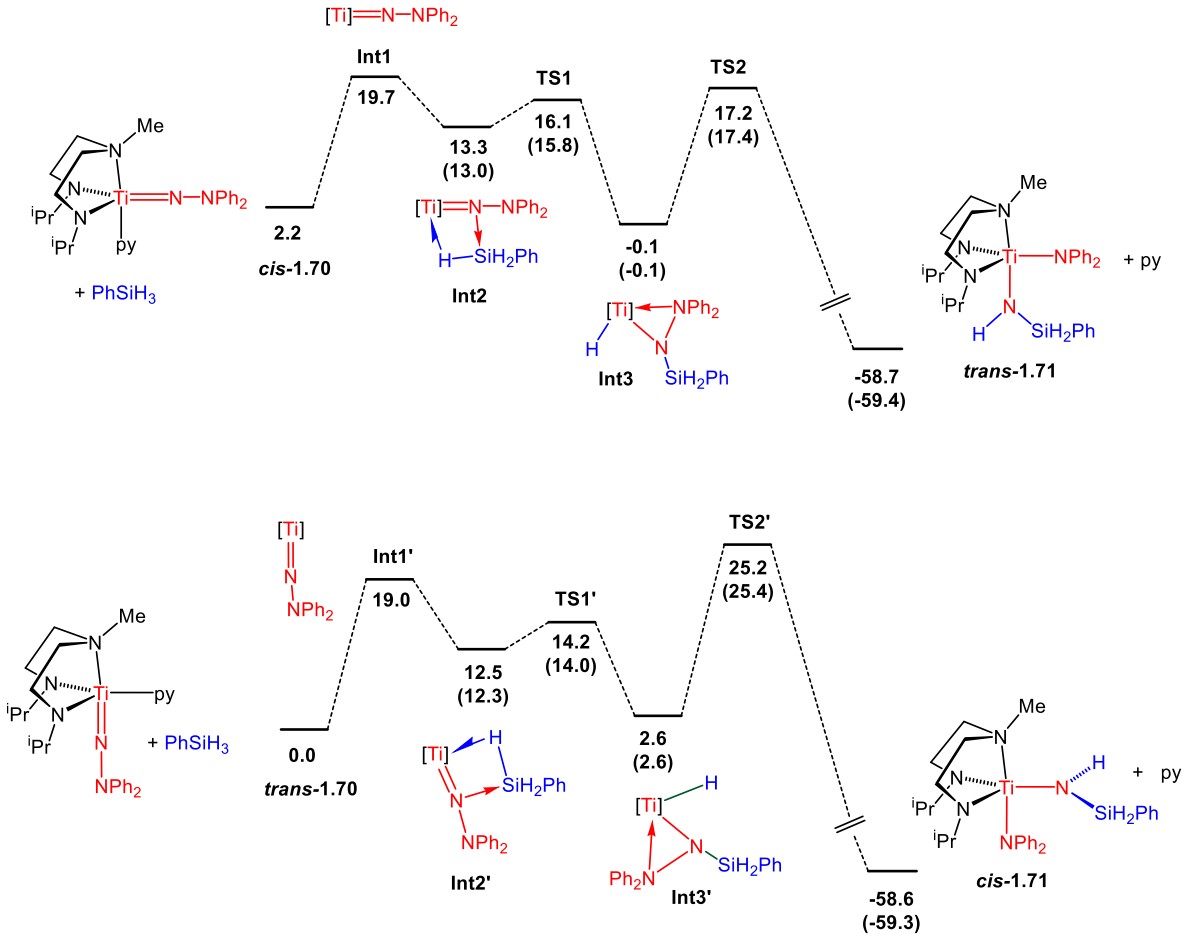

Figure 2.2. DFT mechanism (B3PW91, SCRF with a def2-tzvp basis set) for the reaction of 1.70 with $PhSiH_3$ forming **1.71** and pyridine. Gibbs free energies (kcal mol^{-1}, T = 298 K) for minima, maxima and transition states (labelled **TSx**) are shown in bold relative to **1.70** and $PhSiH_3$. [Ti] represents $Ti(N_2{}^{iPr}N^{Me})$. The corresponding values for the reactions with $PhSiD_3$ leading to **1.71-*d*$_3$** are given in parentheses.

By this full DFT study it can be concluded that the highest points located on the lowest energy reaction pathway involve either the pyridine loss to form **Int1** ($\Delta G^{\ddagger}$ = 17.5 kcal mol^{-1}) or the hydride transfer and N–N bond cleavage to yield the final product ***cis*-1.71** ($\Delta G^{\ddagger}$ = 17.3 kcal mol^{-1}). However, the difficulty to locate the transition state associated with the pyridine dissociation makes it difficult to draw a conclusion. The computed mechanism is consistent with the experimental observations reported below.

Experimentally, comparison of the reaction of **1.70** with $PhSiH_3$ or $PhSiD_3$, either by initial rates (at -10 °C) or by a competition experiment between **1.70** and an excess of $PhSiH_3$ and $PhSiD_3$ (at RT) established a kinetic isotope effect in the range 1.34 – 1.41 for both types of experiment, comparable to values found for Si–H addition to Ti=S and Ti=O bonds.[28,29] It was also found that the presence of an excess of pyridine decreased the rate of reaction (although competing unknown side-reactions prevented a detailed analysis). Likewise, reaction of the DMAP analogue of **1.70**, $Ti(N_2^{iPr}N^{Me})(NNPh_2)(DMAP)$ (4, DMAP = 4-dimethylaminopyridine), with $PhSiH_3$ proceeded considerably more slowly to form **1.71**. Consequently, both pyridine (or DMAP) loss and E–H (E = Si or B) bond cleavage are kinetically important to the rate-determining steps for the cleavage reaction. DFT calculations showed that the dissociation of DMAP to form **Int1** and **Int1'** is less favoured than for pyridine, and the ΔG are 19.6 and 18.4 kcal mol^{-1} for the ***cis*-1.70** and the ***trans*-1.70** DMAP analogues, respectively (the reference of zero Gibbs free Energy is the trans isomer, while the cis is 2.1 kcal mol^{-1} less stable).

The full mechanism was also calculated for the reaction of **1.70** with $PhSiD_3$ and the corresponding energies are given in parentheses in Figure 2.2 . The final product is 0.7 kcal mol^{-1} lower in energy and **TS2** is 0.2 kcal mol^{-1} higher in energy. In agreement with the aforementioned experimental results, the kinetic isotope effect of 1.16 was calculated, reflecting the contribution of the isotope sensitive hydride transfer to the overall rate. By arbitrarily decreasing the relative G of **Int1** to 18.0 kcal mol^{-1} (from 19.7 kcal mol^{-1}) and allowing the hydride transfer to dominate the rate, the calculated isotope effect is 1.33. Furthermore, by removing the pyridine dissociation barrier completely the maximum possible KIE for the hydride transfer step was calculated to be 1.37. This demonstrates the sensitivity of the calculated KIE to small changes in the calculations and the upper limit that might be expected. The same set of calculations was performed with the def2-qzvpp basis set for the SCRF calculations as reported in Figure 2.3 for comparison.

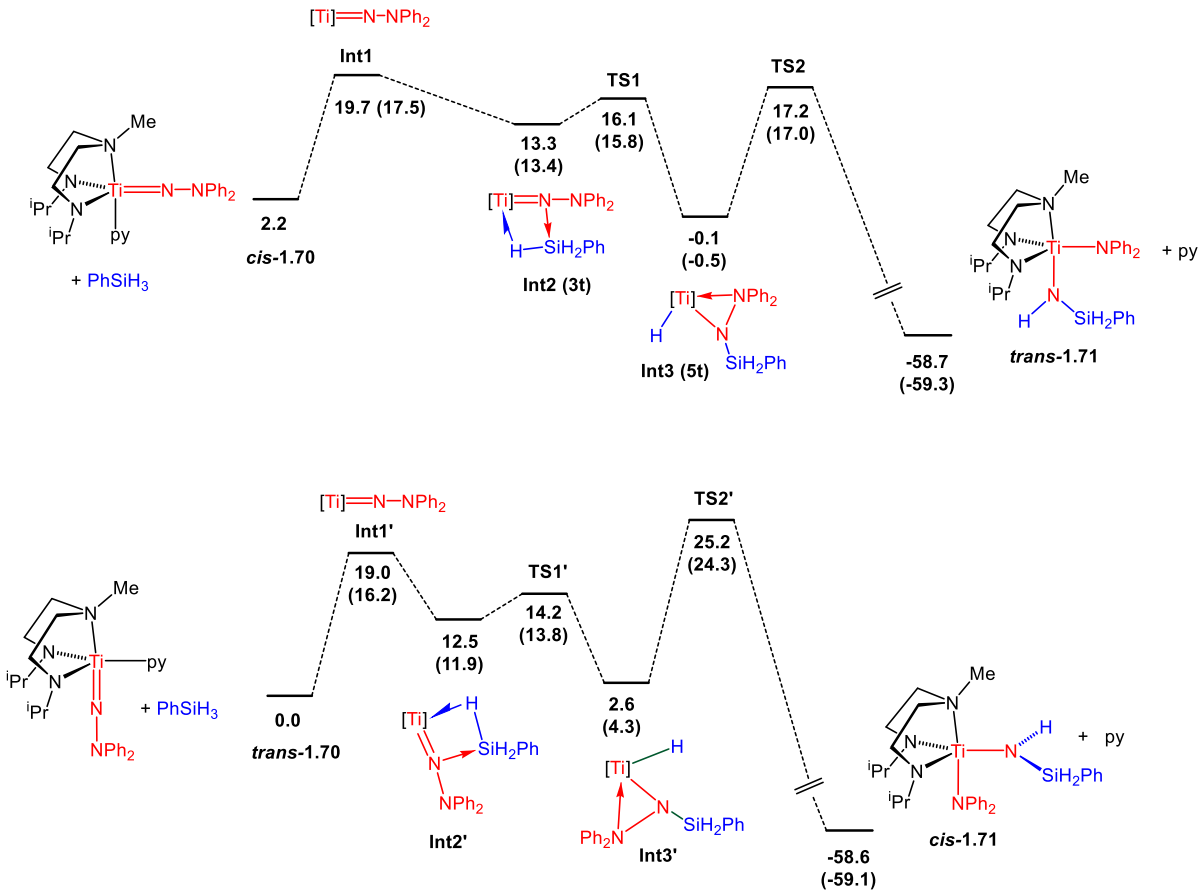

Figure 2.3. DFT mechanism (SCRF with a def2-tzvp or def2-qzvpp basis set, in parentheses) for the reaction of **1.70** with $PhSiH_3$ forming **1.71** and pyridine. Gibbs free energies (kcal mol^{-1}, T = 298 K) for minima, maxima and transition states (labelled **TSx**) are shown in bold relative to **1.70** and $PhSiH_3$. [Ti] represents $Ti(N_2{}^{iPr}N^{Me})$.

In both pathways the numbers differ slightly and the same conclusions can be drawn from both set of results.

2.5 DFT Mechanism of the reaction of $Ti(N_2{}^{iPr}N^{Me})(NNPh_2)(py)$ (1.70) with boranes

The unprecedented reactions of **1.70** with silanes prompted us to explore the corresponding reaction with a variety of boranes. Promising results led us to investigate the reactivity of half-sandwich compounds with the same set of boranes. A detailed discussion about the reactivity of **1.38**, **1.39** and **1.40** will be presented in the next Chapter. This Section will focus on the experimental and computational results of $Ti(N_2{}^{iPr}N^{Me})(NNPh_2)(py)$ (**1.70**) with boranes.

In particular, reactions with pinacolborane, cathecolborane, dimesitylborane ($HBMes_2$) and 9-borabicyclo(3.3.1)nonane (9-BBN) were experimentally investigated by Dr. Laura

Stevenson. A full computational study was performed on the reaction of **1.70** with 9-BBN and $HBMes_2$. Reaction of **1.70** with 1 equiv. of 9-BBN dimer gave clean conversion to the borylamide $Ti(N_2^{iPr}N)\{N(H)BC_8H_{14}\}(NPh_2)$ (**1.73**) together with $py{\cdot}HBC_8H_{14}$. In solution, **1.73** exists predominantly as the cis isomer (3:1 ratio of *cis*:*trans*) which was characterized by X-ray crystallography. Overall, the N_α atom of **1.70** has inserted into the B–H bond of the borane with concomitant reductive cleavage of the N_α–N_β bond. This is also the first reaction of this type for a single metal centre. The analogous reaction product $Ti(N_2^{iPr}N^{Me})\{N(H)BMes_2\}(NPh_2)$ (**2.3**) along with $py{\cdot}HBMes_2$ was obtained following reaction with two equivalents of Mes_2BH which also exists as a mixture of *cis* and *trans* isomers (85:15). Both reactions are shown in Scheme 2.1.

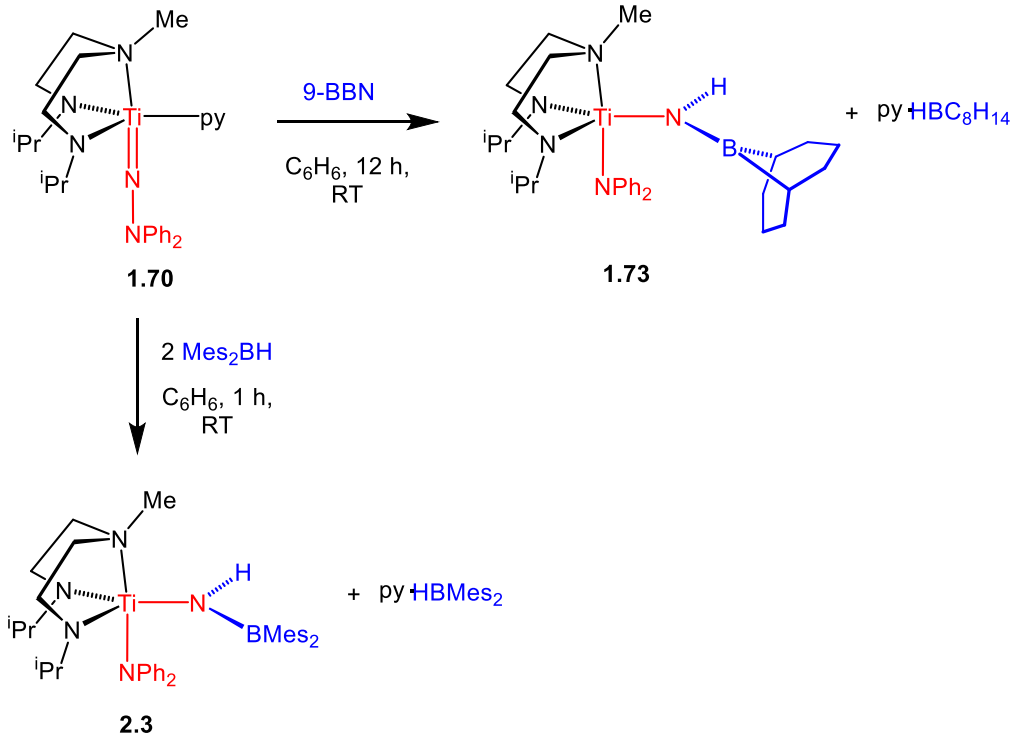

Scheme 2.1 Reaction of $Ti(N_2^{iPr}N^{Me})(NNPh_2)(py)$ (**1.70**) with 9-BBN and $HBMes_2$.

Compounds **1.73** and **2.3** both contain a five-coordinate titanium centre with approximately trigonal bipyramidal geometry and the diamide-amine ligands bound in a κ^3-*fac* manner. The borylamide moiety occupies the equatorial position *cis* to the NMe donor and the NPh_2 ligand occupies the remaining coordination site, in both cases. The Ti(1)-N(1) bond distances of 1.9693(15) and 1.9954(18) Å for **1.72** and **2.3** are typical of amide(1-) interactions with a longer bond found in **2.3** due to the large steric bulk of the Mes substituents. Both N(1) atoms have approximately planar geometry with angle subtended about N(1) calculated to be 359.82(26) and 358.14(30) ° respectively.

However, the borylamide moiety is significantly twisted out of the equatorial plane, with a N(4)/(5)-Ti(1)-B(1)-H(1) torsion angle of 30.1 and 67.6 ° for **1.73** and **2.3** respectively, indicating that the lone pair on N(1) is not well positioned for a π-bonding interaction with titanium. The large steric bulk of the two Mes substituents compared to the bicyclic -C_8H_{14} moiety cause the borylamide moiety to twist further out of the equatorial plane. The N(1)-B(1) bond distances of 1.405(3) and 1.409(3) Å for **1.73** and **2.3** are typical of species of the type $R_2N–BR'_2$ which have significant N=B double bond character *via* $N_{2p}\rightarrow B_{2p}$ π donation.[30]

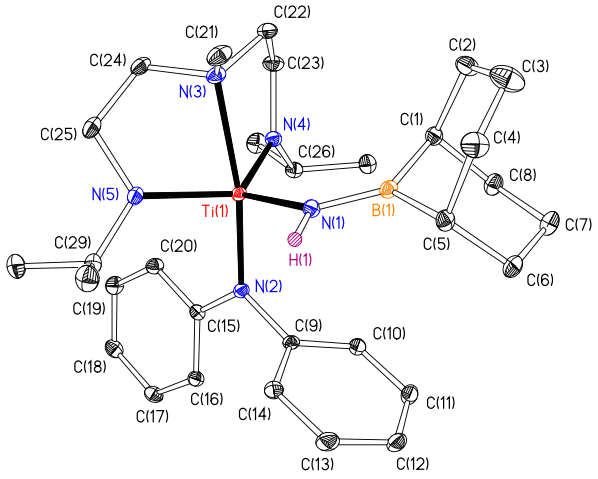

Figure 2.4. Displacement ellipsoid plots[26] (20% probability) of $Ti(N_2^{iPr}N^{Me})\{N(H)BC_8H_{14}\}(NPh_2)$ (**1.73**). Carbon-bound H atoms are omitted for clarity.

DFT calculations indicate an analogous mechanism to that for $PhSiH_3$. All the reported results were performed with the new methodology (optimizations with B3PW91/D3(bj) and a def2-svp basis set, followed by SCRF single point calculations with B3PW91/D3(bj) and a def2-qzvpp basis set). The full pathway from the *cis* isomer of **1.70** with 9-BBN monomer is shown in Figure 2.5. The Gibbs free energy values reported are referenced to ***trans*-1.70** + 9-BBN monomer (0.0 kcal mol^{-1}). Dissociation of pyridine is followed by the formation of an adduct (**Int2_B**), prior to 1,2-B–H addition. The increased acceptor ability of boron compared to silicon results in a stronger adduct. This is clear from the optimized geometry that shows a short B–N distance of 1.586 Å which is not far in value from the calculated B–N distance in the final product (1.414 Å) and a significant lengthening of the $Ti=N_\alpha$ bond from 1.729 to 1.843 Å. As reported before, the

$Ti{=}N_a$ lengthening was less evident with $PhSiH_3$, as a confirmation of the better accepting capability of the boron atom.

Thus, as expected **Int2_B** is lower in energy than the silicon adduct **Int2**. Similarly, the intermediate resulting from B–H addition (**Int3_B**) is lower in energy than the corresponding silicon intermediate (**Int3**) although the barrier is slightly higher (6.4 *vs.* 2.8 kcal mol^{-1}). This is consistent with a stronger B–H (than Si–H) bond requiring more energy to break.[31] The lower energy of **Int3_B** is likely due to the formation of a strong B–N bond. The final hydride transfer step to yield **1.73** has an associated barrier of 19.6 kcal mol^{-1} making this the rate-limiting step in the reaction sequence. It is worth pointing out that neither dissociation of 9-BBN dimer and reaction of the second equivalent of 9-BBN monomer with pyridine have not been included in the calculations. The bond lengths and angles in the DFT structure of **1.73** are in good agreement with the real values.

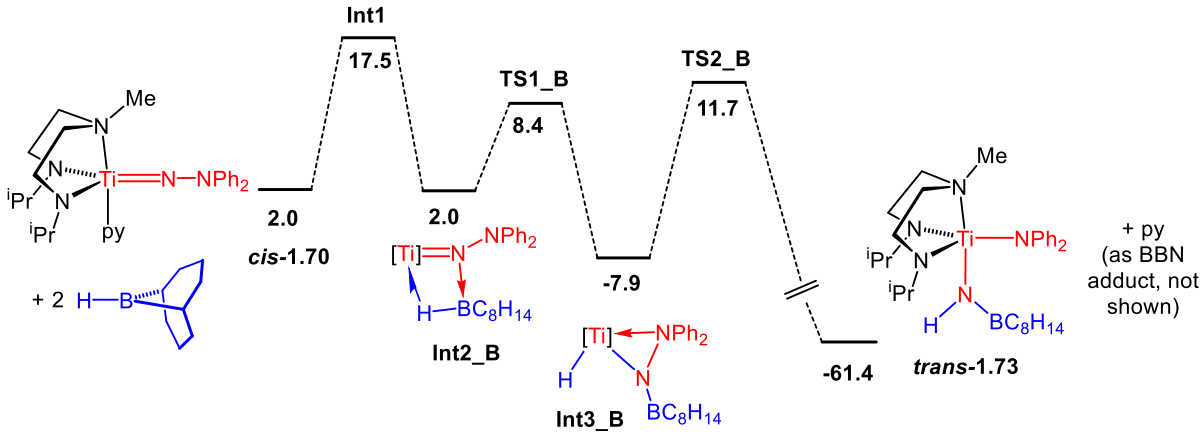

Figure 2.5. DFT mechanism for the reaction of **1.70** with 9-BBN monomer forming **1.73** and pyridine. Gibbs free energies (kcal mol^{-1}, T = 298 K) for minima, maxima and transition states (labelled **TSx_B**) are shown in bold relative to **1.70** and 9-BBN monomer. [Ti] represents $Ti(N_2{}^{iPr}N^{Me})$. ΔG for adduct formation has been excluded.

As reported above, the DFT mechanism described was calculated for the reaction of the cis isomer of **1.70** with 9-BBN monomer. However, 9-BBN exists exclusively as a dimer in non-donor solvents according to kinetic studies on the hydroboration of alkenes with 9-BBN.[32] Dissociation of 9-BBN dimer has been reported to have a rate constant of 1.5 x 10^{-4} s^{-1} and with an estimated barrier of 22.6 kcal mol^{-1}, in benzene at room temperature. Attempts to locate the transition state for 9-BBN dimer dissociation using DFT were

unsuccessful. However, as mentioned, the Gibbs free energy of reaction was calculated 20.0 kcal mol^{-1}. This value could be useful to get an estimate of the lowest possible barrier of dissociation. This also suggests that the 9-BBN dimer dissociation is possibly the highest energy TS as the barrier is comparable if not higher than the final hydride transfer step.

Experiments were performed to support the mechanism and elucidate the kinetics. The reaction of Ti($N_2^{iPr}N^{Me}$)($NNPh_2$)(py) (**1.70**) and 9-BBN dimer (1:1 ratio) in C_6D_6 at room temperature was monitored by ^1H NMR spectroscopy and the evolution of Ti($N_2^{iPr}N^{Me}$){N(H)BC_8H_{14}}(NPh_2) (**1.73**) measured by integration over a period of time. In particular, the initial rates method was used to effectively calculate the rate, d[**1.73**]/d*t* at time = 0, and to estimate the order of reaction. In general, to establish the order of a reaction two methods could be potentially used, the pseudo-first order conditions and the initial rates. Previous work in our group has successfully used the initial rate method to analyse the kinetics of the catalytic diamination of hydrazines with internal alkynes with amide supported titanium compounds.[33] The rate of reaction was found to be ten times slower than the reaction with $PhSiH_3$ (1.28(3) x 10^{-5} mol dm^{-3} s^{-1}). Kinetically, the reaction was found to be zero-order in **1.70**. An initial rate of 1.09(1) x 10^{-5} mol dm^{-3} s^{-1} obtained when two equivalents of **1.70** were used. As previously reported for $PhSiH_3$, when the reaction was monitored with the DMAP analogue of **1.70** only a marginal decrease in the initial rate was observed suggesting a rate-determining step after (or before) formation of the base-free intermediate. The reaction can be modelled by using the same methodology already established for hydroboration of alkenes, reported in literature[32] as outlined in Scheme 2.3.

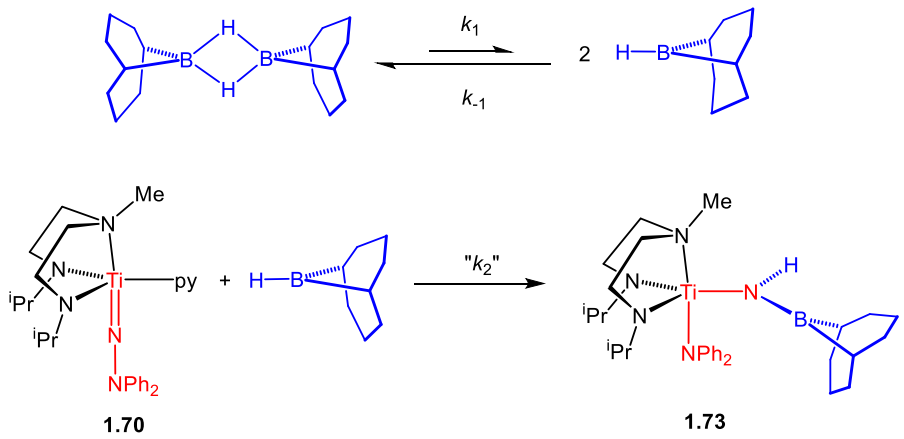

Scheme 2.3

$$\text{Rate} = \frac{k_1 k_2[\mathbf{1.70}][\text{9-BBN dimer}]}{k_{-1}[\text{9-BBN}] + k_2[\mathbf{1.70}]} \qquad (2.5)$$

$$\text{Rate} = k_1[\text{9-BBN dimer}] \qquad (\text{if } k_{-1}[\text{9-BBN}] << k_2[\mathbf{1.70}]) \qquad (2.6)$$

$$\left[\frac{k_1}{k_{-1}}\right]^{1/2} k_2[\mathbf{1.70}][\text{9-BBN dimer}]^{1/2} \quad (\text{if } k_{-1}[\text{9-BBN}] >> k_2[\mathbf{1.70}]) \qquad (2.7)$$

As in the hydroboration chemistry, reactions with reactive alkenes demonstrate a first-order dependence on 9-BBN dimer due to rate-limiting dimer dissociation. In comparison, hydroboration with unreactive alkenes demonstrate a half-order dependence on 9-BBN due to a rate limiting B–H addition. For this chemistry the steady-state approximation to 9-BBN monomer leads to the rate equation shown in Equation 2.5. This approximation is valid because the rate of formation and the rate of consumption of 9-BBN monomer are similar. The approximation k_{-1}[9-BBN] << k_2[**1.70**] can be applied when the k_2 step is fast. This leads to the equation shown in Equation 2.6 and the rate will show a first-order dependence on 9-BBN dimer. Alternatively, if the k_2 step is slower than 9-BBN dimer formation, the rate equation can be written as shown in Equation 2.7. It is important to point out that the rate constant k_2 is used to denote all the reaction steps in the reaction of **1.70** with 9-BBN monomer. This is of course a simplification but for the purpose of the experiments it works perfectly. The dependence of the rate on 9-BBN dimer concentration, at constant Ti concentration, was therefore used to determine

whether 9-BBN dimer dissociation or hydride transfer, is rate-limiting. Initial rates in this set of experiments scaled linearly with 9-BBN dimer, consistent with Equation 2.6. Moreover, the rate constant for 9-BBN dimer dissociation (k_1) can be estimated to be between 2.3 and 5.9 x 10^{-4} s^{-1}, which corresponds to a free energy of activation of 21.8(1) - 22.4(1) kcal mol^{-1}. These values are in excellent agreement with the values reported in the literature (k_1 = 1.5 x 10^{-4} s^{-1} and $\Delta G^{\ddagger}$ = 22.6 kcal mol^{-1}) and crucially are higher in energy than the calculated barrier for hydride transfer. In conclusion, these experimental evidences, in combination with the proposed DFT calculations point out a mechanism in which the 9-BBN dimer dissociation is the RDS.

As mentioned above, the reaction of **1.70** with Mes_2BH proceeds more quickly than with 9-BBN, reaching 100% conversion after one hour. Mes_2BH is a dimer in the solid state but exists as an equilibrium mixture of monomer and dimer in a benzene solution. This is consistent with a fast reaction of **1.70** with monomer boranes. Due to the speed of the reaction a kinetic analysis has not been carried out. DFT mechanism has been computed and is reported in Figure 2.6.

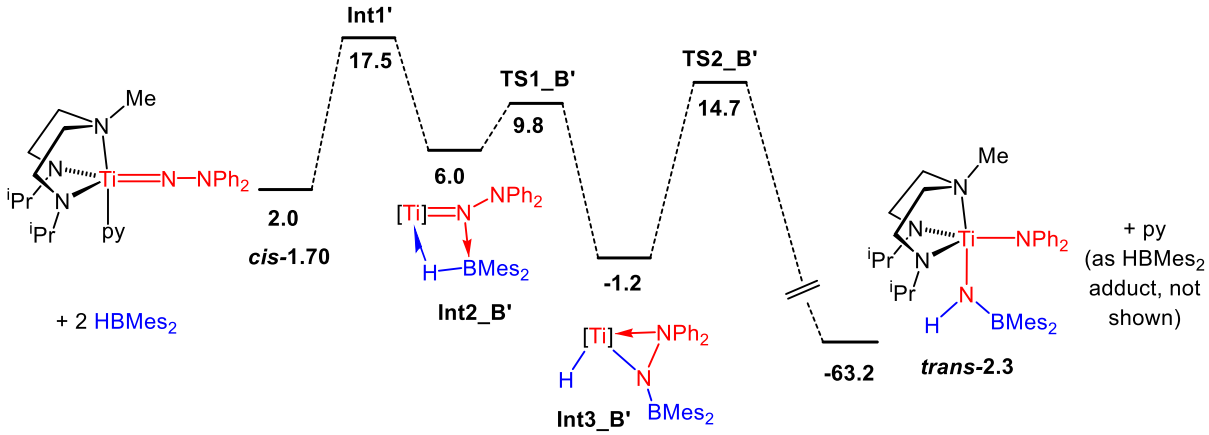

Figure 2.6 DFT mechanism for the reaction of ***cis*-1.70** with $HBMes_2$ monomer (def2-qzvpp basis set for SCRF calculations) forming ***trans*-2.3** and pyridine. Gibbs free energies (kcal mol^{-1}, T = 298 K) for minima, maxima and transition states (labelled **TSx_B'**) are shown in bold relative to **1.70** and $HBMes_2$ monomer. [Ti] represents $Ti(N_2^{iPr}N^{Me})$.

The Gibbs free energy of $HBMes_2$ dimer dissociation was calculated to be 8.9 kcal mol^{-1}. The reaction pathway is identical to the mechanisms evaluated before for both $PhSiH_3$ and 9-BBN. **Int3_B'** is higher in energy than the corresponding intermediate observed for

9-BBN, **Int_3B** (-1.2 *vs.* -7.9 kcal mol^{-1}) possibly because of steric bulk of the Mes groups. The highest barrier is associated with the final hydride transfer step to yield **2.3**, with a barrier of 15.9 kcal mol^{-1}. This value is lower than the one found for 9-BBN (19.6 kcal mol^{-1}) in line with the experimental results. These results suggest that the rate determining step should be associated either with the pyridine dissociation, with a relative Gibbs free energy of 17.5 kcal mol^{-1} or with the final hydride transfer. However due to decomposition and broad overlapping resonances this could not be proved experimentally. A single experiment was performed, starting from the DMAP analogue of **1.70** which shows that DMAP dissociation is slower than py dissociation.

2.6 Reaction of Ti($N_2^{iPr}N^{Me}$)($NNPh_2$)(py) (1.70) with H_2

The 1,2-addition of dihydrogen to metal-ligand multiple bonds has been reported for several Group 4 complexes.[29,34,35] Unfortunately no reaction was observed between Ti($N_2^{iPr}N^{Me}$)($NNPh_2$)(py) (**1.70**) and H_2 under 2-3 atm. The DFT mechanism was calculated in order to shed light on these observation and is shown in Figure 2.7.

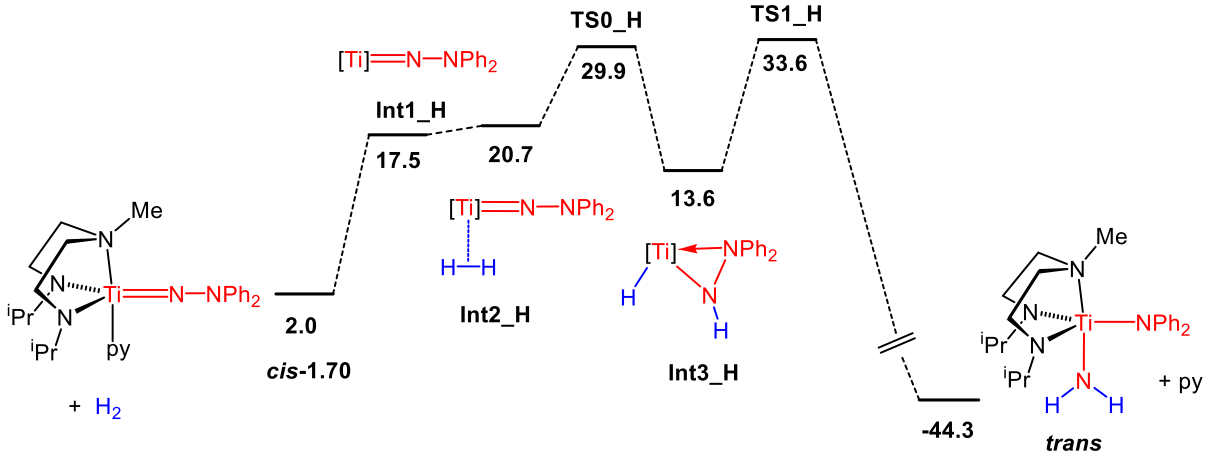

Figure 2.7. DFT mechanism for the reaction of **1.70** with H_2. Gibbs free energies (kcal mol^{-1}, T = 298 K) for minima, maxima and transition states (labelled **TSx_H**) are shown in bold relative to 1.70 and H_2. [Ti] represents Ti($N_2^{iPr}N^{Me}$).

The final products are low in energy indicating that the reaction is thermodynamically feasible. Following formation of the pyridine free species **Int1** the formation of the adduct **Int2_H** is slightly uphill. By examining the total energies of the two intermediates, **Int1_H** and **Int2_H** however, it is noted that **Int2_H** is more stable by 5.62 kcal mol^{-1}. The Gibbs energy position of **Int2_H** is certainly the result of H_2 binding energy not being strong enough to compensate from the loss of entropy, this is why it is uphill as compared to **Int1_H**.

The relative G of **Int2_H** is higher in energy than the analogous intermediates found with $PhSiH_3$ and 9-BBN. This is attributed to the lack of acceptor ability of H_2, resulting in reduced stabilisation. The 1,2-addition step is also endergonic as the formation of one N–H bond and one Ti–H bond is not enough to compensate for the energy required to break the very strong H–H bond. As the intermediates are high in energy the corresponding transition states are also high in energy leading to a kinetically inaccessible reaction pathway. These observations are in line with what has been reported for the

hydrazido compound Cp*Ti{MeC(N^{i}Pr)$_2$}(NNMe$_2$) (**1.39**), which also showed no reactivity with H_2.[15]

2.7 Reaction and attempted DFT Mechanism of Ti($N_2^{iPr}N^{Me}$){N(H)SiH_2Ph}(NPh_2) (1.71) with silanes

As reported in Section 2.1, **1.70** reacts with a variety of silanes. The reactivity of the reaction product of **1.70** with $PhSiH_3$. Ti($N_2^{iPr}N^{Me}$){N(H)SiH_2Ph}(NPh_2) **1.71**, with other silanes and $PhSiD_3$ was also tested. Reaction of Ti($N_2^{iPr}N^{Me}$){N(H)SiH_2Ph)}(NPh_2) (**1.71**) with one equivalent of $PhSiD_3$ led to slow incorporation of deuterium into the Si–H sites exclusively. The ^{1}H NMR spectrum indicated the presence of hydrogen in free phenylsilane (Equation 2.8). After 24 hours at room temperature there was *ca.* 30% incorporation of D into **1.71**. This might suggest reversible formation of **1.71**. However, during this time no deuterium was incorporated into the N–H site of **1.71** as established by ^{1}H and ^{2}H NMR spectroscopy.

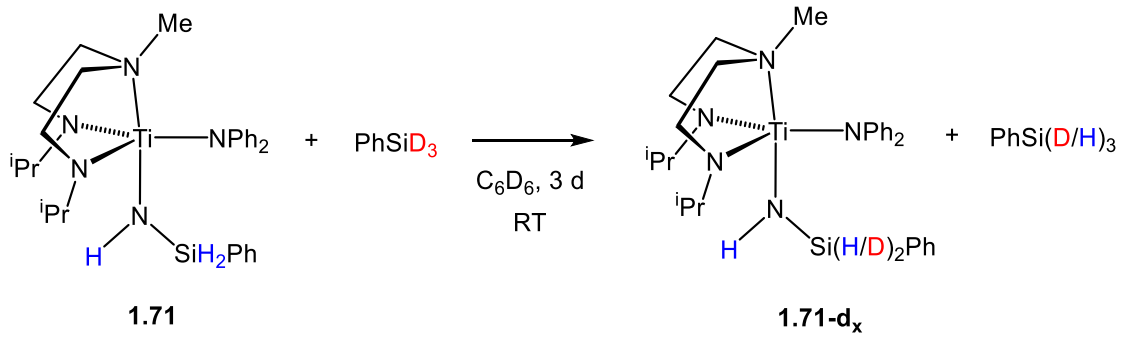

1.71 **1.71-d_x**

Equation 2.8

This prompted us to investigate a potential mechanism in more detail. When **1.71** was mixed with one equivalent of 3,5-$C_6H_3(CF_3)_2SiH_3$ an equilibrium mixture of **1.71** and **2.1** was observed. When more equivalents of 3,5-$C_6H_3(CF_3)_2SiH_3$ were added complete conversion was observed. Therefore, it was clear that the reaction of **1.71** with silanes could result in the exchange of the SiH_2Ph moiety. This could also explain the H/D exchange reaction shown in Equation 2.8. DFT calculations were performed in order to elucidate the reaction mechanism.

The proposed mechanism for this exchange reaction is shown in Scheme 2.4. An initial imido intermediate is formed (**1.71_Int1)** from **1.71** and $HNPh_2$ elimination. 1,2-addition of Si–H to the Ti=N bond to yield the bis(silyl)amide-hydride species **1.71_Int2** can occur. Rotation around the Ti–N bond places the original silyl substituent (labelled blue) close to the Ti–H bond to yield compound **1.71_Int3** and the final 1,2-elimination reforms an imido intermediate now with the new silylamide substituent (labelled green,

1.71_Int4). No intermediates were observed during the course of any of the exchange reactions.

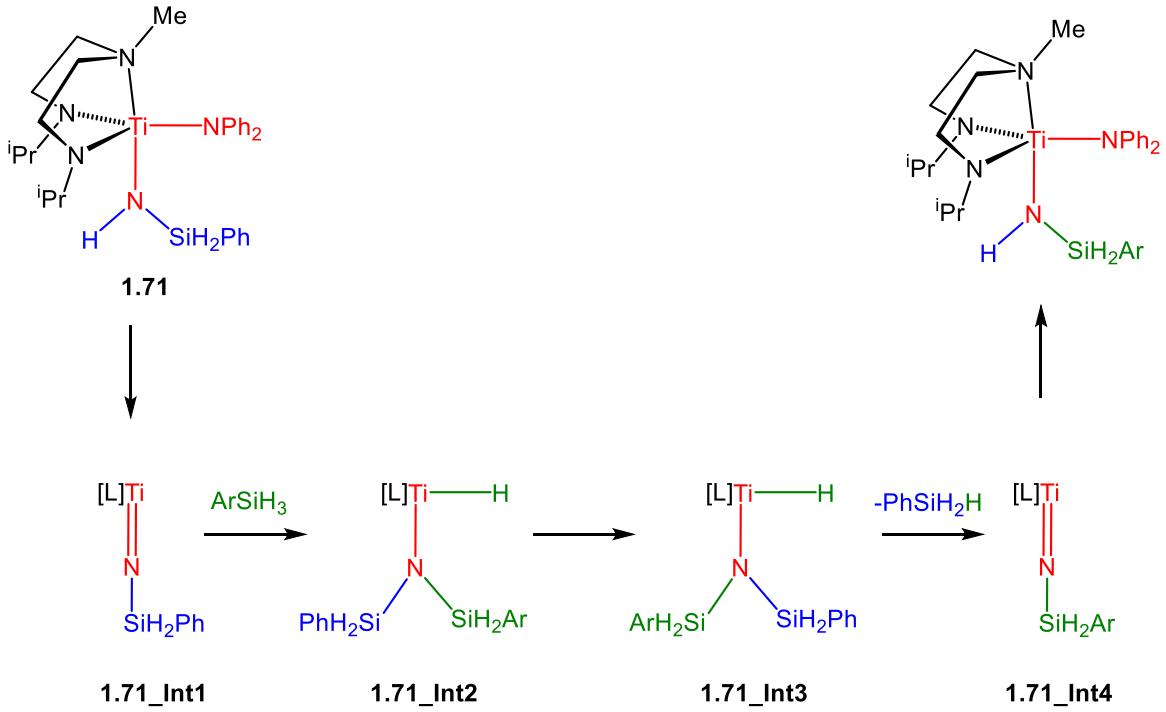

Scheme 2.4

Of particular interest was the formation of **1.71_Int1** that could happen after the transfer of the Ti-N(H)SiH_2Ph proton either to the $–NPh_2$ ligand to form **1.71_IntA**, or to one of the Ti-N_{amide} atoms of the supporting ligand to yield **1.71_IntB** (Scheme 2.5). Transfer to the Ti-N_{amine} apical nitrogen atom is unlikely to happen due to the lower basicity of this atom. Unfortunately, none of these species was observed experimentally. A variety of experiments were performed in order to verify this mechanism.

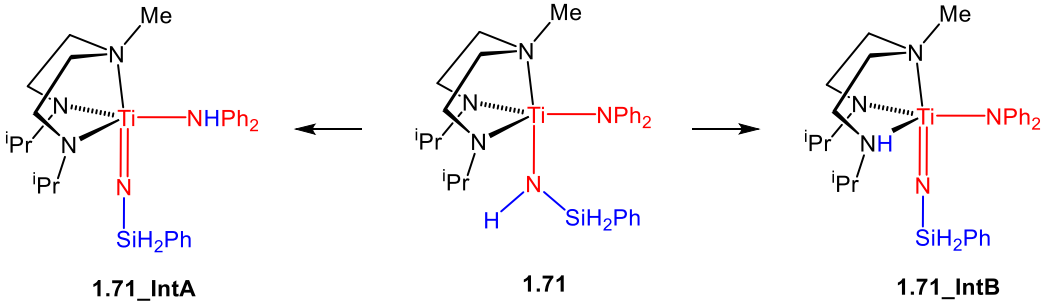

Scheme 2.5. Two possible mechanisms for the formation of an imido intermediate from **1.71**.

Compound **1.71** was mixed with an equivalent of Tol_2NH on the NMR tube scale as a probe for the formation of **1.71_IntA** from **1.71**. If **1.71_IntA** is readily accessible, then exchange between the weakly bound neutral ligand -$NHPh_2$ and the sterically and electronically similar Tol_2NH would occur. However, no reaction occurred at room temperature over 24 hours. On heating at 70 °C for two hours a new set of resonances where observed along with Ph_2NH, heating for further 22 hours did not increase the conversion and the two species were present in a 1:1 ratio. The new species exists as a mixture of two isomers and has been tentatively assigned as $Ti(N_2^{iPr}N^{Me})\{N(H)SiH_2Ph\}(NTol_2)$ containing the $NTol_2$ ligand. The observation of $Ti(N_2^{iPr}N^{Me})\{N(H)SiH_2Ph\}(NTol_2)$ cannot prove that **1.71_IntA** is accessible under the experimental reaction conditions.

To further understand which of the two proposed mechanisms to yield the imido intermediate **1.71_Int1** was the preferred one, a reaction of **1.71** with 3,5-$C_6H_3(CF_3)_2SiH_3$ was carried out in the presence of an equivalent of Tol_2NH. No incorporation of $NTol_2$ into either **1.71** or **2.1** was observed confirming that the reaction of **1.71** with silanes is unlikely to proceed *via* **1.71_IntA** and is thought to instead undergo transfer of the Ti–N(H)SiH_2Ph proton to one of the $Ti–N_{amide}$ atoms to yield **1.71_IntB** . Works reported by our group showed the ability of the N_{amide} atoms of the supporting ligand to accept a proton, often resulting in unexpected reactivity products.[26]

DFT calculations were used to support the experimental results and to gain further insights. Two potential pathways were calculated in order to establish if the imido compound **1.71_Int1** was accessed *via* **1.71_IntA** or *via* **1.71_IntB** .

Pathway A, reported in Figure 2.8 proceeds *via* ***trans*-1.71_IntA** , which is uphill with respect to compound **1.71** and accessed via a barrier of $\Delta G^{\ddagger}$ = 25.5 kcal mol^{-1}. Calculations performed on the *cis* isomer show that the barrier is even higher, namely $\Delta G^{\ddagger}$ = 32.2 kcal mol^{-1}. When the labile neutral ligand, $HNPh_2$, is removed from both isomers a four-coordinate compound (**IntA**) is formed, in which the multiple bond occupies a position intermediate between axial and equatorial as shown in Figure 2.9. This result is unexpected as the $Ti=N_{\alpha}$ should be stabilized more if trans to the N_{apical}.

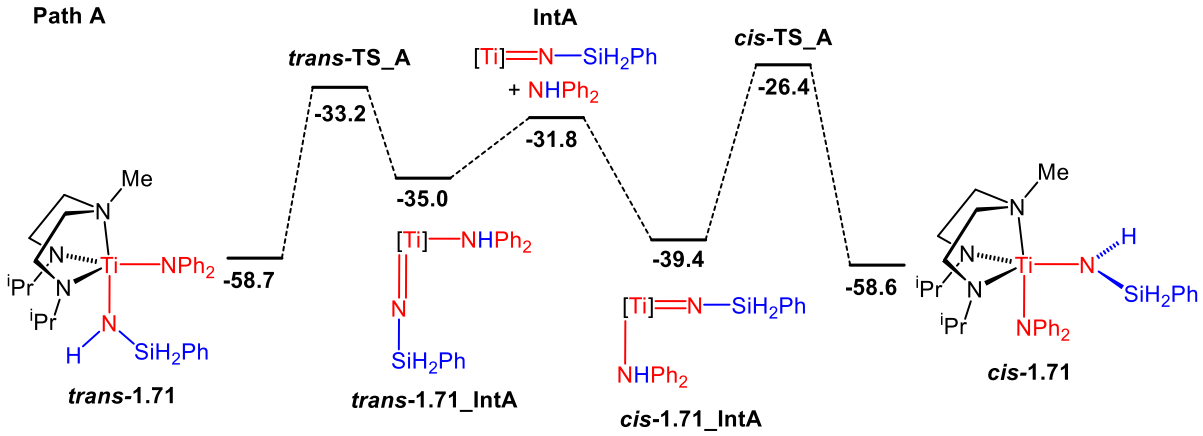

Figure 2.8. DFT mechanism for the formation of an imido intermediates from 1.71. Gibbs free energies (kcal mol^{-1}, T = 298 K) for minima, maxima and transition states (labelled **TS_x**) are shown in bold relative to *trans*-1.70. [Ti] represents $Ti(N_2^{iPr}N^{Me})$.

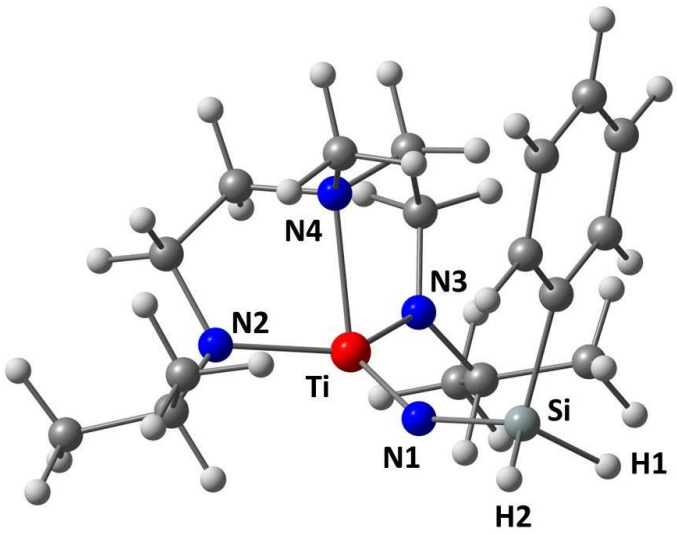

Figure 2.9. DFT gas phase optimized structure of **IntA**. C-bound H atoms omitted. Selected distances (Å): Ti–N_1 1.720, N_1–Si 1.709, Si–H_1 1.503.

Coordination of $HNPh_2$ to the Ti atom in a position cis to the N_{apical} yield ***cis*-1.71-IntA**. Finally, addition of SiH_3Ph across Ti=N_α bond led to ***cis*-1.71**.

A second pathway, Path B, involving the migration of the Ti-N(H) atom to one of the Ti-N_{amide} atoms of the supporting ligand was also evaluated.

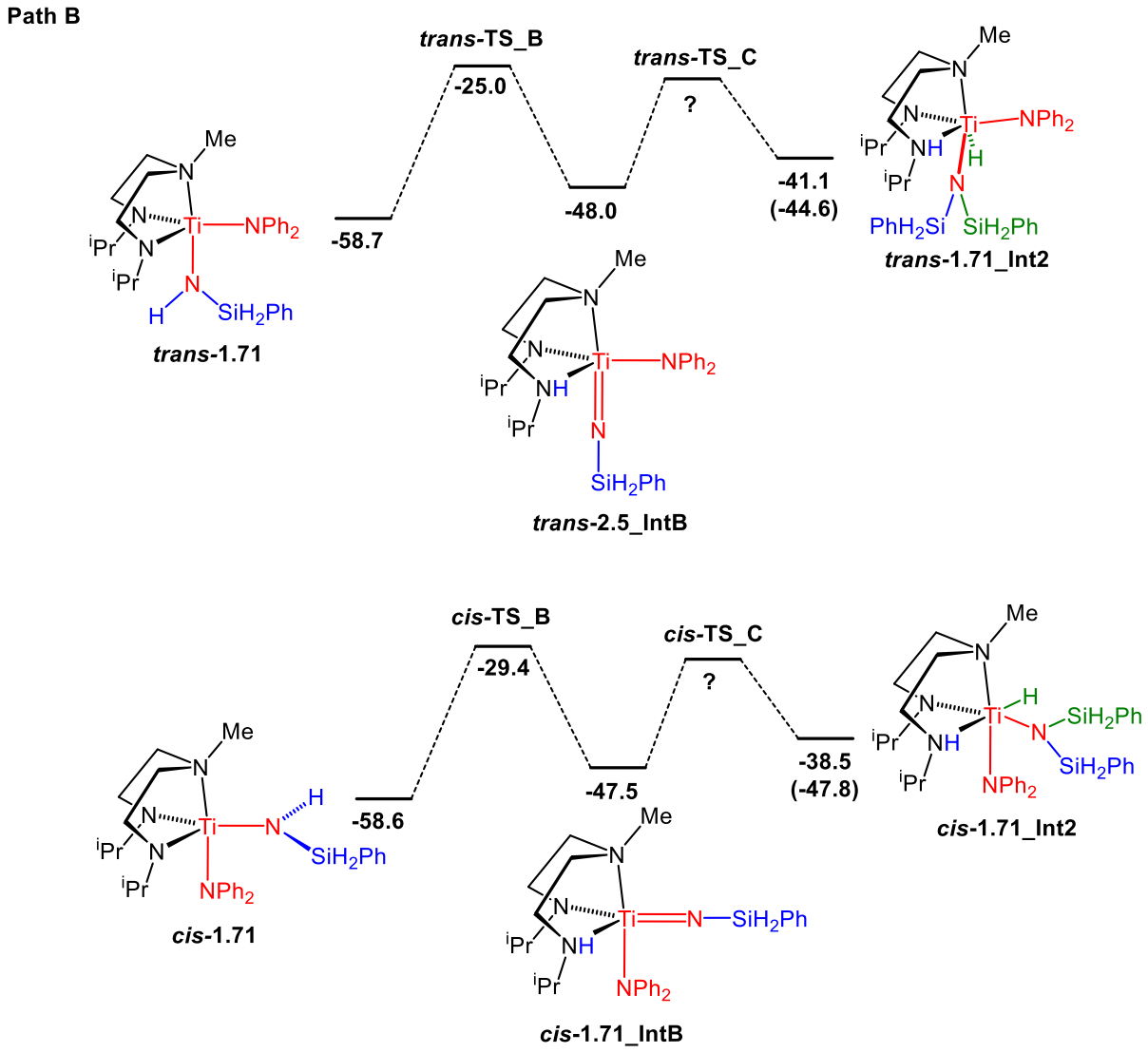

Figure 2.10. DFT mechanism for the formation of imido intermediates from **1.71** and subsequent reaction with $PhSiH_3$ or 3,5-$(CF_3)_2C_6H_3SiH_3$. Gibbs free energies (kcal mol^{-1}, T = 298 K) for minima, maxima and transition states (labelled **TS_x**) are shown in bold relative to ***trans*-1.70**. [Ti] represents $Ti(N_2^{iPr}N^{Me})$.

As reported in Figure 2.10, the energy of both the intermediates *cis* and *trans* **1.71_IntB** are low, but the barriers to reach them are $\Delta G^{\ddagger}$ = 29.3 and 33.7 kcal mol^{-1} respectively. This is again in contrast with a reaction that proceeds at room temperature. Furthermore, from cis or trans **1.71_IntB** it was not possible to locate the transition states associated with the addition of another $PhSiH_3$ molecule across the $Ti{=}N_{\alpha}$ bond. The stability of the resulting compounds, namely *cis* **1.71_Int2** and *trans* **1.71_Int2** was promising. The same single point calculations were performed for the analogous products of the reaction

of 3,5-$C_6H_3(CF_3)_2SiH_3$ with *cis* or *trans* **1.71_IntB** (reported in brackets in Figure 2.10). Additional stabilization was conferred by the electron-withdrawing groups on the Ph ring. To conclude, even though Pathway B was more promising, it was not possible to fully understand the mechanism and establish the preferred pathway.

2.8 Conclusions

The reactions of Ti($N_2^{iPr}N^{Me}$)($NNPh_2$)(py) (**1.70**) with the Si–H and B–H bonds of silanes and boranes and with H_2 have been discussed both experimentally and computationally. This reactivity is novel and provides the first examples of E-H bond induced reductive cleavage of a hydrazide N-N bond. Kinetic experiments and DFT studies proved that the mechanism proceed via E (Si or B) bond addition across the Ti=N_α bond to yield a silyl or borylhydrazido-hydride intermediates. The final products are obtained after the hydride transfer to N_α accompanied by N-N bond cleavage. Interestingly, the reaction of **1.70** with 9-BBN shows a different rate determining step than the reaction of **1.70** with $PhSiH_3$ and $HBMes_2$. While for the reaction of $PhSiH_3$ dissociation of pyridine from **1.70** and the hydride-transfer step have comparable barriers and thus both contribute to the rate determining step, for the reaction with 9-BBN, dissociation of 9-BBN dimer was found to be rate limiting. This is clearly due to the high dissociation barrier of 9-BBN dimer in solution.

The silyl and borylamido products were isolated and in the case of Ti($N_2^{iPr}N^{Me}$){N(H)$SiHPh_2$}(NPh_2) (**1.71**), Ti($N_2^{iPr}N^{Me}$){N(H)BC_8H_{14}}(NPh_2) (**1.73**) and Ti($N_2^{iPr}N^{Me}$){N(H)$BMes_2$}(NPh_2) (**2.3**) were structurally characterised.

The silylamido compound Ti($N_2^{iPr}N^{Me}$){N(H)SiH_2Ph}(NPh_2) (**1.71**) can undergo further reaction with both silanes and boranes. The subsequent reaction with silanes is proposed to proceed *via* an imido intermediate following transfer of the Ti–N(H)SiH_2Ph hydrogen atom to one of the Ti–N_{amide} atoms. Si–H addition to the newly formed imido bond yields a bis(silyl)amide compound which then can undergo rotation, followed by elimination of either silane to reform an imido intermediate. This process can occur reversibly allowing the silyl group to be readily exchanged. Experimental data are fully consistent with this mechanism. However, it was not possible to locate all of the transition states by DFT.

Compound Ti(N_2^{iPr}N)($NNPh_2$)(py) (**1.70**) does not react with H_2 because of the high bond strength and the lack of acceptor ability of H_2 which led to high Gibbs free energy intermediates along the reaction pathway.

Following the promising results described in this Chapter, the reactivity of the cyclopentadienyl-amidinate supported compounds Cp*Ti{MeC(N^iPr)$_2$}($NNMe_2$) (**1.39**), Cp*Ti{MeC(N^iPr)$_2$}($NNPh_2$) (**1.38**) and Cp*Ti{MeC(N^iPr)$_2$}($NNCPh_2$) (**1.40**) was investigated with the same set of boranes.

2.9 References

1 L. Stevenson, S. Mellino, E. Clot and P. Mountford, *J. Am. Chem. Soc.*, 2015, **137**, 10140–10143.

2 P. J. Walsh, M. J. Carney and R. G. Bergman, *J. Am. Chem. Soc.*, 1991, **113**, 6343–6345.

3 Y. Li, Y. Shi and A. L. Odom, *J. Am. Chem. Soc.*, 2004, **126**, 1794–1803.

4 S. Banerjee and A. L. Odom, *Organometallics*, 2006, **25**, 3099–3101.

5 A. A. Dissanayake and A. L. Odom, *Chem. Commun.*, 2012, **48**, 440–442.

6 H. Herrmann, J. L. Fillol, H. Wadepohl and L. H. Gade, *Angew. Chem. Int. Ed.*, 2007, **46**, 8426–8430.

7 T. Gehrmann, J. L. Fillol, H. Wadepohl and L. H. Gade, *Angew. Chem. Int. Ed.*, 2009, **48**, 2152–2156.

8 T. Gehrmann, M. Kruck, H. Wadepohl and L. H. Gade, *Chem. Commun.*, 2012, **48**, 2397–2399.

9 T. Gehrmann, S. A. Scholl, J. L. Fillol, H. Wadepohl and L. H. Gade, *Chem. - Eur. J.*, 2012, **18**, 3925–3941.

10 A. J. Blake, J. M. McInnes, P. Mountford, G. I. Nikonov, D. Swallow and D. J. Watkin, *J. Chem. Soc. Dalton Trans.*, 1999, 379–392.

11 J. D. Selby, C. D. Manley, M. Feliz, A. D. Schwarz, E. Clot and P. Mountford, *Chem. Commun.*, 2007, **733**, 4937–4939.

12 A. D. Schofield, A. Nova, J. D. Selby, C. D. Manley, A. D. Schwarz, E. Clot and P. Mountford, *J. Am. Chem. Soc.*, 2010, **132**, 10484–10497.

13 P. J. Tiong, A. D. Schofield, J. D. Selby, A. Nova, E. Clot and P. Mountford, *Chem. Commun.*, 2010, **46**, 85–87.

14 A. D. Schofield, A. Nova, J. D. Selby, A. D. Schwarz, E. Clot and P. Mountford,

Chem. Eur. J., 2011, **17**, 265–285.

15 P. J. Tiong, A. Nova, E. Clot and P. Mountford, *Chem. Commun.*, 2011, **47**, 3147–3149.

16 A. D. Schwarz, C. S. Onn and P. Mountford, *Angew. Chem. Int. Ed.*, 2012, **51**, 12298–12302.

17 J. Unruangsri, H. Morgan, A. D. Schwarz, A. D. Schofield and P. Mountford, *Organometallics*, 2013, **32**, 3091–3107.

18 P. J. Tiong, A. Nova, A. D. Schwarz, J. D. Selby, E. Clot and P. Mountford, *Dalton Trans.*, 2012, **41**, 2277–2288.

19 P. J. Tiong, L. R. Groom, E. Clot and P. Mountford, *Chem. Eur. J.*, 2013, **19**, 4198–4216.

20 B. A. MacKay, R. F. Munha and M. D. Fryzuk, *J. Am. Chem. Soc.*, 2006, **128**, 9472–9483.

21 S. P. Semproni, E. Lobkovsky and P. J. Chirik, *J. Am. Chem. Soc.*, 2011, **133**, 10406–10409.

22 M. Hirotsu, P. P. Fontaine, P. Y. Zavalij and L. R. Sita, *J. Am. Chem. Soc.*, 2007, **129**, 12690–12692.

23 M. D. Fryzuk, B. A. MacKay, S. A. Johnson and B. O. Patrick, *Angew. Chem. Int. Ed.*, 2002, **41**, 3709–3712.

24 B. A. MacKay, S. A. Johnson, B. O. Patrick and M. D. Fryzuk, *Can. J. Chem.*, 2005, **83**, 315–323.

25 S. P. Semproni and P. J. Chirik, *Eur. J. Inorg. Chem.*, 2013, **2**, 3907–3915.

26 L. C. Stevenson, DPhil Thesis, University of Oxford, 2015.

27 F. Weigend and R. Ahlrichs, *Phys. Chem. Chem. Phys.*, 2005, **7**, 3297–3305.

28 Z. K. Sweeney, J. L. Polse, R. G. Bergman and R. A. Andersen, *Organometallics*, 1999, **18**, 5502–5510.

29 T. E. Hanna, E. Lobkovsky and P. J. Chirik, *Inorg. Chem.*, 2007, **46**, 2359–2361.

30 D. A. Fletcher, R. F. McMeeking and D. Parkin, *J. Chem. Inf. Comput. Sci.*, 1996, **36**, 746 (Cambridge Structural Database version 5.37).

31 J. E. Huheey, E. A. Keiter and R. L. Keiter, *Inorganic Chemistry: Principles of Structure and Reactivity*, 1993.

32 H. C. Brown, J. Chandrasekharan and K. K. Wang, *Pure Appl. Chem.*, 1983, **55**, 1387–1414.

33 L. R. Groom, DPhil Thesis, University of Oxford, 2014.

34 T. E. Hanna, I. Keresztes, E. Lobkovsky, W. H. Bernskoetter and P. J. Chirik, *Organometallics*, 2004, **23**, 3448–3458.

35 J. L. Polse, R. A. Andersen and R. G. Bergman, *J. Am. Chem. Soc.*, 1998, **120**, 13405–13414.

3.1 Overview

This Chapter describes the reactions of the imido, hydrazido and alkylidene hydrazido compounds Cp*Ti{MeC(N^{i}Pr$_2$)$_2$}(NTol) (**3.1**), Cp*Ti{MeC(N^{i}Pr$_2$)$_2$}(NNMe$_2$) (**1.39**), Cp*Ti{MeC(N^{i}Pr$_2$)$_2$}(NNPh$_2$) (**1.38**), Cp*Ti{MeC(N^{i}Pr$_2$)$_2$}(NNCPh$_2$) (**1.40**) with the B–H bonds of boranes, which represent a number of new types of reactions in transition metal-ligand multiple bond chemistry. The nature and mechanism of these reactions were investigated experimentally, with kinetic studies, and computationally, by means of DFT calculations. The synthetic studies also led to a new route to a titanium borylimido compound and a new mechanism for dehydrogenative coupling of amines and boranes which will be presented at the end of this Chapter.

The computational studies have been performed in collaboration with Prof. Philip Mountford at the University of Oxford and Dr. Eric Clot at Université of Montpellier, France. Part of the reported work has been recently published.[1]

3.2 Introduction

As extensively discussed in the previous Chapters, Group 4 hydrazides and imides of the type (L)M=NR and (L)M=NNR$_2$ have been studied for decades. Several examples of stoichiometric and catalytic reactions of titanium imides and hydrazides have been reported in the Introduction. Although reactions of the aforementioned compounds with unsaturated substrates, such as CO$_2$, CS$_2$ and heterocumulenes have been explored in detail,[2–17] E–H (E = heteroatom) bond activation reactions were less studied. In particular, as described in Chapter 2, while the Si–H bond activation of silanes was reported in our group,[15,18] the same reactions with the B–H bond of boranes have been only recently developed.[1] Chen and co-workers described the first structurally authenticated example of the 1,2-addition of a B–H bond of a transition metal imide.[19] The resulting hydride species was trapped with a second equivalent of borane to yield an organohydroborate ligand. In 2015, Walter and co-workers reported activation of B–H bonds of boranes by a base-free thorium terminal imido compound, namely [η^5-1,2,4-(Me$_3$C)$_3$C$_5$H$_2$]$_2$Th=N(p-tolyl).[20]

In 2007, Lancaster and co-workers reported the synthesis of the four-coordinate amidoborate complexes Ti(NR$_2$)$_3${NH$_2$B(C$_6$F$_5$)$_3$} (R = Me or Et) achieved by reaction of homoleptic titanium amides Ti(NR$_2$)$_4$ (R = Me or Et) with the Brønsted acidic reagent H$_3$NB(C$_6$F$_5$)$_3$.[21] More recently, the same research group published the synthesis of a

zirconocene complex, $Cp_2Zr\{NH_2B(C_6F_5)_2\}H_2$ which exhibits an agostic Zr-H-B interaction and is in equilibrium with the hydride product, $Cp_2Zr(H)\{NH_2B(C_6F_5)_2H\}$. These complexes was obtained by reaction of Cp_2ZrCl_2 with $Li[H_2NB(C_6F_5)_2H]$ and are formally borane adducts of amido compounds.[22] In 2012, they reported an authenticated adduct of $HB(C_6F_5)_2$ on the parent metallocene imido complex $Cp_2Hf{=}NH$, namely $Cp_2Hf\{NHB(C_6F_5)_2H\}$.[22]

In 2014, our research group has found the first reductive N_α–N_β bond cleavage reactions (Equation 3.1) of a hydrazido compound by using organic boranes (containing B–H bonds) and silanes (containing Si–H bonds). This was achieved with the diamide-amine supported complex $Ti(N_2N^{Me})(NNPh_2)(py)$ (**1.70**) and has been discussed in detail in Chapter 2.

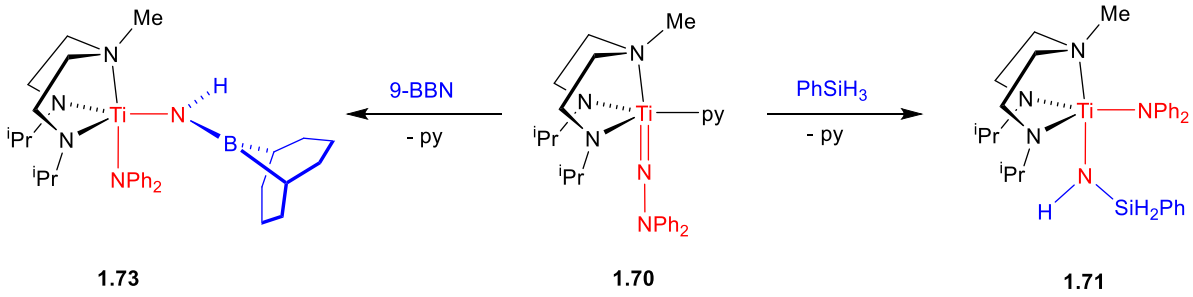

1.73 **1.70** **1.71**

Equation 3.1

These promising results encouraged us to further explore the reactions of Ti=NR (R = ^{t}Bu or Tol) and $Ti{=}NNR_2$ (R_2 = Me_2, Ph_2 or CPh_2) complexes bearing a different ligand set. The Cp*-amidinate supported titanium systems were found to be particularly interesting. A variety of complexes, namely $Cp^*Ti\{MeC(N^iPr_2)_2\}(NTol)$ (**3.1**), $Cp^*Ti\{MeC(N^iPr_2)_2\}(NNR_2)$ (R = Me_2 (**1.39**), R = Ph_2 (**1.38**) or R = CPh_2 (**1.40**)) were synthesised from the imido complex $Cp^*Ti\{MeC(N^iPr)_2\}(N^tBu)$ (**1.37**) *via* an exchange reaction with hydrazine or hydrazone (Equation 3.2).[18,23]

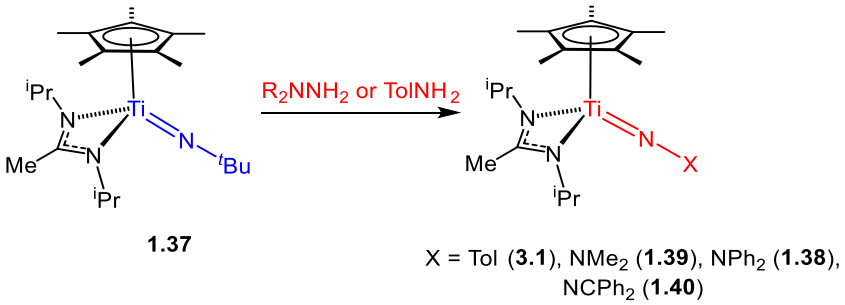

1.37

Equation 3.2

Our research group previously studied the Si–H bond reactions with these half- sandwich compounds. Reaction of Cp*Ti{MeC(N^{i}Pr)$_2$}(NNMe$_2$) (**1.39**) with silanes gave the reversible Si–H bond 1,2-addition to the Ti=N$_\alpha$ multiple bond where the effective N$_\beta$ coordination was required to stabilise the dialkyl hydrazide(1−) product (Equation 3.3**)**.[24] The corresponding diphenylhydrazide compound Cp*Ti{MeC(N^{i}Pr)$_2$}(NNPh$_2$) (**1.38**) showed no reactivity with silanes and neither did the imido analogues Cp*Ti{MeC(N^{i}Pr$_2$)$_2$}(NR) (R = ^{t}Bu or Tol). The analogous cyclopentadienyl-amidinate supported compound Cp*Ti{MeC(N^{i}Pr)$_2$}(NNCPh$_2$) (**1.40**) undergoes the same Si–H bond activation reaction with both primary and secondary silanes to give Cp*Ti{MeC(N^{i}Pr)$_2$}{N(PhSiH$_2$)N(CHPh$_2$)} (Equation 3.4), which was assigned as adduct on N$_\alpha$, based on Equation 3.3. However, based on the collected experimental data alone, it was not possible to rule out an adduct on N$_\beta$.

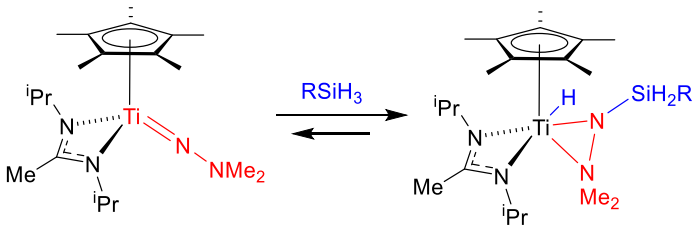

1.39

Equation 3.3

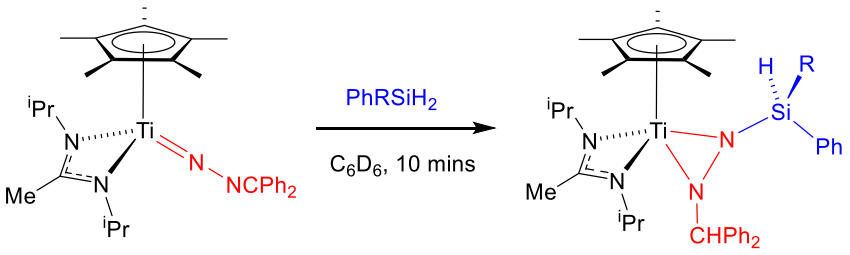

1.40 R = Ph or H

Equation 3.4

Following this line of research, the Author decided to investigate the reactivity of the aforementioned Ti=NR (R = ^{t}Bu or Tol) and Ti=N–X (X = NMe_2, NPh_2, $NCPh_2$ or O^{t}Bu) half-sandwich compounds toward the B–H bond activation with a variety of boranes. Boranes with different electronic and steric features were synthesised in order to understand the underlying factors guiding these reactions. The half-sandwich compounds were targeted to explore the effect of a different ligand set on the reactivity with boranes. Finally, the choice to investigate the reactivity of both imides and hydrazides was led by the hope to access a novel B–H induced reductive cleavage of the Nα–Nβ bond.

3.3 Selection of titanium complexes and boranes

Following the promising results reported in our research group the reactivity of a variety of half-sandwich compounds was explored (Figure 3.1). Next, the starting boranes were selected and synthesised (Figure 3.2, shown in their monomeric form).

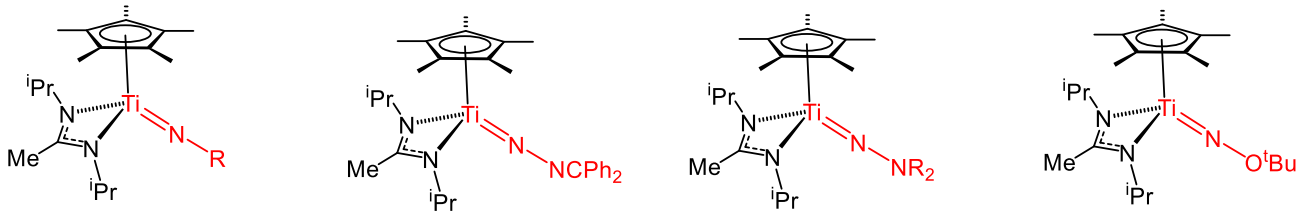

R = ^{t}Bu (**1.37**), Tol (**3.1**) R_2 = Me_2 (**1.39**), Ph_2 (**1.38**)

Figure 3.1. Titanium complexes selected for the reactions with boranes.

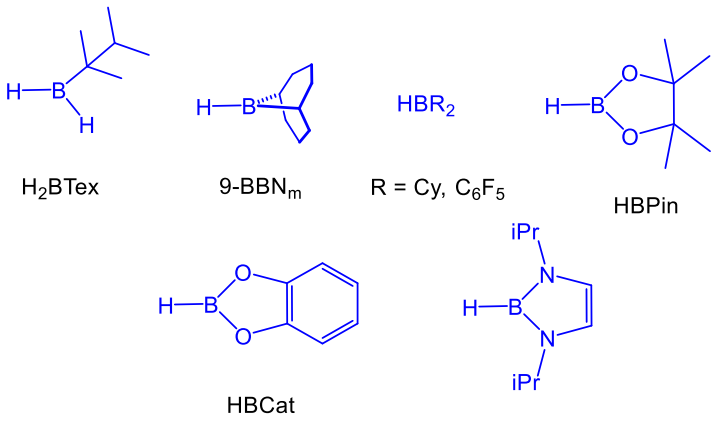

Figure 3.2. Library of boranes tested (shown in their monomeric form, where appropriate).

As it was found that the reaction of Ti(N_2N^{Me})($NNPh_2$)(py) (**1.70**) with alkylboranes such as $HBMes_2$ and 9-BBN led to a reductive cleavage of the N_α–N_β bond (Equation 3.1, left), the reactivity with both primary and secondary alkyl-boranes, namely $HBMes_2$, 9-BBN, $HBCy_2$ and H_2BTex was investigated. The aim was to understand the effect of the steric bulk on the reactivity. Next, boranes with different electronic features were explored. It was reported by Dr. Laura Stevenson that reactions of Ti(N_2N^{Me})($NNPh_2$)(py) (**1.70**) with HBPin and HBCat led to two six-coordinate titanium compounds (reaction product with HBPin shown in Equation 3.5) with a diolate ligand and a new N(Me)($CH_2CH_2N^iPr$)($CH_2CH_2N(^iPr)B(H)NNPh_2$) group.[25] The driving force behind the reactions with HBPin and HBCat was thought to be the formation of strong Ti–O bonds, assisted by the nucleophilic nature of the amido nitrogen of N_2N^{Me}.

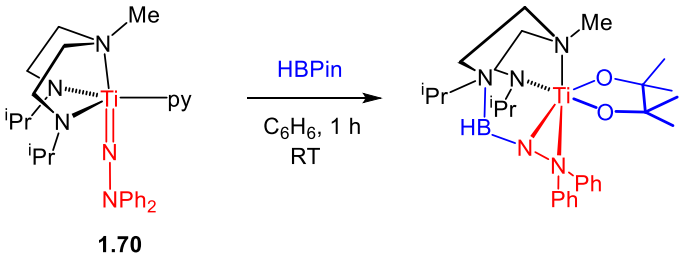

Equation 3.5

For these reasons both HBPin and HBCat were also reacted with the half-sandwich compounds depicted in Figure 3.1. To better understand the effect of heteroatoms attached to the boron atom, HB(N^iPrCH_2)$_2$ was also tested. The effect of the N atoms could be comparable to that of the O atoms but some differences might arise. Firstly, the B–O bond strength is much higher than the B–N bond strength. Secondly, oxygen is more

electronegative than nitrogen and the lone pair donation from N to the vacant p orbital on B is stronger.[26] Finally, $HB(C_6F_5)_2$ was synthesised and reacted, to see the effect of electron withdrawing groups such as the pentafluorophenyl rings.

3.4 Reactions of imido complexes Ti=NR with boranes

Reactions of Cp*Ti{MeC(N^{i}Pr)$_2$}(N^{t}Bu) (**1.37**) with any boranes were unsuccessful and gave no reaction even under forcing conditions (high temperatures and/or long reaction times). Reactions of Cp*Ti{MeC(N^{i}Pr)$_2$}(NTol) (**3.1**) with selected boranes are shown in Scheme 3.1.

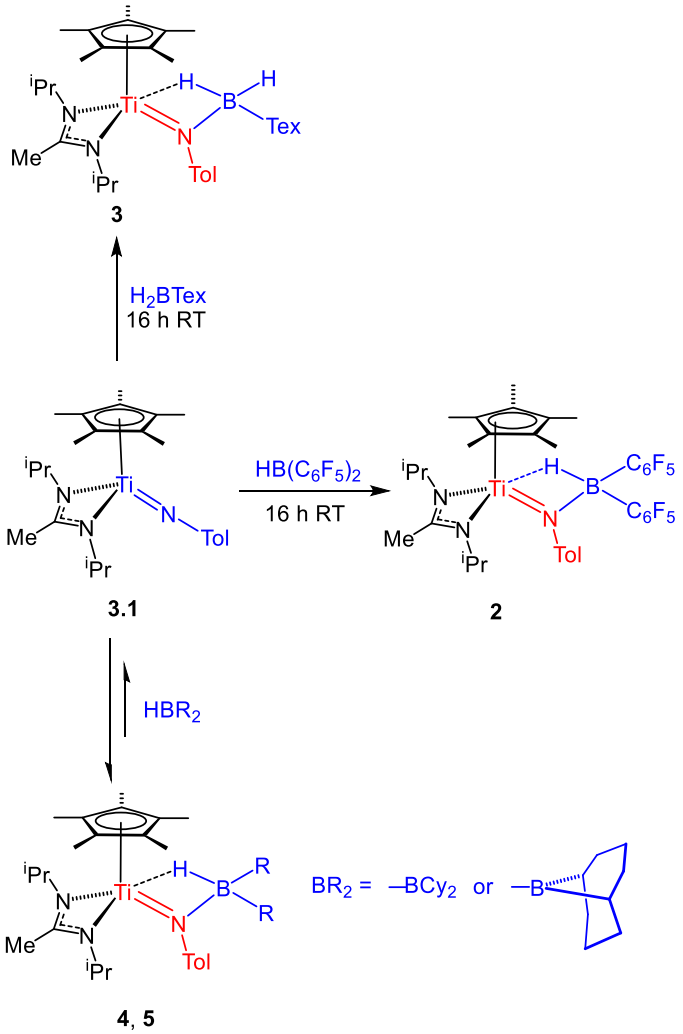

Scheme 3.1. Reactions of Cp*Ti{MeC(N^{i}Pr)$_2$}(NTol) (**3.1**) with selected boranes.

NMR tube scale reactions of **3.1** with HB(C$_6$F$_5$)$_2$ or H$_2$BTex proceeded cleanly to completion. On the preparative scale in benzene, the product of the reaction of **3.1** with HB(C$_6$F$_5$)$_2$, namely Cp*Ti{MeC(N^{i}Pr$_2$)$_2$}{(NTol)HB(C$_6$F$_5$)$_2$} (**2**) was isolated as a brown powder in 60% yield after 16 h at RT. Cp*Ti{MeC(N^{i}Pr$_2$)$_2$}{(NTol)H$_2$BTex} (**3**) was isolated as a dark yellow powder after 16 h at RT in 75% yield. The ^{11}B chemical shifts of **2** and **3** are -7.68 and 1.46 ppm respectively. Although the B-H resonances could not be observed in the ^{1}H NMR spectra of **2** or **3**, presumably because of quadrupolar coupling, the infrared spectrum of Cp*Ti{MeC(N^{i}Pr$_2$)$_2$}{(NTol)H$_2$BTex} (**3**) confirmed the

presence of two (B–H) bonds, namely at 2327 cm^{-1} for the terminal B–H and at 1908 cm^{-1} for the bridging B–H while the B–H stretching mode is found to be 1939 cm^{-1} in **2**. In the case of **2** the presence of a doublet in the ^{11}B NMR is diagnostic of an intact B-H bond. The coupling constant was 59.8 Hz, ^{1}J(H,B). The coupling constants are a useful tool to understand the nature of the bond. In general, for two-center two-electron bonds the value of *J* is larger than for three-centre two-electron bonds. The value found is in line with the one reported by Lancaster and co-workers,[22] namely in $Cp_2Hf\{NHB(C_6F_5)_2H\}$, where ^{1}J(H,B) = 63 Hz. The value for the free $HB(C_6F_5)_2$ is not known, as it is 90% in dimeric form in solution, however the coupling constant for the borane adduct $H_3N{\bullet}B(C_6F_5)_2H$ is 102 Hz.[22] The reduction of this value, observed in **2**, is further evidence of agostic interaction to the metal. For the other complexes shown in Scheme 3.1 the ^{11}B NMR displayed a broad singlet, thus other methodologies such as the IR were used to elucidate the structure. Diffraction-quality crystals of **2** and **3** were grown from pentane solutions at RT. The molecular solid state structures, which confirm that depicted in Scheme 3.1, are shown in Figure 3.3, and selected bond lengths and angles are listed in Table 3.1. The B-bonded H atoms in **2** and **3** were located in the Fourier difference maps and positionally and isotropically refined.

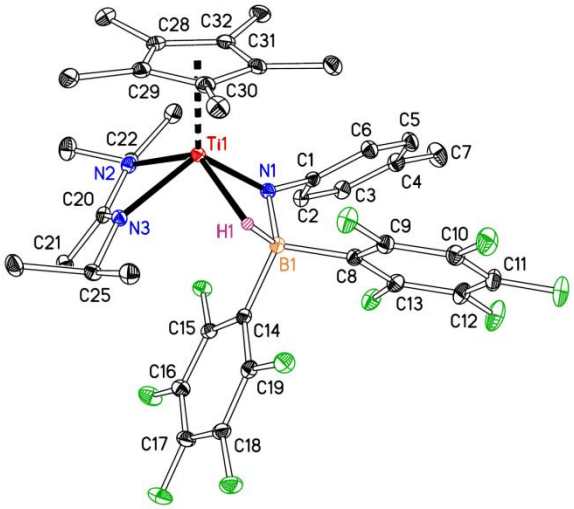

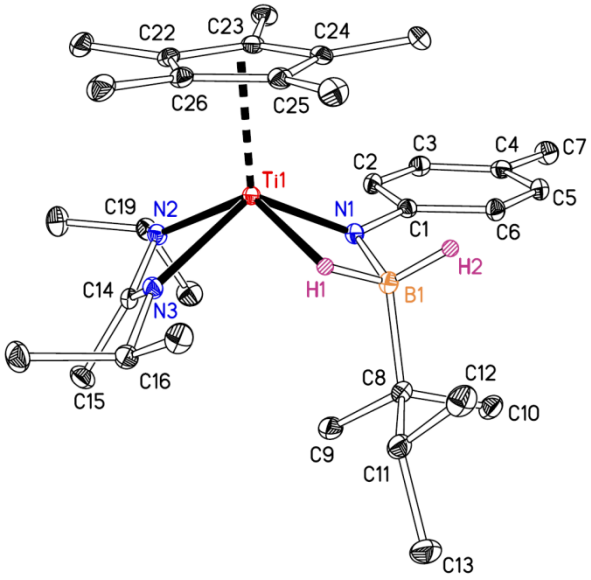

Figure 3.3. Displacement ellipsoid plot (25% probability) of Cp*Ti{MeC(N^{i}Pr$_2$)$_2$}{(NTol)HB(C$_6$F$_5$)$_2$} (**2**) (top) and Cp*Ti{MeC(N^{i}Pr$_2$)$_2$}-{(NTol)H$_2$BTex} (**3**) (bottom). C-bound H atoms are omitted for clarity. H atoms are drawn as spheres of an arbitrary radius.

Table 3.1. Selected bond distances (Å) and angles (°) for Cp*Ti{MeC(N^{i}Pr$_2$)$_2$}{(NTol)HB(C$_6$F$_5$)$_2$} (**2**) and Cp*Ti{MeC(N^{i}Pr$_2$)$_2$}{(NTol)H$_2$BTex} (**3**).

Parameter	**2**	**3**
Ti(1)–N(1)	1.8725(9)	1.8813(7)
Ti(1)–N(2)	2.0950(9)	2.0817(7)
Ti(1)–N(3)	2.0910(8)	2.1194(7)
Ti(1)–H(1)	2.009(13)	1.914(13)
Ti(1)–Cp$_{cent}$	2.308	2.055
N(1)–B(1)	1.5426(14)	1.5466(11)
B(1)–H(1)	1.187(14)	1.233(13)
B(1)–H(2)		1.131(13)
B(1)–C(8)	1.6296(14)	1.6473(13)
N(1)–Ti(1)–Cp$_{cent}$	124.7	119.0
N(2)–Ti(1)–Cp$_{cent}$	114.0	114.5
N(3)–Ti(1)–Cp$_{cent}$	121.2	117.2
N(1)–Ti(1)–N(2)	99.94(4)	103.69(3)
Ti(1)–N(1)–B(1)	91.62(6)	91.38(5)
N(1)–B(1)–C(8)	113.69(8)	117.54(7)

The two structures confirm the formation of adducts featuring B coordinated to N and H coordinate to the titanium atom. Both **2** and **3** have 4-legged piano stool geometries; the distances and angles are within the expected general ranges. The Ti(1)–N(1) distance of ca. 1.87–1.88 Å for both **2** and **3** are significantly lengthened compared to the typical values of 1.70–1.73 Å found in analogues of **3.1**. The N(1)–B(1) distance of ca. 1.54–1.55 Å is in line with values reported for nitrogen-boron dative bonds.[22,27] The N(1)–B(1) distance of 1.5426(14) Å in **2** can be directly compared with that of 1.509(10) Å in Lancaster's Cp$_2$Hf{(NHB(C$_6$F$_5$)$_2$H} mentioned earlier.[22] The shorter distance in this case

implies stronger B–N bonding which may be attributed to the absence of any bulky N-substituent in the hafnium bond and the reduced steric crowding in general. The ^{11}B NMR chemical shift of -7.68 ppm in **2** is less negative than in the hafnium example (δ = -27.5 ppm in the same solvent), again consistent with higher B-N bonding in the latter case. The Ti(1)–H(1) distances are significantly longer than the experimental values for the Si–H addition products with silanes (Cp*Ti{MeC(N^{i}Pr)$_2$}(H){N(PhSiH$_2$)NMe$_2$}, range ca. 1.56–1.64 Å) previously found in our research group.[15] Note that, in **2** the Ti(1)–H(1) bond is longer (2.009(13) *vs.* 1.914(13) Å) than in **3** and consequently the B(1)–H(1) is shorter (1.187(14) *vs.* 1.233(13) Å). This can be explained by the electron-withdrawing nature of the C_6F_5 groups which render the boron atom more Lewis acidic.

On the NMR tube scale in C_6D_6 the reactions with 9-BBN and HBCy$_2$ yielded adducts where the B atom is coordinated to Nα and presumably the hydrogen to titanium atom as observed in compounds **2** and **3**, namely Cp*Ti{MeC(N^{i}Pr$_2$)$_2$}{(NTol)HB(C$_8$H$_{14}$)} (**4**) and Cp*Ti{MeC(N^{i}Pr$_2$)$_2$}{(NTol)HBCy$_2$} (**5**). When performed on preparative scale, **4** could be isolated as a sticky oil which could not be purified further; while **5** could not be obtained in an isolated form. Both compounds **4** and **5** were thus characterized in solution.

However, other evidence was used for the reaction of Cp*Ti{MeC(N^{i}Pr$_2$)$_2$}(NTol) **(3.1**) with 9-BBN to confirm the proposed structure. The absence of any Ti–H hydride in the ^{1}H NMR (Figure 3.4) is indicative of an adduct. The ^{11}B NMR spectrum is indicative of tetracoordinate boron appearing at a chemical shift of 10.2 ppm. It is reported in literature that ^{11}B shifts are more upfield for complexes where B is tetracoordinated.[28]

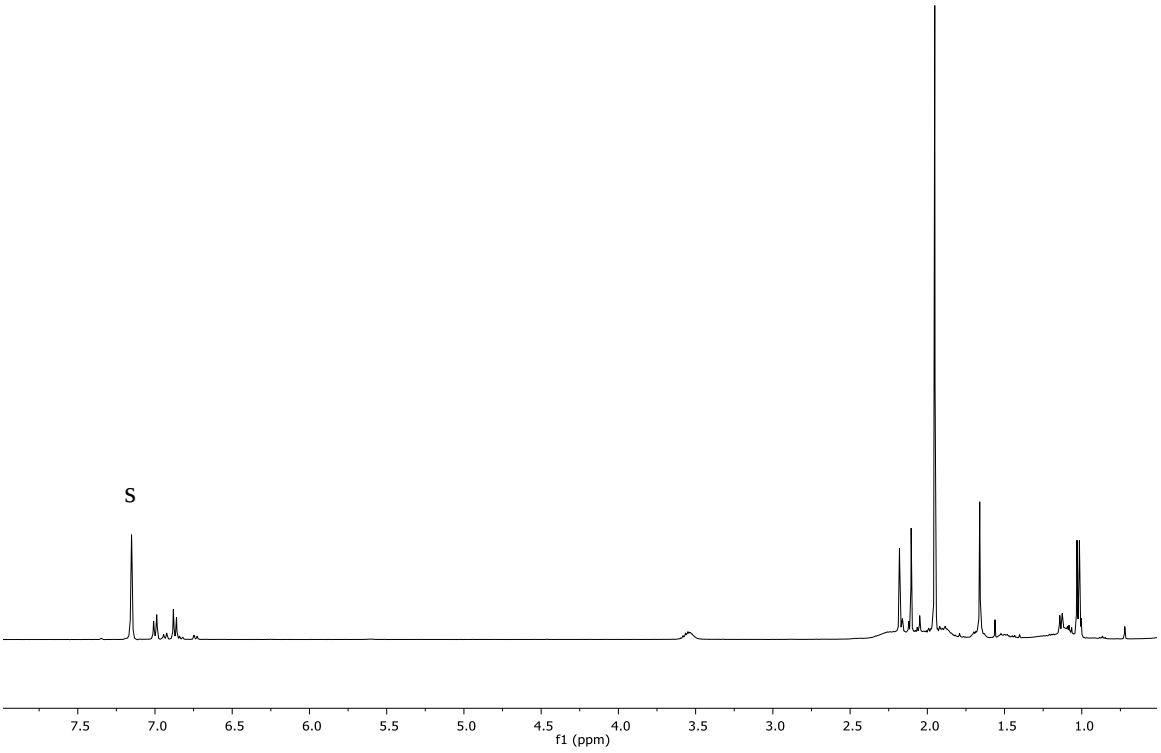

Figure 3.4. ^{1}H NMR spectrum (400.1 MHz) of Cp*Ti{MeC(N^{i}Pr$_2$)$_2$}{(NTol)HB(C$_8$H$_{14}$)} (**4**). in C_6D_6 at 298 K. Residual protio-solvent is labelled 's'.

The reversibility of the reaction of **3.1** + 0.5 9-BBN to give **4** allowed a thermodynamic analysis by VT NMR and the Van't Hoff plot in toluene-*d*$_8$ is reported in Figure 3.5. When monitored at low temperature (from 298 K to 243 K) no further conversion to the product **4** was observed. When monitored at high temperature (from 298 K to 343 K) conversion to the starting material and free 9-BBN was observed. Values of Δ_rG (298 K) and Δ_rH (298 K) were respectively found to be -2.5(1) and -9.5(2) kcal mol^{-1} in line with an equilibrium reaction. 9-BBN exists as a dimer in solution, as explained in Chapter 2, thus the dissociation of half-dimer to form a monomer was also taken into account and the aforementioned values are the sum of the two consecutive reactions depicted in Scheme 3.2.

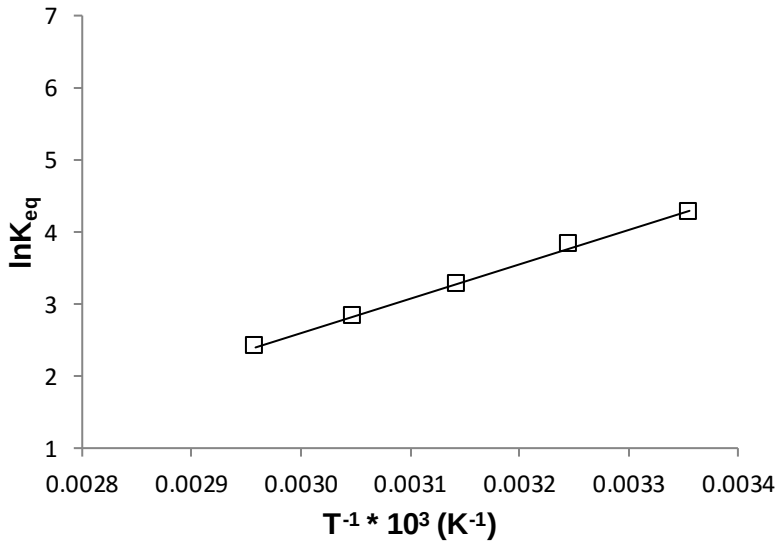

Figure 3.5. van't Hoff plot for the reaction Cp*Ti{MeC(N^{i}Pr)$_2$}(NTol) (**3.1**) + 0.5 9-BBN = Cp*Ti{MeC(N^{i}Pr$_2$)$_2$}{(NTol)HB(C$_8$H$_{14}$)} (**4**). Δ_rH = -9.5(2) kcal mol^{-1}, Δ_rS = -23.3(7) cal mol^{-1} K^{-1}, Δ_rG = -2.5(1) kcal mol^{-1} (R^2 = 0.998).

To further confirm the strength of the adducts, two NMR scale reactions in C_6D_6 of **3** with 1 equiv. of HB(C$_6$F$_5$)$_2$ or 1 equiv. of H$_2$BTex were performed. Immediate conversion to **2** or **3** and free 9-BBN was observed at RT, confirming that the two isolated adducts are stronger than Cp*Ti{MeC(N^{i}Pr$_2$)$_2$}{(NTol)HB(C$_8$H$_{14}$)} (**4**).

Unfortunately reactions with the other boranes reported in Section 3.3 were not successful. In some cases, the reactions did not proceed even under forcing conditions (high temperatures or long reaction times), while in other cases they were associated with a high percentage of decomposition products.

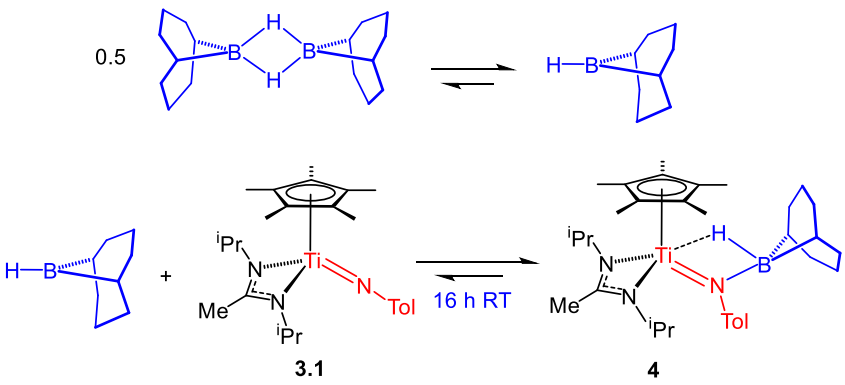

Scheme 3.2. Steps in the reaction of **3.1** with 9-BBN.

3.5 Computational studies of Cp*Ti{MeC(N^{i}Pr$_2$)$_2$}(NTol) (3.1)

Further evidence of the reaction products reported in Section 3.4 were obtained with the aid of DFT calculations. All the calculations on the real systems described in this Chapter were performed according to the following methodology: geometry optimisations using the B3PW91 functional with the titanium atom represented by the relativistic effective core potential (RECP) from the Stuttgart group and the associated basis set,[29] augmented by an f polarization function and the remaining atoms represented by a def2-svp basis set.[30] The SCRF single point calculations were performed with a def2-qzvpp basis set for all atoms.[31] Dispersion interactions were taken into account with the d3(bj) corrections in both the optimizations and the single point calculations.[32] ^{11}B NMR calculations were performed with the Gauge-Independent Atomic Orbital (GIAO) method and a pcS-2 basis set, using BF_3OEt_2 as reference for ^{11}B NMR shifts.[33] Calculations on sterically-pruned model systems were performed with the same methodology for the geometry optimizations without dispersion interactions in the optimization process. The SCRF single point calculations were performed with a def2-tzvp basis set[31] for all atoms with and without dispersion interactions. A detailed description of the methodology and a DFT introduction is described in Chapter 7.

The computed distances in models **2** and **3** are in line with the experimental results. The DFT structures of **3** and **4** are shown in Figure 3.6, and selected differences associated with the Ti{N(Tol)HBR^{1}R^2} moiety are given in the figure caption for all three structures, **2**, **3** and **4**. For **2** and **3** the agreement between the experimental structures is good, with the longest discrepancies being found for the Ti–H and B–H distances for absolute values. Nonetheless the trends are faithfully reproduced between and within **2** and **3**, in comparison with **2** and **3**.The Ti–H distance in **2** (DFT: 1.950 Å, X-ray: 2.009(13) Å) is shorter than in **3** (1.904 and 1.914(13) Å); likewise B–H_b is longer than B–H_t in **3**, and B–H_t is slightly shorter in both **2** and **2** compared to **3** and **3** (difference = 0.012 and 0.046(19) Å respectively) for $HB(C_6F_5)_2$ and H_2BTex, respectively). The DFT structure of **4** is comparable to those in **2** and **3**. In **4** the B–H transfer seems most advanced with Ti–H_b = 1.848 Å and B–H_b = 1.336 Å, but the N_{im}–B distance is the same as for **3** and longer than in **2**. These structural variations are consistent with the different coordination environment at boron in the three compounds.

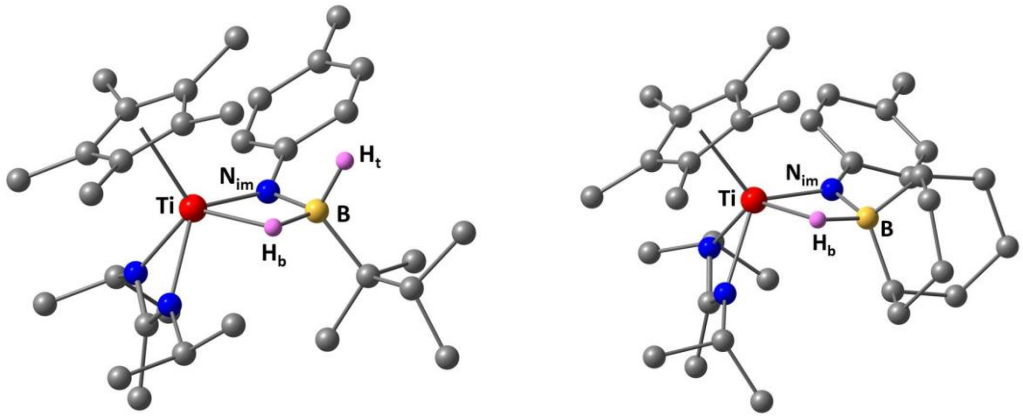

Figure 3.6. DFT gas phase optimized structures of Cp*Ti{MeC(N^{i}Pr$_2$)$_2$}{(NTol)H$_2$BTex} (**3**, left) and Cp*Ti{MeC(N^{i}Pr$_2$)$_2$}{(NTol)HB(C$_8$H$_{14}$)} (**4**, right). C-bound H atoms omitted. Selected distances (Å) for Cp*Ti{MeC(N^{i}Pr$_2$)$_2$}{(NTol)HB(C$_6$F$_5$)$_2$} (**2**, not shown above): Ti–H$_b$ 1.950, B–H$_b$ 1.297, Ti–N$_{im}$ 1.879, B–N$_{im}$ 1.523; for **3**: Ti–H$_b$ 1.904, B–H$_b$ 1.309, B–H$_t$ 1.231, Ti–N$_{im}$ 1.869, B–N$_{im}$ 1.542; for **4**: Ti–H$_b$ 1.853, B–H$_b$ 1.336, Ti–N$_{im}$ 1.853, B–N$_{im}$ 1.542.

The computed B–H frequencies were found to be 1939, 2306 ν(B–H$_t$) and 1891 ν(B–H$_b$), and 1755 cm^{-1} for **2**, **3**, and **4** respectively in agreement with the ν(B–H) experimental results. The ^{11}B NMR values were calculated to be -6.7, 2.0 and 8.0 ppm for **2**, **3** and **4** respectively (compared to -7.7, 1.4 and 10.4 ppm experimentally found for **2**, **3** and **4**). The Gibbs free energies of reaction of Cp*Ti{MeC(N^{i}Pr)$_2$}(NTol) (**3.1**) with 9–BNN, HB(C$_6$F$_5$)$_2$ and H$_2$BTex were also computed by means of DFT calculations as shown in Table 3.2. All the values are referenced to Cp*Ti{MeC(N^{i}Pr)$_2$}(NTol) (**3.1**) which was set as the zero energy reference (0.0 kcal mol^{-1}). Note that all the three boranes exist as dimers in solution, thus it was necessary to evaluate the Gibbs free energies associated with the dissociation of 0.5 equiv. of dimeric species. The Gibbs free energies were negative for HB(C$_6$F$_5$)$_2$ and H$_2$BTex in line with exogenic reactions. The computed Gibbs free energy value for the formation of **4**, 0.8 kcal mol^{-1}, is in good agreement with the experimental one (-2.5(1) kcal mol^{-1}). The balance between the coordination of 9-BBN$_{monomer}$ and the need to dissociate the dimer gives the poor coordination observed by NMR.

Table 3.2. Computed SCRF solvent Gibbs free energy values (benzene at RT) for the reactions of **3.1** with boranes, at 298.15 K.

	$\Delta_r G$ (kcal mol^{-1})
0.5 $HB(C_6F_5)_{2dimer} \rightarrow HB(C_6F_5)_{2monomer}$	10.6
0.5 $H_2BTex_{dimer} \rightarrow H_2BTex_{monomer}$	7.0
0.5 $9\text{-}BBN_{dimer} \rightarrow 9\text{-}BBN_{monomer}$	10.0
3.1 + $HB(C_6F_5)_{2monomer} \rightarrow$ **2**	-29.7
3.1 + $H_2BTex_{monomer} \rightarrow$ **3**	-30.5
3.1 + $9\text{-}BBN_{monomer} \rightarrow$ **4**	-9.2
3.1 + 0.5 $HB(C_6F_5)_{2dimer} \rightarrow$ **2**	-19.1
3.1 + 0.5 $H_2BTex_{dimer} \rightarrow$ **3**	-23.5
3.1 + 0.5 $9\text{-}BBN_{dimer} \rightarrow$ **4**	0.8

From these values and the DFT structures discussed above it is clear that the $\Delta_r G$ values are similar for both H_2BTex and $HB(C_6F_5)_2$ which led us to conclude that the stability of the adducts is primarily driven by the steric bulk which is not offset by the electron withdrawing groups in the secondary borane $HB(C_6F_5)_2$.

3.6 Reactions of Cp*Ti{MeC(N^{i}Pr$_2$)$_2$}(NNCPh$_2$) (1.40) with boranes

Following the results reported in Section 3.5, we decided to explore how the presence of a substituent in β position in complexes of the type Ti=N–X affects the reactivity with boranes. Inspired by 1,2-addition reactions between Cp*Ti{MeC(N^{i}Pr$_2$)$_2$}(NNCPh$_2$) (**1.40**) and silanes published by our research group,[18] we investigated the reactivity of **1.40** with the boranes reported in Section 3.3. Reaction of Cp*Ti{MeC(N^{i}Pr$_2$)$_2$}(NNCPh$_2$) (**1.40**) with PhSiH$_3$ previously yielded Cp*Ti{MeC(N^{i}Pr)$_2$}{N(PhSiH$_2$)N(CHPh$_2$)} (**3.2**) where the Si atom is attached to Nα. Unfortunately it was not possible to grow diffraction quality crystals of **3.2**. The proposed structure was however supported by Si–H 1,2-addition reactions reported in literature by Bergman and co-workers between Cp*$_2$Ti{NNC(H)Tol} and PhSiH$_3$ which gave hydride-alkylidene hydrazide(1-) product analogous to the one formed from Cp*Ti{MeC(N^{i}Pr)$_2$}(NNMe$_2$) (Equation 3.3).[34] In their reaction, the first formed isomer had to undergo rotation of the tolyl group on the alkylidene hydrazide fragment to form the sterically less congested stable isomer. It was thus proposed that the reactions between **1.40** and PhSiH$_3$ proceeded through initial Si–H 1,2-addition reactions to form an hydride-alkylidene hydrazide(1–) intermediate **3.2_Int** analogous to those reported by Bergman. The intermediate then undergoes hydride transfer to form the finally observed product **3.2** (Equation 3.6).

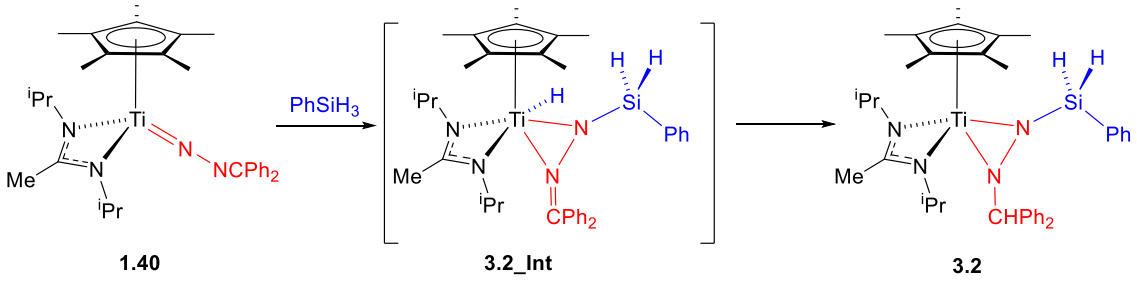

Equation 3.6

Following these results, we hoped that reactions of **1.40** with boranes would give more stable products in contrast to the aforementioned reactions of the imido compound Cp*Ti{MeC(N^{i}Pr$_2$)$_2$}{(NTol) (**3.1**). On the NMR tube scale, Cp*Ti{MeC(N^{i}Pr$_2$)$_2$}(NNCPh$_2$) (**1.40**) reacted quantitatively with a range of boranes, namely H$_2$BTex, HBCy$_2$, 9-BBN and HBPin to form the B–H addition products depicted in Equation 3.7.

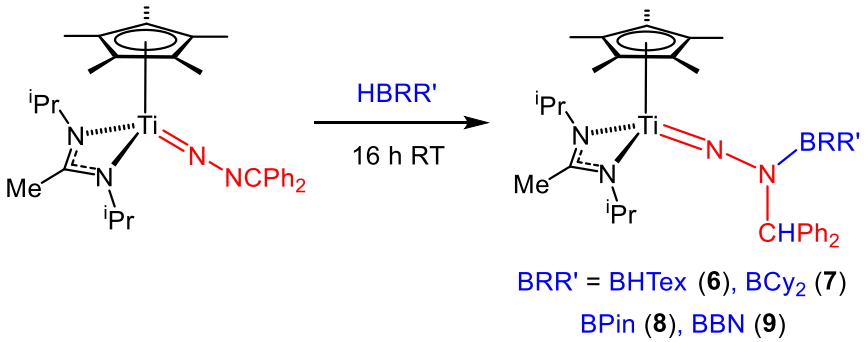

Equation 3.7

On the preparative scale, reactions of the alkylidene hydrazide **1.40** with HBPin and 9-BBN were complete after 16 h at RT and confirmed 1,2 B–H addition across the N_{β}=CPh_2 bond in products **8** and **9**, which were isolated in 70% and 50% yields respectively and characterized by NMR and IR spectroscopy, elemental and X-ray analysis. The ^{1}H NMR shows a diagnostic C<u>H</u>Ph_2 signal at 5.55 and 5.56 ppm for **8** and **9** respectively. In comparison the C<u>H</u>Ph_2 signal was found at 5.23 ppm in Cp*Ti{MeC(N^{i}Pr)$_2$}{N($PhSiH_2$)N($CHPh_2$)} (**3.2**). The molecular solid state structures of **8** and **9**, are shown in Figure 3.7, and selected bond lengths and angles are listed in Table 3.3.

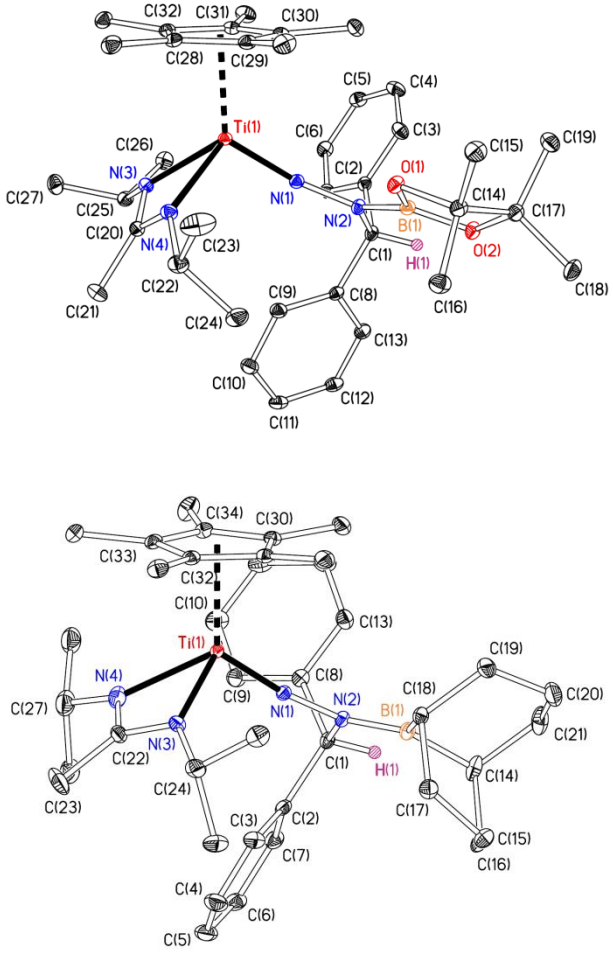

Figure 3.7. Displacement ellipsoid plot (25% probability) of Cp*Ti{MeC(N^{i}Pr)$_2$}{NN(BPin)CHPh$_2$} (**8**) (top) and Cp*Ti{MeC(N^{i}Pr)$_2$}-{NN(BC$_8$H$_{14}$)CHPh$_2$} (**9**) (bottom). C-bound H atoms except H(1) are omitted for clarity.

Table 3.3. Selected bond distances (Å) and angles (°) for Cp*Ti{MeC(N^{i}Pr)$_2$}{NN(BPin)CHPh$_2$} (**8**) and Cp*Ti{MeC(N^{i}Pr)$_2$}-{NN(BC$_8$H$_{14}$)CHPh$_2$} (**9**).

Parameter	**8**	**9**
Ti(1)–N(1)	1.7280(8)	1.7256(16)
Ti(1)–N(3)	2.1071(8)	2.1052(18)
Ti(1)–N(4)	2.1243(8)	2.119(2)
Ti(1)–Cp$_{cent}$	2.077	2.082
N(1)–N(2)	1.3723(11)	1.380(2)
N(2)–B(1)	1.4186(13)	1.407(3)
B(1)–O(1)	1.3794(12)	
B(1)–O(2)	1.3798(12)	
B(1)–C(18)		1.577(3)
B(1)–C(14)		1.583(3)
N(1)–Ti(1)–Cp$_{cent}$	124.77	124.89
N(3)–Ti(1)–Cp$_{cent}$	119.70	116.94
N(4)–Ti(1)–Cp$_{cent}$	121.47	117.16
Ti(1)–N(1)–N(2)	168.09(6)	172.82(14)
N(1)–N(2)–B(1)	119.69(8)	122.67(16)
N(1)–N(2)–C(1)	118.30(7)	113.55(15)
C(1)–N(2)–B(1)	119.69(8)	123.44(16)

Compound **8** and **9** feature three-legged piano stool geometry around titanium. The average Ti=Nα distance of **8** and **9** is *ca.* 1.727(2) Å which is shorter compared to that of the starting Cp*Ti{MeC(N^{i}Pr)$_2$}(NNCPh$_2$) (**1.40**) (1.751(2) Å). In **1.40**, a detailed DFT analysis suggests that the longer Ti=Nα is due to an antibonding interaction between the π_h-type Ti=Nα bonding orbital and the Nβ=CPh$_2$ π-bonding orbital which is not present in the products **8** and **9**. In comparison the Nα–Nβ distances are shorter than in **1.40** (1.329(2) Å) for both **8** and **9**.

The sums of the N(1)–N(2)–R angles (360.0(2) and 359.7(5) °) reveal effectively planar geometry at the N(2) atom. The N(2)–B(1) bond length are comparable but that of **8** is marginally shorter because of competing π-donation from the Pin O atoms, consistent with a single bond but significant donation *via* $N_{2p}\rightarrow B_{2p}$ π-interactions.[27]

Low temperature NMR studies were performed with the hope of finding an hydride-alkylidene hydrazide(1–) intermediate analogous to that found by Bergman.[34] Unfortunately, when reactions of Cp*Ti{MeC(N^{i}Pr)$_2$}(NNCPh$_2$) (**1.40**) with either HBPin or 9-BBN were monitored starting from 243 K and warming up to 298 K no intermediates were observed. Reaction of **1.40** with H_2BTex yielded an analogous product, namely **6** (Equation 3.7), isolated in 70% yield as yellow oil and characterized by NMR and elemental analysis. Compound **7** was fully characterized by NMR and IR spectroscopy. As for the reactions of Cp*Ti{MeC(N^{i}Pr)$_2$}(NTol) (**3.1**) DFT evidence of the proposed structure will be presented in the next Section. Interestingly the reaction of Cp*Ti{MeC(N^{i}Pr)$_2$}(NNCPh$_2$) (**1.40**) with HB(C$_6$F$_5$)$_2$ showed three intermediates along the reaction pathway (Scheme 3.3).

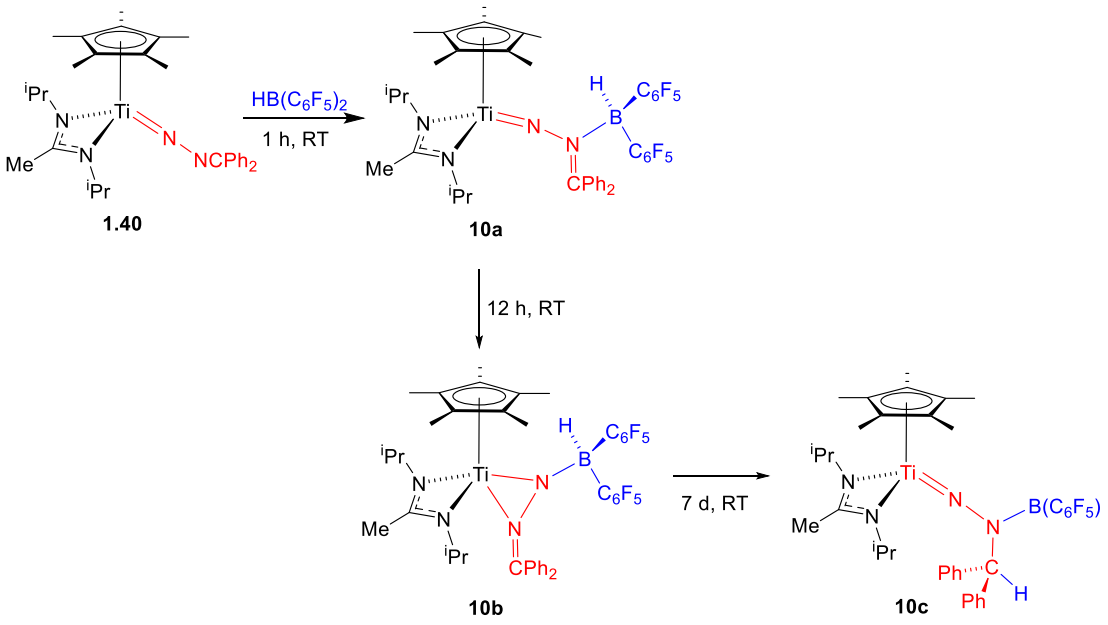

Scheme 3.3. Reaction products of Cp*Ti{MeC(N^{i}Pr)$_2$}(NNCPh$_2$) (**1.40**) and HB(C$_6$F$_5$)$_2$.

On the NMR tube scale the reaction proceeds *via* an adduct on the Nβ first (1 h, RT), namely Cp*Ti{MeC(N^{i}Pr)$_2$}{NNHB(C$_6$F$_5$)$_2$CPh$_2$} (**10a**) which was fully characterized on the NMR scale after 1 h at 0 °C in toluene-*d*$_8$ and by means of IR spectroscopy. This labile compound quickly converts to an adduct on Nα, namely

$Cp^*Ti\{MeC(N^iPr)_2\}\{NHB(C_6F_5)_2NCPh_2\}$ (**10b**) which is analogous to those observed for all the reactions of $Cp^*Ti\{MeC(N^iPr)_2\}(NTol)$ (**3.1**) with boranes, reported in Section 3.5. **10b** was successfully isolated as orange oil in 62% yield and characterized by IR, NMR and elemental analysis. Only after 7/8 days at RT the product of 1,2 B–H addition across the N_β=CPh_2 bond, $Cp^*Ti\{MeC(N^iPr)_2\}\{NNB(C_6F_5)_2CHPh_2\}$ (**10c**), characterized by diagnostic $CHPh_2$ resonances at 6.15 and 77.1 ppm in the ^1H and ^{13}C NMR respectively, along with undefined decomposition products, was observed. Unfortunately, due to a high percentage of decomposition it was not possible to isolate **10c**.

The connectivity of the proposed adducts, **10a** and **10b** was confirmed *via* HOESY NMR (^1H–^{19}F), infrared spectroscopy ν(B–H) bonds and with the aid of DFT calculations, described in the next Section. The absence of any ν(Ti–H) bonds in the IR spectrum for both **10a** and **10b** is evidence that the B–H bond is still intact. This was further supported by the lack of Ti–H in the ^1H NMR (Figure 3.8, compound **10b**). The ^{11}B NMR does not show resolved coupling with ^1H in both complexes. Bands at 2591 cm^{-1} in the IR spectrum of **10a** and at 1945 cm^{-1} in that of **10b** were instead observed, in line with a possible B–H bond. The ^{11}B NMR chemical shifts were -8.54 and -9.72 ppm for **10a** and **10b** respectively, evidence of tetracoordinated boron atoms.

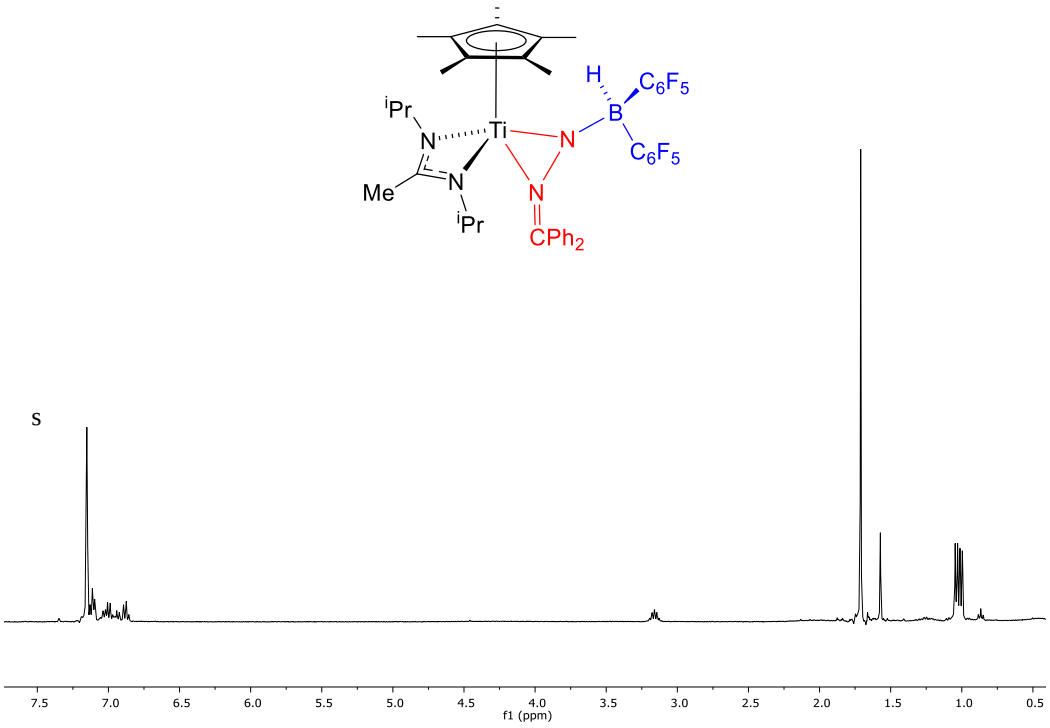

Figure 3.8. ^1H NMR spectrum (400.1 MHz) of $Cp^*Ti\{MeC(N^iPr)_2\}\{NHB(C_6F_5)_2NCPh_2\}$ (**10b**) in C_6D_6 at 298.15 K. Residual protio-solvent is labelled 's'.

3.7 Computational studies on Cp*Ti{MeC(N^{i}Pr$_2$)$_2$}(NNCPh$_2$) (1.40)

As further evidence for the proposed adducts **10a** and **10b** DFT studies were performed for the reactions of **1.40** with HBPin, 9-BBN and HB(C$_6$F$_5$)$_2$. The computational methodology used is the same as described in Section 3.5. Firstly, the Gibbs free energies (including solvent and dispersion interactions) of the experimental and hypothetical compounds **10a**, **10b**, **10a_HBPin**, **10b_HBPin**, **10a_9-BBN**, **10b_9-BBN**, **8**, **9** and **10c** were computed. It was experimentally found that, for reactions of **1.40** with either HBPin or 9-BBN, no adduct was detected, even when starting at low temperature. The Gibbs free energies reported in Table 3.4 are in line with the experimental results. All the values are referenced to Cp*Ti{MeC(N^{i}Pr)$_2$}(NNCPh$_2$) (**1.40**) which was set as the zero of energy. As reported before for reactions of **3.1** with boranes, the contribution of the dissociation of boranes from dimer to monomer must be taken into account for 9-BBN and HB(C$_6$F$_5$)$_2$ (Table 3.4). HBPin is a monomer in solution instead.

Table 3.4. SCRF solvent Gibbs free energy values (benzene at RT) for the reactions of **1.40** with boranes, at 298.15 K.

	$\Delta_r G$ (kcal mol^{-1})
0.5 9-BBN$_{dimer}$ → 9-BBN$_{monomer}$	10.0
0.5 HB(C$_6$F$_5$)$_{2dimer}$ → HB(C$_6$F$_5$)$_{2monomer}$	10.6
1.40 + HBPin$_{monomer}$ → **10a_HBPin**	16.1
1.40 + 9-BBN$_{monomer}$ → **10a_9-BBN**	-4.2
1.40 + HB(C$_6$F$_5$)$_{2monomer}$ → **10a**	-17.6
1.40 + HBPin$_{monomer}$ → **10b_HBPin**	2.6
1.40 + 9-BBN$_{monomer}$ → **10b_9-BBN**	-11.6
1.40 + HB(C$_6$F$_5$)$_{2monomer}$ → **10b**	-17.7
1.40 + HBPin$_{monomer}$ → **8**	-15.9
1.40 + 9-BBN$_{monomer}$ → **9**	-29.4
1.40 + HB(C$_6$F$_5$)$_{2monomer}$ → **10c**	-27.1
1.40 + 0.5 9-BBN$_{dimer}$ → **10a_9-BBN**	5.8
1.40 + 0.5 HB(C$_6$F$_5$)$_{2dimer}$ → **10a**	-7.0
1.40 + 0.5 9-BBN$_{dimer}$ → **10b_9-BBN**	-1.6
1.40 + 0.5 HB(C$_6$F$_5$)$_{2dimer}$ → **10b**	-7.1
1.40 + 0.5 9-BBN$_{dimer}$ → **9**	-19.6
1.40 + 0.5 HB(C$_6$F$_5$)$_{2dimer}$ → **10c**	-15.5

As reported in Table 3.4 the reactions to the final 1,2 B–H addition products for all the boranes, even without taking into account the additional energetic expense to dissociate the borane dimers. When considering the formation of the two adducts it is clear that reactions of **1.40** and HB(C$_6$F$_5$)$_2$ leading to **10b** is exergonic in line with **10b** being more stable than **10a**, as is experimentally observed. The DFT structures for **10a** and **10b** are shown in Figure 3.9. These were computed on the basis of the HOESY NMR (^{1}H–^{19}F) and IR experimental results. In particular, **10a** was found to be a B–H adduct with B connected to the N$_\beta$ atom, where there is interaction through space between the phenyl ring in **1.40** (NNCPh$_2$ group) and an aromatic ring of HB(C$_6$F$_5$)$_2$. The average interplanar spacing between the two rings is ca. 3.35 Å (range 2.8 to 3.5 Å). The arene–perfluoroarene interaction has been known for over 40 years, and has been shown to occur in numerous 1:1 complexes of arenes and fluoroarenes.[35]

The IR frequency at 2591 cm^{-1} suggested that the B–H bond is intact with no significant elongation thus possibly without any coordination of B–H to $N\beta=\underline{C}Ph_2$. For comparison, the computed B–H frequencies were 2459 and 2589 cm^{-1} in $HB(C_6F_5)_{2dimer}$ and $HB(C_6F_5)_{2monomer}$ respectively. The computed structure of **10a** reflects these results, and displays a ν(B–H) bond frequency of 2468 cm^{-1}. In addition all the H–F distances are in line with the NMR data. Compound **10b** was found to be a B–H adduct with B connected to the $N\alpha$ atom and possibly the B–$\underline{H}$ to titanium, as suggested by the ν(B–H) bond frequency at 1945 cm^{-1}. The computed structure of **10b** displays a ν(B–H) bond frequency of 1915 cm^{-1}. It is important to note that, due to the lack of experimental evidence, the structures of the aforementioned adducts are hypothetical. The same adducts were computed for HBPin and 9-BBN on the assumption of a similar geometry.

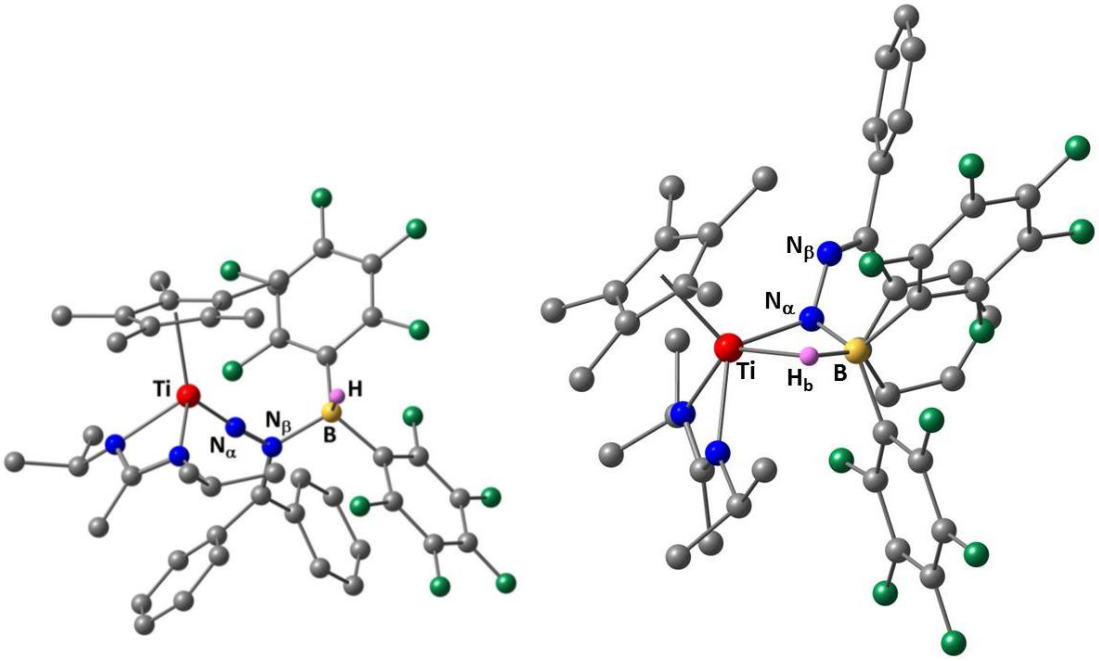

Figure 3.9. DFT gas phase optimized structures of Cp*Ti{MeC(N^{i}Pr)$_2$}{NNHB(C$_6$F$_5$)$_2$CPh$_2$} (**10a**, left) and Cp*Ti{MeC(N^{i}Pr)$_2$}{NHB(C$_6$F$_5$)$_2$NCPh$_2$} (**10b**, right). C-bound H atoms omitted. Selected distances (Å) for **10a**: Ti–N$_\alpha$ 1.732, N$_\alpha$–N$_\beta$ 1.318, N$_\beta$–B 1.607, B–H 1.219; for **10b**: Ti–H$_b$ 1.940, Ti–N$_\alpha$ 1.785, N$_\alpha$–N$_\beta$ 1.351, N$_\alpha$–B 1.553, B–H$_b$ 1.295.

DFT attempts were performed in order to elucidate the mechanism for reactions of **1.40** with boranes. Based on the stability of the three products formed in the reaction of **1.40** with HB(C$_6$F$_5$)$_2$ it was assumed that the conversion of **10a** to **10b** is reversible. Initial formation of the most stable product, **10b**, is followed by a quick conversion to **10a**, which then undergoes a B–H activation reaction to give the final product **10c**.

3.8 Reactions of Cp*Ti{MeC(N^{i}Pr$_2$)$_2$}(NNMe$_2$) (1.39) and Cp*Ti{MeC(N^{i}Pr$_2$)$_2$}(NNPh$_2$) (1.38) with boranes

Following the successful outcome of Cp*Ti{MeC(N^{i}Pr$_2$)$_2$}(NTol) (**3.1**) and Cp*Ti{MeC(N^{i}Pr$_2$)$_2$}(NNCPh$_2$) (**1.40**), the reactivity of complexes Cp*Ti{MeC(N^{i}Pr$_2$)$_2$}(NNR$_2$) (R$_2$ = Me$_2$ (**1.39**) or Ph$_2$ (**1.38**)) was then explored. In this Section the reactions of the hydrazide complexes **1.38** and **1.39** with boranes will be presented. Kinetic studies were performed to elucidate the mechanism of reaction of **1.39**

with 9-BBN will then be discussed. Finally, DFT studies on the bonding, by means of Natural Bonding Orbitals (NBO) calculations and a proposed mechanism of reaction of **1.39** with 9-BBN will be illustrated.

3.8.1 Reactions with $HB(C_6F_5)_2$ and HBPin: experimental and computational results

Following initial screening NMR tube scale reactions of **1.38** and **1.39** with a series of boranes (Section 3.3), it was found that bulky Cp*Ti{MeC(N^{i}Pr$_2$)$_2$}(NNPh$_2$) (**1.38**) showed rather limited reactions whereas **1.39** gave clean products with HBPin, 9-BBN and $HB(C_6F_5)_2$ representing a spectrum of electron-deficiency at the boron atom. On the preparative scale, reactions of **1.39** with $HB(C_6F_5)_2$ and HBPin gave the analytically pure adduct Cp*Ti{MeC(N^{i}Pr$_2$)$_2$}(N(HB(C$_6$F$_5$)$_2$NMe$_2$) (**11**) and the borylhydrazido-hydride compound Cp*Ti{MeC(N^{i}Pr)$_2$}(H){N(BPin)NMe$_2$} (**12**) (Scheme 3.4) in 80% and 50% yield, respectively. Compound **11** was a red oil which could not be crystallized, whereas **12** gave green, diffraction-quality crystals (Figure 3.10).

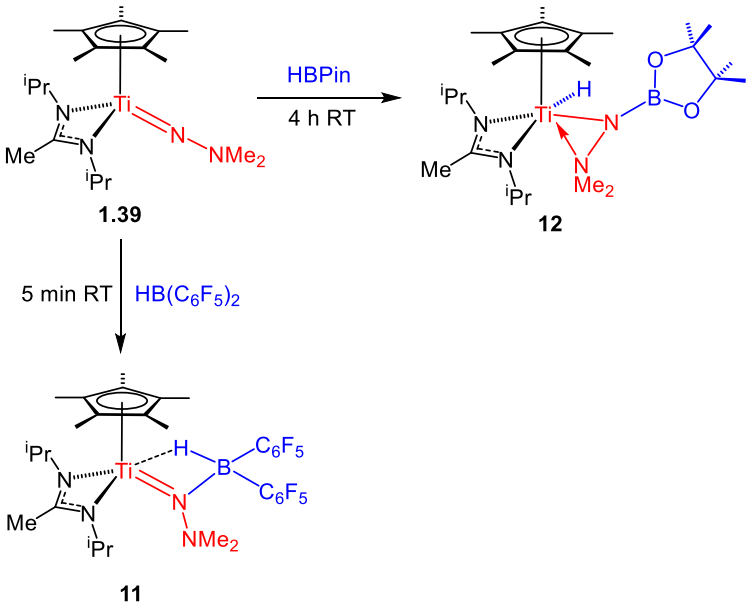

Scheme 3.4. Reactions of Cp*Ti{MeC(N^{i}Pr$_2$)$_2$}(NNMe$_2$) (**1.39**) with HBPin and $HB(C_6F_5)_2$.

Although compound **12** is stable for weeks both in solution and in the solid state at RT, upon heating to 70 ^{o}C in C_6D_6 decomposition occurs to a mixture of unidentified products. Compound **12** represents only the third fully authenticated B–H bond 1,2-addition product of a transition metal imide or hydrazide, the first being very recently reported for a rare terminal scandium imide[19] and the second for a thorium terminal imido

metallocene.[20] It was noted that **12** did not react further with HBPin or other boranes (*cf.* reaction with 9-BBN below).

The solid state structure of **12**, which confirms that depicted in Scheme 3.4, is shown in Figure 3.10, and selected bond lengths and angles are listed in Table 3.5.

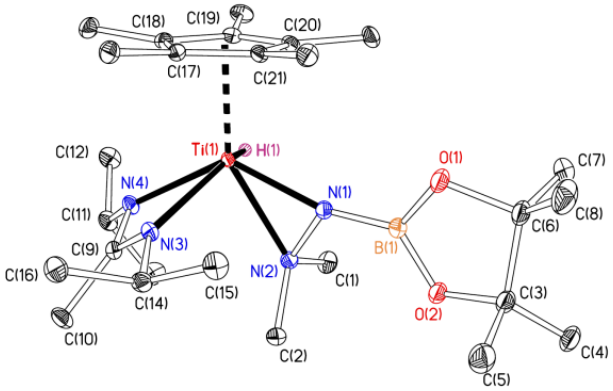

Figure 3.10. Displacement ellipsoid plot (25% probability) of Cp*Ti{MeC(N^{i}Pr)$_2$}(H)-{N(BPin)NMe$_2$}(**12**). C bound H atoms are omitted for clarity.

Table 3.5. Selected bond distances (Å) and angles (°) for Cp*Ti{MeC(N^{i}Pr)$_2$}(H){N(BPin)NMe$_2$} (**12**).

Parameter	**12**
Ti(1)–N(1)	1.9664(10)
Ti(1)–N(2)	2.2173(11)
Ti(1)–N(3)	2.1835(10)
Ti(1)–N(4)	2.1893(10)
Ti(1)–H(1)	1.701(19)
Ti(1)–Cp$_{cent}$	2.082
N(1)–N(2)	1.4399(14)
N(1)–B(1)	1.4183(17)
B(1)–O(1)	1.3817(17)
N(1)–Ti(1)–Cp$_{cent}$	114.83
N(3)–Ti(1)–Cp$_{cent}$	113.26
N(4)–Ti(1)–Cp$_{cent}$	116.67
Ti(1)–N(1)–N(2)	79.58(6)
N(2)–N(1)–B(1)	119.40(10)

The molecular structure confirms the 1,2-addition of B–H to Ti=Nα and reveal five-legged piano stool geometry. Figure 3.10 shows that N(1), N(3), N(4) and H(1) atoms in **12** are approximately co-planar. The new N(BPin)NMe$_2$ ligand is κ^2-coordinated as reported for the reactions of **1.39** with silanes.[15] The solution NMR data are consistent with this as shown by the inequivalent -NMeMe groups. The Ti(1)–N(1) and N(1)–N(2) distances of *ca.* 1.97 and 1.44 Å respectively are significantly lengthened compared to those of 1.723(3) and 1.386(2) Å in **1.39**. These values lie at the longer end of the ranges previously found for κ^2-coordinated hydrazido(1–) complexes (Ti–Nα: 1.832 - 2.005 (mean ca. 1.90) Å; Nα–Nβ: 1.236 - 1.458 (mean ca. 1.41) Å; 14 examples[27]) and are consistent with the disruption of the Ti–Nα triple bond and a change from *sp* hybridisation

for N(1) in **1.39** to sp^2 in **12**. This is confirmed by a N(2)–N(1)–B(1) angle of ca. 119 ° and a N(1)–B(1) bond distance of 1.4183(17) Å consistent with a single nitrogen boron bond. The ^{1}H NMR data confirm the presence of a Ti-H at 5.57 ppm along with inequivalent N(BPin)N$\underline{Me}_2$ groups. The Ti(1)–N(1) and N(1)–N(2) are in line with those previously reported for the analogous compound Cp*Ti{MeC(N^{i}Pr)$_2$}(H){N(PhSiH$_2$)NMe$_2$} (1.96(3) and 1.46(4) Å respectively). The N(1)–H(1) is instead slightly longer (1.701(19) *vs.* 1.64(4) Å).[15]

It was noted that HBPin did not react with Cp*Ti{MeC(N^{i}Pr$_2$)$_2$}(NTol) (**3.1**), contrary to the reaction of **3.1** with PhSiH$_3$, reflecting lower Lewis acidity (or hydridicity of H) of the B atom due to the presence of two oxygen atoms. DFT calculations were used to confirm that the κ^2-coordination of the N(BPin)NMe$_2$ ligand is a key element to stabilize the borylhydrazido-hydride product. The SCRF Gibbs free energies of the experimental and hypothetical hydrazido(1–) complexes with or without N$_\beta$ coordinated to titanium were indeed computed. The Gibbs free energy value of **12** was found to be -16.7 kcal mol^{-1} while that of the hypothetical product **12_Nbeta** without the N(BPin)NMe$_2$ ligand κ^2-coordination was -2.1 kcal mol^{-1}(values referenced to (**1.39** + HBPin), set at 0 kcal mol^{-1}).

The NMR and IR spectra of **11** indicate that in this case no B–H bond cleavage occurs. The NMR spectrum shows no Ti–H resonance and equivalent N$\underline{Me}_2$ groups (Figure 3.11). Moreover, the ν(B–H) mode in **11** appears at 1990 cm^{-1} in the IR spectrum, indicative of an elongation of B–H bonds, presumably because of the B–H coordination to the titanium atom.

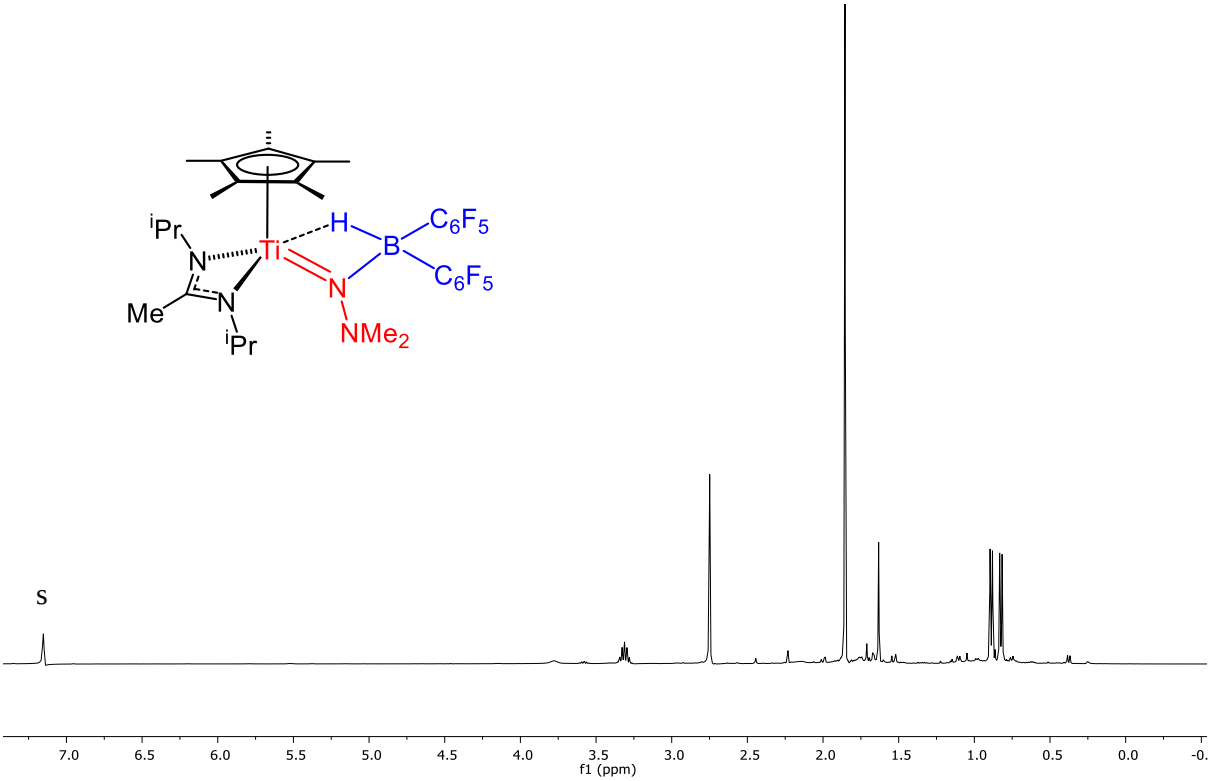

Figure 3.11. ^{1}H NMR spectrum (400.1 MHz) of Cp*Ti{MeC(N^{i}Pr$_2$)$_2$}(N(HB(C$_6$F$_5$)$_2$NMe$_2$) (**11**) in C$_6$D$_6$ at 298.15 K. Residual protio-solvent is labelled 's'.

Compound **11** is assigned the structure shown in Scheme 3.4, analogous to the reaction products previously found for the reaction of Cp*Ti{MeC(N^{i}Pr$_2$)$_2$}(NTol) (**3.1**) with boranes, namely B–H adducts with B coordinated to Nα. To rule out an alternative Nβ coordinated adduct, like the alkylation product [Cp*Ti{MeC(N^{i}Pr)$_2$}(NNMe$_2$Me)]$^{+}$ previously found in our research group and formed by reaction of **1.39** with MeI,[23] DFT calculations of the experimental product, **11**, and the hypothetical one, **11_Nbeta**, were performed (Figure 3.12). The most compelling evidence were the ν(B–H) frequency found to be 1912 cm^{-1} in **11** and 2412 cm^{-1} in **11_Nbeta**, which supported the proposed structure. Moreover, the Gibbs free energy (including solvent and dispersion interactions) of **11** was 11.3 kcal mol^{-1} lower than **11_Nbeta**, namely -29.9 kcal mol^{-1} *vs.* -18.6 kcal mol^{-1} for **11_Nbeta** (values referenced to **(1.39** + HB(C$_6$F$_5$)$_2$), set at 0.0 kcal mol^{-1}). The hypothetical product formed by B–H bond cleavage (the analogous **12**) has a G$_{rel}$ = -21.8 kcal mol^{-1}, confirming that the Nα adduct is the more thermodynamically stable product.

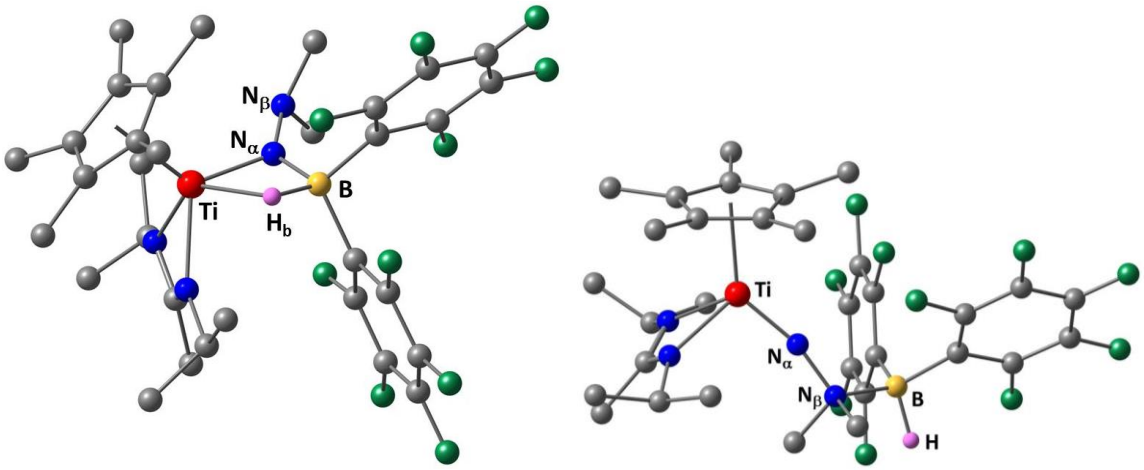

Figure 3.12. DFT optimized structures of Cp*Ti{MeC(N^{i}Pr)$_2$}{NBH(C$_6$F$_5$)$_2$NMe$_2$} (**11,** left) and Cp*Ti{MeC(N^{i}Pr)$_2$}{NNHB(C$_6$F$_5$)$_2$Me$_2$} (**11_Nbeta**, right*)*. C-bound H atoms omitted. Selected distances (Å) for **11**: Ti–H$_b$ 2.041, B–H$_b$ 1.291, Ti–N$_\alpha$ 1.850, N$_\alpha$–B 1.531, N$_\alpha$–N$_\beta$ 1.395; for **11_Nbeta**: Ti– N$_\alpha$ 1.721, N$_\beta$–B 1.671, B–H 1.216, N$_\alpha$–N$_\beta$ 1.407.

The highly symmetric spectrum presented in Figure 3.11 is indicative of a highly symmetric complex, where the Ti-N-B-H atoms lie in the vertical plane that bisects the Cp* ring, or of a fluxional complex. Based on the X-ray structure reported above for the reaction of Cp*Ti{MeC(N^{i}Pr)$_2$}(NTol) + HB(C$_6$F$_5$)$_2$, namely complex **2**, which is indicative of a non-symmetric complex, a fluxional complex was hypothesized. In addition to that, complex **2** also presents a highly symmetric ^{1}H NMR, again indicative of fluxionality or high symmetry. In this case, the ^{1}H NMR at low temperature (-80°C, in tol-d$_8$), shows significant broadening without spitting of the signals, however cooling was not sufficient to resolve the signals. Therefore, we decided to characterize complexes **2** and **11** at RT. Other examples of fluxionality of analogous compounds were reported in our group, namely for reactions of half-sandwich amidinate complexes with CO$_2$, which resulted in non-symmetric products that can undergo a low energy fluxional process, described as an interconversion of two enantiomeric forms.[36]

3.8.2 Reactions with 9-BBN

Reaction of either Cp*Ti{MeC(N^{i}Pr)$_2$}(NNMe$_2$) (**1.39**) or Cp*Ti{MeC(N^{i}Pr)$_2$}(NNPh$_2$) (**1.38**) with 0.5 equiv of 9-BBN dimer in C$_6$D$_6$ at RT or 60 °C respectively, gave *ca* 50% conversion of the titanium complex and all of the borane to a 1:1 mixture of two boron-

containing products as well as H_2 (as judged by a ^1H NMR singlet at 4.46 ppm) according to NMR spectroscopy. Scaling up the reaction of **1.39** with 1 equiv. of 9-BBN dimer gave quantitative conversion of both starting materials to the borylimide $Cp^*Ti\{MeC(N^iPr)_2\}(NBC_8H_{14})$ (**1**) and the aminoborane $Me_2NBC_8H_{14}$[37] which was separated from **1.39** by careful vacum sublimation (T = 90 °C, p = 10^{-5} mbar) affording **1** in 95% purity (Equation 3.9). Compound **1.38** also reacted quantitatively with 9-BBN dimer in C_6D_6 at 60 °C to form **1** and $Ph_2NBC_8H_{14}$[38] together with H_2. It was not possible to fully separate $Ph_2NBC_8H_{14}$ from **1** on scale-up. The lower volatility of the aminoborane led to longer sublimation times and/or higher temperatures, giving thermal degradation of **1**.

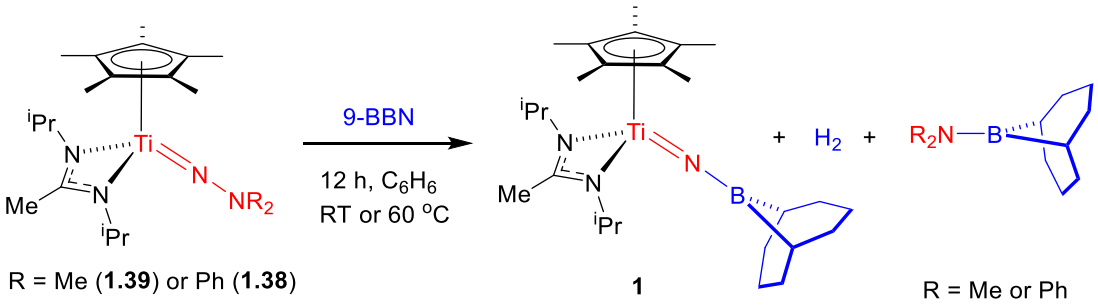

Equation 3.9

Hoping to obtain an easier separation of $Ph_2NBC_8H_{14}$ from the desired product, **1**, other starting hydrazido compounds with half-sandwich supporting ligands, were synthesised, namely Cp*Ti{PhC(N^{i}Pr)$_2$}(NNPh$_2$) (**13**) and Cp*Ti{MeC(NCy$_2$)$_2$}(NNPh$_2$) (**14**). However both compounds react in the same manner with 9-BBN and the separation of $Ph_2NBC_8H_{14}$ from the respective borylimido products, namely Cp*Ti{PhC(N^{i}Pr)$_2$}(NBC$_8$H$_{14}$) (**15**) and Cp*Ti{MeC(NCy)$_2$}(NBC$_8$H$_{14}$) (**16**) on scale-up was even more difficult.

The solid state structure of **1** is shown in Figure 3.13 and confirms the formation of the new borylimido ligand. Selected bond lengths and angles are listed in Table 3.6. Terminal transition metal borylimides are extremely rare and there are no established synthetic routes.[39–43] Only two examples have been reported for Group 4, both during the course of this Thesis, these being Mindiola's Ti(NBEt$_2$)(NTol$_2$){HC(C^{t}BuNDipp)$_2$} (Dipp = 2,6-C$_6$H$_3$^{i}Pr$_2$) (**1.88**) prepared from the corresponding parent imide (Ti=NH functional group) and 2 equivs. of NaHBEt$_3$, potentially *via* a nitrido intermediate[42] and the terminal borylimido complex, (PN)$_2$Ti=BCat (**1.89),** obtained via salt methathesis reaction of the titanium salt, [μ$_2$-K(OEt$_2$)]$_2$[(PN)$_2$Ti=N]$_2$ (PN = N-(2-(diisopropylphosphino)-4-methylphenyl)-2,4,6-trimethylanilide) and ClBcat (cat = catechol).[43] The Ti(1)–N(1) bond length of 1.731(3) Å in **1** is identical within error to the Ti=NR distances in the xylylimido analogue (1.738(2) Å) all of which have formal Ti≡N triple bonds ($\sigma^2\pi^4$). In addition, the N(1)–B(1) distance of 1.402(4) Å is typical of species of the type R$_2$N–BR'$_2$ which have significant N=B double bond character *via* $N_{2p}\rightarrow B_{2p}$ π-donation. The conversion of a terminal hydrazide to a borylimide is a previously unknown reaction. Mechanistically, based on the other observations reported above, namely the reaction of **1.39** with HBPin, it was proposed that this proceeds first of all *via* 1,2 B–H addition to Ti=Nα to form an intermediate analogous to Cp*Ti{MeC(N^{i}Pr)$_2$}(H){N(NMe$_2$)BPin}

(**12**). The reaction can be reversed starting from **1** and Ph_2NNH_2, reforming **1.38** and H_2N–BBN.[44]

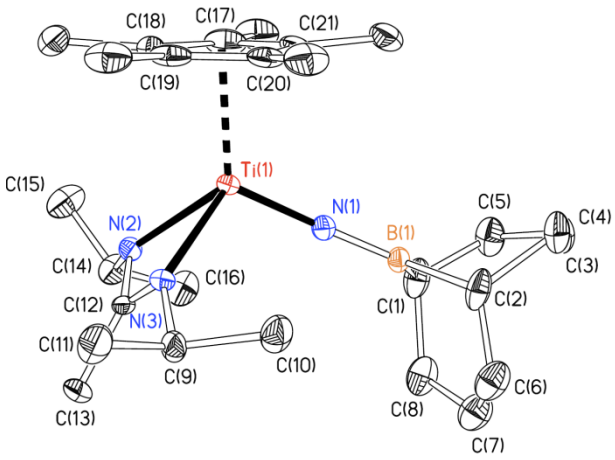

Figure 3.13. Displacement ellipsoid plot (20% probability) of Cp*Ti{MeC(N^iPr)$_2$}(NBC_8H_{14}) (**1**). H atoms are omitted for clarity.

Table 3.6. Selected bond distances (Å) and angles (°) for Cp*Ti{MeC(N^iPr)$_2$}(NBC_8H_{14}) (**1**).

Parameter	**1**
Ti(1)–N(1)	1.731(3)
Ti(1)–N(2)	2.091(4)
Ti(1)–N(3)	2.065(4)
$Ti(1)–Cp_{cent}$	2.070
N(1)–B(1)	1.402(4)
B(1)–C(1)	1.523(12)
B(1)–C(2)	1.580(8)
$N(1)–Ti(1)–Cp_{cent}$	118.94
$N(2)–Ti(1)–Cp_{cent}$	122.41
$N(3)–Ti(1)–Cp_{cent}$	122.26
Ti(1)–N(1)–B(1)	178.4(3)
N(2)–Ti(1)–N(1)	107.65(19)
N(3)–Ti(1)–N(1)	108.6(2)

Molecular orbital and NBO analyses[45] of the DFT structure of **1** support this interpretation by finding two Ti–N π-bonding interactions, one of which is significantly stabilized (π_v) by delocalization into the otherwise vacant 2p AO of B(1) oriented perpendicular to the N(1)-B(1)-C(1)-C(2) plane (Figure 3.14).

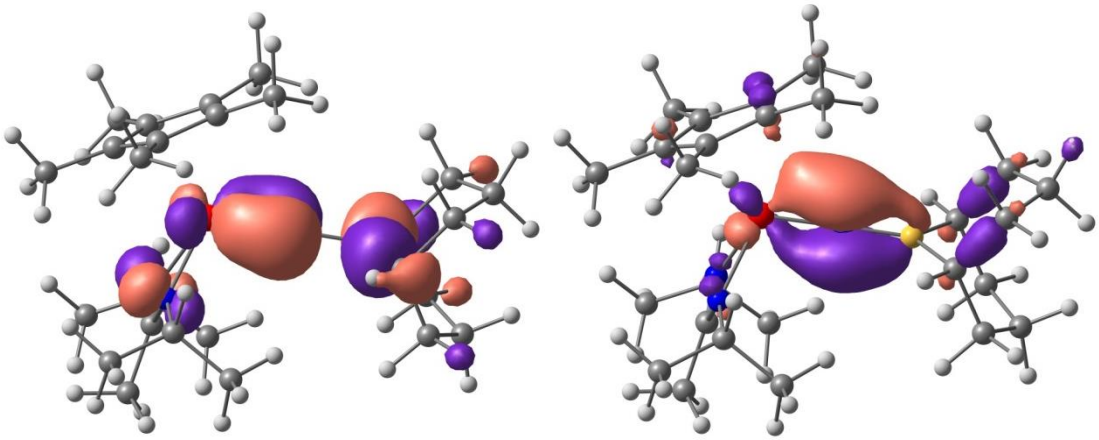

Figure 3.14. Isosurfaces and energies of frontier molecular orbitals in Cp*Ti{MeC(NMe)$_2$}(NBC$_8$H$_{14}$) (**1**).

As further confirmation, a Natural Bonding Orbital (NBO) analysis was performed. NBO are an useful tool to create effective atomic orbitals for each atom in the molecule environment and examine the bonding from a "Lewis-like" perspective. The delocalization of NBOs creates Natural Localized Molecular Orbitals (NLMOs), which are defined as the least delocalized orbitals in the molecule, unitary equivalent to Canonical Molecular Orbitals.[45] The Ti–N bond is formed by one σ and two π components. NLMOs associated to the triple Ti–Nα bond as deduced from the NBO analysis show that π_2(Ti–Nα) has a significant delocalization toward the boron atom (Figure 3.15).

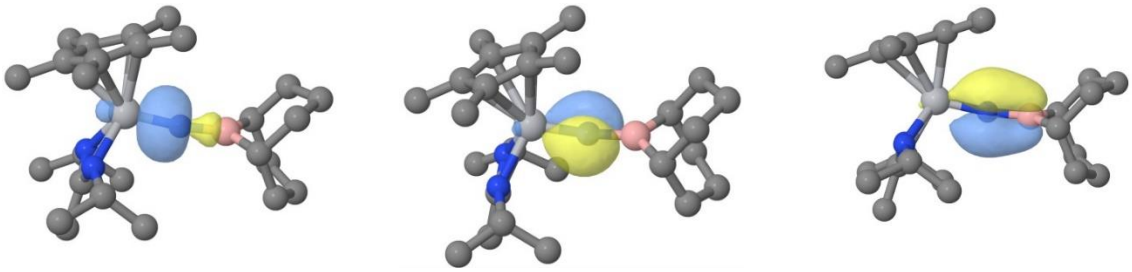

σ(Ti-Nα) π_1(Ti-Nα) π_2(Ti-Nα)

Figure 3.15. NLMO (Natural Localized Molecular Orbital) associated with the triple Ti–Nα bond as deduced from the NBO analysis. H atoms have been omitted for clarity.

A detailed Molecular Orbital and NBO analysis, including a comparison with model imido and hydrazido half-sandwich titanium compounds, will be presented in the next Chapter. In order to understand the reaction mechanism, kinetic and computational studies were performed and will be discussed in the coming Section.

3.8.3 Studies of the formation of Cp*Ti{MeC(N^{i}Pr)$_2$}(NBC$_8$H$_{14}$) (1)

A series of NMR tube scale kinetic studies were next performed in order to understand the mechanism of formation of Cp*Ti{MeC(N^{i}Pr)$_2$}(NBC$_8$H$_{14}$) (**1**). As mentioned before, the stoichiometry required to fully convert **1.39** (or **1.38**) + 9-BBN dimer to **1** and Me$_2$NBC$_8$H$_{14}$ (or Ph$_2$NBC$_8$H$_{14}$) was 1:2 (Ti:B). When **1.39** (or **1.38**) was reacted with 0.5 equiv. of 9-BBN dimer at RT or 60 °C the reaction reached only 50% completion in terms of titanium. Mechanistically, based on the reaction of Ti(N$_2$N^{Me})(NNPh$_2$)(py) (**1.70**) and 9-BBN dimer discussed in Chapter 2, we initially proposed that reactions of **1.39** (**1.38**) and 9-BBN dimer proceed via 1,2 B–H addition to Ti=Nα to form an intermediate analogous to Cp*Ti{MeC(N^{i}Pr)$_2$}(H){N(BPin)NMe$_2$} (**12**) (labelled **1_Int1** in Scheme 3.5). Hydride transfer to the Nα atom and reductive Nα–Nβ bond cleavage would then form Cp*Ti{MeC(N^{i}Pr)$_2$}{N(H)BC$_8$H$_{14}$}(NR$_2$) (**1_Int2**), analogous to Ti(N$_2^{iPr}$N){N(H)BC$_8$H$_{14}$}(NPh$_2$) (**1.73**). Subsequent 1,2-elimination of R$_2$NH from **1_Int2** would form **1** and R$_2$NH. Finally R$_2$NH and 9-BBN would react to form H$_2$ and R$_2$NBC$_8$H$_{14}$.

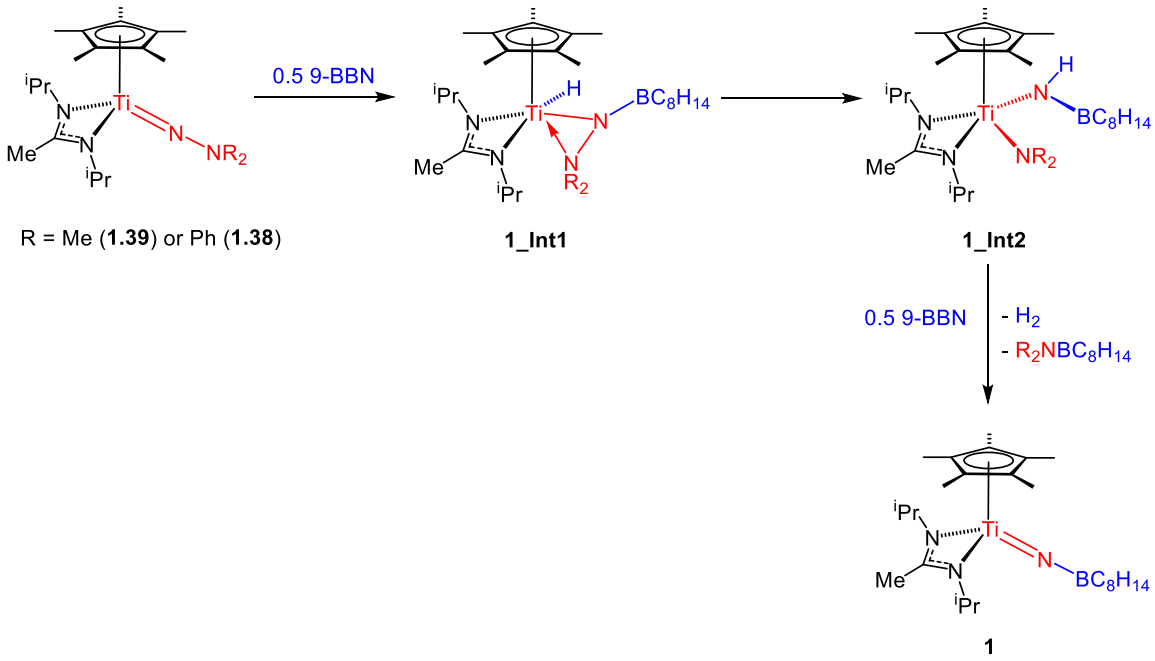

Scheme 3.5. Proposed reaction mechanism for Cp*Ti{MeC(N^{i}Pr)$_2$}(NNR$_2$) (R$_2$ = Me$_2$ (**1.39**) or Ph$_2$ (**1.38**)) + 9-BBN dimer.

Firstly, a series of experiments were performed to test the proposed mechanism. Secondly, DFT calculations were used to elucidate this and other potential reaction pathways.

Experimentally, the reaction of Cp*Ti{MeC(N^{i}Pr)$_2$}(NNMe$_2$) (**1.39**) and 9-BBN dimer (1:1 ratio) in C_6D_6 at room temperature was monitored by ^{1}H NMR spectroscopy and the evolution of **1** measured by integration over a period of time. It was observed that H_2 elimination was concerted to formation of **1** and $Me_2NBC_8H_{14}$, as opposed to Me_2NH elimination followed by off-metal reaction with 0.5 equiv. of 9-BBN dimer. This was confirmed by the absence of any resonance associated with free Me_2NH at RT during the course of the reaction. The same results were observed for reaction of **1.38** + 9-BBN at 60 °C. A control reaction was then performed, where Cp*Ti{MeC(N^{i}Pr)$_2$}(NBC$_8$H$_{14}$) (**1**) was reacted with Ph_2NH and 0.5 equiv. of 9-BBN dimer. It was observed that the reaction was only complete in 48 h at 60 °C and quantitatively formed $Ph_2NBC_8H_{14}$ and H_2. As the reaction time was longer than that to fully convert **1.38** + 9-BBN dimer (16 h, 60 °C) this ruled out any mechanism not involving concerted formation of Cp*Ti{MeC(N^{i}Pr)$_2$}(NBC$_8$H$_{14}$) (**1**), $Ph_2NBC_8H_{14}$ and H_2. DFT evidence reported later in this Section will support this hypothesis.

Low temperature experiments were then performed for Cp*Ti{MeC(N^{i}Pr)$_2$}(NNMe$_2$) (**1.38**) + 9-BBN dimer. The reaction between **1.39** and 9-BBN dimer (1:1 ratio) in toluene-d_8 at 273 K was monitored by ^{1}H NMR spectroscopy and the evolution of **1** measured by integration over a period of time. The ^{1}H NMR spectrum shows 90% conversion of **1.39** + 9-BBN to an intermediate proposed to be **1_Int1** (Scheme 3.5) which was characterized on the NMR scale in toluene-d_8 at 273 K. Attempts to fully isolate this intermediate were unsuccessful due to its instability under vacuum. Nonetheless, a series of experimental evidence was obtained. The ^{1}H NMR spectrum in C_6D_6 shows a diagnostic Ti–H resonance at 6.25 ppm (Figure 3.17), while the ^{11}B shift is at 28 ppm. Upon formation of **1_Int1**, free 9-BBN was still present in solution, as confirmation that **1_Int1** has no further molecules of borane coordinated to it. DFT calculations confirmed a ^{11}B chemical shift at 32 ppm for the suggested intermediate. The DFT gas phase optimized structure is shown in Figure 3.16.

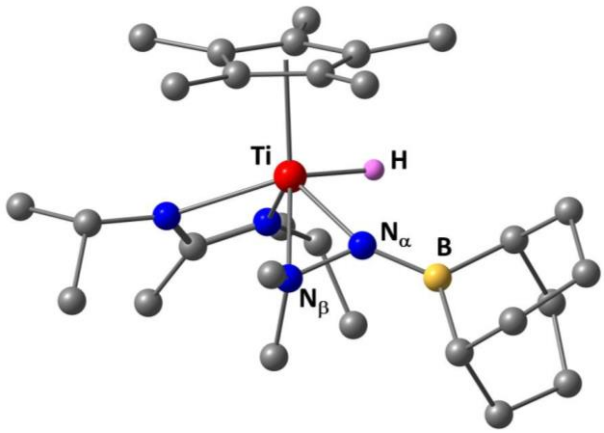

Figure 3.16. DFT gas phase optimized structure of Cp*Ti{MeC(N^{i}Pr)$_2$}(H){N(BPin)NMe$_2$} (**1_Int1**).C-bound H atoms omitted. Selected distances (Å): Ti–H 1.660, Ti–N$_\alpha$ 1.956, N$_\alpha$–N$_\beta$ 1.416, B–N$_\alpha$ 1.400.

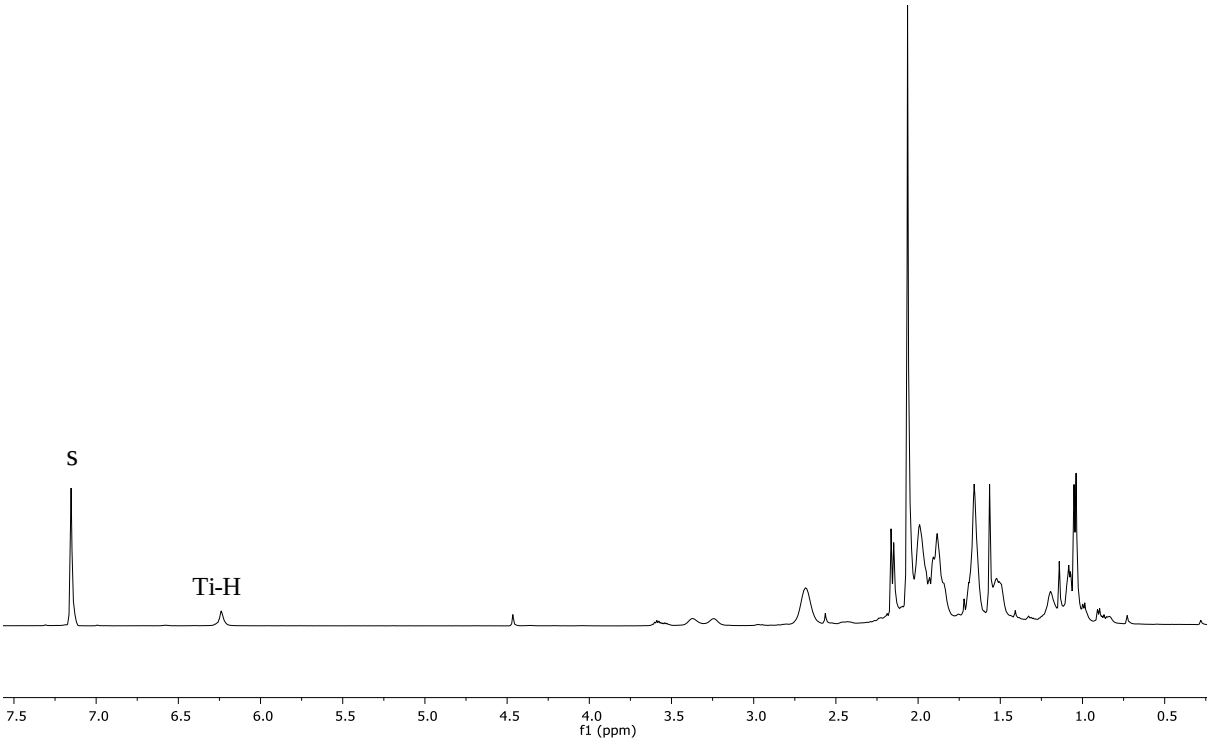

Figure 3.17. ^{1}H NMR spectrum (400.1 MHz) of **1_Int1** in C_6D_6 at 278 K. Residual protio-solvent labelled 's'.

Warming the NMR sample after 1h at 298 K results in the disappearing of **1_Int** + 9-BBN and the formation of Cp*Ti{MeC($N^{i}Pr$)$_2$}(NBC_8H_{14}) (**1**), H_2 and $Me_2NBC_8H_{14}$. For Cp*Ti{MeC($N^{i}Pr$)$_2$}($NNPh_2$) (**1.38**) no reaction was observed at RT, while on heating no intermediate was detected in solution. The reaction can be thus simplified in three subsequent steps as depicted in Scheme 3.6.

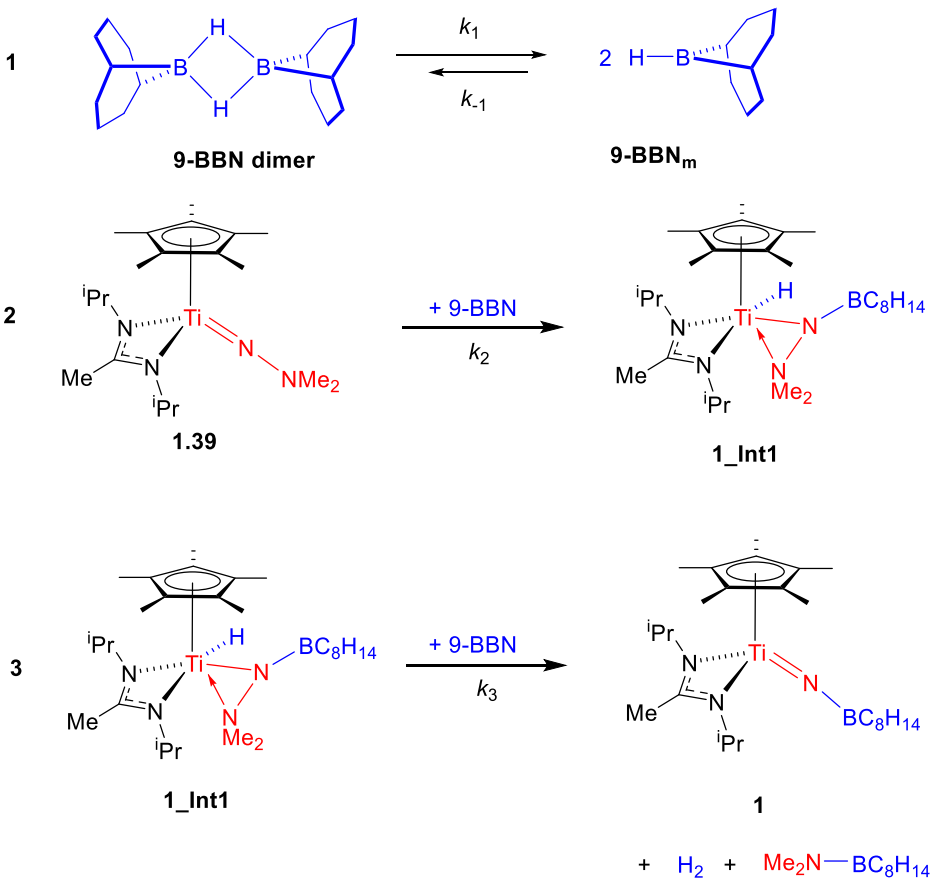

Scheme 3.6. Steps in the reaction of Cp*Ti{MeC(N^{i}Pr)$_2$}(NNMe$_2$) (**1.39**) with 1 equiv. of 9-BBN dimer.

Given that after 1 h at RT **1.39** was 90% converted to **1_Int1** the first two steps, namely 9-BBN dissociation from dimer to monomer (Step **1** in Scheme 3.6) and reaction of **1.39** with 9-BBN to form **1_Int** (Step **2** in Scheme 3.6) were studied together and independently from the last step (Figure 3.18). The conversion of **1_Int** to **1** was then explored.

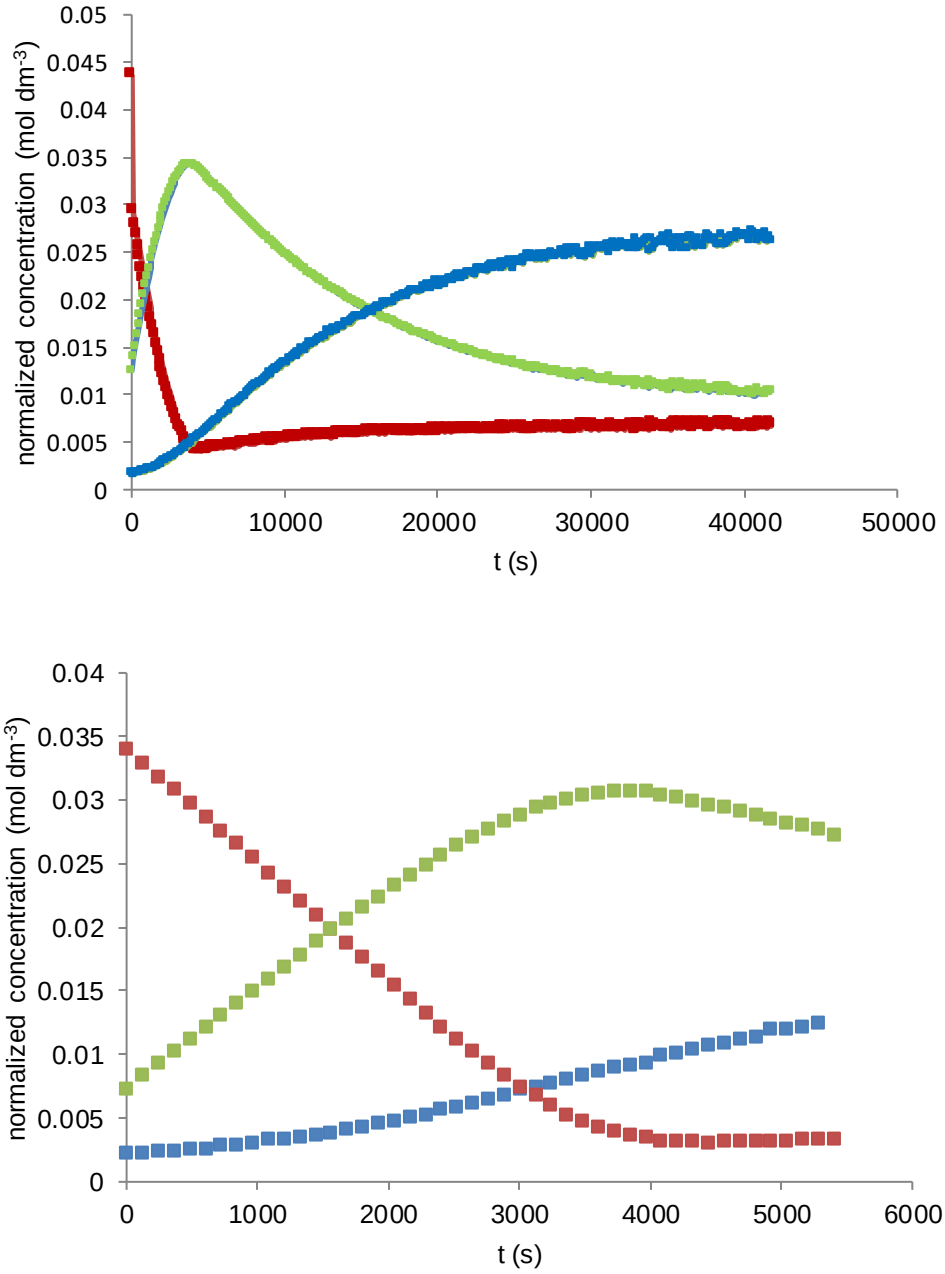

Figure 3.18. Decay of Cp*Ti{MeC(N^{i}Pr)$_2$}(NNMe$_2$) (**1.39**, red), formation of **1_Int1** (green) and growth of **1** (blue) at 273 K (top) and at RT in C_6D_6 (bottom), for the early stages of formation of **1**.

As already explained in Chapter 2, the two steps of the reaction can be modelled by using the same methodology established for hydroboration of alkenes, reported in literature as outlined below.[46–48]

$$\text{Rate} = \frac{k_1 k_2[\mathbf{1.39}][\text{9-BBN dimer}]}{k_{-1}[\text{9-BBN}] + 0.5\, k_2[\mathbf{1.39}]} \quad (3.10)$$

$$\text{Rate} = 2\, k_1[\text{9-BBN dimer}] \quad (\text{if } k_{-1}[\text{9-BBN}] << k_2[\mathbf{1.39}]) \quad (3.11)$$

$$\text{Rate} = \left[\frac{k_1}{k_{-1}}\right]^{1/2} k_2[\mathbf{1.39}][\text{9-BBN dimer}]^{1/2} \quad (\text{if } k_{-1}[\text{9-BBN}] >> k_2[\mathbf{1.39}]) \quad (3.12)$$

Full derivation of Equations 3.10 – 3.12 is given in the Appendix. As in the hydroboration chemistry, reactions with reactive alkenes demonstrate a first-order dependence on 9-BBN dimer due to rate-limiting dimer dissociation. In comparison, hydroboration with unreactive alkenes demonstrate a half-order dependence on 9-BBN due to a rate limiting B–H addition. For this chemistry the steady-state approximation to 9-BBN monomer leads to the rate equation shown in Equation 3.10. This approximation is valid because the rate of formation and the rate of consumption of 9-BBN monomer can be considered equal. The approximation k_{-1}[9-BBN] << k_2[**1.39**] can be applied when the k_2 step is fast. This leads to the equation shown in Equation 3.11 and the rate will show a first-order dependence on 9-BBN dimer. Alternatively, if the k_2 step is slower than 9-BBN dimer formation, the rate equation can be written as shown in Equation 3.12. It is important to point out that the apparent rate constant k_2 is used to denote all the reaction steps in the reaction of **1.39** with 9-BBN monomer to form **1_Int1**. This is of course a simplification.

Therefore, by establishing the dependence of the rate on 9-BBN dimer concentration, at constant titanium concentration, it should be possible to determine whether 9-BBN dimer dissociation or hydride-transfer is the rate limiting step. To establish the order of a reaction two methods could be potentially used, the pseudo-first order conditions and the initial rates, as explained in Chapter 2. However, due to solubility issues the pseudo order conditions cannot be performed when an excess of 9-BBN dimer is present in this reaction. The initial rates instead can provide an accurate description. The initial rates method was used to effectively calculate the rate of the starting material consumption, d[**1.39**]/dt at time = 0. Previous work in our group has successfully used this method to analyse the kinetics of the catalytic diamination of hydrazines with internal alkynes with

amide supported titanium compounds.[49] The initial rates method involves repeating the same experiment several times, using a different initial concentration of one reactant, and keeping all other reactant concentrations (and temperature) the same in each experiment. In this case, the method has been applied for **1_Int1** formation by varying either [9-BBN] or [**1.39**]. The graph of [**1_Int**] *vs.* time for the stoichiometric reaction at 298.15 K in C_6D_6 gave the non-linear plot shown in Figure 3.19. Graphical software (Origin) was used to fit a curve to all of the data points, thus describing the evolution of product throughout the kinetic study (Equation 3.13, 'y_0', 'A_1' and 'B_1' are empirical constants). The curve was then differentiated to obtain an equation for the gradient, and the gradient calculated at time = 0 s (Equation 3.14). This allows the initial rate of reaction to be calculated (Figure 3.19, stoichiometry 1:1, [**1.39**]:[9-BBN dimer]). The initial rates method is accurate when the reaction is relatively slow.

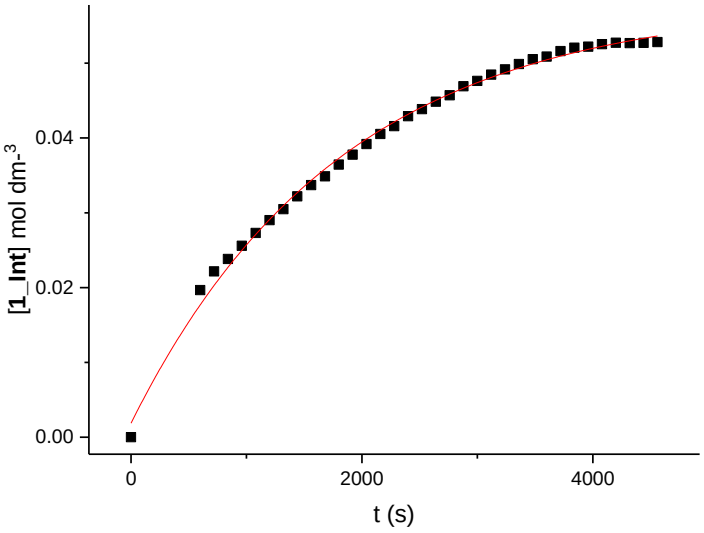

Figure 3.19. Plot of Cp*Ti(H){MeC(N^{i}Pr)$_2$}(N(NMe$_2$)BC$_8$H$_{14}$) ([**1_Int1**]) *vs.* time plotted in Origin for a 1:1 stoichiometry [**1.39**]:[9-BBN dimer] at RT in C_6D_6. The best-fit line (r^2 = 0.98198) shown gave A_1 = -0.0563(6), B_1 = 1818(61) giving an initial rate of 3.1 (1) x 10^{-5} mol dm^{-3} s^{-1}.

$$[\mathbf{1_Int}] = y_0 + A_1 e^{t/B_1} \qquad (3.13)$$

$$\frac{d[\mathbf{1_Int}]}{dt} = \frac{A_1 e^{t/B_1}}{B_1} \qquad \left(\frac{d[\mathbf{1_Int}]}{dt}\right)_{t=0} = \frac{A_1}{B_1} \qquad (3.14)$$

When the concentration of 9-BBN dimer was kept constant and **1.39** was varied, zero order dependence was observed on titanium, in line with Equation 3.11. When the reaction between **1.39** and 9-BBN dimer (0.5, 1, 1.5 and 2 equiv. of 9-BBN dimer, 0.022 - 0.087 mol dm^{-3}, Figure A1, Appendix) was monitored at 298.15 K in C_6D_6 the evolution of **1_Int1** followed a similar behaviour as detailed above and therefore initial rates in each case were obtained using the initial rates method (initial rate = 2.6(1) x 10^{-5}, 3.1(1) x 10^{-5}, 4.9(4) x 10^{-5} and 7.4(4) mol dm^{-3} s^{-1} for 0.5, 1, 1.5 and 2 equivalents of 9-BBN dimer respectively). As shown in Figure 3.20, the initial rates scale linearly with $[\text{9-BBN dimer}]_0$ (top plot) consistent with Equation 3.11. Importantly the initial rates do not scale linearly with $[\text{9-BBN dimer}]_0^{0.5}$ and thus Equation 3.12 does not apply.

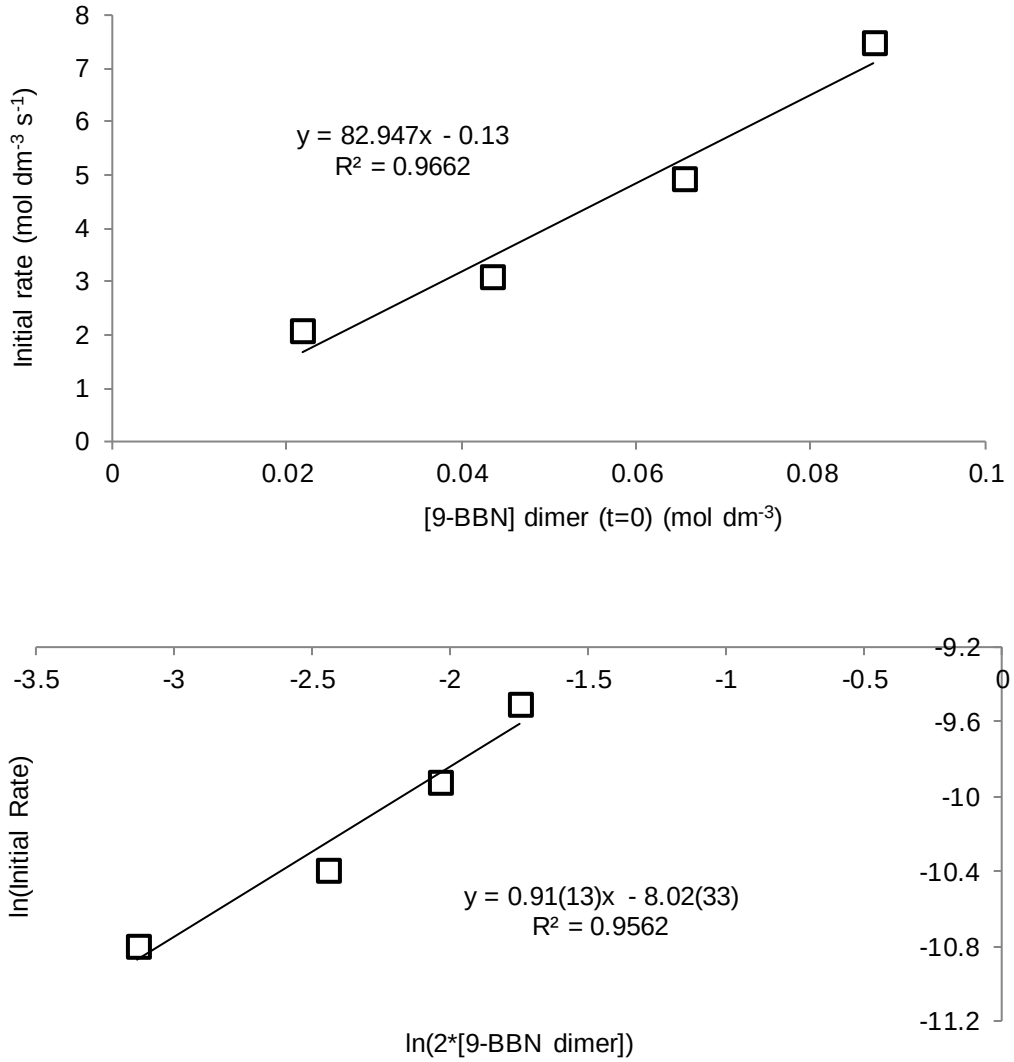

Figure 3.20. Top: Plot of initial rate vs. $[9\text{-BBN dimer}]_0$ for the reaction of **1.39** with 9-BBN dimer, R^2 = 0.980. Bottom: logarithmic plot of ln(Initial rate) *vs.* ln(2*[9-BBN dimer]), R^2 = 0.9562. Gradient of the slope = 0.91(13).

In order to obtain the exact order of the dependence on 9-BBN dimer concentration the logarithmic plot shown in Figure 3.20 was used (bottom plot). Both Equations 3.11 and 3.12 can be written in the general form shown in Equation 3.15 at constant Ti concentration. Therefore, the order of the reaction in 9-BBN dimer can be obtained from the gradient of the logarithmic plot (Equation 3.16).

As can be seen the gradient is close to one within error, also indicating a first-order dependence on 9-BBN dimer due to rate-limiting 9-BBN dimer dissociation, consistent with Equation 3.11.

$$\text{initial rate} = k_{obs}[\text{9-BBN dimer}]^n \quad (3.15)$$

$$\ln(\text{initial rate}) = n \ln([\text{9-BBN dimer}]) + \ln(k_{obs}) \quad (3.16)$$

From the intercept, k_1 was calculated to be 3.3(9) x 10^{-4}, which corresponds to a Gibbs free energy of activation of 22.2 kcal mol^{-1}. This value is in line with the experimental results reported in literature[47,50] for 9-BBN dissociation (k_1 = 1.5 x 10^{-4} s^{-1} and $\Delta G^{\ddagger}$ = 22.6 kcal mol^{-1}) and in line with the computed barriers (*vide infra*). Unfortunately, the third step of the reaction does not follow a simple rate equation thus it was not possible to perform an initial rate analysis. Even on the NMR scale reaction, formation of **1** in presence of an excess of 9-BBN dimer is associated with major unidentified decomposition products after the formation of **1_Int1**.

DFT calculations were next carried out in order to help elucidate the reaction mechanism and to fully understand why the reaction of **1.39** with HBPin stops at the borylhydrazido-hydride intermediate Cp*Ti{MeC(N^{i}Pr)$_2$}(H){N(BPin)NMe$_2$} (**12**), while reaction with 9-BBN proceeds to the borylimido compound Cp*Ti{MeC(N^{i}Pr)$_2$}(NBC$_8$H$_{14}$) (**1**) . Initially, a set of calculations were performed on the small model system CpTi{MeC(NMe)$_2$}(NNMe$_2$) (**1.39Q**), and replacing HBPin with HB(OMe)$_2$ and 9-BBN with HBMe$_2$. For simplicity in these model systems both boranes were considered to be monomers. Then the same calculations were performed on the real system to have a better description. The computational methodology has been described in Section 3.5. Initially, a mechanism identical to the one described for Ti(N$_2^{iPr}$N^{Me})(NNPh$_2$)(py) (**1.70**) and boranes, fully explained in Chapter 2, was postulated**.** Experimental evidence described in Section 3.8.3 ruled out this potential mechanism. DFT calculations are shown in Figure 3.21. All the Gibbs free energies reported are referenced to **1.39Q** which is set at 0.0 kcal mol^{-1}.

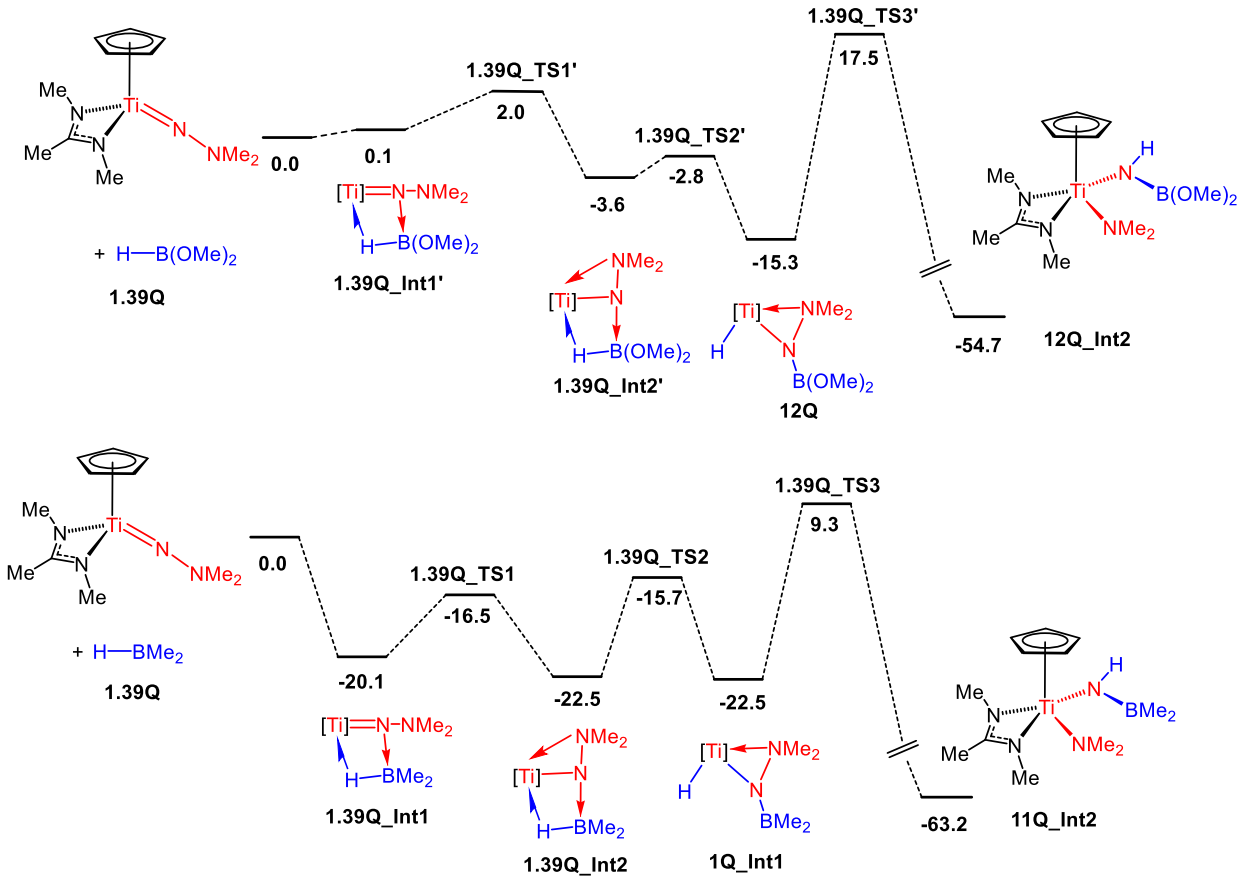

Figure 3.21. DFT mechanism (B3PW91, SCRF with a def2-tzvp basis set and including dispersion interactions) for the reaction of CpTi{MeC(NMe)$_2$}(NNMe$_2$) (**1.39Q**) with HB(OMe)$_2$ (*top*) and HBMe$_2$ (*bottom*) forming CpTi{MeC(NMe)$_2$}{N(H)BOMe$_2$}(NMe$_2$) (**12Q_Int2**) and CpTi{MeC(NMe)$_2$}{N(H)BMe$_2$}(NMe$_2$) (**1Q_Int2**) respectively. Gibbs free energies (kcal mol^{-1}, T = 298.15 K) for minima, maxima and transition states (labelled **1.39Q_TSx**) are shown in bold relative to **1.39Q** and HB(OMe)$_2$ (or HB(OMe)$_2$) respectively. [Ti] represents CpTi{MeC(NMe)$_2$}.

As can be seen, in both cases the RDS is associated with the final hydride transfer from the titanium atom in **1.39Q_Int1'** (or **1.39Q_Int1**) to N$_\alpha$ and a highly exergonic reductive N$_\alpha$–N$_\beta$ bond cleavage, to give **12Q_Int2** (or **11Q_Int2**) for HB(OMe)$_2$ (or HBMe$_2$). In both cases the barrier is high for reactions that proceed at RT, namely 32.8 kcal mol^{-1} and 29.8 kcal mol^{-1} for HB(OMe)$_2$ and HBMe$_2$. These values are in agreement with the experimental results reported above; reaction of **1.39** with HBPin gave the borylhydrazido-hydride product (**12Q**), while in reaction of **1.39** with 9-BBN dimer no free HNMe$_2$ was observed. In addition, this hypothetical pathway is unable to

discriminate between HBPin and 9-BBN, in disagreement with what was experimentally observed. For this reason other potential mechanisms for the reaction of **1.39Q** with $HBMe_2$ were tested. From the experimental details obtained it was clear that the reaction mechanism proceeds until the intermediate observed on the NMR scale **1_Int1** (model compound **1Q_Int1**, Figure 3.21). From this intermediate, it was hypothesized that the second molecule of borane ($HBMe_2$) could potentially coordinate to N_β *via* the B atom and release simultaneously H_2 and Me_2NBMe_2 to afford the final borylimido compound $CpTi\{MeC(NMe)_2\}(NBMe_2)$ (**1Q**). The potential mechanism is shown in Figure 3.22.

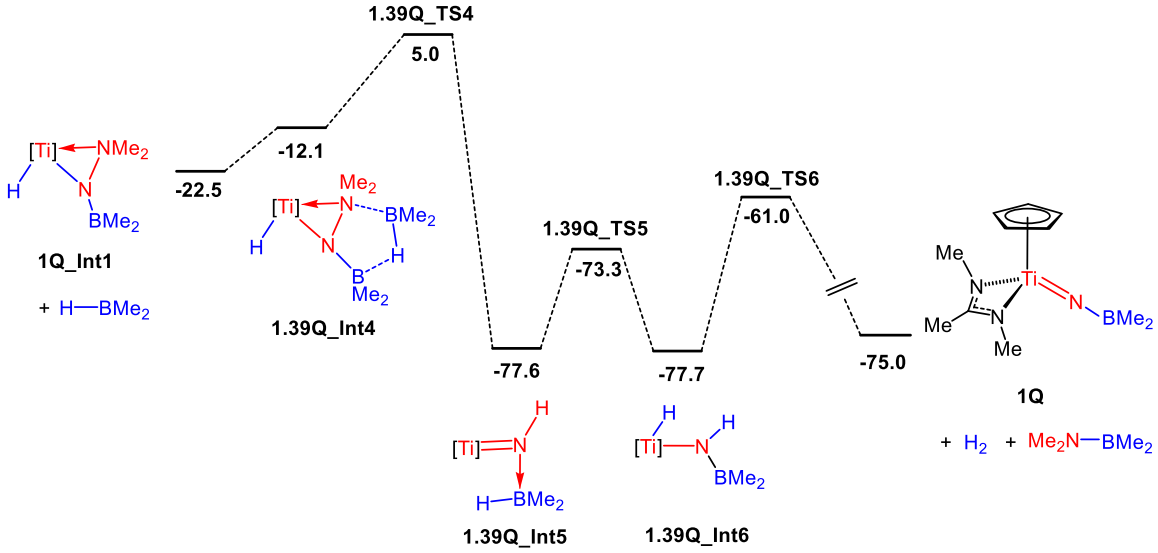

Figure 3.22. DFT mechanism (B3PW91, SCRF with a def2-tzvp basis set and including dispersion interactions) for the reaction of $CpTi\{MeC(NMe)_2\}(NNMe_2)$ (**1Q_Int1**) with a second molecule of $HBMe_2$ forming $CpTi\{MeC(NMe)_2\}\{NBMe_2\}$ (**1Q**), H_2 and Me_2NBMe_2. Gibbs free energies (kcal mol^{-1}, T = 298.15 K) for minima, maxima and transition states (labelled **1.39Q_TSx**) are shown in bold relative to **1Q_Int1** and $HBMe_2$. [Ti] represents $CpTi\{MeC(NMe)_2\}$.

As shown in Figure 3.22, from **1Q_Int1** a second molecule of $HBMe_2$ can coordinate to the N_β *via* the B atom. A five-membered transition state, where the N_α–N_β bond is cleaved and a N-H bond is formed, leads to **1.39Q_Int5** and releases Me_2NBMe_2. From this intermediate the process to get the final product is facile. A first H migration from B to titanium (**1.39Q_TS5**, $\Delta G^{\ddagger}$ = 4.3 kcal mol^{-1}) is followed by release of H_2 (**1.39Q_TS6**, $\Delta G^{\ddagger}$ = 16.7 kcal mol^{-1}). According to this mechanism, the RDS step is associated with the five-membered TS (**1.39Q_TS4**) which is lower than the RDS observed in the previous

mechanism, namely 27.5 *vs.* 29.7 kcal mol^{-1} starting from **1Q_Int1** (Figure 3.21, bottom). Other attempts with different coordination modes of the second molecule $HBMe_2$ to either $N\alpha$ or $N\beta$ did not give results consistent with the experiments. For completeness, the reaction mechanism described in Figure 3.21 was computed for the reactions of **1.39** with HBPin and 9-BBN by using real systems and the computational methodology described in Section 3.5. All the Gibbs free energy values are referenced to (**1.39** + borane), which is set at 0.0 kcal mol^{-1}. For HBPin, the monomer borane is considered while for 9-BBN, the values are referenced to 0.5 9-BBN dimer (Figure 3.23).

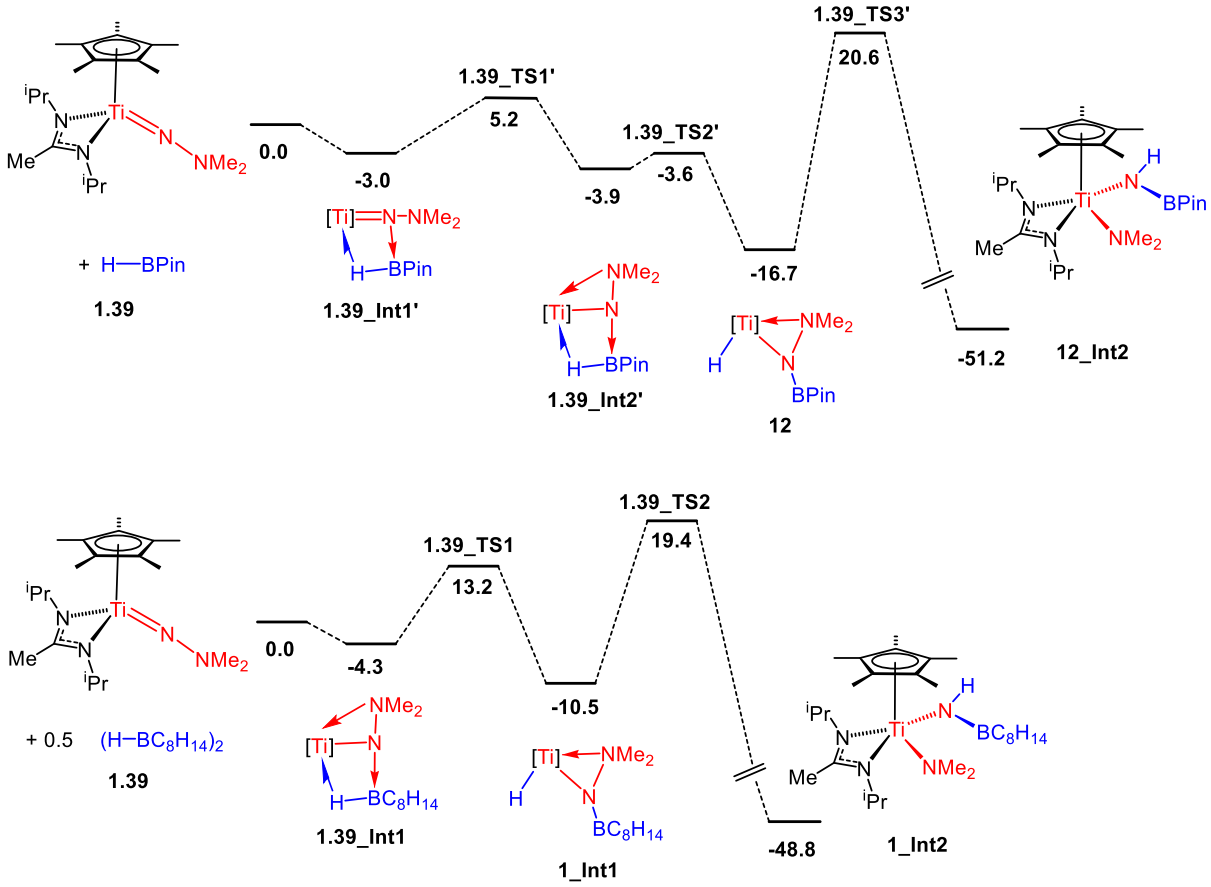

Figure 3.23. DFT mechanism (B3PW91, SCRF with a def2-qzvpp basis set and including dispersion interactions) for the reaction of Cp*Ti{MeC(N^{i}Pr)$_2$}(NNMe$_2$) (**1.39**) with HBPin (top) and 9-BBN (bottom) forming Cp*Ti{MeC(N^{i}Pr)$_2$}{N(H)BPin}(NMe$_2$) (**12_Int2**) and Cp*Ti{MeC(N^{i}Pr)$_2$}{N(H)BC$_8$H$_{14}$}(NMe$_2$) (**1_Int2**) respectively. Gibbs free energies (kcal mol^{-1}, T = 298.15 K) for minima, maxima and transition states (labelled **1.39_TSx**) are shown in bold relative to **1.39** and 9-BBN (or HBPin). [Ti] represents Cp*Ti{MeC(N^{i}Pr)$_2$}.

Starting from the reaction of **1.39** with HBPin (Figure 3.23), the results are in line with the experimental results as expected. An initial formation of an adduct (**1.39_Int1'**), is followed by chelation of Nβ to titanium. Cleavage of B–H bond gives the experimentally observed product **12**. The hypothetical hydride transfer step to yield **12_Int2** has an associated barrier of 37.2 kcal mol^{-1} making this step unfeasible. Moving on to 9-BBN, the reaction mechanism to give **1_Int1** is facile**.** The final hydride transfer step to yield **1_Int2** has an associated barrier of 29.4 kcal mol^{-1} which again is high for a reaction complete in 12 h at RT. Attempts to compute alternative mechanisms were unsuccessful. The analogue of the five-membered TS proposed for the small model system (**1.39Q_TS4**, Figure 3.22) was found to have a relative Gibbs free energy of 37.5 kcal mol^{-1}.(**TS5_memberred**, optimized structure reported in the XYZ Appendix). In summary, the mechanism of the reaction was unfortunately not fully elucidated. Experimental and computational evidence suggest that the formation of Cp*Ti{MeC(N^iPr)$_2$}(H){N(BC_8H_{14})NMe_2} (**1_Int1**) is facile and governed by the dissociation of 9-BBN dimer, which is the RDS. The conversion of this intermediate to the final product is slower and associated with decomposition products which made the kinetic analysis difficult.

3.9 Other reactions

Reactions of Cp*Ti{MeC(N^iPr_2)$_2$}(NTol) (**3.1**), Cp*Ti{MeC(N^iPr_2)$_2$}($NNMe_2$) (**1.39**), Cp*Ti{MeC(N^iPr_2)$_2$}($NNPh_2$) (**1.38**) and Cp*Ti{MeC(N^iPr_2)$_2$}($NNCPh_2$) (**1.40**) with several other molecules containing element hydrogen bonds were also attempted. These include ^{t}BuSH, diisobutylaluminium hydride, $TMPAlH_2$ (TMP = 2,2,6,6-tetramethylpiperidine) and Mes_2SnH_2. In all cases a mixture of species were observed of which no one could be isolated or identified. Some evidence was obtained for a dehydrogenative coupling reaction with Mes_2SnH_2. However, the results were not reproducible or well behaved and were therefore not pursued further. Finally, reactions of Cp*Ti{MeC(N^iPr_2)$_2$}(NO^tBu) (**3.3**) with boranes and silanes were attempted. Unfortunately all of them resulted in decomposition of the starting titanium compound or in a mixture of species.

3.10 Conclusion and Outlook

Reactions of Cp*Ti{MeC(N^iPr_2)$_2$}(NTol) (**3.1**), Cp*Ti{MeC($N^iP/$)$_2$}($NNMe_2$) (**1.39**), Cp*Ti{MeC(N^iPr_2)$_2$}($NNPh_2$) (**1.38**) and Cp*Ti{MeC(N^iPr_2)$_2$}($NNCPh_2$) (**1.40**) with a

range of silanes and boranes were described in this Chapter. Reactions of Cp*Ti{MeC(N^{i}Pr)$_2$}(NTol) (**3.1**) with boranes gives adducts where the B atom is coordinated to Nα and the hydrogen to titanium. For Cp*Ti{MeC(N^{i}Pr)$_2$}(NNCPh$_2$) (**1.40**), reactions with both pinacolborane (HBPin) or 9-BBN give B–H addition across the N=C double bond, while reaction with HB(C$_6$F$_5$)$_2$ proceeds *via* two intermediates, namely a boron adduct on Nβ Cp*Ti{MeC(N^{i}Pr)$_2$}{NNBH(C$_6$F$_5$)$_2$CPh$_2$} (**10a**), followed by a boron adduct on Nα and Cp*Ti{MeC(N^{i}Pr)$_2$}{NBH(C$_6$F$_5$)$_2$NCPh$_2$} (**10b**), before leading to the final product, Cp*Ti{MeC(N^{i}Pr)$_2$}{NNB(C$_6$F$_5$)$_2$CHPh$_2$} (**10c**). The reactivity of the analogues hydrazido compounds Cp*Ti{MeC(N^{i}Pr$_2$)$_2$}(NNMe$_2$) (**1.39**) and Cp*Ti{MeC(N^{i}Pr$_2$)$_2$}(NNMe$_2$) (**1.38**) is different, resulting in either the product of 1,2-addition across the Ti=N bond with HBPin (for **1.39** only), or the borylimido compound Cp*Ti{MeC(N^{i}Pr)$_2$}{NBC$_8$H$_{14}$} (**1**) with one equivalent of 9-BBN dimer. Reactions of both **1.38** and **1.39** with 9-BBN dimer thus result in complete Nβ atom transfer to substrate and encompasses the overall reduction of R$_2$NNH$_2$ with 9-BBN to the corresponding borylamines R$_2$NB$_8$H$_{14}$ (R$_2$ = Ph$_2$ or Me$_2$) and H$_2$, in a new type of dehydrogenative coupling reaction[51] and provide the first examples of Si–H and B–H induced reductive cleavage of a hydrazide N–N bond on half-sandwich titanium complexes. Computational studies, including DFT and NBO calculations have been performed in order to support the experimental data and to propose a mechanism for the reactions of the hydrazide complexes **1.38** and **1.39** with 9-BBN dimer.

3.11 References

1 L. Stevenson, S. Mellino, E. Clot and P. Mountford, *J. Am. Chem. Soc.*, 2015, **137**, 10140–10143.

2 P. J. Walsh, M. J. Carney and R. G. Bergman, *J. Am. Chem. Soc.*, 1991, **113**, 6343–6345.

3 Y. Li, Y. Shi and A. L. Odom, *J. Am. Chem. Soc.*, 2004, **126**, 1794–1803.

4 S. Banerjee and A. L. Odom, *Organometallics*, 2006, **25**, 3099–3101.

5 A. A. Dissanayake and A. L. Odom, *Chem. Commun.*, 2012, **48**, 440–442.

6 H. Herrmann, J. L. Fillol, H. Wadepohl and L. H. Gade, *Angew. Chem. Int. Ed.*, 2007, **46**, 8426–8430.

7 T. Gehrmann, J. L. Fillol, H. Wadepohl and L. H. Gade, *Angew. Chem. Int. Ed.*, 2009, **48**, 2152–2156.

8 T. Gehrmann, M. Kruck, H. Wadepohl and L. H. Gade, *Chem. Commun.*, 2012, **48**, 2397–2399.

9 T. Gehrmann, S. A. Scholl, J. L. Fillol, H. Wadepohl and L. H. Gade, *Chem. - Eur. J.*, 2012, **18**, 3925–3941.

10 A. J. Blake, J. M. McInnes, P. Mountford, G. I. Nikonov, D. Swallow and D. J. Watkin, *J. Chem. Soc. Dalt. Trans.*, 1999, 379–392.

11 J. D. Selby, C. D. Manley, M. Feliz, A. D. Schwarz, E. Clot and P. Mountford, *Chem. Commun.*, 2007, **733**, 4937–4939.

12 A. D. Schofield, A. Nova, J. D. Selby, C. D. Manley, A. D. Schwarz, E. Clot and P. Mountford, *J. Am. Chem. Soc.*, 2010, **132**, 10484–10497.

13 P. J. Tiong, A. D. Schofield, J. D. Selby, A. Nova, E. Clot and P. Mountford, *Chem. Commun.*, 2010, **46**, 85–87.

14 A. D. Schofield, A. Nova, J. D. Selby, A. D. Schwarz, E. Clot and P. Mountford, *Chem. Eur. J.*, 2011, **17**, 265–285.

15 P. J. Tiong, A. Nova, E. Clot and P. Mountford, *Chem. Commun.*, 2011, **47**, 3147–3149.

16 A. D. Schwarz, C. S. Onn and P. Mountford, *Angew. Chem. Int. Ed.*, 2012, **51**, 12298–12302.

17 J. Unruangsri, H. Morgan, A. D. Schwarz, A. D. Schofield and P. Mountford, *Organometallics*, 2013, **32**, 3091–3107.

18 P. J. Tiong, L. R. Groom, E. Clot and P. Mountford, *Chem. Eur. J.*, 2013, **19**, 4198–4216.

19 J. Chu, X. Han, C. E. Kefalidis, J. Zhou, L. Maron, X. Leng and Y. Chen, *J. Am. Chem. Soc.*, 2014, **136**, 10894–10897.

20 E. Zhou, W. Ren, G. Hou, G. Zi, D.-C. Fang and M. D. Walter, *Organometallics*, 2015, **34**, 3637–3647.

21 A. J. Mountford, W. Clegg, S. J. Coles, R. W. Harrington, P. N. Horton, S. M. Humphrey, M. B. Hursthouse, J. a Wright and S. J. Lancaster, *Chem. Eur. J.*, 2007, **13**, 4535–4547.

22 E. A. Jacobs, A. Fuller, S. J. Coles, G. A. Jones, G. J. Tizzard, J. A. Wright and S. J. Lancaster, *Chem. Eur. J.*, 2012, **18**, 8647–8658.

23 P. J. Tiong, A. Nova, L. R. Groom, A. D. Schwarz, J. D. Selby, A. D. Schofield, E. Clot and P. Mountford, *Organometallics*, 2011, **30**, 1182–1201.

24 P. J. Tiong, A. Nova, A. D. Schwarz, J. D. Selby, E. Clot and P. Mountford, *Dalton Trans.*, 2012, **41**, 2277–2288.

25 L. C. Stevenson, DPhil Thesis, University of Oxford, 2015.

26 D. S. Matteson, *Stereodirected Synthesis with Organoboranes*, Springer, 2012.

27 D. A. Fletcher, R. F. McMeeking and D. Parkin, *J. Chem. Inf. Comput. Sci.*, 1996, **36**, 746 (Cambridge Structural Database version 5.37).

28 P. Pardasani, R. T. Pardasani and A. Pelter, in *Chemical shift: Datasheet from Landolt-Börnstein - Group III Condensed Matter*, eds. R. R. Gupta and M. D. Lechner, Springer-Verlag Berlin Heidelberg, p. Volume 35A.

29 S. Doye, *Synlett*, 2004, **2004**, 1653–1672.

30 A. Schäfer, H. Horn and R. Ahlrichs, *J. Chem. Phys.*, 1992, **97**, 2571–2577.

31 F. Weigend and R. Ahlrichs, *Phys. Chem. Chem. Phys.*, 2005, **7**, 3297–3305.

32 S. Grimme, S. Ehrlich and L. Goerigk, *J. Comput. Chem.*, 2011, **32**, 1456–1465.

33 F. Jensen, *J. Chem. Theory Comput.*, 2008, **4**, 719–727.

34 A. W. Kaplan, J. L. Polse, R. A. Andersen and R. G. Bergman, *J. Am. Chem. Soc.*, 1998, **120**, 11649–11662.

35 S. Lorenzo, G. R. Lewis and I. Dance, *New J. Chem.*, 2000, **24**, 295–304.

36 A. E. Guiducci, C. L. Boyd, E. Clot and P. Mountford, *Dalton Trans.*, 2009, 5960–5979.

37 L. Komoroski, A. Meller and K. Niedenzu, *Inorg. Chem.*, 1990, **29**, 538.

38 A. G. M. Barrett, M. R. Crimmin, M. S. Hill, P. B. Hitchcock and P. A. Procopiou, *Organometallics*, 2007, **26**, 4076–4079.

39 M. D. Fryzuk, B. A. MacKay, S. A. Johnson and B. O. Patrick, *Angew. Chem. Int. Ed.*, 2002, **41**, 3709–3712.

40 A. A. Danopoulos, C. Redshaw, A. Vaniche, G. Wilkinson, B. Hussain-Bates and M. B. Hursthouse, *Polyhedron*, 1993, **12**, 1061–1071.

41 K. Weber, K. Korn, A. Schorm, J. Kipke, M. Lemke, A. Khvorost, K. Harms and J. Sundermeyer, *Z. Anorg. Allg. Chem.*, 2003, **629**, 744–754.

42 K. Searles, B. Pinter, C. H. Chen and D. J. Mindiola, *Organometallics*, 2014, **33**, 4192–4199.

43 L. N. Grant, B. Pinter, T. Kurogi, M. E. Carroll, G. Wu, B. C. Manor, P. J. Carroll and D. J. Mindiola, *Chem. Sci.*, 2017, **8**, 1209–1244.

44 R. Köster and G. Seidel, *J. Lieb. Ann. der Chemie*, 1977, **1977**, 1837–1846.

45 F. Weinhold and C. R. Landis, *Chem. Educ. Res. Pr.*, 2001, **2**, 91–104.

46 J. R. Schwierl and H. C. Brown, *J. Org. Chem.*, 1993, **58**, 1546–1552.

47 H. C. Brown, J. Chandrasekharan and K. K. Wang, *Pure Appl. Chem.*, 1983, **55**, 1387–1414.

48 K. K. Wang and H. C. Brown, *J. Org. Chem.*, 1980, **45**, 5303–5306.

49 L. R. Groom, DPhil Thesis, University of Oxford, 2014.

50 J. Chandrasekharan and H. C. Brown, 1985, 518–520.

51 H. C. Johnson, T. N. Hooper and A. S. Weller, *Top. Organomet. Chem.*, 2015, 153.

4.1 Overview

This Chapter describes the computational studies on the bonding and reactivity of novel titanium borylimides. The systematic approach used to synthesise these titanium borylimido compounds, starting from three different synthons, namely Ti{NB(NAr'CH)$_2$}Cl$_2$(NHMe$_2$)$_2$ (**4.1**), Ti{NB(NAr'CH)$_2$}Cl$_2$(py)$_3$ (**4.2**), and Cp*Ti{NB(NAr'CH)$_2$}Cl(py) (**4.3**) and by subsequently installing the desired supporting ligands, will be described. The most relevant experimental results obtained by Dr. Ben Clough, Post-Doctoral researcher in our research group will be presented[1] and a full computational study of the bonding of compounds with sandwich and half-sandwich structures will be explained in detail and connected to both to the experimental results already presented in Chapter 3, and to the previously studied alkyl- and arylimido counterparts. The novel reactivity of a borylimido half-sandwich compound with CO_2, CS_2 and aldehydes will also be explored. All the experimental results have been performed by Dr. Ben Clough and by Martin Slusarczyk, respectively Post-Doctoral researcher and DPhil student in our group at the University of Oxford. The reported computational results have been performed in collaboration with Prof. Philip Mountford at the University of Oxford and Dr. Eric Clot at Université Montpellier, France.

4.2 Introduction

As fully described in Chapter 2, Group 4 imido and hydrazido compounds have been studied in great detail. Of particular interest were the Group 4 imides of the type (L)M=N–R (R= alkyl or aryl), which formally contain a metal-nitrogen triple bond ($\sigma^2\pi^4$). As extensively described in previous chapters, the presence of a nitrogen atom in the β position in the parent hydrazido compounds of the type (L)M=NNR$_2$ often led to a completely different reactivity which was associated with the reductive cleavage of the N–N bond.[2–5] Despite both imido and hydrazido complexes having been extensively explored and detailed studies of the bonding and the reactivity being performed, less attention has been paid to complexes where the nitrogen in β position has been substituted by another heteroatom, X, to give (L)M=N–XR$_n$. Only recently, the synthesis of the first Group 4 alkoxyimide complex, (L)Ti=NOR, obtained by using a protonolysis route with Ti(NMe$_2$)$_2$Cl$_2$ and ^{t}BuONH$_2$ was reported.[6] The reactivity of related cyclopentadienyl-amidinate supported alkoxyimido complexes with a wide range of substrates such as heterocumulenes, aldehydes, ketones and nitriles was studied.

Following this line of research, the incorporation of a boron atom in the β position was also investigated in our group with the hope of accessing both novel Ti=N_α and N_α–B_β bond reactivity. The serendipitous discovery of the two borylimido compounds reported in Chapter 3, namely (^{tBu}NacNac)Ti(NBEt$_2$)(NTol$_2$) (**1.88**, ^{tBu}NacNac = HC{C(^{t}Bu)NAr'}$_2$), produced through reaction of 2 equiv. NaHBEt$_3$ with the parent imido (compound featuring a terminal NH) reported by Mindiola and co-workers,[7] and Cp*Ti{MeC(N^{i}Pr)$_2$}(NBC$_8$H$_{14}$) (**1**),[8] led our group to investigate how to incorporate a boron atom in the β position in a systematic manner. In particular, well established routes previously reported for the titanium imido, hydrazido and alkoxyimido chemistry were explored. In work previously developed by this research group and others, synthons of the type Ti(NR)Cl$_2$(L)$_n$ (R = ^{t}Bu, aryl, NPh$_2$, O^{t}Bu; L = py, 4-NC$_5$H$_4$^{t}Bu; n = 2 or 3)[9,10,11,12] and Ti(NR)Cl$_2$(NHMe$_2$)$_2$ (R = alkyl, aryl, NPh$_2$, NO^{t}Bu)[9,10,13–15] proved to be versatile entry points to new complexes through displacement of the Cl or Lewis base ligands with anionic or neutral donors. A general route to the latter type involves the reaction of Ti(NMe$_2$)$_2$Cl$_2$ with the required amine, N,N-substituted hydrazine or alkoxyamine[9,10,13–17] and, in some cases, reaction of those compounds with pyridine results in the pyridine-coordinated complexes Ti(NR)Cl$_2$(py)$_3$.[13,18] From these synthons it was possible to install a dianionic, tridentate diamide-amine ligand RN{(CH$_2$)$_n$NSiMe$_3$}$_2$ (R = Me, n = 2 ($N_2^{SiMe_3}N^{Me}$) or n = 3 (N_2N^{Me}); R = SiMe$_3$, n = 2 ($N_2N^{SiMe_3}$)) along with the related diamide pyridine ligands (2-C$_5$H$_4$N)CMe(CH$_2$NSiMe$_2$R)$_2$ (R = Me (N_2N^{py}) or R = ^{t}Bu ($N_2^{TBS}N^{py}$)) which have been demonstrated to be very effective to promote the reactivity of the Group 4 metal-nitrogen multiple bond in literature.[2,5,11,19–28] As explained in more detail before, the N_{amide} π-donors increase the reactivity of the metal-nitrogen multiple bond and lead to catalytic and stoichiometric reactivity. For example, reaction of Ti(N_2N^{Me})(NNPh$_2$)(py) with alkynes gives an insertion reaction of the alkyne into the N_α–N_β bond forming the vinylimide complex Ti(N_2N^{Me}){NC(Ph)C(Me)NPh$_2$}(py), as shown in Equation 4.1.[2]

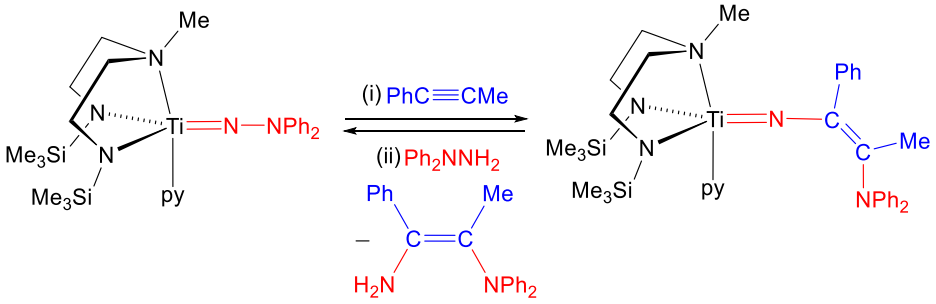

Equation 4.1

Compounds with a sandwich or half-sandwich structure have also been studied in the past years in our group. For example the cyclopentadienyl-amidinate complexes Cp*Ti{MeC(N^{i}Pr)$_2$}(NTol) (**3.1**)[29] , Cp*Ti{MeC(N^{i}Pr)$_2$}(NNR$_2$) (R = Ph (**1.38**) or Me (**1.39**)[30] and Cp*Ti{MeC(N^{i}Pr)$_2$}(NNCPh$_2$) (**1.40**)[31] can be synthesised from the readily-prepared Cp*Ti{MeC(N^{i}Pr)$_2$}(N^{t}Bu) (**1.37**)[29] *via* *tert*-butylimide-arylamine/hydrazine exchange reactions (Figure 4.1).

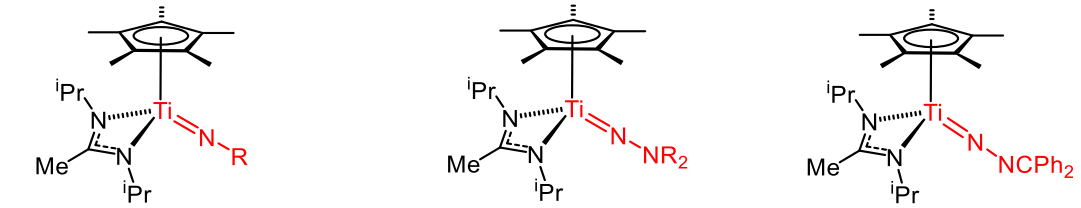

R = ^{t}Bu (**1.37**) or Ar (**3.1**) R = Ph (**1.38**) or Me (**1.39**) **1.40**

Figure 4.1. Examples of cyclopentadienyl-amidinate supported complexes synthesised in our group.[29–31]

Both routes described above were extended to borylimido chemistry using the borylamine H$_2$NB(NAr'CH)$_2$, where Ar' = Dipp. Following the results described in Chapter 3, reactions using the conventional dialkyl- or diarylborylamines, namely H$_2$NBMes$_2$ and H$_2$N-BBN, were also attempted without any successful outcome as described in the following Sections.

4.3 Synthesis of new titanium borylimido compounds

This Section will summarize the main experimental results performed by Dr. Ben Clough to synthesise novel titanium borylimido compounds. Firstly, the preparation of the synthon Ti{NB(NAr'CH)$_2$}Cl$_2$(NHMe$_2$)$_2$ (**4.1**) will be presented. Subsequently,

compounds with sandwich and half-sandwich structures will be discussed. Finally the attempted exchange reactions among imido and borylimido compounds will be reported.

4.3.1 Synthesis of $Ti\{NB(NAr'CH)_2\}Cl_2(NHMe_2)_2$ (4.1)

As reported previously in our group, monomeric species of the type $Ti(NR)Cl_2(NHMe_2)_2$ (R = alkyl, aryl, NPh_2, O^tBu) were obtained from reaction of $Ti(NMe_2)_2Cl_2$ with the respective primary amine, aniline, diphenylhydrazine or *tert*-butoxyamine.[9–12,18] In the same way, the borylamine $H_2NB(NAr'CH)_2$ was reported by Dr. Ben Clough to react cleanly with $Ti(NMe_2)_2Cl_2$ to form the borylimido complex $Ti\{NB(NAr'CH)_2\}Cl_2(NHMe_2)_2$ (**4.1**) *via* proton transfer (Equation 4.2).[1]

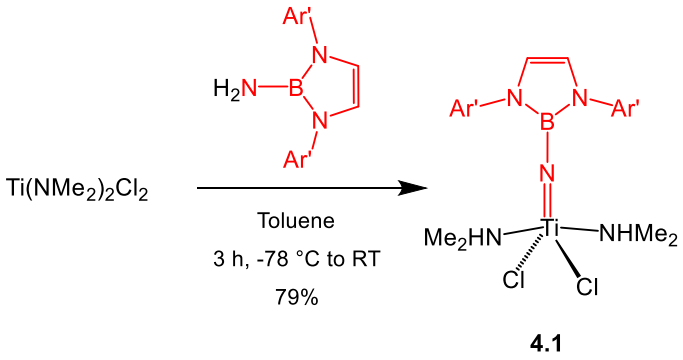

Equation 4.2

The solid state structure is shown in Figure 4.2. In the solid state, $Ti\{NB(NAr'CH)_2\}Cl_2(NHMe_2)_2$ (**4.1**) has an approximately trigonal bipyramidal geometry in which the two $NHMe_2$ ligands occupy axial positions and the Cl and $NB(NAr'CH)_2$ ligands occupy equatorial positions. The orientation of the borylimido ligand is such that it lies between the planes defined by the mutually *trans* Cl atoms and the mutually *trans* amine ligands; the angle between the Cl(1)–Ti(1)–Cl(2) plane and the {N(1),B(1),N(2),N(3)} plane is *ca* 61.0°. **4.1** can be compared with the array of previously structurally characterised complexes of the type $Ti(NR)Cl_2(NHMe_2)_2$ (R = alkyl, aryl, O^tBu)[9,10,13–15,17,18] all of which share a largely similar molecular geometry. Of particular interest here is the Ti–N–B linkage. The short Ti(1)–N(1) distance of 1.7027(11) Å and the near-linear Ti(1)–N(1)–B(1) angle of 178.19(9)°, which implies sp hybridisation at N(1), are both consistent with a titanium–nitrogen triple bond ($\sigma^2\pi^4$). The N(1)–B(1) distance of 1.4374(16) Å is consistent with a single bond, falling within the range (*ca* 1.34 – 1.51 Å) of all N–B single bonds with sp hybridised N and three-coordinate B in the Cambridge Structural Database.[32] Past experimental and

computational work has found that Ti–N_{im} bond lengths typically follow the trend Ti–N_{alkyl} < Ti–NO^{t}Bu < Ti–N_{aryl} < Ti–NNPh$_2$ (N_{im} is used to represent the multiply-bonded nitrogen in imido, hydrazido, alkoxyimido and borylimido compounds), and this is indeed the case for the respective analogues of **4.1** (although no hydrazide has been structurally characterised). The Ti(1)–N(1) bond length of 1.7027(10) Å in **4.1** places within the range reported for a series of eight arylimido complexes Ti(NAr)Cl$_2$(NHMe$_2$)$_2$ (avg. Ti–N_{im} = 1.703 Å, range 1.694(4) – 1.708(2) Å), and is longer than in both the alkylimide Ti(N^{i}Pr)Cl$_2$(NHMe$_2$)$_2$ (1.672(2) Å) and the *tert*-butoxyimido analogue (1.688(3) and 1.691(3) Å for the two crystallographically independent molecules).[9,13]

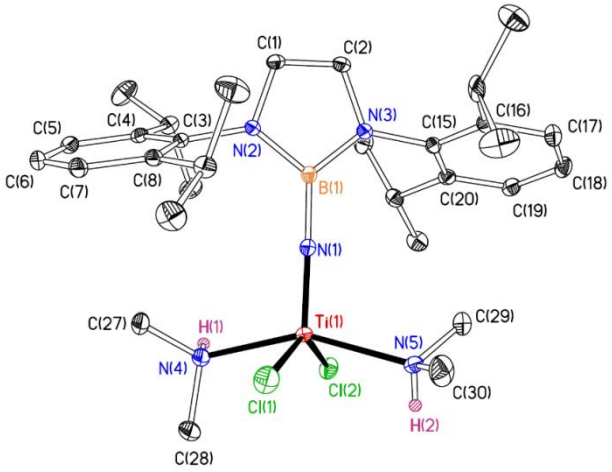

Figure 4.2. Displacement ellipsoid plot (25% probability) of Ti{NB(NAr'CH)$_2$}Cl$_2$(NHMe$_2$)$_2$ (**4.1**).[1] C-bound H atoms are omitted for clarity. H(1) and H(2) are drawn as spheres of an arbitrary radius.

As reported in the introduction the same reaction shown in Equation 4.2 was attempted for the two dialkyl- and diarylborylamines, namely H$_2$NBC$_8$H$_{14}$ and H$_2$NBMes$_2$. Unfortunately, neither of these two reactions was successful. In each case, an insoluble precipitate was observed in the NMR tube, and in the reaction of Ti(NMe$_2$)$_2$Cl$_2$ with H$_2$NBC$_8$H$_{14}$, Me$_2$NBC$_8$H$_{14}$ was identified, suggesting that an amide exchange process takes place and leads to decomposition of the titanium starting material. To explain the difference in reactivity and the steric and energetic features of the three borylimido experimental or hypothetical complexes, DFT calculations were performed and will be discussed in the next Section. This synthon was successfully used by Dr. Ben Clough to eventually obtain borylimido compounds with tridentate nitrogen-based supporting ligands. The experimental details will not be presented in this Thesis.

4.3.2 Synthesis of titanium borylimido complexes with sandwich and half-sandwich structures

As discussed in the introduction, two routes were successfully established to access the borylimido chemistry. The second route, described in this Section, namely imide/borylamine exchange, was used to produce six new complexes with sandwich and half-sandwich structures, utilising either a Cp or a Cp* ligand. To synthesise the half-sandwich complexes, compound Cp*Ti{NB(NAr'CH)$_2$}Cl(py) (**4.3**), was targeted first. The reaction was successfully achieved through a reaction in the melt, assisted by the removal of H_2N^tBu under dynamic vacuum, Equation 4.3.

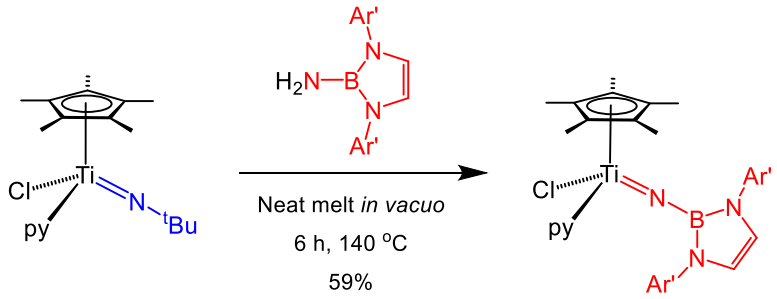

4.3

Equation 4.3

Also in this case, the reactions of Cp*Ti(N^{t}Bu)Cl(py) with $H_2NBC_8H_{14}$ and H_2NBMes_2 were investigated, with the aim of forming the respective dialkyl- or diarylborylimido complexes. Unfortunately, no success was found with either of these substrates, with both solution and melt conditions being attempted. At low temperatures in a C_6D_6 solution, no reaction was observed in either case, whilst forcing conditions employed in higher temperature solution reactions, or in melts, ultimately resulted only in decomposition of the titanium starting material. Following the success of the amidinate-supported borylimido complex, Cp*Ti{MeC(N^{i}Pr)$_2$}(NBC$_8$H$_{14}$) (**1**), obtained from the related hydrazide and 9-BBN, as discussed in Chapter 3, an analogous reaction was attempted. The salt metathesis reactions of **4.3** with either Li[MeC(N^{i}Pr)$_2$] or Li[PhC(N^{i}Pr)$_2$] were not successful. This is suspected to be due to prevention of complexation by steric constrains.

Alternative monoanionic N,N-bidentate ligands with reduced steric profiles such as the aminopyrrolide ligand $N^{pyr}N^{Me2}$ (Me_2NCH_2(2-NC_4H_3)), which has been used in Group 4 imido chemistry in recent years,[33] were targeted (Scheme 4.1). The solid state structure of the isolated product, namely Cp*Ti(hpp){NB(NAr'CH)$_2$} (**1.91**) is shown in Figure 4.3.

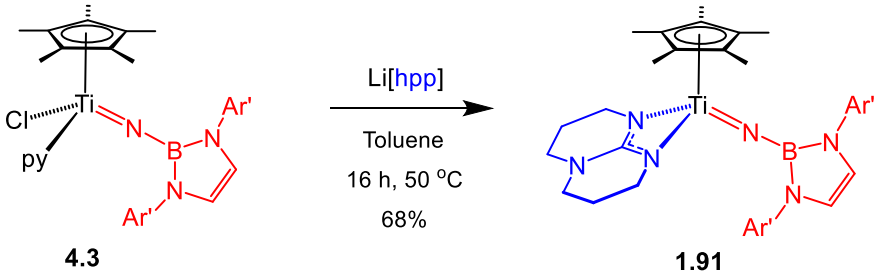

Scheme 4.1. Synthesis of Cp*Ti(hpp){NB(NAr'CH)$_2$} (**1.91**) from Cp*Ti{NB(NAr'CH)$_2$}Cl(py) (**4.3**).

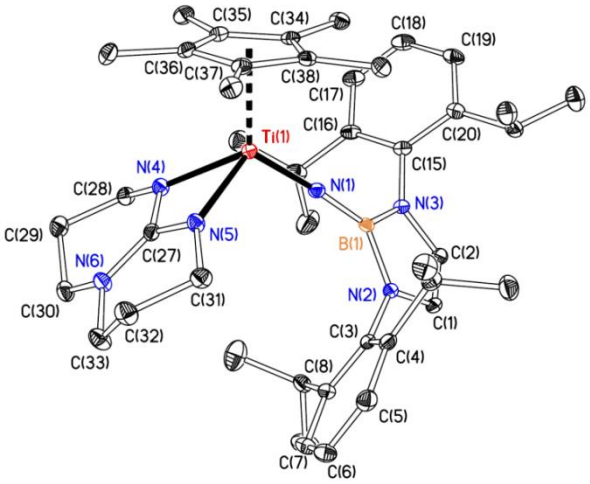

Figure 4.3. Displacement ellipsoid plots (20% probability) of Cp*Ti(hpp){NB(NAr'CH)$_2$} (**1.91**).[1] H atoms are omitted for clarity.

Compound **1.91** has a three-legged piano stool geometry, with an η^5-C_5Me_5 ligand, η^1-borylimido ligand and a κ^2-N,N'-bound ligand (hpp or $N^{pyr}N^{Me2}$, respectively). Comparison of the metric parameters of the Ti–N–B linkage show that the borylimido moiety bears Ti–N triple bond and N–B single bond: the Ti(1)–N(1) is 1.743(2) Å, the N(1)–B(1) distance is 1.422(3) Å, along with the Ti(1)–N(1)–B(1) angle of 176.00(17)°, in agreement with all of the structural characterisations discussed previously. As compared to the half-sandwich compound described in Chapter 3, namely Cp*Ti{MeC(N^{i}Pr)$_2$}(NBC$_8$H$_{14}$) (**1**), complex **1.91** has a slightly longer Ti–N distance (1.743(2) Å *vs.* 1.731(3) Å) along with a shorter N–B distance (1.422(3) Å *vs.* 1.402(4) Å). This arises from the nitrogen atoms that form the backbone of the borolyl ring in **1.91**, which partially donate into the vacant boron 2p orbital, preventing a full donation from the Nα and thus elongating the Nα–B distance. This effect will also be described in the next Section with the aid of DFT calculations.

Moving on to the titanium complexes with a bent metallocene sandwich structure, these were of particular interest in our research group, due to the absence of any metallocene borylimido complex in literature and were successfully synthesised by Dr. Ben Clough. In particular, the synthesis of $Cp_2Ti\{NB(NAr'CH)_2\}(py)$ (**1.92**) was reported to occur by reaction of the synthon, $Ti\{NB(NAr'CH)_2\}Cl_2(py)_3$ (**4.2**), with 2 equivalents of NaCp (Equation 4.4).

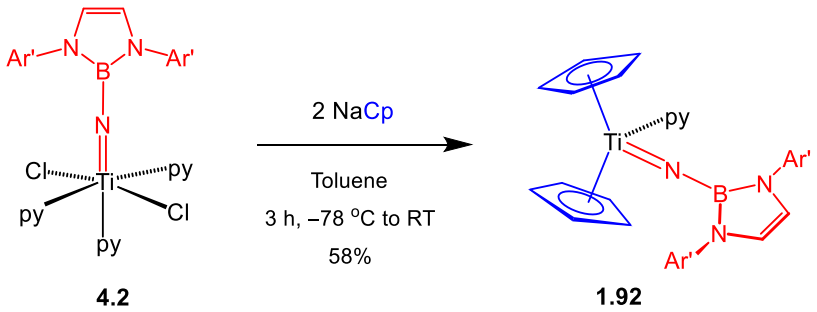

4.2 **1.92**

Equation 4.4

The solid state structure is shown in Figure 4.4. The structure displays a bent Cp_2Ti moiety which is coordinated to both the borylimido ligand and a pyridine donor ligand. The structure of this novel borylimido complex can be compared to the previously reported imido and hydrazido complexes, $Cp_2Ti(N^tBu)(py)$ (**1.5**) and $Cp_2Ti(NNPh_2)(py)$ (**4.4**).[34,35] The Cp rings of **1.92** are η^5-coordinated to the metal with Ti–C bonds in the range 2.4022(18) – 2.6053(18) Å, and an average Ti–Cp centroid distance of 2.18 Å. Close inspection of the Ti–C bonds of **1.92** reveals that the upper Cp ring (as drawn in Figure 4.4) has a considerable ring-slip away from the borylimido ligand and the ideal geometry (of five equal Ti–C distances). That is, C(28) and C(29) have Ti–C distances of 2.6050(18) and 2.6053(18) Å respectively, whilst those for C(27), C(30) and C(31) are shorter at 2.4943(17), 2.4423(18) and 2.4325(18) Å. Thus the bonding situation for this Cp ring may be viewed as moving towards an η^2,η^3-coordination mode, as result of a strong trans-influence.

As a comparison, the Ti–C lengths in the "lower" Cp ring are in the range *ca* 2.402 – 2.503 Å and so the ring-slipping effect is not appreciable in that ring. The Ti(1)–N(1) bond length of 1.7549(13) Å is comparable to the $Ti–N_{im}$ distance in the hydrazide **4.4** (1.757(2) Å),[35] and longer than in the imide **1.5** (1.723(6) Å),[34] and is consistent with a Ti–N triple bond. A small departure from linearity is encountered in the Ti(1)–N(1)–B(1) angle, which has the value 159.65(12)°. This is likely due to unavoidable steric

constraints imposed by the large substituents of the borylimido ligand, in addition to electronic effects which will be discussed in the next Section by aid of DFT calculations.

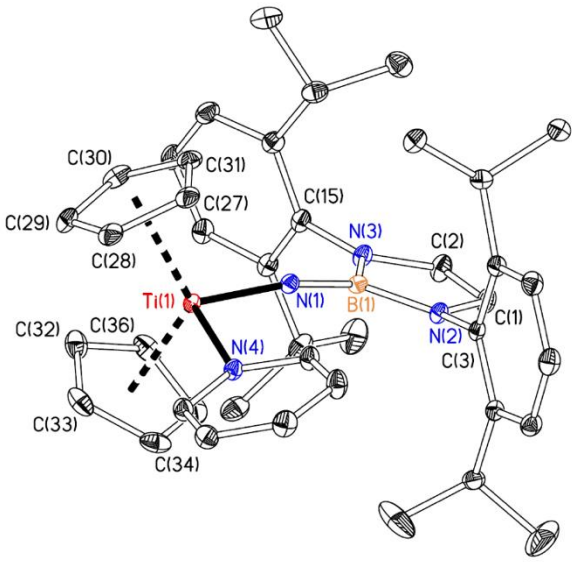

Figure 4.4. Displacement ellipsoid plot (20% probability) of $Cp_2Ti\{NB(NAr'CH)_2\}(py)$ (**1.92**).[1] H atoms are omitted for clarity.

4.4 Computational studies of bonding in half-sandwich borylimides

As the previously-reported hydrazido compounds of the type $Cp^*Ti\{MeC(N^iPr)_2\}(NNR_2)$ were initially prepared from $Cp^*Ti\{MeC(N^iPr)_2\}(N^tBu)$ (**1.37**) and the corresponding hydrazines at room temperature using the *tert*-butyl imide-hydrazine exchange strategy an analogous approach was attempted by Dr. BenClough, former DPhil in our research group. The aforementioned approach was used starting from the alkylimido complex $Cp^*Ti(hpp)(N^tBu)$ (**4.5**) and the borylamine $H_2NB(NAr'CH)_2$. The reaction led to an equilibrium mixture of starting materials and the desired final product **1.91** as shown in Equation 4.5. Furthermore, the reactions performed by reacting either $Cp^*Ti(hpp)(N^tBu)$ (**4.5**) or $Cp^*Ti(N^tBu)Cl(py)$ with the dialkylborylamine, $H_2NBC_8H_{14}$, were unsuccessful. Thus, DFT calculations were performed in order to better understand the energetics of bond dissociation and formation in these amine exchange reactions.

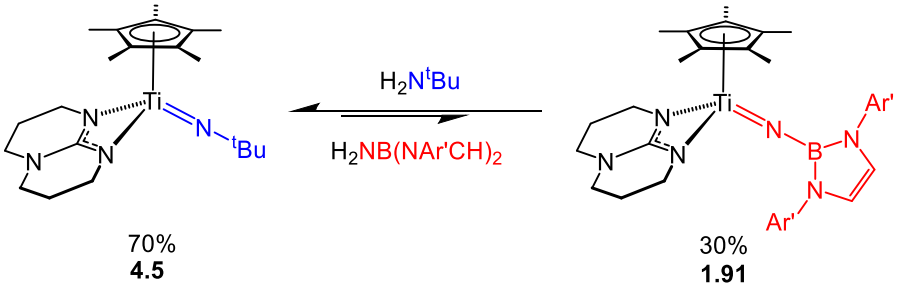

Equation 4.5

In this Section, a full computational analyses, including Molecular Orbitals (MO), Quantum theory of atoms in molecules (QTAIM) and Natural Bonding Orbitals (NBO), of model half-sandwich complexes will be presented to elucidate the differences between the $NB(NAr'CH)_2$ ligand and dialkylborylimido ligands such as that in the BBN-substituted compound **1**. The bonding nature of the metallocene compound $Cp_2Ti\{NB(NAr'CH)_2\}(py)$ (**1.92**) will also be presented and compared to the parent imido and hydrazido compounds.

4.4.1 Molecular Orbital Analysis of half- sandwich complexes

Starting from the Cp*-half-sandwich structures, DFT geometry optimisation calculations were carried out on the model systems $CpTi\{MeC(NMe)_2\}(NR)$ (**1Q_R**; R = Me, Ph, BMe_2, $B(NMeCH)_2$) using the B3PW91 functional[36,37] and def2-svp basis set[38] for all atoms, followed by single point calculations in the gas phase with a def2-tzvp basis set.[39] For these sterically-pruned model systems dispersion interactions and solvent corrections were not included. This computational methodology is used for all of the model systems described in this Chapter. In **1Q_B(NMeCH)$_2$**, $NB(NMeCH)_2$ is used as a model for the real $NB(NAr'CH)_2$ ligand, and the hpp ligand is approximated as the $MeC(NMe)_2$ amidinate to give direct comparisons with previously reported computational results on model imides and hydrazides, whilst **1Q_BMe$_2$** is a model of the real BBN-substituted compound $Cp^*Ti\{MeC(N^iPr)_2\}(NBC_8H_{14})$ (**1**). Selected calculations performed with the hpp ligand, as described later in this Section, will show that there is no significant difference between complexes with amidinate or hpp ligands. The frontier molecular orbitals (FMOs) of the model imido and borylimido dianions $[NMe]^{2-}$, $[NPh]^{2-}$, $[NBMe_2]^{2-}$ and $[NB(NMeCH)_2]^{2-}$ will be compared first, and then the FMOs of the $[CpTi\{MeC(NMe)_2\}]^{2+}$ fragment will be described. Finally, after an elucidation of both

components involved in the bonding, the MOs of the model compounds **1Q_R** will be presented. Although all real systems have been simplified with smaller model systems, this was crucial to understand better the role played by the single components in each FMO.

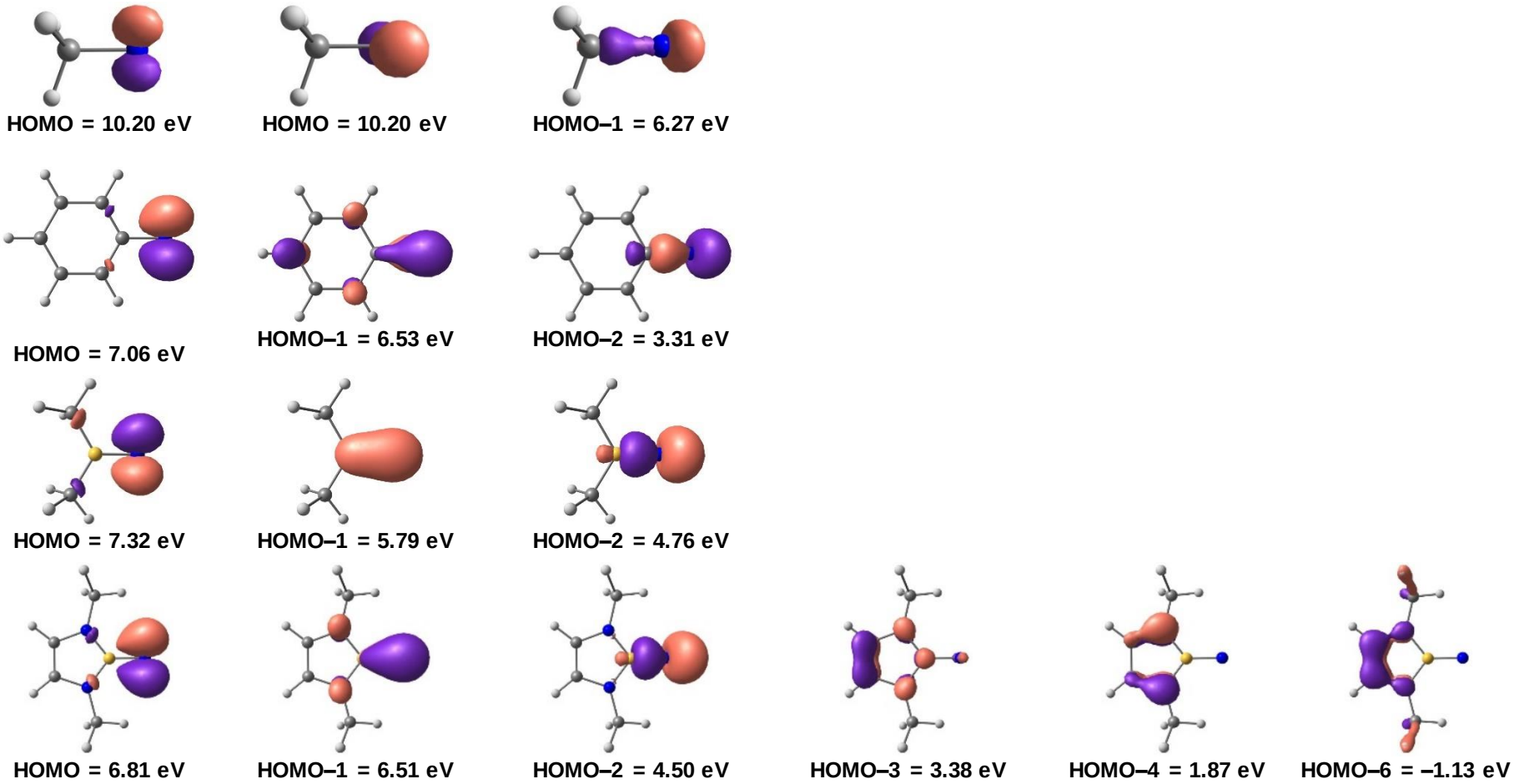

Figure 4.5. Isosurfaces and energies of the frontier molecular orbitals (σ and 2π) in the model imido-type dianions $[NMe]^{2-}$, $[NPh]^{2-}$, $[NBMe_2]^{2-}$ and $[NB(NMeCH)_2]^{2-}$, along with the π-bonding MOs of the boryl ring in $[NB(NMeCH)_2]^{2-}$.

Figure 4.5 shows the three highest occupied MOs for the four model imido-type fragments $[NMe]^{2-}$, $[NPh]^{2-}$, $[NBMe_2]^{2-}$ and $[NB(NMeCH)_2]^{2-}$, these being the nitrogen-based σ-donor orbital and two π-donor orbitals in each case. All the energies reported in Figure 4.5 are positive, as reported for anions. The positive eigenvalues reflects the unbound state of the electrons. The $[NMe]^{2-}$ fragment has two degenerate and orthogonal MOs (N lone pairs) at an energy of 10.20 eV. The σ-donor orbital is the HOMO–1 at 6.27 eV. Having no electron-withdrawing substituent, the FMOs of $[NMe]^{2-}$ are considerably higher in energy than the ones of the other dianonic fragments, whose energy can be lowered by donation into vacant orbitals. Moving to $[NPh]^{2-}$, now the two nominally π-symmetry N lone pairs are of different energy. The HOMO lies parallel to the phenyl ring, so does not have any interaction with the π orbitals of that ring. In contrast, the lone pair perpendicular to the ring partially donates into an unoccupied ring π orbital to form the HOMO–1 which is stabilised by 0.53 eV relative to the HOMO. The HOMO–2 is the σ-donor orbital, which is stabilised by 2.96 eV relative to that of $[NMe]^{2-}$ by the electron-withdrawing phenyl group.

In $[NBMe_2]^{2-}$ the degree of stabilization of the HOMO–1 relative to the HOMO is even higher (1.53 eV) due to a significant degree of donation of the N lone pair to the empty B 2p orbital. The σ contribution to the bond is highlighted in the HOMO-2, which has energy of 4.76 eV. In $[NB(NMeCH)_2]^{2-}$, the situation is more complicated. The lone pair perpendicular to the boryl ring is similarly stabilised by donation to the B 2p orbital, although the extra stabilization is only 0.30 eV, due to competing donation from the nitrogen atoms that form the backbone of the borolyl ring. The electronegativity of the adjacent nitrogen atoms in the borolyl backbone stabilises the σ-donor orbital more in comparison to the methyl substituents in the $[NBMe_2]^{2-}$ fragment. Additionally, Figure 4.5 displays three further occupied MOs of $[NB(NMeCH)_2]^{2-}$ which represent the 6π electrons of the aromatic borolyl ring.

The model dicationic fragment $[CpTi\{MeC(NMe)_2\}]^{2+}$ was also studied from a molecular orbital point of view. Selected FMOs, some of which are expected to act as the acceptor orbitals for an imido-type dianion, are depicted in Figure 4.6. The LUMO is a purely non-bonding metal d orbital, while the two π-accepting orbitals are the LUMO+1 and LUMO+2 which can be thought as the metal d orbitals involved in the formation of an imido-type ligand bonding. The LUMO+3 acts as the σ-acceptor, and the LUMO+4 is a

metal–ligand antibonding orbital with δ symmetry and thus is not involved with the bonding of an imido ligand.

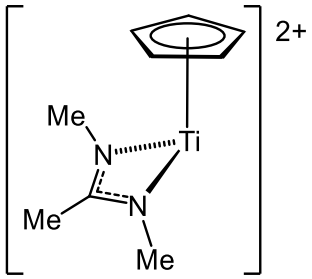

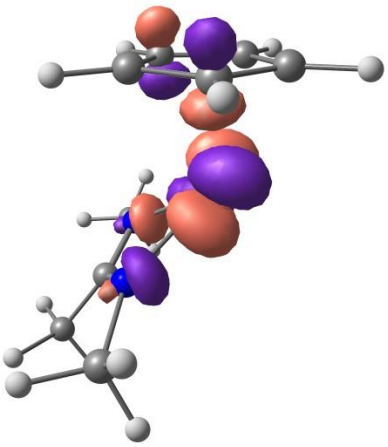

LUMO+4 = –10.4 eV

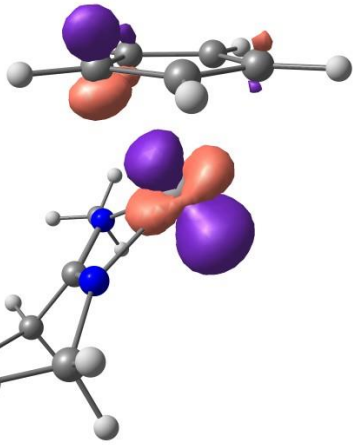

LUMO+3 = –11.6 eV

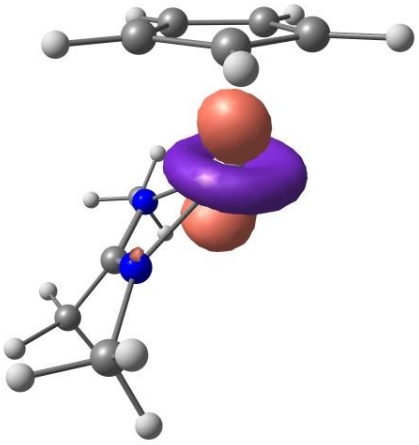

LUMO+2 = –11.9 eV

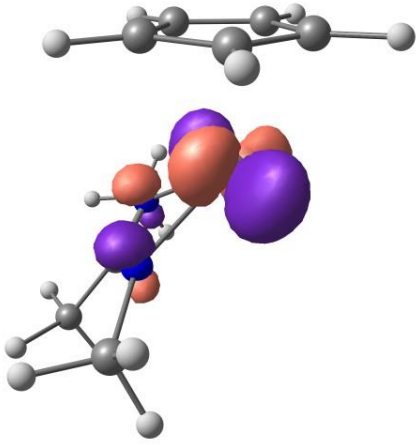

LUMO+1 = –12.3 eV

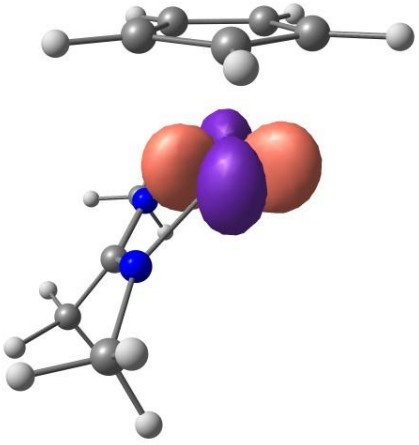

LUMO = –12.6 eV

Figure 4.6. Isosurfaces and energies of frontier molecular orbitals in the model dicationic fragment $[CpTi\{MeC(NMe)_2\}]^{2+}$.

After a clear description of the FMOs of both the imido-type dianions and the dicationic metal fragments, the electronic structure of the model compounds can be elucidated. The notation is the following: the MO denoted π_v lies in the approximate molecular mirror plane and the other lies perpendicular to it (π_h). It has been previously shown that the π_h energies are relatively insensitive to the N_α-substituents and vary non-systematically due to different degrees of mixing with the out-of-phase $2p_\pi$ contribution of amidinate N atoms.[40] Although the two π-symmetry lone pairs of $[NMe]^{2-}$ are degenerate (C_{3v} symmetry), the two π-components of the metal–nitrogen multiple bond that form **1Q_Me** are not isoenergetic as they have different symmetries and involve mixing with different acceptor orbitals at the metal centre. The HOMO–1 of **1Q_Me** has an energy of –5.68 eV and lies parallel to the vertical $Ti–Cp_{cent}$ vector (Figure 4.7), whilst the π_h component is the HOMO–2 with an energy of –6.17 eV. Additionally, the HOMO (–5.49 eV) is an amidinate ligand-based orbital, with a substantial delocalization and Ti-N π character.

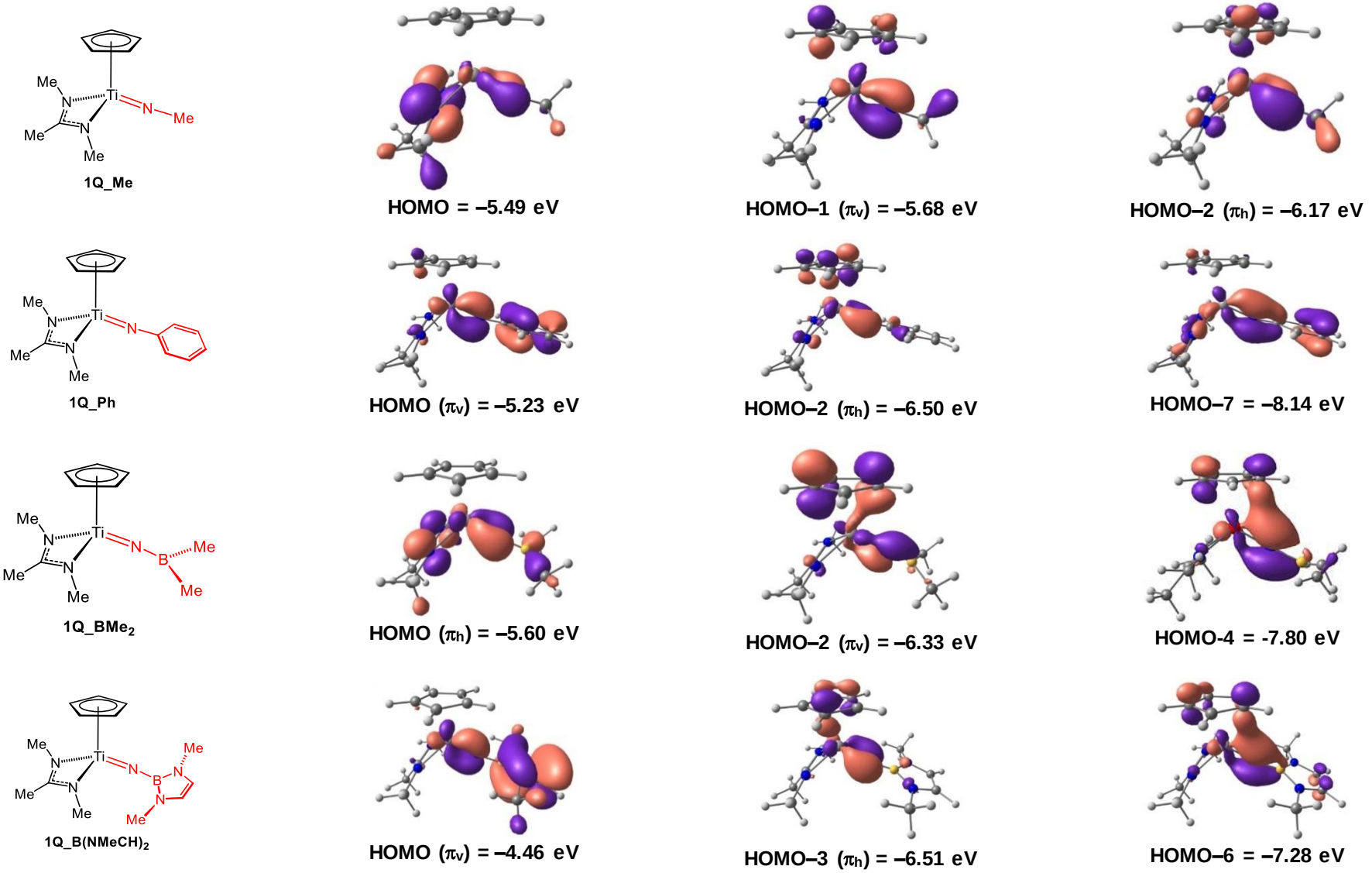

Figure 4.7. Isosurfaces and energies of frontier molecular orbitals in the model compounds, [CpTi{MeC(NMe)$_2$}(NR) (**1Q_R**; R = Me, Ph, BMe$_2$, B(NMeCH)$_2$).

Compared to CpTi{MeC(NMe)$_2$}(NMe) (**1Q_Me**), the phenyl substituent in **1Q_Ph** leads to a destabilisation of π_v by +0.45 eV due to a π^* antibonding interaction with one of the occupied ring MOs. The HOMO–2 is the Ti–N π_h component, which is formed from the higher energy of the two π-symmetry N lone pairs depicted in $[NPh]^{2-}$ in Figure 4.6. This is 0.33 eV lower in energy than the π_h in **1Q_Me** due to the electron-withdrawing nature of the phenyl group compared with methyl. The counterpart of the HOMO in **1Q_Ph** is the HOMO–7 which is Ti–N π_v bonding and also shows significant donation of a Ti–N π component into the phenyl ring. The HOMO–1 is a mainly amidinate ligand-based lone pair, similar to the HOMO of **1Q_Me**.

The structure of the model borylimido complexes is now analysed. The π_h component of the metal-nitrogen multiple bond in **1Q_BMe$_2$** lies at an energy of –5.60 eV and has features comparable to the alkylimido analogue **1Q_Me** where the HOMO-2 is at –6.17 eV. Although the HOMO–2 and the HOMO-4 of **1Q_BMe$_2$** show significant mixing with Cp π-bonding orbitals, inspection of atomic contributions show that these two MO best incorporate the π_v component. HOMO-2 is 0.73 eV more stable than the π_h as this is formed from the HOMO–1 of $[NBMe_2]^{2-}$ which is significantly stabilised by donation of the N lone pair into the empty B 2p orbital, and the HOMO-4 lies at -7.80 eV. As in **1Q_Ph**, the complete Ti–N π_v interaction is distributed among several MOs.

Finally, the π MOs of the model borylimide **1Q_B(NMeCH)$_2$** are comparable in form to those of the model phenylimide **1Q_Ph**. In particular, the π_v component of both models is the HOMO, which is high in energy due to an antibonding interaction between this component of the multiple bond and a filled π orbital of the respective phenyl or borylimido ring. However, that of **1Q_B(NMeCH)$_2$** is significantly higher in energy than that of **1Q_Ph** (–4.46 *vs* –5.23 eV), this being due to the electropositive nature of boron. As expected, the π_h component is lower in energy (–6.51 eV) as no significant interaction with the vacant orbital on the boron atom occurs. Similar to **1Q_Ph** and **1Q_BMe$_2$**, the HOMO–6 of **1Q_B(NMeCH)$_2$** represents a backbonding interaction from a metal–nitrogen π component into an empty π orbital of the boryl ring, this effect originating from the HOMO–1 of the $[NB(NMeCH)_2]^{2-}$ fragment.

As reported above, to test the validity of using CpTi{MeC(NMe)$_2$}{NB(NMeCH)$_2$} (**1Q_B(NMeCH)$_2$**) as a model for the real compound Cp*Ti(hpp){NB(NAr'CH)$_2$} (**4.5**), calculations were also run on the hpp-supported model CpTi(hpp)(NMe) (**4.5Q_Me**) and compared with **1Q_Me**. The three highest occupied MOs of each model are shown in

Figure 4.8, along with their energies. It is found that these MOs of **4.5Q_Me** are analogous in form to those of **1Q_Me** although are consistently higher in energy, possibly arising from the guanidinate nitrogen making the ligand more electron rich. The HOMO of each model is a ligand-based orbital with significant delocalization into the Ti-N π bond (at energies of –5.49 and –5.31 eV for **1Q_Me** and **4.5Q_Me** respectively). The HOMO–1 is the π_v MO, and the HOMO–2– is the π_h MO in each case.

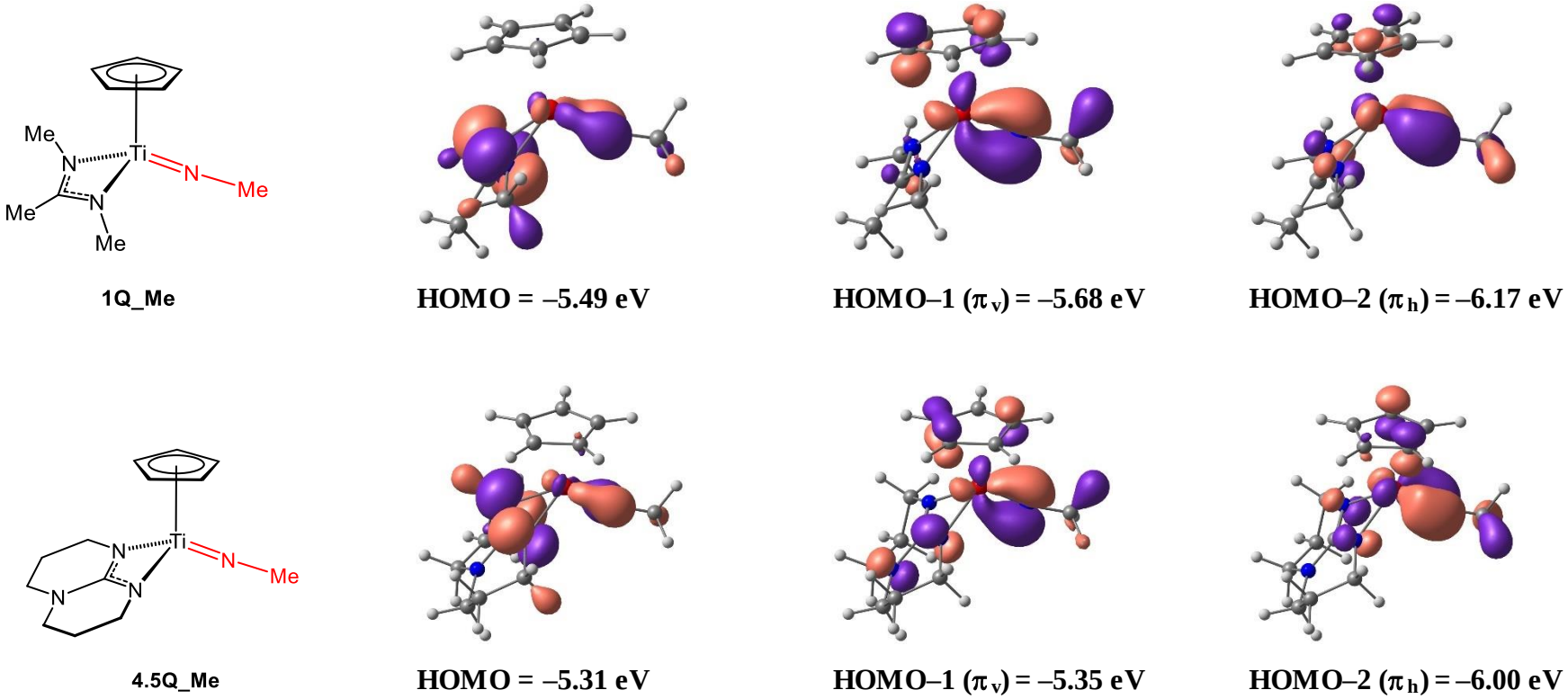

Figure 4.8. DFT model compounds CpTi{MeC(NMe)$_2$}(NMe) (**1Q_Me**, top) and CpTi(hpp)(NMe) (**4.5Q_Me**, bottom), and associated isosurfaces and energies of the three highest occupied MOs.

4.4.2 Bond dissociation energies, QTAIM and NBO calculations of half-sandwich compounds

To further understand the differences in energetics between borylamines and other amine derivatives, bond dissociation energies of the model titanium–nitrogen multiple bonds were calculated. The bond dissociation energy is considered the sum of three components: the interaction energy ($E_{interaction}$) between the atoms involved in the formation of the multiple bond, in addition to the relaxation energies (E_{relax}) of the two resulting fragments (from the geometries of the fragments in the complexes to the lowest energy relaxed geometries) (Equation 4.6). The three components and the summed bond dissociation energies are all listed in Table 4.1. From this table it is clear that the model borylimides have the greatest bond dissociation energies, so are considered to be the strongest titanium–nitrogen linkages by this measure. In particular, **1Q_B(NMeCH)$_2$** and **1Q_BMe$_2$** have ΔE_{BD} values of 119.6 and 132.3 kcal mol^{-1}, respectively, which compare to 109.7 and 108.2 kcal mol^{-1} for the model imides **1Q_Me** and **1Q_Ph**.

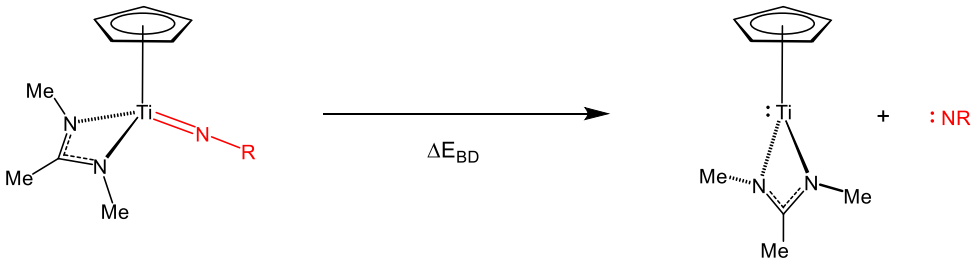

1Q_R **1Q_frag**

Equation 4.6

Table 4.1. Relaxation energies (E_{relax}), interaction energies ($E_{interaction}$) and bond dissociation energies (ΔE_{BD} = E_{relax} (1Q_frag) + E_{relax} (NR) + $E_{interaction}$) for a range of titanium–nitrogen multiply bonded model complexes. All fragments are in the triplet state, and all energies are given in kcal mol^{-1}.

NR	E_{relax} (**1Q_frag**)	E_{relax} (NR)	$E_{interaction}$	ΔE_{BD}
NMe	–7.9	–1.2	118.8	109.7
NPh	–7.9	–2.2	118.3	108.2
$NBMe_2$	–7.9	–5.9	146.1	132.3
$NB(NMeCH)_2$	–7.9	–1.2	128.7	119.6

The bond dissociation energies described above showed that the model borylimides actually have stronger Ti–N multiple bonds than their imido counterparts. However, it was experimentally reported that borylamines do not readily exchange with a *tert*-butylimido ligand and in the reactions of **4.5**, that H_2N^tBu and anilines do give exchange with a borylimido ligand. However, it must be noted that, to obtain the full picture, the N–H bond energies of the relevant amine and borylamine substrates must be considered. A full understanding of these processes thus requires an analysis of both the N-H and Ti-N bonds.

For this purpose, a set of QTAIM (Quantum Theory of Atoms in Molecules) calculations[41] and a full NBO analysis[42] were performed in collaboration with Prof. Philip Mountford and Dr. Eric Clot. QTAIM calculations might be useful to extract some key parameters needed to elucidate the nature of the bonding in molecules. In general, diagnostic parameters that can be analysed when performing a QTAIM calculation are the following:

1. The delocalization index, δ(A-B), of a bond A–B, which is a measure of the number of electron pairs delocalised or shared between the two atoms and can relate to the formal bond order for series of similar compounds
2. The Laplacian, $\nabla^2\rho$, which is a measure of the concentration of electron density at a particular point. When $\nabla^2\rho > 0$ the electron density is locally depleted from

the BCP, and where $\nabla^2\rho < 0$ the electron density is locally concentrated at the bond critical point, which is an indication of a covalent bond.

3. The ellipticity, ε, measures the extent to which the density is preferentially accumulated into a given plane containing the bond path. It is equal to 0 if the bond is cylindrically symmetrical (e.g. for the single bond in ethane or for the triple bond in acetylene).
4. The total energy density *H* is the sum of the total kinetic energy (*G*) and potential energy (*V*) densities at the BCP. *H* is negative for interactions with a significant sharing of electrons, and its magnitude reflects the "covalence" of the interaction.
5. The electron density, ρ, at the BCP. A larger ρ can indicate a stronger bond for a given pair of atoms.

The key QTAIM parameters are listed in Tables 4.2 and Table 4.3, along with calculated stretching frequencies (ν) and force constants (*k*) of the N–H bonds in the respective amines H_2NR which will be discussed below. In the following tables and plots, a colour coding scheme is employed to visually highlight the different types of metal–nitrogen multiple bonded functional groups. Blue data correspond to borylimido functional groups, red to arylimides and green to hydrazides, whilst the black data refer to the model methylimide **1Q_Me**. Different types of titanium nitrogen multiple bonded functional groups were analysed separately, in order to better understand the particular features of each group.

Table 4.2. Selected QTAIM data (atomic units) in model complexes of the type CpTi{MeC(NMe)$_2$}(NR) (**1Q_R**; R = BMe$_2$, B(NMeCH)$_2$, BMe$_2$NH$_3$, Me, 4-C$_6$H$_4$CF$_3$, Ph, 4-C$_6$H$_4$NH$_2$, NMe$_2$, NMe$_2$_planar), associated Ti–N$_{im}$ and N$_{im}$–R bond distances (d, Å) in the optimised structures, and energies (kcal mol^{-1}) for Ti–N bond dissociation (ΔE_{BD}), amine exchange from **1Q_Me** (ΔE_{exch}) and double N–H bond dissociation of the respective amine (ΔE_{2N-H}). Values for ρ (electron density), $\nabla^2\rho$ (electron density Laplacian), and ε (ellipticity) were obtained at the bond critical point. δ(A–B) is the delocalisation index for the stated pair of atoms.

1Q_R	d(Ti–N$_{im}$)	d(N$_{im}$–R)	ΔE_{BD}	ΔE_{exch}	ΔE_{2N-H}	δ(Ti–N$_{im}$)	ρ(Ti–N$_{im}$)	$\nabla^2\rho$(Ti–N$_{im}$)	ε(Ti–N$_{im}$)	δ(N$_{im}$–R)
1Q_BMe$_2$	1.706	1.415	132.3	11.7	225.8	1.590	0.206	0.712	0.211	0.535
1Q_B(NMeCH)$_2$	1.694	1.429	119.6	0.8	202.3	1.632	0.212	0.727	0.063	0.482
1Q_BMe$_2$NH$_3$	1.674	1.504	117.2	5.7	204.7	1.772	0.222	0.765	0.032	0.407
1Q_Me	1.679	1.417	109.7	0.0	191.5	1.673	0.209	0.819	0.091	1.046
1Q_4-C$_6$H$_4$CF$_3$	1.708	1.361	111.6	–2.4	191.0	1.498	0.196	0.770	0.152	1.128
1Q_Ph	1.702	1.366	108.2	–1.8	188.2	1.534	0.199	0.780	0.134	1.112
1Q_4-C$_6$H$_4$NH$_2$	1.700	1.369	103.3	–2.8	182.4	1.550	0.200	0.781	0.110	1.107
1Q_NMe$_2$	1.699	1.346	94.6	–6.5	170.0	1.551	0.193	0.811	0.041	1.287
1Q_NMe$_2$_planar	1.712	1.320	93.3	–7.0	168.1	1.501	0.182	0.841	0.210	1.351

Table 4.3. QTAIM charges (*Q*, units of *e*) of fragments of model complexes of the type CpTi{MeC(NMe)$_2$}(NR) (**1Q_R**; R = BMe_2, $B(NMeCH)_2$, BMe_2NH_3, Me, 4-$C_6H_4CF_3$, Ph, 4-$C_6H_4NH_2$, NMe_2, NMe_2_planar), and average ν(N–H) (cm^{-1}) and force constants *k*(N–H) (mDyne $Å^{-1}$) associated with the respective amine H_2NR.

1Q_R	*Q*(NR)	*Q*(Ti)	ν(N–H) (avg.)	*k*(N–H) (avg.)
1Q_BMe_2	–0.887	1.972	3644.2	8.4
1Q_$B(NMeCH)_2$	–0.851	1.967	3684.2	8.6
1Q_BMe_2NH_3	–0.747	1.940	3606.2	8.2
1Q_Me	–0.802	1.944	3555.0	8.0
1Q_4-$C_6H_4CF_3$	–0.912	1.967	3646.5	8.4
1Q_Ph	–0.874	1.958	3630.5	8.3
1Q_4-$C_6H_4NH_2$	–0.838	1.950	3609.5	8.2
1Q_NMe_2	–0.749	1.910	3479.1	7.6
1Q_NMe_2_planar	–0.695	1.884	3443.5	7.5

The main results obtained to correlate the QTAIM and the BDE results are reported in Figure 4.9. There exist (in principle) two measures of the titanium–nitrogen multiple bond strength which may be accessed both experimentally and through computation: the Ti–N bond distance and the bond dissociation energy (ΔE_{BD}). Here, each of these will be correlated with QTAIM parameters and their variation with imide substituent R discussed. Firstly, however, it is noted that the Ti–N bond distances and bond dissociation energies in the family of compounds **1Q_R** are not themselves correlated, as shown in Figure 4.9 (top left). Indeed, when the Ti–N_{im} bond distance in **1Q_Me** was lengthened by 0.071 Å (from 1.679 Å in the optimised structure to 1.750 Å), the total electronic energy of the resulting model complex increases by 1.3 kcal mol^{-1} only, signifying that the electronic energy of the system (and by extension, ΔE_{BD}) is not strongly dependent on the value of this metric, which relates mainly to π interactions with the substituent R.

The variation in the Ti–N_{im} bond distance in this family of model complexes is considered. This distance anti-correlates with the delocalisation index δ(Ti–N_{im}) of that bond, as seen in Figure 4.9 (top right, R^2 = 0.866). Using the Ti–N_{im} distance of 1.679 Å in **1Q_Me** as a starting point, the model arylimides **1Q_4-$C_6H_4CF_3$**, **1Q_Ph** and **1Q_$C_6H_4NH_2$** all have longer distances, and correspondingly smaller delocalisation indices. In an arylimide, there are two contributing π effects. Firstly, a backbonding interaction exists from a Ti–N π bond to an unoccupied π* orbital of the aryl ring, and secondly, there is donation from a filled π orbital of the aryl ring into a π* orbital of the Ti–N bond. Together, these two effects result in a reduction of the bond order of the Ti–N multiple bond and a lengthening of the bond. The data here suggest that the former effect is dominant, as this effect is greatest for the electron-poor ring in **1Q_4-$C_6H_4CF_3$** group, giving a bond distance of 1.708 Å and δ(Ti–N_{im}) of 1.498, and least for the electron-rich ring in **1Q_4-$C_6H_4NH_2$**, giving a bond distance of 1.700 Å and δ(Ti–N_{im}) of 1.550.

The same effect is seen in the model hydrazides, though in this case arises from donation of the N_β lone pair into a π* orbital of the Ti–N multiple bond. This effect is greatest when N_β is forced to be planar as a more linear alignment of the lone pair with the Ti–N π bond is possible.

Finally, the model borylimides, **1Q_B(NMeCH)$_2$** and **1Q_BMe_2**, were explored. These have longer Ti–N_{im} distances than **1Q_Me** due to delocalisation of the Ti-N_{im} π_v bond pair to the 2p orbital of boron. This effect is lessened for **1Q_B(NMeCH)$_2$** as there is competing donation to the 2p orbital by the nitrogen atoms in the backbone of the borolyl moiety, and is also found to be negated by the coordination of NH_3 to boron in the model **1Q_BMe_2NH_3**. It is also found that the Ti–N bond dissociation energies of **1Q_R** correlate extremely well with the calculated N–H bond dissociation energies of the corresponding amines H_2NR, as shown in Figure 4.9 (centre right, R^2 = 0.988), and in turn with the average N–H bond force constants which reflect only N–H σ-bonding effects. The anti-correlation between the average force constant k(N–H) and the electron density Laplacian is also shown in Figure 4.9 (bottom left). These results therefore confirm a relationship between the strength of the N–H bonds of an amine H_2NR and the metal–nitrogen multiple bond strength in the corresponding imido derivative, arising from the σ-donor ability of the NR fragment. In cases where NR is a strong σ-donor, such as for R = BMe_2 and $B(NMeCH)_2$ the N–H bonds of the amine are strongest and ΔE_{BD} values are the greatest (132.3 and 119.6 kcal mol^{-1} respectively). When considering the

much smaller ΔE_{BD} values in the model hydrazides **1Q_NMe$_2$** and **1Q_NMe$_2$_planar** (94.6 and 93.3 kcal mol^{-1} respectively) it is now apparent that these are due to the poorer σ-donor ability of the $NNMe_2$ fragments, which arises largely from the electronegativity of the N_β-containing group.

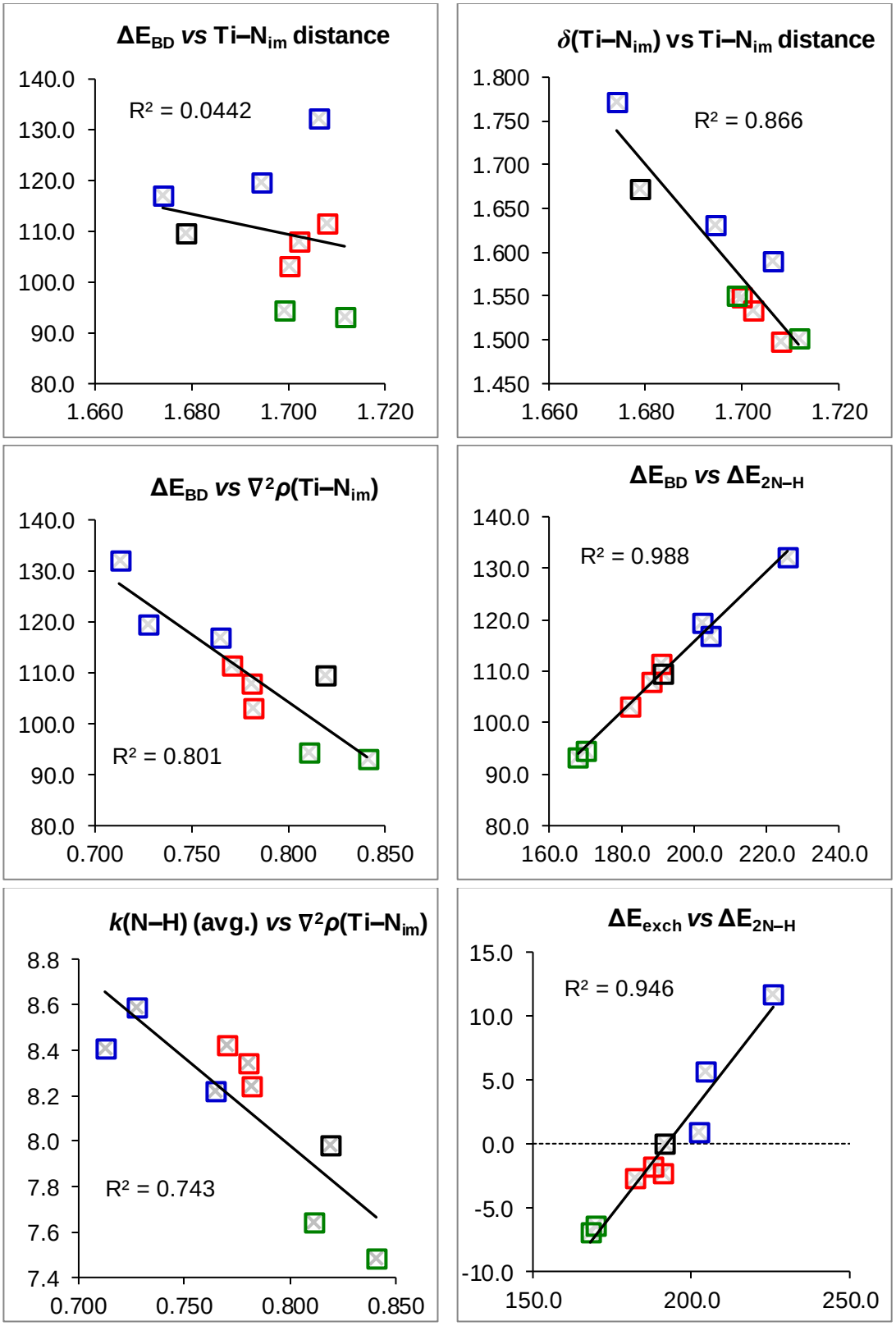

Figure 4.9. Selected relationships between QTAIM parameters (atomic units) and bond dissociation and exchange energies (kcal mol^{-1}), N–H bond force constants (k, mDyne Å^{-1}) and Ti–N$_{im}$ bond distances (Å).

Another set of QTAIM studies was performed on variants of the model complexes **1Q_R** in which the Ti–N_{im} bond distances of all of the complexes were fixed at 1.700 Å which is close to the average of the optimised distances. These new models are denoted **1Q_R_fixed** and the newly calculated QTAIM parameters for the Ti–N_{im} bond are listed in Table 4.4, along with graphical plots of their relationships with the bond dissociation energies obtained from the original models **1Q_R** in Figure 4.10. This strategy aimed to isolate the underlying donor ability of the NR fragment from the π effects which dominate variation in the Ti–N_{im} bond distance.

Firstly, there is a strong correlation (R^2 = 0.874) between the Ti–N_{im} bond dissociation energies in **1Q_R** and the electron densities at the BCP, ρ, in **1Q_R_fixed** (Figure 4.10, top left). Correlations of ρ with binding energies are known for a number of different types of bond, and can be used as a measure of bond covalency.[43] In this study, ρ is found to be greatest for the borylimides (blue data points), corresponding to the greatest ΔE_{BD} values, and smallest for the hydrazides (green data points), these having the smallest ΔE_{BD} values. Thus, ρ appears to reflect increasing covalency of the Ti–N_{im} bond with more electron-releasing NR fragments. A strong negative correlation (R^2 = 0.834) also exists between ΔE_{BD} and the Laplacian of the electron density at the BCP, $\nabla^2\rho$ (Figure 4.10, top right). The Laplacian is defined as the sum of three curvatures of electron density at the BCP: λ_1 and λ_2 are negative and lie in two coordinates perpendicular to the bond path, while λ_3, the curvature along the bond path, is positive.[43] It is the two negative components of the Laplacian which measure the concentration of electron density along the bond path, and give the negative correlation mentioned above. Although the Laplacian does not correlate well and does not reflect the covalent character of the Ti-N bond (the value is positive for all the computed complexes) the two components that reflect the electron density along the bond path correlate well with the BDE. Indeed, plotting ΔE_{BD} against the negative λ component which has the highest magnitude (by convention λ_1), a strong negative correlation (R^2 = 0.908) is again observed (Figure 4.10, centre left). It must be noted that, while the λ_3 component stays more or less constant amongst the complexes, the most electron-releasing NR fragments give the most negative λ_1 values. This, therefore, reflects the greatest degree of electron density concentration along the bond path for the strongest bond. However the Laplacian is not a good indicator of the covalent bonding in this cases as compared to the total energy density described below and the electron density at the BCP.

Turning next to measures of energy density, there is a strong correlation (R^2 = 0.873) between ΔE_{BD} and the total energy density (the sum of potential and kinetic energy densities) at the BCP, *H* (Figure 4.10, centre right). *H* is known to be negative for covalent interactions, with its increasing magnitude reflecting a greater degree of covalency.[43] This follows the same trends described above for the electron-releasing nature of the respective NR fragments. Inspection of the potential (*V*) and kinetic (*G*) energy components of *H* show that, in this study, the variation of the total energy density is dominated by *V*, with a plot of ΔE_{BD} against *V* giving a similarly strong correlation (R^2 = 0.826; Figure 4.10, bottom left). In contrast, there is no significant relationship between *G* and ΔE_{BD}.

A negative correlation (R^2 = 0.839) is found, however, between ΔE_{BD} and the composite QTAIM parameter G/ρ (Figure 4.10, bottom right). For a homonuclear bond, this ratio has been reported to increase with the bond order, whilst in polar bonds the increasing magnitude of this ratio corresponds to an increasing bond polarity.[44] It is the latter correlation which is relevant in this study, where the ratio is greatest for the most polar Ti–N_{im} bonds (hydrazides containing electronegative N_β) and smallest for the least polar Ti–N_{im} bonds (borylimides containing electropositive B). Interestingly, the G/ρ value of **1Q_BMe$_2$NH$_3$_fixed** is considerably smaller than that of **1Q_Me_fixed** (1.428 *vs* 1.508), despite these two models being isoelectronic (1.428 *vs* 1.508). This highlights the fact that this metric is dominated by the electronegativity of the atom directly bonded to N_{im}. Indeed, the G/ρ value of **1Q_BMe$_2$NH$_3$_fixed** is closer to those of the two other model borylimides **1Q_BMe$_2$** and **1Q_B(NMeCH)$_2$** (1.400 and 1.405 respectively).

Table 4.4. Selected QTAIM data (atomic units) for the Ti–N_{im} bond (fixed at 1.700 Å) in model complexes of the type CpTi{MeC(NMe)$_2$}(NR) (**1Q_R_fixed**; R = BMe_2, $B(NMeCH)_2$, BMe_2NH_3, Me, 4-$C_6H_4CF_3$, Ph, 4-$C_6H_4NH_2$, NMe_2, NMe_2_planar). All other bond metrics remained unchanged from the optimised structures. Values for ρ (electron density), $\nabla^2\rho$ (electron density Laplacian), ε (ellipticity), H (total energy density), G (kinetic energy density) and V (potential energy density) were obtained at the bond critical point. δ is the delocalisation index of the Ti–N_{im} bond. λ_1 and λ_2 are curvatures of the electron density in two coordinates perpendicular to the bond path, while λ_3 is the curvature of the electron density along the bond path.

1Q_R_fixed	δ	ρ	$\nabla^2\rho$	ε	λ_1	λ_2	λ_3	H	G	V	G/ρ
1Q_BMe_2_fixed	1.596	0.210	0.719	0.208	–0.366	–0.303	1.388	–0.114	0.294	–0.407	1.400
1Q_$B(NMeCH)_2$_fixed	1.627	0.209	0.722	0.063	–0.339	–0.318	1.379	–0.113	0.293	–0.406	1.405
1Q_BMe_2NH_3_fixed	1.749	0.208	0.740	0.032	–0.318	–0.308	1.366	–0.112	0.297	–0.408	1.428
1Q_Me_fixed	1.653	0.199	0.793	0.096	–0.298	–0.272	1.362	–0.101	0.300	–0.401	1.508
1Q_4-$C_6H_4CF_3$_fixed	1.506	0.200	0.780	0.150	–0.321	–0.279	1.379	–0.103	0.298	–0.401	1.490
1Q_Ph_fixed	1.536	0.200	0.783	0.133	–0.315	–0.278	1.377	–0.103	0.298	–0.401	1.494
1Q_4-$C_6H_4NH_2$_fixed	1.549	0.200	0.781	0.111	–0.312	–0.281	1.374	–0.103	0.298	–0.401	1.491
1Q_NMe_2_fixed	1.550	0.192	0.809	0.041	–0.277	–0.266	1.352	–0.095	0.297	–0.391	1.545
1Q_NMe_2_planar_fixed	1.515	0.188	0.859	0.205	–0.274	–0.228	1.361	–0.089	0.304	–0.394	1.618

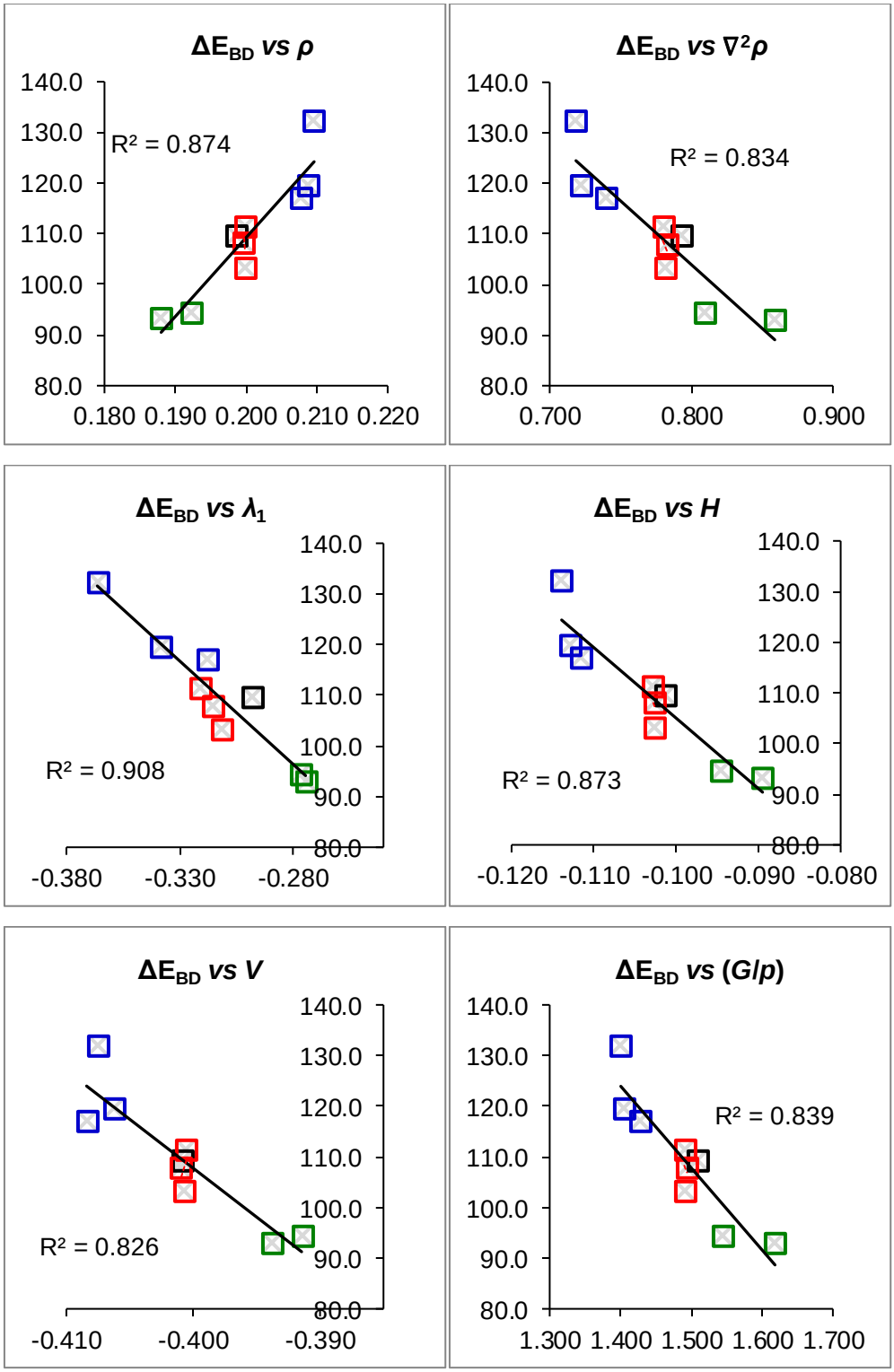

Figure 4.10. Selected relationships of QTAIM parameters (atomic units) of the Ti–N_{im} bond of the models **1Q_R_fixed** with bond dissociation energies (kcal mol^{-1}) of the models **1Q_R**.

It is also noted that the delocalisation indices (δ) in the family of *fixed-distance* models **1Q_R_fixed** correlate strongly with the Ti–N_{im} bond distances in the *relaxed* species

1Q_R (R^2 = 0.823), whilst δ of **1Q_R_fixed** does not correlate well with the bond dissociation energies of **1Q_R** (R^2 = 0.231). This confirms that the low energy variation in the Ti–N_{im} bond distances across the range of models **1Q_R** does not have a significant effect on the calculated bond dissociation energies in those models, and validates this approach of fixing the Ti–N_{im} bond distance to reveal more underlying relationships with QTAIM parameters.

A natural bonding orbital (NBO) study was then performed on the family of model complexes **1Q_R_fixed**. In this methodology, the models were set up with no formal bond being present between Ti and N_{im} (although the Ti–N_{im} distance is set at 1.700 Å). Instead, N_{im} bears three NBOs which ideally contain two electrons each, these representing three N lone pairs: one with σ symmetry and two with π symmetry. These three NBOs then mix with accepting NBOs on the Ti centre to create three natural localised molecular orbitals (NLMOs) which are strictly occupied by two electrons each and represent the one σ and two π components (π_{para} and π_{perp}) of the metal–nitrogen multiple bond in a Lewis structure sense.[42] Inspection of the percentage titanium participation in each of these NLMOs is a means to evaluate the σ- or π-donor ability of the respective NBO; a greater weight on Ti indicates greater donation of electron density from N_{im}, i.e. a greater degree of covalency. This data is listed in Table 4.5.

Inspection of the titanium participation in the σ NLMO shows that this is largest for the borylimides (blue) and smallest for the hydrazides (green), indicating a relationship with the electronegativity of the substituent R. Thus, NR fragments with more electropositive R groups are stronger σ donors and, as expected from the QTAIM studies described above, a strong correlation (R^2 = 0.798) is found between ΔE_{BD} and % Ti (σ) (Figure 4.11, left). The titanium participation in π_{perp} scales in the opposite direction, due to the π effects of the R substituent which have previously been described (e.g. donation of an N_β lone pair into a Ti–N π* orbital or donation of Ti–N π electrons into an empty B 2p orbital), although this correlates less well with ΔE_{BD}. No clear relationship is seen between the identity of R and Ti participation in π_{para}.

Table 4.5. Percentage Ti participation (% Ti) in Ti–N_{im} NLMOs, and hybridisation (proportion of p character, sp^x) of the Ti–N and N–R σ bonds, obtained from NBO calculations on model complexes of the type CpTi{MeC(NMe)$_2$}(NR) (**1Q_R_fixed**; R = BMe_2, $B(NMeCH)_2$, BMe_2NH_3, Me, 4-$C_6H_4CF_3$, Ph, 4-$C_6H_4NH_2$, NMe_2, NMe_2_planar).

1Q_R_fixed	%Ti (σ)	%Ti (π_{para})	%Ti (π_{perp})	sp^x (Ti–N σ)	sp^x (N–R σ)
1Q_BMe_2_fixed	20.4	30.2	17.2	1.94	0.54
1Q_$B(NMeCH)_2$_fixed	19.4	26.1	25.7	1.53	0.78
1Q_BMe_2NH_3_fixed	20.3	25.8	30.0	1.05	1.01
1Q_Me_fixed	18.0	28.7	29.1	0.64	1.78
1Q_4-$C_6H_4CF_3$_fixed	17.4	27.1	24.6	0.83	1.43
1Q_Ph_fixed	17.6	27.4	25.8	0.81	1.45
1Q_4-$C_6H_4NH_2$_fixed	17.5	27.1	26.9	0.78	1.48
1Q_NMe_2_fixed	17.0	25.2	34.1	0.45	2.36
1Q_NMe_2_planar_fixed	16.7	22.9	37.2	0.51	2.19

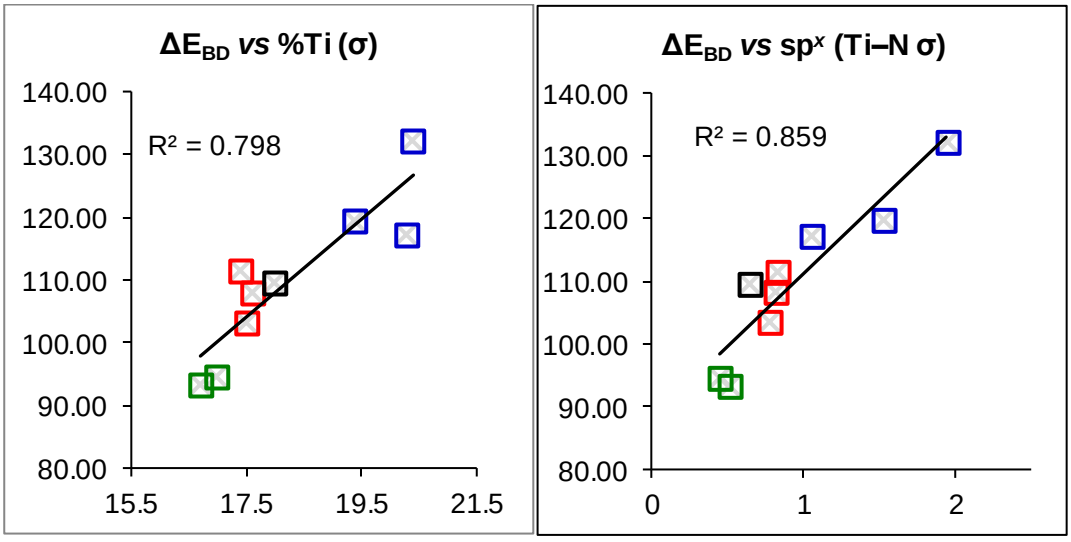

Figure 4.11. Relationships of bond dissociation energies (kcal mol^{-1}) of the models **1Q_R** with percentage titanium participation in the σ NLMO (%Ti (σ), left) and with the degree of 2p character (sp^x) in the same NLMO (right) in **1Q_R_fixed**.

Furthermore, the hybridisation of the N-based NLMO in the Ti–N and N–R σ bonds (data in Table 4.5) were analysed to give further insight on the effect of electronegativity of the R substituent on the NR fragment's σ-donor ability. It was found that the Ti–N bond has the greatest degree of 2p character for the borylimides (blue, electropositive B) and the smallest degree of 2p character for the hydrazides (green, electronegative N_β). The degree of 2p character in the N–R σ bond anti-correlates with that in the Ti–N σ bond. Greater 2p character in the Ti–N bond corresponds to greater polarisation of the NLMO towards the Ti centre, thus this parameter scales with the percentage of titanium participation in it. Correspondingly, ΔE_{BD} may also be related to the proportion of 2p character in the σ NLMO, with a strong correlation ($R^2 = 0.859$) again being observed (Figure 4.11, right).

In summary, these QTAIM and NBO studies have shown that two measures of metal–nitrogen multiple bond strength, the bond distance and the bond dissociation energy, are separable and arise from distinct electronic factors. The variation in the $Ti–N_{im}$ bond distance is found to be dominated by π interactions with the substituent at the N_{im} atom, whilst variation in the bond dissociation energy is found to arise primarily from the underlying σ-donor ability of the NR fragment, which in turn relates to the electronegativity or electropositivity of the R substituent.

4.4.3 Exchange energetics and relationship between the N-H and Ti-N BDEs

Once the individual features of both the Ti-N and N-H bonds in the model amido, hydrazido and borylimido complexes were elucidated, the energetics of the exchange processes depicted the model thermodynamic cycle (Scheme 4.2) in which the Ti=NR of **1Q_Me**, exchanges with H_2NPh, H_2NBMe_2, $H_2NB(NMeCH)_2$, were calculated. The overall energy of this exchange (ΔE_{exch}) can be expressed as the sum of four stepwise bond dissociation energies (BDEs): ΔE_1 (Ti=NR homolysis), ΔE_2 (substrate H-N homolysis), $-\Delta E_3$ (Ti=N formation) and $-\Delta E_4$ (product H-N bond formation) ($\Delta E_{exch} = \Delta E_1 + \Delta E_2 - \Delta E_3 - \Delta E_4$). This enables the assessment of the overall impact of both N-H and Ti=N bond dissociations on ΔE_{exch}.

The energies of the four processes, along with the total ΔE_{exch} are listed in Table 4.6. It can be seen that both borylamines give positive ΔE_{exch} values: 0.8 and 11.7 kcal mol^{-1} for $H_2NB(NMeCH)_2$ and H_2NBMe_2 respectively. In contrast, exchange with the model aniline H_2NPh gives –1.8 kcal mol^{-1}. Inspection of how the ΔE_2 and ΔE_3 values vary with the R group show that there is greater variation in the former, that is the breaking of the N–H bonds in the H_2NR reagent, implying that this is the dominant component of ΔE_{exch}. In particular, for H_2NBMe_2, ΔE_2 is very large (225.8 kcal mol^{-1}), and it is only slightly smaller for $H_2NB(NMeCH)_2$ (202.3 kcal mol^{-1}). This can consequently explain that failure of the experimental reactions to produce borylimides through exchange of an imido ligand with a borylamine reported above, it is apparent that the strong N–H bonds in the model borylamines more than compensate for the effect of the stronger Ti–N bonds in the respective model borylimido complexes. One way to look at the BDE values for amines is to look at the stability of the radical generated from the first N-H homolytic bond cleavage, namely ·NHR. In the case of R = alkyl, the radical will be stabilized because of positive inductive effects. In the case of R = Ph, there will be competing effects arising from the Ph ring, namely a stabilization by virtue of delocalization and a destabilization arising from the electron withdrawing nature of the phenyl ring. In the case of R = BMe_2, the inductive effect will destabilize the radical because of the electropositive nature of the boron. The higher the stability of the radical, the lower the BDE required to break the N-H bond. In this assumption, the BDE will be lower for H_2NMe, than for H_2NBMe_2 while for H_2NPh the BDE will be the result of the predominant effect. For example, for the benzyl radical $PhCH_2$·, the BDE is lower than

for the tertiary alkyl radical, $(CH_3)_3C\cdot$, indicating that the delocalization effect over compensate for the inductive destabilizing effect. These ΔE_2 values for the borylamines may be compared with 188.2 kcal mol^{-1} for H_2NPh, whilst the corresponding ΔE_3 value is 108.2 kcal mol^{-1}. These results align with the experimental evidence that anilines are reported to give exchange with the *tert*-butylimide, that the borylimido ligand in **4.5** was reported to be readily displaced by H_2N^tBu. The ΔE_{exch} were also computed for the model systems CpTi(hpp)(NMe) (**4.5Q_R**); R = Ph, BMe_2, $B(NMeCH)_2$ and values were found to be -2.5, 10.2 and 0.0 kcal mol^{-1} for H_2NPh, H_2NBMe_2 and $H_2NB(NMeCH)_2$ respectively, in line with the results reported above for the amidinate ligand.

These findings may also be of relevance to the failure of the reaction between $Ti(NMe_2)_2Cl_2$ and $H_2NBC_8H_{14}$. Whilst reaction with $H_2NB(NAr'CH)_2$ produces **4.1**, the analogous compound **4.1_BBN** cannot be prepared. These findings imply that this failure may be due to the stronger N–H bonds in $H_2NBC_8H_{14}$ relative to the other borylamine, making this protonolysis reaction unfeasible, and allowing instead the observed deleterious side reaction which forms $Me_2NBC_8H_{14}$.

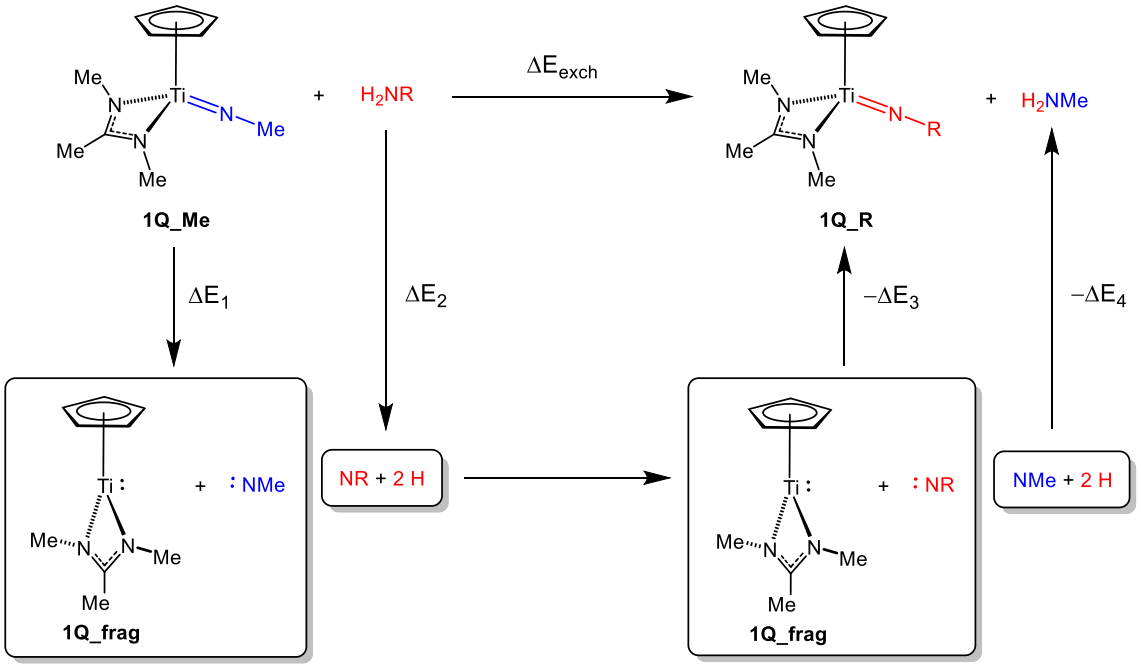

Scheme 4.2. Energy decomposition scheme for the exchange reactions of **1Q_NMe** with amine derivatives H_2NR.

Table 4.6. ΔE values (kcal mol^{-1}) for the four processes depicted in Scheme 4.2, along with the total ΔE_{exch} (= ΔE_1 + ΔE_2 – ΔE_3 – ΔE_4). All non-H fragments are in the triplet state.

NR	ΔE_1	ΔE_2	ΔE_3	ΔE_4	ΔE_{exch}
NPh	109.7	188.2	108.2	191.5	–1.8
$NBMe_2$	109.7	225.8	132.3	191.5	11.7
$NB(NMeCH)_2$	109.7	202.3	119.6	191.5	0.8

To get the full picture, SCF gas phase energies and Gibbs free energies were then evaluated for the hypothetical isodesmic reactions. The SCF gas phase energies are reported in Figure 4.12 using the model systems **1Q_R**, in which the methylimido ligand **1Q_Me** is exchanged with the borylamines to give the respective model borylimido compound and free methylamine.

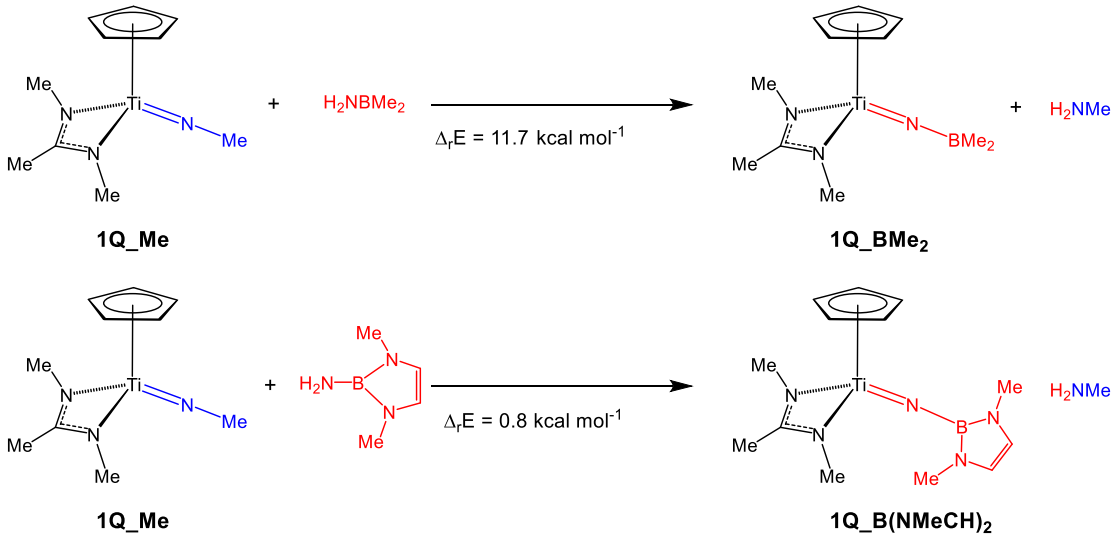

Figure 4.12. DFT computed electronic energies (kcal mol^{-1}) for the isodesmic reaction illustrated.

The reaction with $H_2NB(NMeCH)_2$ has a Δ_rE of 0.8 kcal mol^{-1}, in line with an equilibrium reaction, while it can be seen that the reaction with the model dialkylborylamine, H_2NBMe_2, has a highly positive Δ_rE of 11.7 kcal mol^{-1}. These two calculated energies, identical in value to the previously reported ΔE_{exch} are in agreement

with the experimental results in which no exchange took place between Cp*Ti(hpp)(N^{t}Bu) and $H_2BC_8H_{14}$, while Cp*Ti(hpp)(N^{t}Bu) and $H_2NB(NAr'CH)_2$ gave an equilibrium mixture of the *tert*-butylimide and the borylimide **1.91**.

The electronic energies values obtained can also be compared with those from previous calculations, although performed with a slightly different computational methodology, namely the same functional but a smaller basis set, of the isodesmic reactions of **1Q_Me** with H_2NPh, H_2NNPh_2[30] these being –2.5 and –5.1 kcal mol^{-1}, respectively. For consistency, the electronic energies values were calculated with the new computational methodology used for the reactions of **1Q_Me** with H_2NPh and H_2NNPh_2. In agreement with the previous computational results, the energies were found to be -1.8 and -4.3 kcal mol^{-1} for H_2NPh and H_2NNPh_2 respectively. In contrast to those Δ_rE values for the two borylamines, these are much more negative, and experimentally, exchange reactions between Cp*Ti{MeC(N^{i}Pr)$_2$}(N^{t}Bu) (**1.37**) and H_2NNPh_2, or anilines are quantitative.[30]

In order to compare the experimental and computational results, solvent calculations were performed on the full systems and the Δ_rG were obtained (Figure 4.13). The computational methodology is the following: geometry optimizations were performed by using B3PW91 functional[37] with a def2-svp basis set[38] followed by single point SCRF calculations within the SMD model.[45] For the SCRF calculations all the atoms were treated with a def2-tzvp basis set[39] and dispersion interactions were taken into account by computing the d3(bj) corrections.[46,47] This computational methodology is used for all the calculations performed on real systems presented in this Chapter. Again, it can be seen that the reaction of Cp*Ti(hpp)(N^{t}Bu) and $H_2NBC_8H_{14}$ is not favourable. Given that $(\mu\text{-}H_2N)_2(BC_8H_{14})_2$ is known to exist in solution as a dimer, the energy of its dissociation to a monomer should be accounted for. When the additional contribution associated with the dimer $(\mu\text{-}H_2N)_2(BC_8H_{14})_2$ dissociation is taken into account (2.2 kcal mol^{-1} for each half dimer forming one monomer), the Δ_rG is even higher (8.2 kcal mol^{-1}).

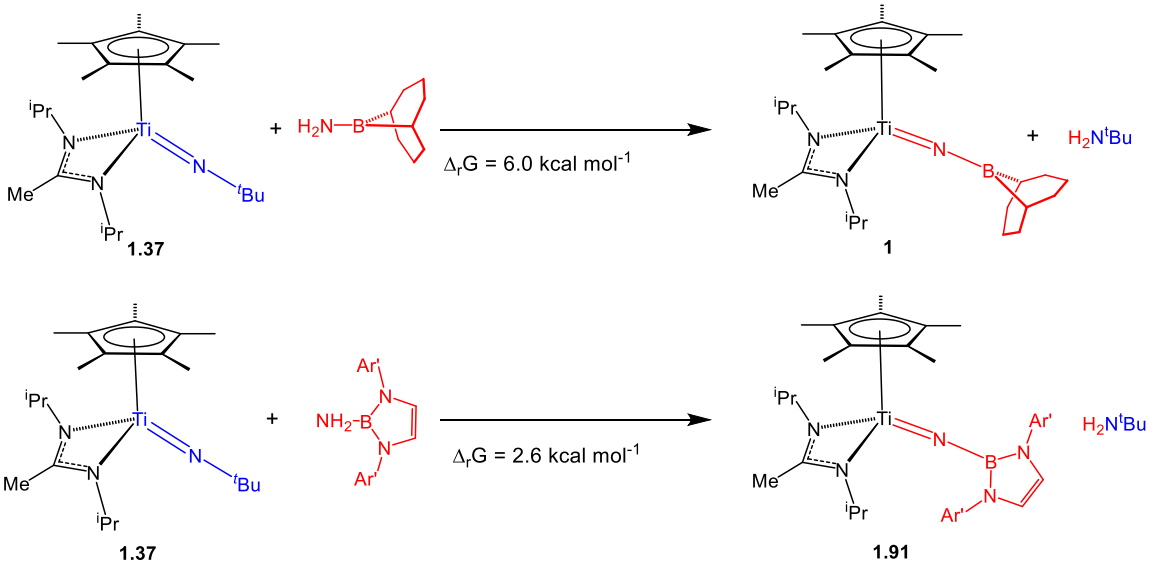

Figure 4.13. DFT computed Gibbs free energies (kcal mol^{-1}) for the isodesmic reaction illustrated.

The same calculations on the full systems were performed for the formation of **4.1, 4.1_BBN** and **4.1_BMes$_2$** from $Ti(NMe_2)_2Cl_2$ and the respective borylamine monomer depicted in Figure 4.14.

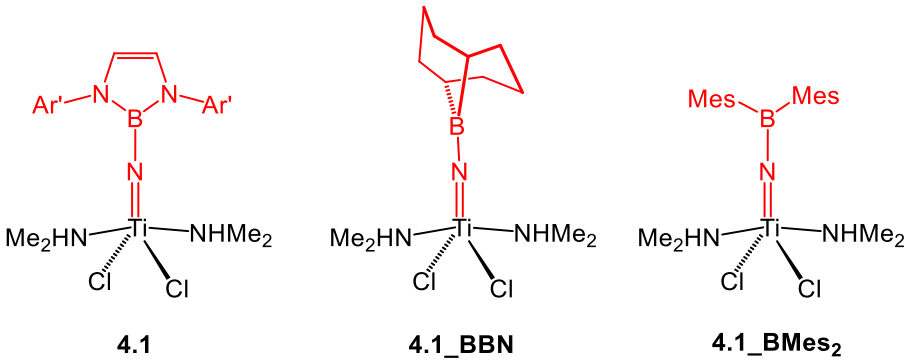

Figure 4.14. Experimental $Ti\{NB(NAr'CH)_2\}Cl_2(NHMe_2)_2$) **4.1** and hypothetical, ($Ti\{NBC_8H_{14}\}Cl_2(NHMe_2)_2$) **4.1_BBN** and ($Ti\{NBMes_2\}Cl_2(NHMe_2)_2$) **4.1_BMes$_2$** and experimental, borylimido compounds.

The Δ_rG values for the three reactions were calculated to be –4.3, 2.3 and –2.0 kcal mol^{-1} respectively. Including the dissociation of half dimer $(\mu\text{-}H_2N)_2(BC_8H_{14})_2$ to form one monomer, the total free energy change for the formation of **4.1_BBN** becomes 4.5 kcal mol^{-1}. Thus it can be seen that the formation of **4.1_BBN** is thermodynamically disfavoured compared with **4.1**, somewhat explaining the different reaction outcome in

this case. In contrast, the formation of **4.1_BMes$_2$** was calculated to be exergonic. It is therefore postulated that an amide-exchange route analogous to that found experimentally for $(\mu\text{-}H_2N)_2(BC_8H_{14})_2$ may be thermodynamically favoured over the desired reaction. By comparing the two optimized structures of **4.1** and **4.1_BBN**, the Ti=N_α bond length was found to be slightly longer in **4.1_BBN** (1.697 vs 1.679 Å), due to the different nature of the substituents on the boron atom in the two complexes. Apart from this, no substantial differences were found in the computed structures. This bond length difference was initially taken as a possible explanation for the different reactivity. In this alkyl- and arylborylamines the donation of the nitrogen lone pair into the vacant 2p orbital on the boron atom should reduce the ability of the amine to pre-coordinate to the metal and the basicity of the nitrogen atom should consequently decrease. However, it was established that pyramidalisation at the nitrogen atom of the borylamines, which is necessary for their coordination to the metal centre, is kinetically accessible, therefore ruling out the suspected involvement of donation of the nitrogen lone pair to the boron 2p orbital as a factor in these reaction outcomes. The Δ_rG values for the three reactions of $Ti(NMe_2)_2Cl_2$ with H_2NMe, H_2NPh and H_2NNPh_2 were also evaluated to verify the reliability of the numbers reported above. The values turned out to be -6.0, -7.7 and -13.0 kcal mol^{-1} respectively, in line with the experimental results previously reported for this set of compounds.[1]

In summary, this full computational analysis has shown that the favourability of imido ligand exchange reactions is mainly associated with the σ-donor ability of the NR fragment, and in relation to the experimental difficulties in forming borylimides through this methodology; this is found to arise from the high N–H bond strengths in the corresponding borylamines. The BDE values are mainly associated with the σ-donor ability of the NR fragments, thus to the electronegativity or electropositivity of the R groups.

4.5 Molecular Orbital Analysis of metallocene complexes

The molecular bonding analysis was next performed on the titanium metallocene complexes. Bent bis-(cyclopentadienyl) derivatives of the transition metals have been a focus of considerable synthetic and theoretical interest for many years. In particular in imido systems of the type $Cp_2M(NR)$, the near-linearity of the M-N-R bond and the formal sp hybridisation of the nitrogen atom, lead to the so called "π-loaded complexes", such as $Cp_2Ti(N^tBu)(py)$, which features an apparent twenty valence electron count.[48] The same situation was encountered by Schrock and co-workers, which rationalised the bonding of planar "20 electron" osmium imido complexes of the type $Os(NR)_3$, by considering one electron lone pair localized in a nitrogen-based nonbonding molecular orbital.[49] Further investigations utilizing photoelectron spectroscopy performed by Green and co-workers[50] has contributed to an understanding of the orbital structure of Cp_2ML_n compounds. In particular, the structure of the molybdenum imido complex, $Cp_2Mo(N^tBu)$ highlighted that competition of the imido π-components against the π-donor orbitals of the Cp ligands prevents full donation of the lone pair to the metal.

The orbital analysis of **1.90** was complex, thus the pyridine-free complexes were analysed first. In this case too, small model systems were used, namely $Cp_2Ti(NR)$ (**1.90Q_R**; R = Me, BMe_2, $B(NMeCH)_2$) in order to have a full comparison with the imido and hydrazido analogues previously studied in our research group.[34,35] The computational methodology was the same reported for the half-sandwich model compounds.

As in the half- sandwich complexes, the FMOs of the $[Cp_2Ti]^{2+}$ fragment will be described. The FMOs of the imido-type dianions $[NMe]^{2-}$, $[NBMe_2]^{2-}$ and $[NB(NMeCH)_2]^{2-}$ have been reported in Figure 4.5. After an elucidation of both components involved in the bonding, the MOs of the model compounds **1.90Q_R** will be presented. Selected FMOs of the $[Cp_2Ti]^{2+}$ fragment, some of which are expected to act as the acceptor orbitals for an-imido type dianion, are depicted in Figure 4.15.

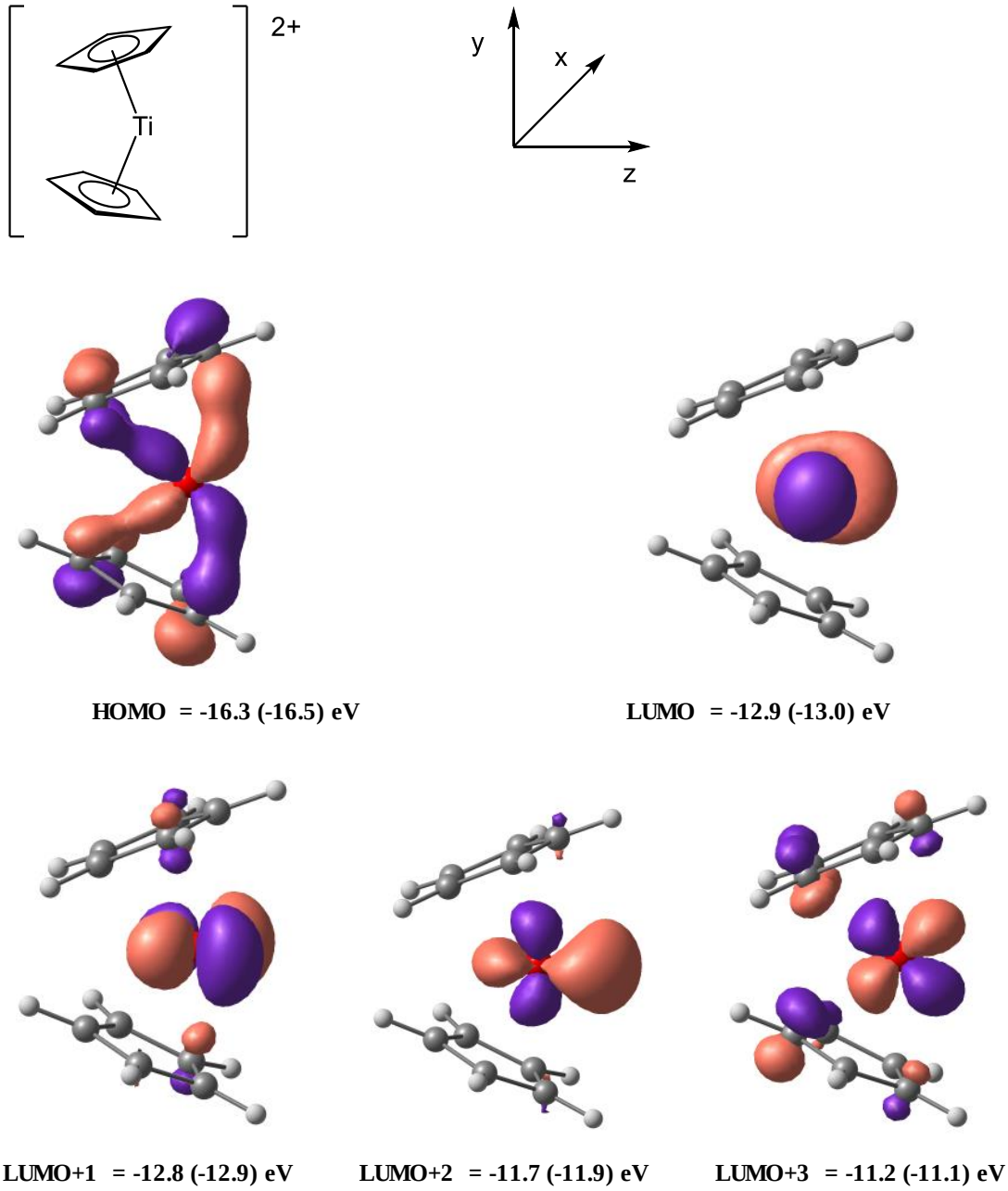

Figure 4.15. Isosurfaces and energies of frontier molecular orbitals in the model dicationic fragment $[Cp_2Ti]^{2+}$, with Cp_{cent}-Ti-Cp_{cent} θ = 128 ° (and θ = 135.2 °).

The HOMO is the π-filled orbital, which finds its antibonding counterpart in the LUMO+3 at -11.2 eV. The LUMO is a non-bonding metal d_{z^2} orbital, the π-accepting orbital is the LUMO+1 which can be thought as the metal d orbital involved in the formation of an imido-type bonding by interaction with the π_h-donor orbital found in the $[NR]^{2-}$ fragment (Figure 4.5). The LUMO+2 is a hybrid $3d_{z^2}/4s$ orbital which best overlaps with the HOMO-2 of the $[NR]^{2-}$ imido-type fragments (Figure 4.5) to form the σ component of the Ti-N bond. From this description it can be noted a clear difference with

the half- sandwich complexes. The AO of $[NR]^{2-}$ would ideally donate into the $3d_{yz}$ AO of $CpTi^{2+}$, but this orbital is already involved in the Ti-Cp bonding forming the HOMO and the LUMO+3. Interaction with NR^{2-} gives, in effect, a 4e-3c interaction between $[NR]^{2-}$, Ti and the relevant SALC of $[Cp_2]^{2-}$. Thus, even in $Cp_2Ti(NR)$, which seems to have a satisfactory 18 valence electron count, one can anticipate one vacant Ti-based AO (mainly the $3d_{x^2}$ based LUMO of $CpTi^{2+}$) and one filled "lone pair" comprising the N $2p_y$ AO of NR^{2-} the relevant SALC of Cp_2^{2+}.[50] Next, the MOs of the model complexes namely $Cp_2Ti(NR)$ (**1.90Q_R**; R = Me, BMe_2, $B(NMeCH)_2$) were analysed (Figure 4.16). In **1.90Q_Me** the HOMO is a non-bonding orbital and lies at -4.97 eV, while the HOMO-1 has an energy of -6.51 eV and is best considered to be the π_h component of the bond. The HOMO-2 is a ligand based orbital and the π_v component is the HOMO-3, at -7.18 eV. Moving on to the borylimido model compounds, in **1.90Q_BMe$_2$** the HOMO is a non-bonding orbital, while the HOMO-1 incorporates the π_h component of the bond and lies at -6.11 eV. The π_v component is present in the HOMO-5, which is significantly stabilized compared to the π_h (by 1.86 eV), due to donation of the N lone pair into the empty B 2p orbital. In **1.90Q_B(NMeCH)$_2$** the HOMO-1 is mainly a non-bonding orbital formed by the HOMO-3 of the $[NB(NMeCH)_2]^{2-}$ fragment, while the π_h component of the bond is best represented by HOMO-3 (-6.87 eV). Finally, HOMO-7 is a mixture of the Ti-Cp bond and the π_v component.

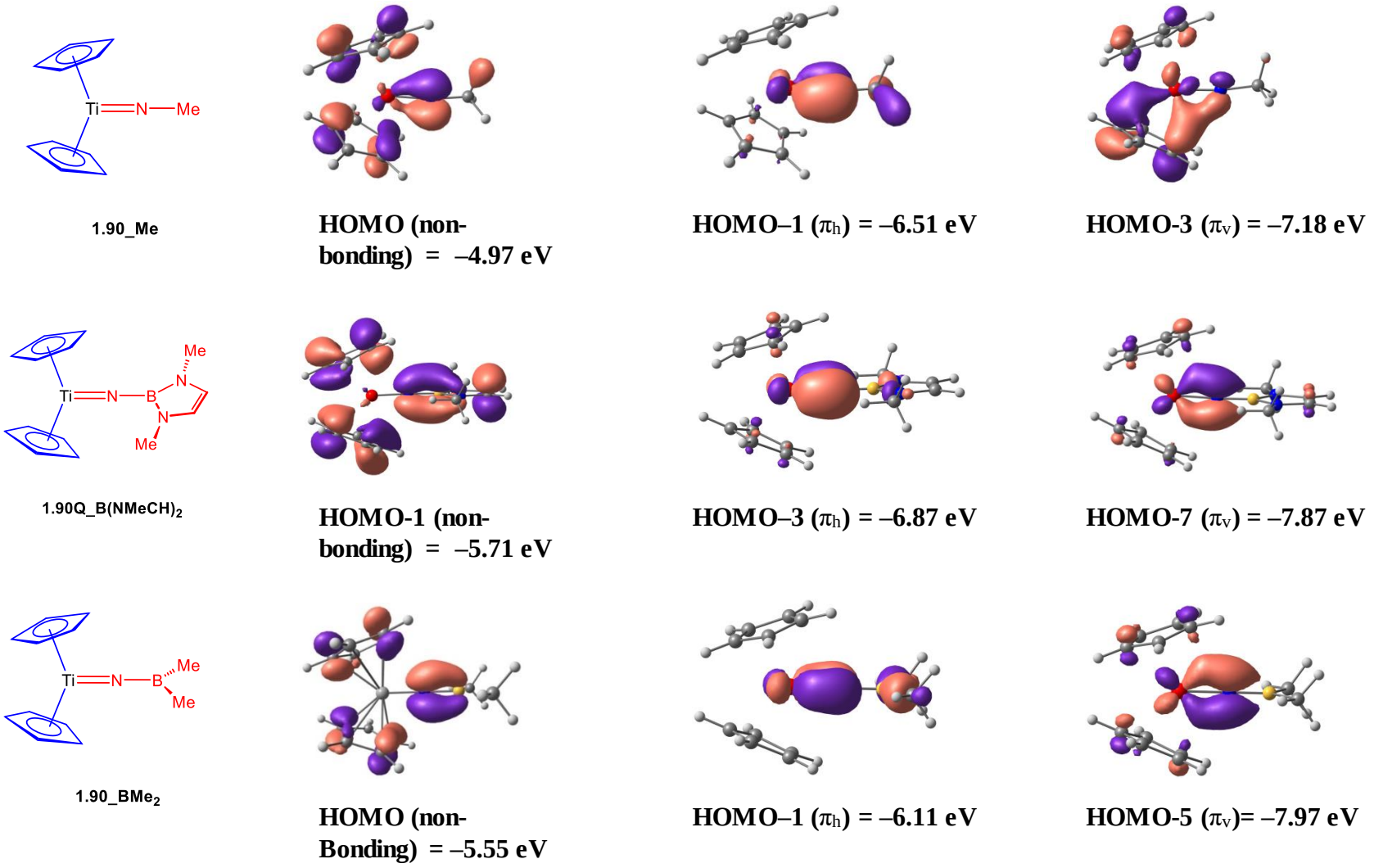

Figure 4.16. Isosurfaces and energies of frontier molecular orbitals in the model compounds, $Cp_2Ti(NR)$ (**1.90Q_R**; R = Me, BMe_2, $B(NMeCH)_2$).

The orbital analysis of the pyridine complex **1.90** is complex, and made more difficult by the lack of (even approximate) molecular symmetry, and by the fact the the $-B(NMeCH)_2$ substituent is itself rotated *ca*. 25° out of the bisecting plane of the Cp_2Ti moiety. This makes distinction between the π_h and the π_v components of the bond rather arbitrary. The MOs of the model complex $Cp_2Ti(NR)(py)$ (**1.90Q_R_py**; R = $B(NMeCH)_2$) were analysed (Figure 4.17). The HOMO is mainly boryl ring based, with some contribution of the in plane Ti=N π bond and is destabilised by an antibonding interaction with the filled π orbitals of the ring. The HOMO-1 is the expected ligand based non-bonding in $Cp_2^RM(E)(L)$ complexes (E = O or NR, L = two- or one- electron donor or none) with significant contribution from the cyclopentadienyl rings. The in plane equatorial bonding mixes with the Cp-Ti bonding in HOMO–3 and HOMO-4. The π_v component is found in HOMO-7 mixing with the Cp=Ti bonding. In the corresponding hydrazide complexes previously studied in our research group, namely $Cp_2Ti(NNPh_2)(py)$, it was noted that the phenyl substituents of the $-NNPh_2$ group were oriented in the plane bisecting the Cp_2Ti moiety.[35]

This orientation was previously noted in $Cp_2Zr(NNPh_2)$DMAP, and is well understood in terms of matching the σ and π orbitals of the hydrazide ligand with the Cp_2M moiety.[4] The π_v component of the bond in $[NNPh_2]^{2-}$ is the HOMO and has the best energy match with the metal acceptor orbitals in $Cp_2Ti(NNPh_2)(py)$. This is in contrast to what has been found in $[NBMe_2]^{2-}$ in which no destabilization of the π_v component of bonding is present, and the where the HOMO is found to be the π_h.

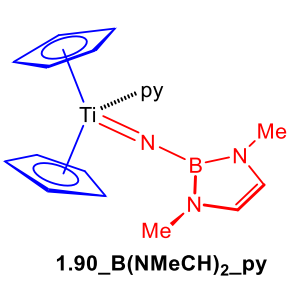

1.90_B(NMeCH)$_2$_py

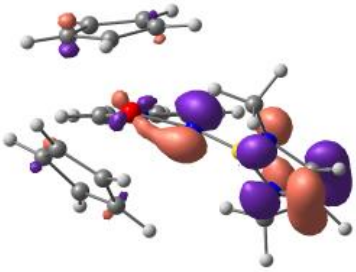

HOMO = -4.21 eV

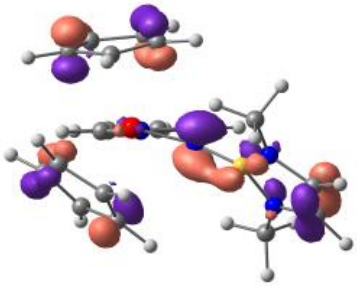

HOMO-1 = -5.20 eV

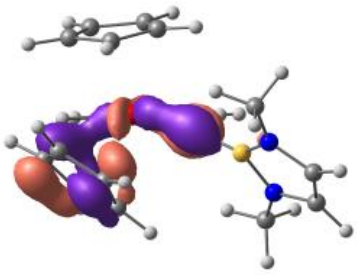

HOMO-3 = -6.33 eV

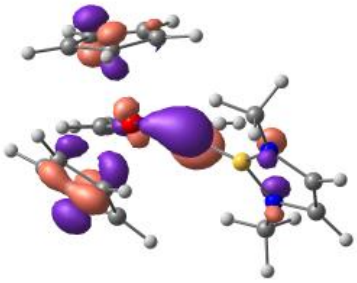

HOMO-4 = -6.52 eV

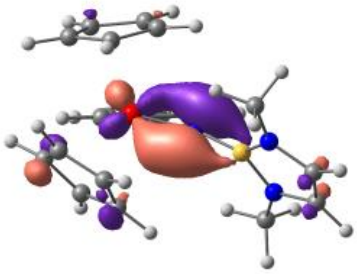

HOMO-7 = -7.39 eV

Figure 4.17. Isosurfaces and energies of frontier molecular orbitals in the model compounds, $Cp_2Ti(NR)(py)$ (**1.90Q_R_py**; R = $B(NMeCH)_2$).

4.6 Experimental and computational studies of reactivity: reactions with CO_2, CS_2, iso(thio)cyanates and TolCHO

The reactivity of the half-sandwich compound Cp*Ti(hpp){NB(NAr'CH)$_2$} **1.91** with CO_2, CS_2 and TolCHO was then investigated both experimentally and by means of DFT calculations. Starting from CO_2 and CS_2 the experimental reactions were reported to proceed at RT (2.5 days in benzene) and at 80 °C (3.5 days in toluene) for CO_2 and CS_2 respectively. In view of analogous reactions of titanium imido and hydrazido complexes with CO_2 and CS_2, initial [2+2] cycloaddition of the heteroallene with the Ti-N multiple bond was expected, potentially followed by extrusion of a boryl-functionalised organic moiety.[29,40,51,52] The experimental results confirmed the reactions to be overall functional group transfer of the borylimido unit onto CE_2 to form ECNB(NAr'CH)$_2$ (E = O (**4.6**), S (**4.7**)), a borylisocyanate and borylisothiocyanate, respectively. The second E atom of CE_2 goes to form one half of the respective oxo- or sulfido-bridged titanium dimer [Cp*Ti(hpp)(μ-E)]$_2$ (E = O (**4.8**), S (**4.9**); Scheme **4.3**).

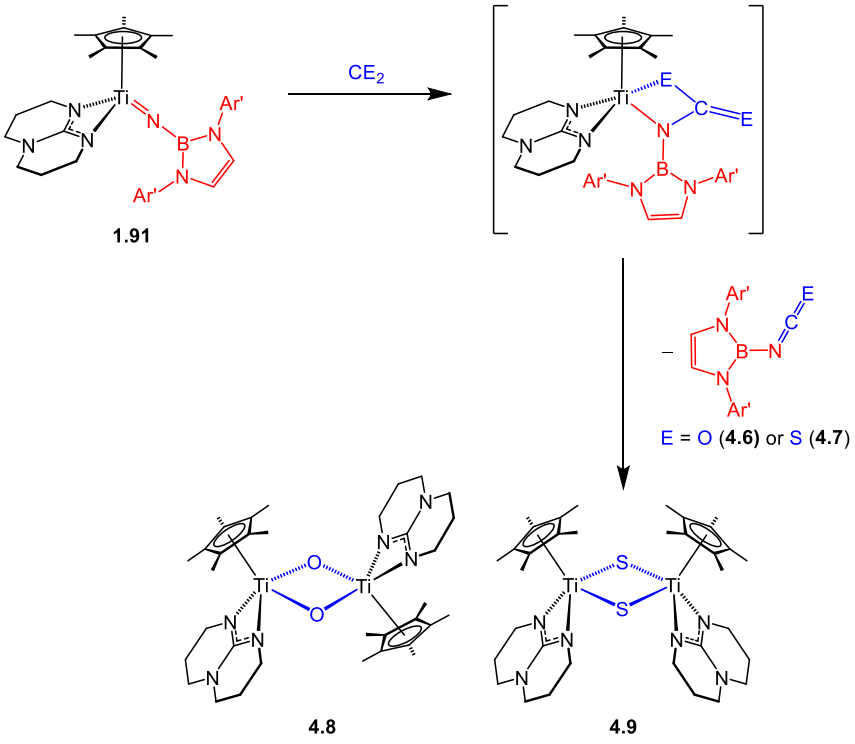

Scheme 4.3. Reactions of Cp*Ti(hpp){NB(NAr'CH)$_2$} (**1.91**) with CO_2 and CS_2. Reaction conditions: E = O: benzene, RT, 2.5 d; E = S: toluene, 80 °C, 3.5 d.

Unfortunately, any attempt to isolate a cycloaddition intermediate was unsuccessful. DFT and experimental studies reported in our group have shown that increasing the steric bulk

of the cyclopentadienyl-amidinate ligand set can kinetically stabilise cycloaddition products toward extrusion. Furthermore, it was reported that the steric demand of the ^{t}Bu group in *tert*-butyl imido complexes leads to extrusion becoming thermodynamically more favourable.[52] With this in mind, it is unsurprising that the very bulky borylimide 1.91 gives only extrusion of the borylisocyanate **4.6**.

To gain further insight into the underlying factors in these metathesis processes the model thermodynamic cycle in Scheme 4.4 in which the Ti=NR of **1Q_NMe** and **1Q_B(NMeCH)$_2$**, exchanges with the C=E (E=O or S) of CO_2, or CS_2 to give **1Q_O** and **1Q_S** was analysed and compared with the published results.[30] It was previously demonstrated experimentally and by means of DFT calculations that the tendency to transfer an imido or hydrazido group from titanium to an organic fragment (CO or CS) was greater for imides, and appears to increase in the order $NNPh_2$ < $NNMe_2$ < NTol ($N^{t}Bu$).[40] The overall energy of this exchange (ΔE_{exch}) can be expressed as the sum of four stepwise bond dissociation energies (BDEs): ΔE_1 (Ti=NR homolysis), ΔE_2 (substrate C=E homolysis), – ΔE_3 (Ti=E formation) and – ΔE_4 (product C=NR bond formation) ($\Delta E_{exch} = \Delta E_1 + \Delta E_2 - \Delta E_3 - \Delta E_4$).

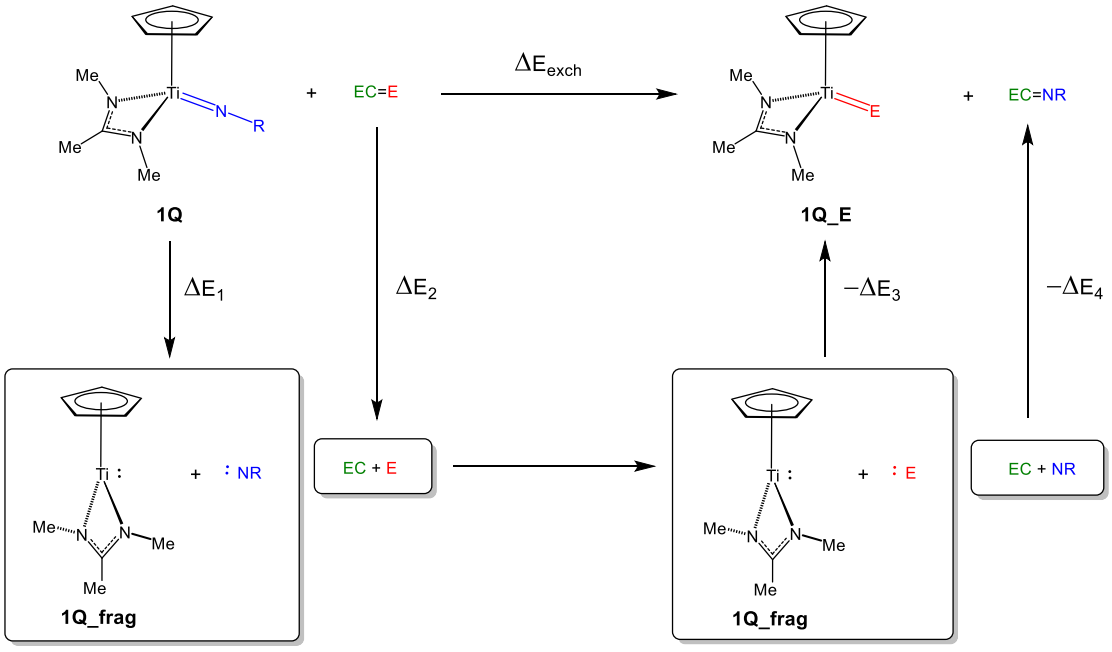

Scheme 4.4. Energy decomposition scheme for selected isodesmic multiple bond exchange reactions of CpTi{MeC(NMe)$_2$}(NR) (R = Me, B(NMeCH)$_2$) with CO_2 and CS_2, and computed bond dissociation energies (ΔE, kcal mol^{-1}). All species are spin state singlets except for the fragments CpTi{MeC(NMe)$_2$}, E, and NR which are spin triplets. ($\Delta E_{exch} = \Delta E_1 + \Delta E_2 - \Delta E_3 - \Delta E_4$).

Table 4.7. ΔE values (kcal mol^{-1}) for the process depicted in Scheme 4.4.

1Q_R	**Ti=NR**	**ΔE_1 (kcal mol^{-1})**
1Q_Me	Ti + NMe	109.7
1Q_Ph	Ti + NPh	108.2
1Q_ B(NMeCH)$_2$	Ti + NB(MeCH)$_2$	119.6
CE$_2$	**EC=E**	**ΔE_2 (kcal mol^{-1})**
CO_2	OC + O	135.7
CS_2	SC + S	114.9
1Q_E	**Ti=E**	**ΔE_3 (kcal mol^{-1})**
1Q_O	Ti + O	166.3
1Q_S	Ti + S	119.9
ECNR	**EC=NR**	**ΔE_4 (kcal mol^{-1})**
OCNMe	OC + NMe	82.7
OCNPh	OC + NPh	74.1
OCNB(NMeCH)$_2$	OC + NB(NMeCH)$_2$	100.4
SCNMe	SC + NMe	120.5
SCNPh	SC + NPh	113.6
SCNB(NMeCH)$_2$	SC + NB(NMeCH)$_2$	138.0

The bond energy of Ti=O is larger than any of the two Ti=NR systems while the Ti=S bond energy is comparable to the Ti=NB(NMeCH)$_2$ BDE and larger than the Ti=NMe BDE. Therefore, in terms of titanium-ligand bond strengths, the metathesis reaction is always favourable for imides, and more for oxide than sulfide bond formation. However, to have a full understanding and assess the contribution of each the ΔE_x in the overall ΔE_{exch}, the substrate and product bond energies should also be investigated. Inspection of the OC=NR bond dissociation energies shows that the OC=NB(NMeCH)$_2$ BDE value is significantly higher than the OC=NMe value (100.4 *vs.* 82.9 kcal mol^{-1}) while the OC=Ph BDE value is lower, namely 74.1 kcal mol^{-1}. This difference could thus not be explained by conjugation effects between the N=C=O π bonds with the π-system of the boryl- or phenyl system. It is postulated that this difference arises from the σ-effect present in the NB(NMeCH)$_2$ fragment, which is connected to the electropositive nature of the boron

atom. However, the relative affinity of the CO fragment is greater for O than for NR. The same considerations apply to the BDE of SC=NB(NMeCH)$_2$, which is 17.5 kcal mol^{-1} higher than the methyl counterpart, SC=NMe, and 24.4 kcal mol^{-1} higher than SC=NPh. In this case the affinity of the SC fragment is higher for the NR fragment than for the S atom. In conclusion, for the reaction with CO_2, the titanium oxygen bond strength is the main driver of the reaction and compensates for the high BDE of CO_2 while for CS_2 the borylisothiocyanate SC=NB(NMeCH)$_2$ plays a major role. Thus, it can be concluded that the bond strength of the EC=NB(NMeCH)$_2$ is the key factor to guide the reaction to the extrusion of the borylisocyanate and borylisothiocyanate products. The values ΔE_{exch} are found to be -11.3 and -23.4 kcal mol^{-1} for OCNB(NMeCH)$_2$ and SCNB(NMeCH)$_2$ respectively. The reactivity with other heterocumulenes was also experimentally investigated, but the reactions were extremely slow (7 to 10 days) and required forcing conditions (80-90 °C). Thus, no computational studies were carried out. The ΔE_{exch} values for the reactions of **1Q_R** with CO_2 and CS_2 are shown in Table 4.8. In all cases the CS_2 reactions are more exothermic. It is clear that the ΔE_{exch} are more favourable (higher in absolute value) for NB(NMeCH)$_2$ > NMe > NPh. This can be explained by the stronger BDE in ECNB(NMeCH)$_2$ then in ECNMe and ECNPh, which more than compensate for the higher Ti=N bond strength in **1Q_ B(NMeCH)$_2$**.

Next, the reaction with TolCHO was investigated. Experimentally, the reaction was reported to proceed at RT by Martin Slusarczyk, DPhil student in our group. Interestingly, the [2+2] cycloaddition product was observed after 30 minutes and isolated, Equation 4.7.

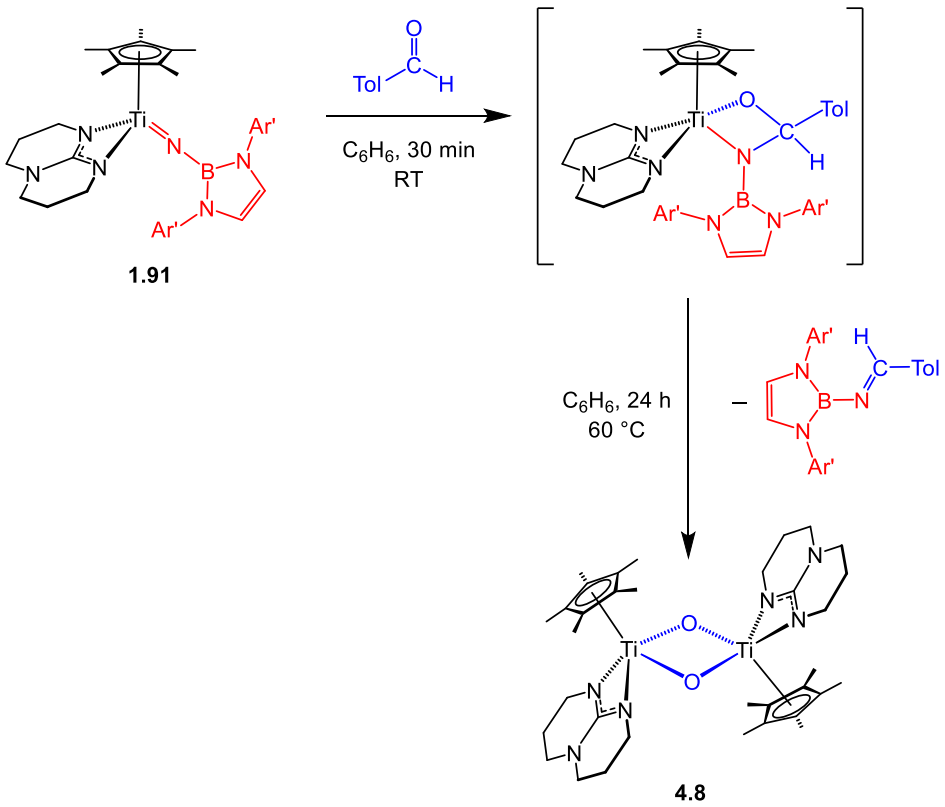

Equation 4.7

After heating at 60 °C the cycloaddition product was then fully converted to the Ti oxo dimer and the organic borylimine Tol(H)C=NB(NAr'CH)$_2$. To date, few synthetic pathways to yield borylimine compounds, were reported in literature.[53–55] In particular, the simple condensation of amines and carbonyls, which is used to form alkylimines, was unsuccessful when starting from the borylamine, H$_2$NB(NAr'CH)$_2$ even under forcing conditions (high temperature or long reaction times). Therefore, also in this case, the model thermodynamic cycle in Scheme 4.5 in which the Ti=NR of **1Q_NMe** and **1Q_B(NMeCH)$_2$**, exchanges with the C=O of PhCHO was analysed to better understand the overall impact of both the Ti=N and the organic frameworks bond dissociation energies. Both results for the organic and inorganic reactions are depicted in Scheme 4.5 and the relevant values are reported in Table 4.9.

Table 4.8. ΔE_{exch} values (kcal mol^{-1}) for the process depicted in Scheme 4.4.

Reaction	ΔE_{exch} **(kcal mol^{-1})**
1Q_Me + CO_2 → **1Q_O** + OCNMe	-3.6
1Q_Ph + CO_2 → **1Q_O** + OCNPh	+3.5
1Q_B(NMeCH)$_2$ + CO_2 → **1Q_O** + OCNB(NMeCH)$_2$	-11.4
1Q_Me + CS_2 → **1Q_O** + SCNMe	-15.8
1Q_Ph + CS_2 → **1Q_O** + SCNPh	-10.4
1Q_B(NMeCH)$_2$ + CS_2 → **1Q_O** + SCNB(NMeCH)$_2$	-23.4

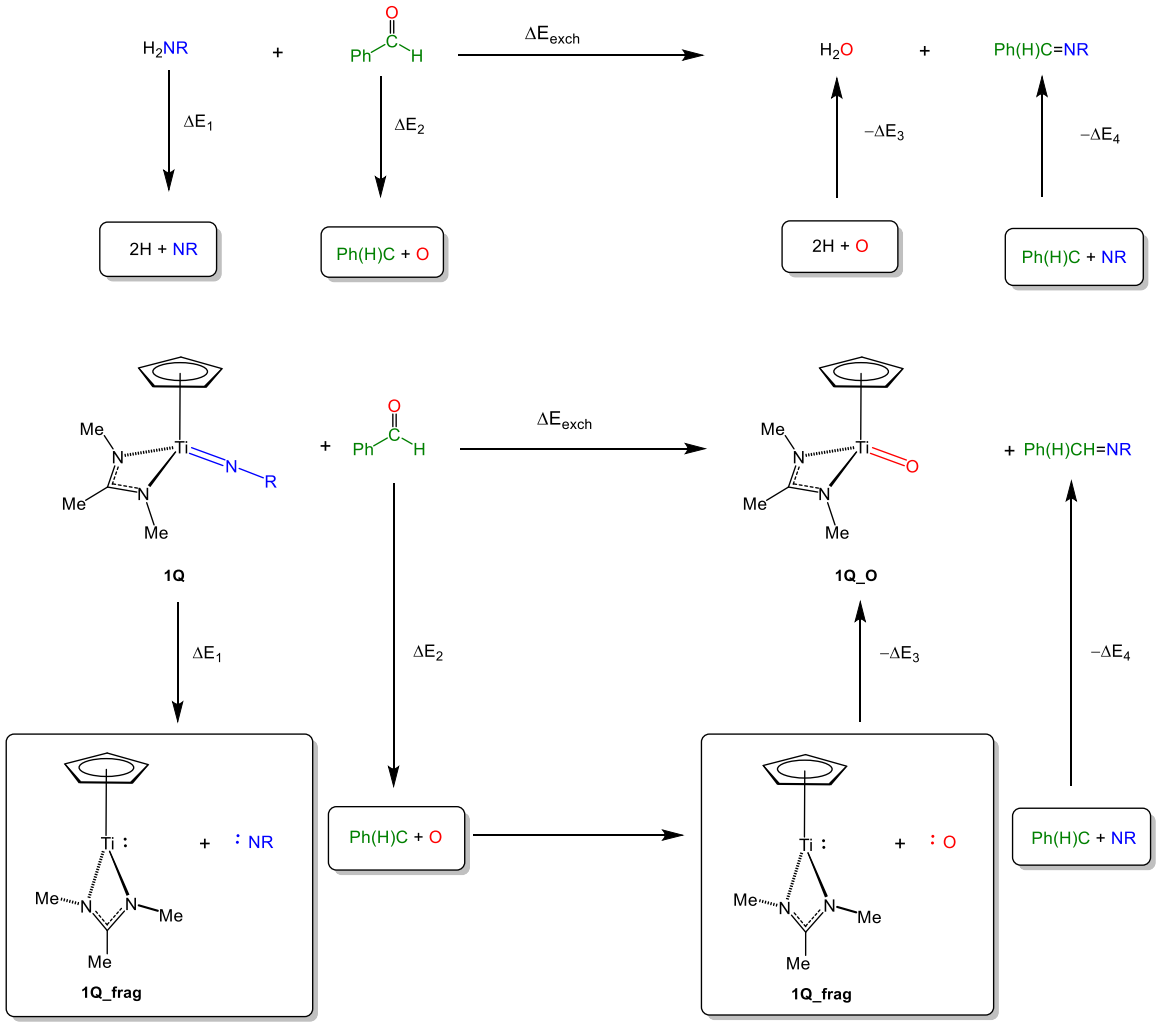

Scheme 4.5. Energy decomposition scheme for selected isodesmic multiple bond exchange reactions of CpTi{MeC(NMe)$_2$}(NR) (R = Me, B(NMeCH)$_2$) with PhCHO, and computed bond dissociation energies (ΔE, kcal mol^{-1}). All species are spin state singlets except for the fragments CpTi{MeC(NMe)$_2$}, X, and NR which are spin triplets and H which is a spin doublet. ($\Delta E_{exch} = \Delta E_1 + \Delta E_2 - \Delta E_3 - \Delta E_4$).

Table 4.9. ΔE values (kcal mol^{-1}) for the process depicted in Scheme 4.5.

1Q_R or H_2NR	**Ti=NR**	**ΔE_1 (kcal mol^{-1})**
1Q_Me	Ti + NMe	109.7
1Q_Ph	Ti + NPh	108.2
1Q_B(NMeCH)$_2$	Ti + NB(MeCH)$_2$	119.6
H_2NMe	2H + NMe	191.5
H_2NPh	2H + NPh	188.2
H_2NB(NMeCH)$_2$	2H + NB(NMeCH)$_2$	202.3
PhCHO	**Ph(H)C=O**	**ΔE_2 (kcal mol^{-1})**
PhCHO	Ph(H)C + O	175.2
H_2O or Ti=O	**Ti=O or HO=O**	**ΔE_3 (kcal mol^{-1})**
H_2O	HO + O	225.9
1Q_O	Ti + O	166.3
PhC(NR)H	**Ph(H)C=NR**	**ΔE_4 (kcal mol^{-1})**
PhC(NMe)H	Ph(H)C + NMe	144.0
PhC(NPh)H	Ph(H)C + NPh	133.4
PhC(NB(NMeCH)$_2$)H	Ph(H)C + NB(NMeCH)$_2$	140.7

Starting from the reaction of **1Q_NMe, 1Q_NPh** and **1Q_B(NMeCH)$_2$** with Ph(H)CO it is clear that the Ti=O bond strength is the key factor to drive the reaction to completion, as reported before for the reaction with CO_2. Although the Ph(H)C=O BDE is higher than the Ph(H)C=NMe, Ph(H)C=NPh and Ph(H)C=NB(NMeCH) BDEs (175.2 *vs.* 144.0, 133.4 and 140.7 kcal mol^{-1} respectively), the Ti=O BDE more than compensates for this contribution and the overall ΔE_{exch} is -22.1, -16.2 and -15.5 kcal mol^{-1} for **1Q_NMe, 1Q_Ph** and **1Q_B(NMeCH)$_2$** respectively, in line with the experimental results (Table 4.9). This differs from the reactions with CO_2 depicted in Scheme 4.4, where there is a bigger difference in RN=CO BDE.

Moving to the organic reaction of H_2NMe and H_2NB(NMeCH)$_2$ with PhCHO it is evident that the release of water is not enough to compensate for both the Ph(H)C=O and the H-N bond strengths in the case of H_2NB(NMeCH)$_2$. Thus, the reaction appears is endothermic

with a value of ΔE_{exch} is 7.5 kcal mol^{-1}, while it is an equilibrium reaction for H_2NMe (0.0 kcal mol^{-1}) and exothermic for H_2NPh (-4.1 kcal mol^{-1}) as depicted in Table 4.10.

Table 4.10. ΔE_{exch} values (kcal mol^{-1}) for the process depicted in Scheme 4.5.

Reaction	ΔE_{exch} (kcal mol^{-1})
1Q_Me + PhCHO → **1Q_O** + Ph(H)CNMe	-22.1
1Q_Ph + PhCHO → **1Q_O** + Ph(H)CNPh	-16.2
1Q_B(NMeCH)$_2$ + PhCHO → **1Q_O** + Ph(H)CNB(NMeCH)$_2$	-15.5
H_2NMe + PhCHO → H_2O + Ph(H)CNMe	0.0
H_2NPh + PhCHO → H_2O + Ph(H)CNPh	-4.1
$H_2NB(NMeCH)_2$ + PhCHO → H_2O + Ph(H)CNB(NMeCH)$_2$	7.5

It is important to note that in all the aforementioned exchange reactions, the dimerization of both titanium oxo- and sulfide- terminal compounds has not been taken into account. It was experimentally found that the oxo- bridged titanium dimer is in a *trans* conformation with respect to the Cp* ligands, while the sulfide- bridged dimer is *cis*. To understand the underlying electronic and steric factors driving these preferences, calculations were performed to evaluate the gas phase SCF energies for the dimerization of the model systems **1.91Q_O** and **1.91Q_S** and the $\Delta_r G$ values for the dimerization of the real systems **1.91_O** and **1.91_S** (Equation 4.8 and 4.9). The SCF gas phase energies show that there is no difference in stability between the cis and the trans isomer in **1.91Q_S**, while the *trans* isomer is 1.4 kcal mol^{-1} more stable than the *cis* isomer in **1.91Q_O**. It is clear that the conformational preferences must arise from steric factors which are not fully taken into account in the small model systems. As reported in Equation 4.9, calculations on the real systems are able to show the contribution of steric bulk. The *cis* isomer of the oxo- dimer is 7.7 kcal mol^{-1} less stable than the *trans* one, as experimentally found by X-ray, while no significant difference (within the computational error) between the cis and the trans sulfide- dimers was found (the *cis* isomer is only 1.7 kcal mol^{-1} less stable than the *trans* one).

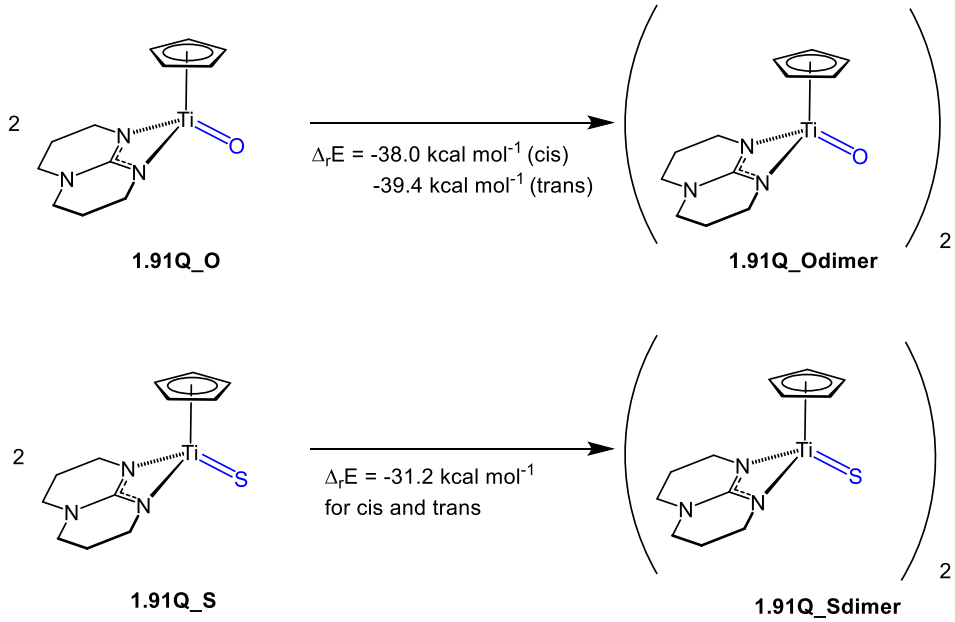

Equation 4.8

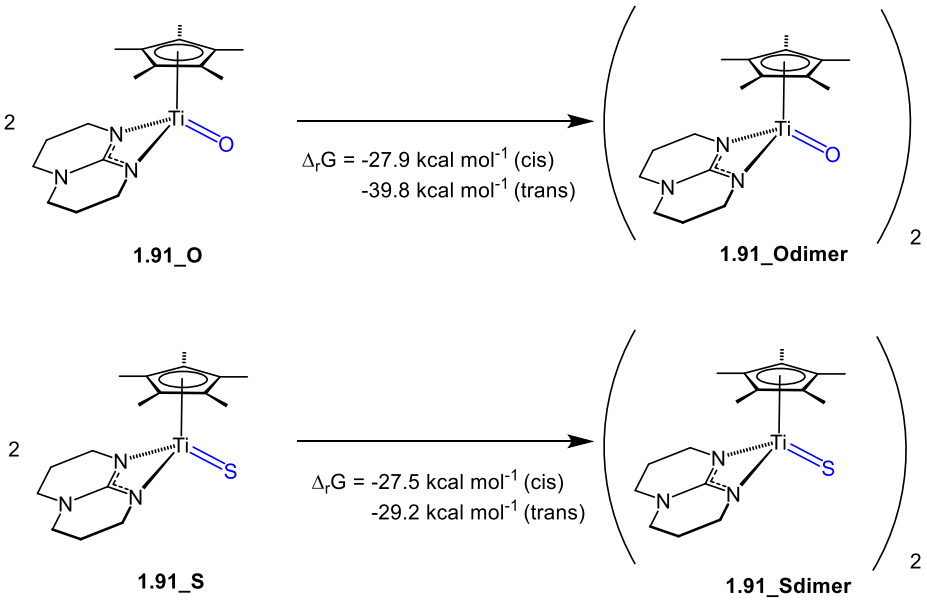

Equation 4.9

4.7 Conclusions

This Chapter has described the synthesis and the computational study of new borylimido complexes of titanium starting from three different synthons, namely $Ti\{NB(NAr'CH)_2\}Cl_2(NHMe_2)_2$ (**4.1**), $Ti\{NB(NAr'CH)_2\}Cl_2(py)_3$ (**4.2**) and $Cp^*Ti\{NB(NAr'CH)_2\}Cl(py)$ (**4.3**) and by subsequently installing the desired supporting ligands by Dr. Ben Clough.

DFT calculations were performed on compounds with sandwich and half-sandwich structures. Results showed that the borylimido functional group is structurally and electronically more similar to an arylimido than an alkylimido ligand. In this particular case, this arises from the presence of the aromatic π system in this 1,3,2-diazaborolyl-type group.

The relevant features of titanium–nitrogen bond in sandwich and half-sandwich model compounds were explored through DFT, QTAIM and NBO calculations. These ultimately showed that the failure of protonolysis reactions of imides with borylamines, and the ready exchange of borylimido ligands with other amines, can be ascribed to the very high N–H bond strengths in the borylamines, which outweighs the corresponding increase in metal–nitrogen bond strength. Furthermore, QTAIM and NBO studies explored the use of the bond distance and bond dissociation energy as two measures of metal–nitrogen multiple bond strength. The variation in the former arises from π interactions with the substituent on the N_{im} atom, whilst the latter varies with the σ-donor ability of the respective NR fragment (ultimately related to the electronegativity or electropositivity of the R group) and is the factor that controls the favourability of imido ligand exchange reactions.

Finally, the reactivity of $Cp^*Ti(hpp)\{NB(NAr'CH)_2\}$ **1.91** with CO_2, CS_2 and TolCHO was then investigated both experimentally and computationally. The experimental results showed that in all cases the reactions resulted in the formation of borylisothiocyanates with concomitant formation of the dimeric titanium compounds $[Cp^*Ti(hpp)(\mu\text{-}E)]_2$ (E = O (**4.8**), S (**4.9**)). The very high N–H bond strengths in the borylamines, along with the $EC{=}NB(NMeCH)_2$ BDEs in the borylisocyanate and the borylisothiocyanate products observed were demonstrated to be crucial factors to achieve the desired reactivity.

4.8 References

1 B. Clough, DPhil Thesis, University of Oxford, 2016.

2 A. D. Schofield, A. Nova, J. D. Selby, A. D. Schwarz, E. Clot and P. Mountford, *Chem. Eur. J.*, 2011, **17**, 265–285.

3 J. Unruangsri, H. Morgan, A. D. Schwarz, A. D. Schofield and P. Mountford, *Organometallics*, 2013, **32**, 3091–3107.

4 P. J. Walsh, M. J. Carney and R. G. Bergman, *J. Am. Chem. Soc.*, 1991, **113**, 6343–6345.

5 H. Herrmann, J. L. Fillol, H. Wadepohl and L. H. Gade, *Angew. Chem. Int. Ed.*, 2007, **46**, 8426–8430.

6 L. R. Groom, A. D. Schwarz, A. Nova, E. Clot and P. Mountford, *Organometallics*, 2013, **32**, 7520–7539.

7 R. Thompson, C.-H. Chen, M. Pink, G. Wu and D. J. Mindiola, *J. Am. Chem. Soc.*, 2014, **136**, 8197–8200.

8 L. Stevenson, S. Mellino, E. Clot and P. Mountford, *J. Am. Chem. Soc.*, 2015, **137**, 10140–10143.

9 A. D. Schwarz, A. Nova, E. Clot and P. Mountford, *Chem. Commun.*, 2011, **47**, 4926–4928.

10 A. D. Schwarz, A. Nova, E. Clot and P. Mountford, *Inorg. Chem.*, 2011, **50**, 12155–12171.

11 J. D. Selby, C. D. Manley, A. D. Schwarz, E. Clot and P. Mountford, *Organometallics*, 2008, **27**, 6479–6494.

12 A. J. Blake, P. E. Collier, S. C. Dunn, W. Li, P. Mountford and O. V Shishkin, *J. Chem. Soc. Dalton Trans.*, 1997, 1549–1558.

13 N. Adams, H. R. Bigmore, T. L. Blundell, C. L. Boyd, S. R. Dubberley, A. J. Sealey, A. R. Cowley, M. E. G. Skinner and P. Mountford, *Inorg. Chem.*, 2005, **44**, 2882–2894.

14 N. Adams, A. R. Cowley, S. R. Dubberley, A. J. Sealey, M. E. G. Skinner and P. Mountford, *Chem. Commun.*, 2001, 2738–2739.

15 T. B. Parsons, N. Hazari, A. R. Cowley, J. C. Green and P. Mountford, *Inorg. Chem.*, 2005, **44**, 8442–8458.

16 M. Müller, C. Maichle-Mössmer and H. F. Bettinger, *J. Org. Chem.*, 2014, **79**, 5478–5483.

17 N. A. H. Male, M. E. G. Skinner, S. Y. Bylikin, P. J. Wilson, P. Mountford and M. Schroder, *Inorg. Chem.*, 2000, **39**, 5483–5491.

18 C. Lorber, R. Choukroun and L. Vendier, *Eur. J. Inorg. Chem.*, 2006, 4503–4518.

19 J. D. Selby, C. D. Manley, M. Feliz, A. D. Schwarz, E. Clot and P. Mountford, *Chem. Commun.*, 2007, **733**, 4937–4939.

20 J. D. Selby, C. Schulten, A. D. Schwarz, A. Stasch, E. Clot, C. Jones and P. Mountford, *Chem. Commun.*, 2008, 5101–5103.

21 A. D. Schofield, A. Nova, J. D. Selby, C. D. Manley, A. D. Schwarz, E. Clot and P. Mountford, *J. Am. Chem. Soc.*, 2010, **132**, 10484–10497.

22 P. J. Tiong, A. D. Schofield, J. D. Selby, A. Nova, E. Clot and P. Mountford, *Chem. Commun.*, 2010, **46**, 85–87.

23 H. Herrmann, J. L. Fillol, H. Wadepohl and L. H. Gade, *Organometallics*, 2008, **27**, 173–174.

24 H. Herrmann, T. Gehrmann, H. Wadepohl and L. H. Gade, *Dalton Trans.*, 2008, 6231–6241.

25 T. Gehrmann, J. L. Fillol, H. Wadepohl and L. H. Gade, *Angew. Chem. Int. Ed.*, 2009, **48**, 2152–2156.

26 T. Gehrmann, G. T. Plundrich, H. Wadepohl and L. H. Gade, *Organometallics*, 2012, **31**, 3346−3354.

27 T. Gehrmann, M. Kruck, H. Wadepohl and L. H. Gade, *Chem. Commun.*, 2012, **48**, 2397–2399.

28 P. E. Collier, S. M. Pugh, H. S. C. Clark, J. B. Love, A. J. Blake, F. G. N. Cloke and P. Mountford, *Inorg. Chem.*, 2000, **39**, 2001–2005.

29 A. E. Guiducci, C. L. Boyd and P. Mountford, *Organometallics*, 2006, **25**, 1167–1187.

30 P. J. Tiong, A. Nova, L. R. Groom, A. D. Schwarz, J. D. Selby, A. D. Schofield, E. Clot and P. Mountford, *Organometallics*, 2011, **30**, 1182–1201.

31 P. J. Tiong, L. R. Groom, E. Clot and P. Mountford, *Chem. Eur. J.*, 2013, **19**, 4198–4216.

32 D. A. Fletcher, R. F. McMeeking and D. Parkin, *J. Chem. Inf. Comput. Sci.*, 1996, **36**, 746 (Cambridge Structural Database version 5.37).

33 M. P. Coles and P. B. Hitchcock, *Organometallics*, 2003, **22**, 5201–5211.

34 S. C. Dunn, P. Mountford and D. A. Robson, *J. Chem. Soc. Dalton Trans.*, 1997, **2**, 293–304.

35 J. D. Selby, M. Feliz, A. D. Schwarz, E. Clot and P. Mountford, *Organometallics*, 2011, **30**, 2295–2307.

36 A. D. Becke, *J. Chem. Phys.*, 1993, **98**, 5648–5652.

37 J. P. Perdew and Y. Wang, *Phys. Rev. B*, 1992, **45**, 13244–13249.

38 A. Schäfer, H. Horn and R. Ahlrichs, *J. Chem. Phys.*, 1992, **97**, 2571–2577.

39 F. Weigend and R. Ahlrichs, *Phys. Chem. Chem. Phys.*, 2005, **7**, 3297–3305.

40 P. J. Tiong, A. Nova, L. R. Groom, A. D. Schwarz, J. D. Selby, A. D. Schofield, E. Clot and P. Mountford, *Organometallics*, 2011, **30**, 1182–1201.

41 R. F. W. Bader, *Atoms in Molecules: A Quantum Theory*, Oxford University Press, Oxford, 1990.

42 F. Weinhold and C. R. Landis, *Chem. Educ. Res. Pr.*, 2001, **2**, 91–104.

43 C. F. Matta and R. J. Boyd, *The Quantum Theory of Atoms in Molecules*, Wiley-VCH, Weinheim, 2007.

44 P. Macchi and A. Sironi, *Coord. Chem. Rev.*, 2003, **238**–**239**, 383–412.

45 A. V Marenich, C. J. Cramer and D. G. Truhlar, *J. Phys. Chem. B*, 2009, **113**, 6378–6396.

46 S. Grimme, S. Ehrlich and L. Goerigk, *J. Comput. Chem.*, 2011, **32**, 1456–1465.

47 S. Grimme, J. Antony, S. Ehrlich and H. Krieg, *J. Chem. Phys.*, 2010, **132**, 154104–154119.

48 J. W. Lauher and R. Hoffmann, *J. Am. Chem. Soc.*, 1976, **98**, 1729–1742.

49 J. T. Anhaus, T. P. Kee, M. H. Schofield and R. R. Schrock, *J. Am. Chem. Soc.*, 1990, **112**, 1642–1643.

50 J. C. Green, M. L. H. Green, J. T. James, P. C. Konidaris, G. H. Maunder and P. Mountford, *J. Chem. Soc., Chem. Commun.*, 1992, 1361–1365.

51 A. E. Guiducci, A. R. Cowley, M. E. G. Skinner and P. Mountford, *J. Chem. Soc. Dalt. Trans.*, 2001, 1392–1394.

52 A. E. Guiducci, C. L. Boyd, E. Clot and P. Mountford, *Dalton Trans.*, 2009, 5960–5979.

53 C. E. Bacon, L. Mansour, J. J. Hayward and J. M. Rawson, *Dalton Trans.*, 2015, **44**, 5284–5287.

54 M. F. Lappert and H. Pyszora, *J. Chem. Soc. A*, 1967, 854–860.

55 B. C. Summerford and S. Road, *J. Chem. Soc. A*, 1968, 1487–1491.

5.1 Overview

This Chapter will describe very recent experimental attempts to isolate the first borylimido complex of a rare earth metal, namely scandium. The main experimental results to synthesise a scandium methyl-borylamide using a β-diketiminate (NacNac)-type supporting ligand incorporating a pendant NMe_2 donor group will be described with the hope of using this complex as a precursor for the desired boryimido complex. Reactivity studies, in particular thermolysis reactions, and reactions with two alkynes will then be summarized. DFT and QTAIM studies will be presented, with the bonding in a model scandium borylimide and its imido counterparts compared, followed by a bonding analysis and a detailed mechanistic study of the reactions of these systems to explain the observed experimental outcomes. All the experimental results were performed by Ben Clough, former DPhil student at University of Oxford and the computational results were performed in collaboration with Prof. Philip Mountford at University of Oxford and Dr. Eric Clot at Université Montpellier, France.

5.2 Introduction

Compared with their Group 4 counterparts, terminal imido complexes of rare earth metals are much more scarce, and advances in their successful synthesis and reactivity have taken place only in the last seven years.[1] Prior to this, the field was limited to the isolation of dimeric complexes or higher-nuclearity clusters which contained bridging imido ligands, as the putative first-formed monomeric complexes had a tendency to form these more stable structures, especially for the larger lanthanides and yttrium.[2–14] Another limiting factor in the synthesis of terminal imido complexes of rare earth metals is the nature of the M=NR multiple bond which is highly polarised, thus more reactive than its counterpart in Group 4 systems, meaning that undesired intra- or intermolecular activations may take place before the terminal imide can be isolated. However, in 2010, Chen and co-workers successfully formed the first isolable terminal imido complex of a rare earth metal.[15] This was achieved using DMAP as a very strong external base, in combination with the introduction of a new bulky β-diketiminate (NacNac)-type supporting ligand with a pendant NMe_2 donor. Heating of $(L^1)Sc(Me)(NHAr')$ (**1.30**, L^1 = $(Ar')NC(Me)CHC(Me)NCH_2CH_2NMe_2$, Ar = 2,6-$C_6H_3{}^iPr_2$) in the presence of DMAP gave the targeted terminal imido complex $(L^1)Sc(NAr')(DMAP)$ (**1.31**, Scheme 5.1). This general strategy required the incorporation of a large amount of steric bulk into both imido and supporting ligands, and the use of DMAP

as a very strong Lewis base to stabilise the complexes and was then followed by other research groups in the last few years.[16,17]

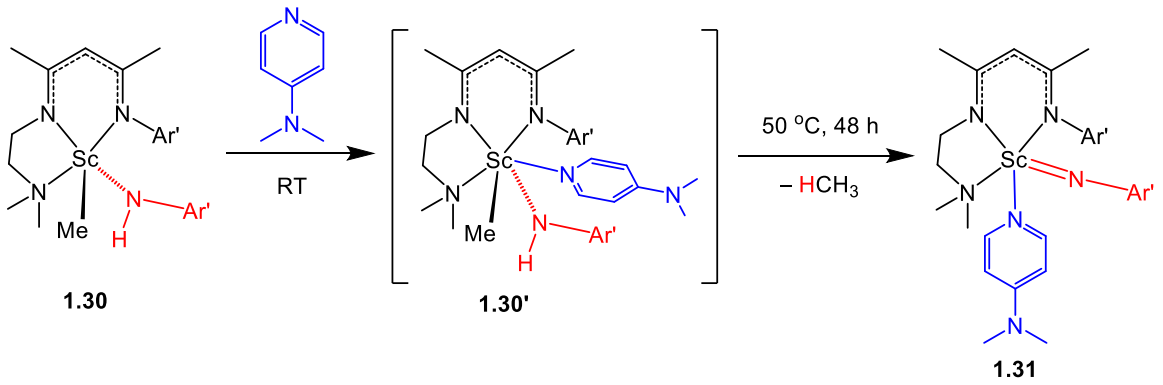

Scheme 5.1.Synthesis of (L^1)Sc(NAr')(DMAP) (**1.31**, Ar = Ar = 2,6-$C_6H_3{}^iPr_2$).[15]

Given the successful syntheses of a number of terminal scandium imides in recent years, the synthesis of a scandium borylimide was targeted by Dr. Ben Clough, former DPhil in our group at the University of Oxford. As the incorporation of a large amount of steric bulk appears to be important in the formation of those terminal imides described above; the very bulky borylamine $H_2NB(NAr'CH)_2$, successfully used for the synthesis of titanium borylimido compounds described in Chapter Four, was used initially. The success of Chen and co-workers in preparing **1.31**, and their subsequent reactivity studies on that imido complex with a wide range of substrates,[18–23] have demonstrated the suitability of the supporting ligand L^1 in this chemistry. The presence of a bulky Ar' group along with the pendant $–CH_2CH_2NMe_2$ donor group was expected to give a flexible environment around the scandium centre. Therefore, L^1 was chosen as the initial supporting ligand in these attempts to form a scandium borylimide, with (L^1)$ScCl_2$ as a starting material. The main experimental results, namely the synthesis of the targeted methyl-borylamido precursor and the thermolysis reactions with a variety of substrates will be presented in Section 5.3 and 5.4 along with a bonding and mechanistic computational study in Section 5.5. Other borylamines were also tested but the experimental results will not be presented in this Thesis.

5.3 Synthesis and characterization of the scandium borylamido complex, (L^1)Sc(Me){NHB(NAr'CH)$_2$} (5.1)

The targeted methyl-borylamide (L^1)Sc(Me){NHB(NAr'CH)$_2$} (**5.1**) was successfully prepared by Ben Clough, following the preparation of (L^1)Sc(Me)(NHAr') (**1.30**) reported by Chen and co-workers.[15] Firstly, (L^1)$ScCl_2$ in THF was reacted with MeLi (1.6 M in Et_2O) to form the dimethylated complex (L^1)$ScMe_2$, which was then reacted *in situ* with 1 equiv.

$H_2NB(NAr'CH)_2$ giving methane elimination over 60 h at RT (Scheme 5.2). This reaction time was significantly longer than that required for the complete formation of **1.30** (24 h at RT), which presumably reflects steric hindrance in the approach of the bulkier borylamine to the scandium centre (compared with H_2NAr').

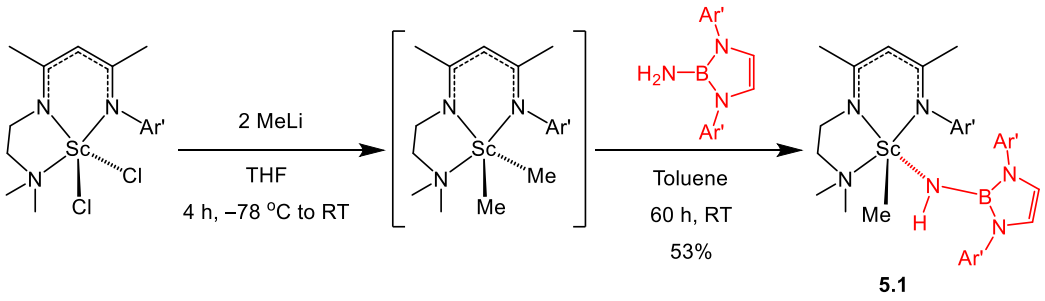

Scheme 5.2. Preparation of $(L^1)Sc(Me)\{NHB(NAr'CH)_2\}$ (**5.1**) from *in situ*-generated $(L^1)ScMe_2$.

The molecular solid state structure of **5.1** is shown in Figure 5.1. Complex **5.1** has a monomeric, five-coordinate structure with square-based pyramidal geometry, in which the tridentate L^1 and the methyl ligand form the base and N(1) of the borylamido ligand resides at the apex. The Sc(1)–N(1) bond distance of 2.0629(8) Å is slightly longer (Δ = 0.016(3) Å) than the corresponding distance in the anilide **1.30** (2.047(3) Å), and the Sc–C bond distance of the methyl ligand of 2.273(1) Å is also longer than that in **1.30** (2.221(4) Å).[15] This probably reflects a steric effect in which the large bulk of the boryl moiety increases the crowding around the Sc centre, thus lengthening the bond distances to the metal, as well as the better donor ability of the $NHB(NAr'CH)_2$ ligand compared with NHAr'. In **5.1**, the borylamide hydrogen is close to a *cis* orientation with respect to the methyl group, with an H–N···Sc–C torsion angle of *ca* 32.2°. This is larger than the corresponding angle in **1.30** of *ca* 9.9°. Chen and co-workers commented that a small angle such as this would make the following α-abstraction process particularly facile.[15]

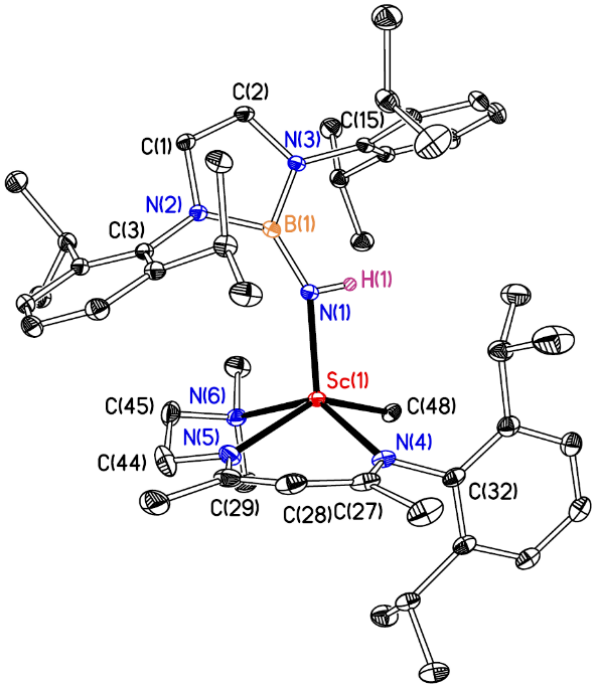

Figure 5.1. Displacement ellipsoid plot (20% probability) of (L^1)Sc(Me){NHB(NAr'CH)$_2$} (**5.1**). C-bound H atoms are omitted for clarity. H(1) is drawn as a sphere of arbitrary radius.[24]

5.4 Reactivity studies of (L^1)Sc(Me){NHB(NAr'CH)$_2$} (5.1): thermolysis reaction and trapping of a transient borylimido complex with alkynes

The main experimental attempts performed to isolate a scandium borylimido complex, starting from (L^1)Sc(Me){NHB(NAr'CH)$_2$} (**5.1**) will now be described. These results will then be supported by DFT studies in Section 5.5. Three thermolysis reactions were initially explored: these being in presence of 1 equiv. of pyridine or DMAP as well as without the addition of an external base. For the base-free thermolysis, heating **5.1** at 60 °C for 16 h gave {MeC(NC$_6$H$_3$^{i}PrCH(Me)CH$_2$)CHC(Me)NCH$_2$CH$_2$NMe$_2$}Sc{NHB(NAr'CH)$_2$} (**5.2**) in which an isopropyl methyl group of the supporting ligand's Ar' moiety appears to have undergone intramolecular C–H activation at the metal centre, a so-called tuck-in or cyclometalation reaction (Scheme 5.3). In the thermolysis reactions in the presence of pyridine or DMAP, toluene solutions of **5.1** with each of those reagents were heated at 60 °C for 16 and 8 h, respectively. The two products (L^1)Sc{NHB(NAr'CH)$_2$}(η^2-4-NC$_5$H$_3$R) (R = H (**5.3**), NMe$_2$ (**5.4**)) were reported to have a borylamide ligand and an η^2-bound pyridyl ligand (or the DMAP counterpart) which has formed from C–H bond activation at the 2-position of the respective Lewis base (Scheme 5.3)

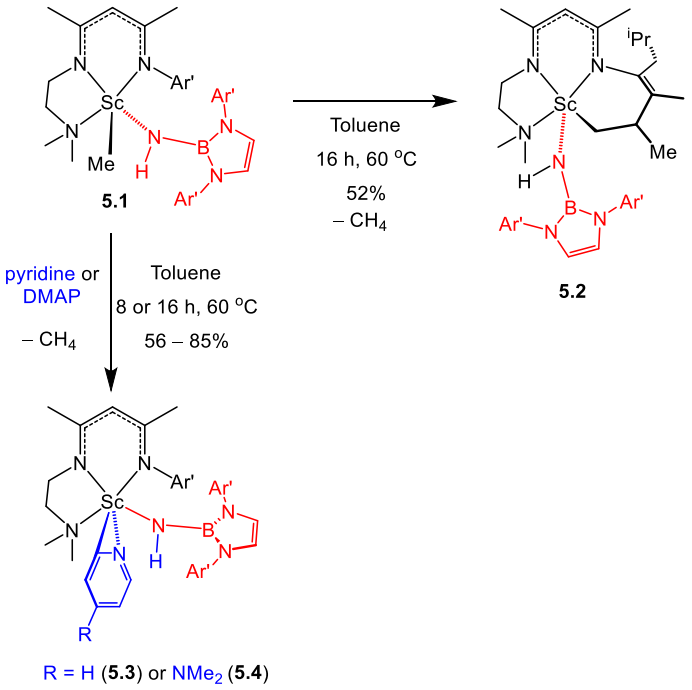

Scheme 5.3. Synthesis of $\{MeC(NC_6H_3{}^iPrCH(Me)CH_2)CHC(Me)NCH_2CH_2NMe_2\}$-Sc$\{NHB(NAr'CH)_2\}$ (**5.2**) and (L^1)Sc$\{NHB(NAr'CH)_2\}(\eta^2$-4-$NC_5H_3R)$ (R = H (**5.3**), NMe_2 (**5.4**)) from (L^1)Sc(Me)$\{NHB(NAr'CH)_2\}$ (**5.1**).

Diffraction-quality crystals were obtained for **5.2** only. The solid state structure is shown in Figure 5.2. Complex **5.2** is confirmed to have a distorted square-based pyramidal geometry similar to that of **5.1** in which one vertex of the basal plane is now a metallated methylene carbon which had been an isopropyl methyl group of the supporting ligand. This forms a new six-membered metallacycle with a distorted boat conformation. The borylamide functionality is again positioned at the pyramidal apex. The Sc(1)–N(1) bond distances of 2.0609(18) and 2.0649(18) Å are comparable to that in **5.1** (2.0629(8) Å). The Sc–C bond distances in the new metallated ligand are 2.249(2) and 2.247(2) Å, which are slightly shorter than the Sc–C bond distance in the methyl ligand of **5.2** (2.2730(10) Å).

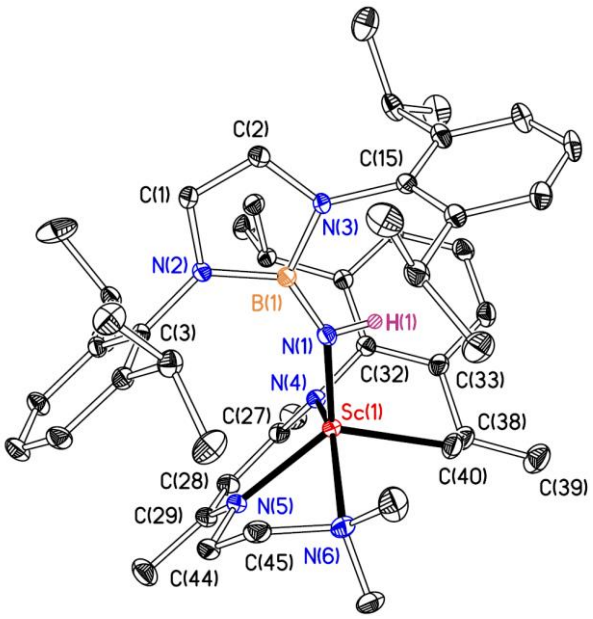

Figure 5.2. Displacement ellipsoid plot (20% probability) of {MeC(NC$_6$H$_3$^{i}PrCH(Me)CH$_2$)CHC(Me)NCH$_2$CH$_2$NMe$_2$}Sc{NHB(NAr'CH)$_2$} (**5.2**).[24] C-bound H atoms are omitted for clarity. H(1) is drawn as a sphere of arbitrary radius.

Experiments were then performed and reported by Dr. Ben Clough in order to elucidate the mechanism of formation of **5.2**, **5.3** and **5.4**. First of all, the three thermolysis reactions were monitored by ^{1}H NMR at 343 K and were reported to have similar experimentally identical first order rate constants (Table 5.1), thus it was initially proposed that they all share a common rate-determining step, namely CH$_4$ elimination. This is further confirmed by the fact that the thermolysis reactions in the presence of pyridine and DMAP to form **5.3** and **5.4** respectively have the same first order rate constants within experimental error despite DMAP being a stronger nucleophile than pyridine by over two orders of magnitude.[25] This implies, therefore, that in those two reactions the coordination of the Lewis base to the metal centre is not involved in the rate-determining step. Isotopic labelling and competition experiments confirmed this hypothesis. When the thermolysis reaction was performed starting from (L^1)Sc(Me){NDB(NAr'CH)$_2$} (**5.1-*d*$_1$**) exclusive conversion to **5.2** was observed. This again suggested that the deuterium was eliminated before the formation of **5.2**, as DCH$_3$, because an alternative mechanism in which the metalation occurs by σ-bond metathesis between Sc–Me and the isopropyl C–H bond would necessarily release CH$_4$. A similar experiment performed in presence of pyridine gave an identical result, the product of the reaction of (L^1)Sc(Me){NHB(NAr'CH)$_2$} (**5.1**) and pyridine-*d*$_5$ was exclusively

$(L^1)Sc\{NDB(NAr'CH)_2\}(\eta^2\text{-}NC_5D_4)$ (**5.3-*d*$_5$**), which suggested that methane release happens before the C-H activation of coordinated pyridine.

Table 5.1. First order rate constants obtained for the base-free thermolysis of $(L^1)Sc(Me)\{NHB(NAr'CH)_2\}$ (**5.1**) to form $\{MeC(NC_6H_3{}^iPrCH(Me)CH_2)CHC(Me)NCH_2CH_2NMe_2\}Sc\{NHB(NAr'CH)_2\}$ (**5.2**), and with pyridine and DMAP to form $(L^1)Sc\{NHB(NAr'CH)_2\}(\eta^2\text{-}4\text{-}NC_5H_3R)$ (R = H (**5.3**), NMe_2 (**5.4**)), in addition to isotopic variants, at 343 K in C_6D_6. Each reaction monitored was run in duplicate.

Starting material	Reagent	Product	k / 10^{-5} s^{-1} (Run 1)	k / 10^{-5} s^{-1} (Run 2)
5.1	-	**5.2**	16.83(3)	15.56(5)
5.1-*d*$_1$	-	**5.2**	1.91(1)	1.82(1)
5.1	pyridine[b]	**5.3**	17.26(3)	16.90(5)
5.1	pyridine-d_5[b]	**5.3-*d*$_5$**	18.66(4)	18.34(8)
5.1	DMAP[b]	**5.4**	17.83(10)	18.04(12)

a. [**5.1**]$_0$ = 0.032 mol dm^{-3}. *b*. [Lewis base]$_0$ = 0.032 mol dm^{-3}.

The base-free thermolysis of **5.1-*d*$_1$** to give **5.2**, and the reaction of **5.1** with pyridine-d_5, were each monitored by ^{1}H NMR arrays. Themolysis of **5.1-*d*$_1$** was found to be significantly slower than that of **5.1** and gave a kinetic isotope effect (KIE) of between 8.15 and 9.25. The value obtained here is comparable to those KIEs reported by Wolczanski and co-workers for α-abstraction reactions in Group 4 and 5 systems which release methane or other alkanes to yield imido functional groups.[26–29,30] When the thermolysis reaction of **5.1** in the presence of pyridine-d_5 was performed, no significant difference was found between the observed first order rate constants from this reaction and the analogous one with protio pyridine. The presence of a large KIE for the breaking of the N–H bond in the starting material **5.1** is indicative of this taking place in the RDS, whilst the absence of a KIE for the C–H bond activation of the pyridine ligand is consistent with that step being rapid and taking place after the RDS and therefore having no influence on the overall rate of reaction.

The proposed reaction mechanism is now shown in Scheme 5.4. In summary, a common rate-determining step (RDS) was proposed, supported by the three reactions having comparable first order rate constants. The initial RDS was proposed to be α-hydrogen abstraction in **5.1** of the borylamide NH by the methyl ligand which leaves a highly reactive scandium borylimido complex (L^1)Sc{NB(NAr'CH)$_2$} (**5.1'**) and releases methane. In the absence of an external substrate, rapid C–H bond activation of a supporting ligand CHMeMe group then occurs at the Sc–N multiple bond (a 1,2-addition) to produce the tuck-in complex **5.2**. When pyridine or DMAP is present, this coordinates to the metal and then undergoes a similar rapid C–H bond activation across the Sc–N multiple bond.

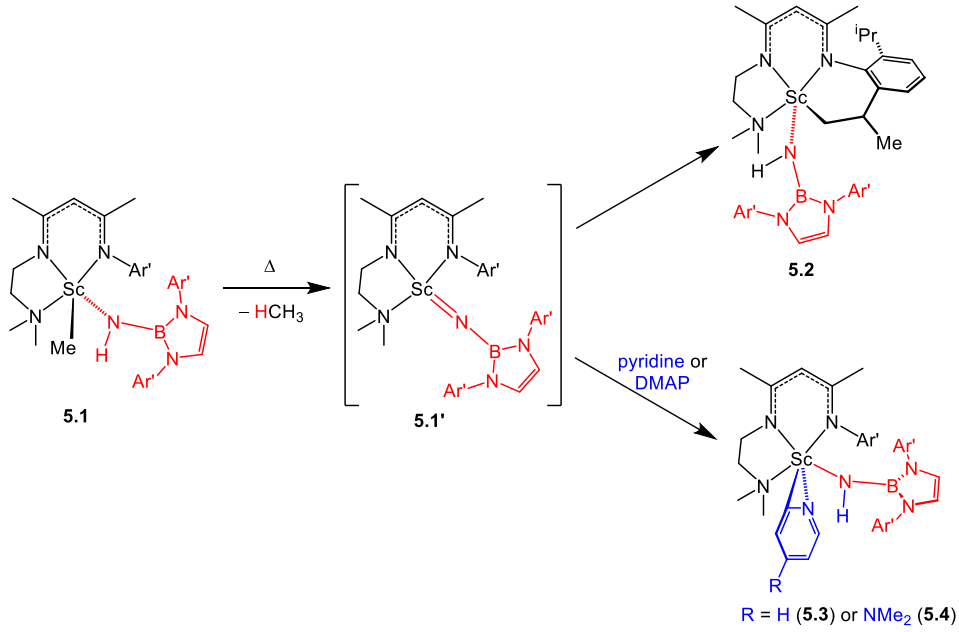

Scheme 5.4. Proposed pathways for the thermolysis reactions of (L^1)Sc(Me){NHB(NAr'CH)$_2$} (**5.1**) to form {MeC($NC_6H_3{}^iPrCH(Me)CH_2$)-CHC(Me)$NCH_2CH_2NMe_2$}Sc{NHB(NAr'CH)$_2$} (**5.2**) and (L^1)Sc{NHB(NAr'CH)$_2$}(η^2-4-NC_5H_3R) (R = H (**5.3**), NMe_2 (**5.4**)).

A series of experiments were next performed in order to elucidate the mechanism to convert the highly reactive scandium borylimido complex (L^1)Sc{NB(NAr'CH)$_2$} (**5.1'**) to the final products of reaction of **5.1** with either py or DMAP and to distinguish between the two steps of coordination and the C-H bond activation of these Lewis bases. Furthermore, experiments were performed to trap the reactive intermediate, **5.1'** which was not possible to isolate during the thermolysis reactions. A detailed discussion has been reported in Dr. Ben Clough's DPhil Thesis.[24] In summary, a series of experiments suggested an equilibrium in the reaction mechanisms after the RDS, as shown in Scheme 5.5.

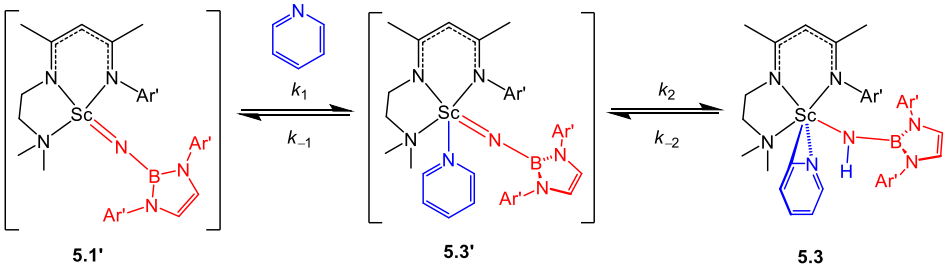

Scheme 5.5. Proposed equilibria in the formation of $(L^1)Sc\{NHB(NAr'CH)_2\}(\eta^2\text{-}NC_5H_4)$ (**5.3**) from $(L^1)Sc\{NB(NAr'CH)_2\}$ (**5.1'**).

For example, a competition experiment between pyridine and DMAP resulted in a product mixture of 53% **5.3** and 47% **5.4**. These results confirmed that the addition to both pyridine and DMAP to the base free intermediate **5.1'** must be reversible under the reaction conditions (343K).

Moreover, it was experimentally found that heating of **5.3** (16 h at 90 °C) resulted in conversion to the tuck-in complex **5.2**, while heating **5.3-*d*$_5$** under the same conditions led to release only of pyridine-d_5, and gave exclusively **5.2** with no incorporation of deuterium. This suggested that the release of pyridine occurs first to return to the base-free borylimido intermediate **5.1'**, which is then followed by intramolecular metalation. This conversion from the kinetic product **5.3** to the thermodynamic product **5.2** is favoured by the entropic gain arising from the released pyridine at higher temperatures, and has been explored by DFT calculations described in the next Section. The equivalent process does not take place for the DMAP analogue **5.3**, for which heating at temperatures above 60 °C on the NMR tube scale results in conversion to a complex mixture of products which cannot be identified.

From the experimental results, it was possible to compare the reactivity of the novel borylamido complex $(L^1)Sc(Me)\{NHB(NAr'CH)_2\}$ (**5.1**) with similar reactions reported by Chen and co-workers on the imido system **1.31**. They used $^t BuCH_2CH_2BC_8H_{14}$ to abstract the Lewis base from the DMAP-stabilised borylimide **1.31**. Heating the base-free complex at 50 °C in the absence of any further added reagent gave quantitative conversion to a tuck-in complex which is a direct structural analogue of **5.2**.[23]

In addition, Chen and co-workers had reported that DMAP coordinates rapidly to **1.30** at RT to give a six-coordinate intermediate (**1.30'**)[15], which is in contrast with the addition of DMAP to the methyl-borylamide **5.1**, for which no coordination to the metal is observed at RT. The difference here is proposed to have a steric basis; with **5.1** having a very bulky

borylamido ligand, the addition of DMAP to give a six-coordinate intermediate would appear to be unfeasible. DFT studies discussed in the next Section will test this hypothesis.

As mentioned in this Section additional experiments were performed in order to trap the transient boryimide **5.1'**, namely thermolysis with two different alkynes, MeCCPh and HCCTol. Reaction of **5.1** with HCCTol was reported to give $(L^1)Sc\{NHB(NAr'CH)_2\}(CCTol)$ (**5.5**) (60 °C, 16 h) which represents 1,2-addition of the alkyne C–H bond across the Sc–N multiple bond of **5.1'** while reaction with MeCCPh gave the azascandacyclobutene complex $(L^1)Sc\{N\{B(NAr'CH)_2\}C(Me)C(Ph)\}$ (**5.6**) (60 °C, 16 h) which represents [2+2] cycloaddition of the internal alkyne across the Sc–N multiple bond of **5.1'**. Only the anti-Markovnikov metallacycle was experimentally observed. This second product was evidence of the transient borylimido complex (Scheme 5.6).

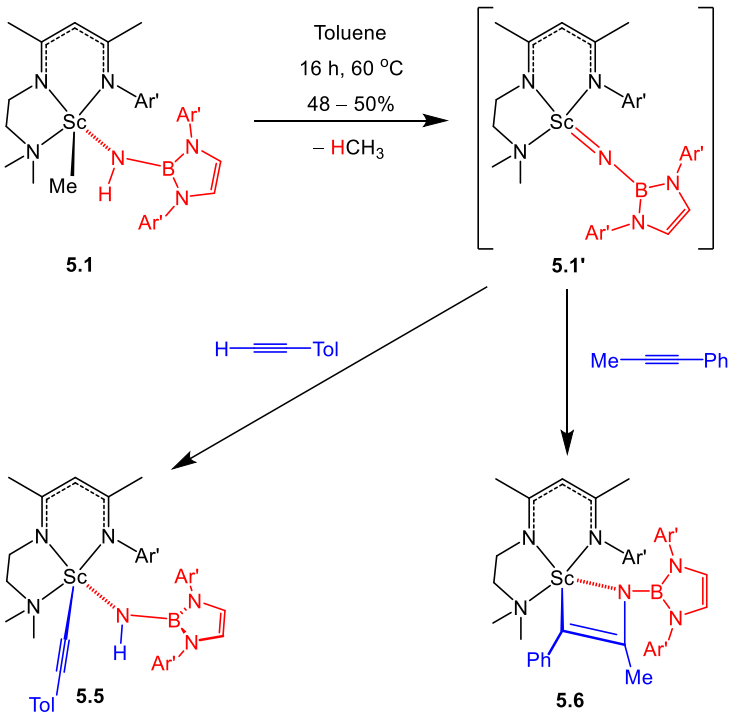

Scheme 5.6. Synthesis of $(L^1)Sc\{NHB(NAr'CH)_2\}(CCTol)$ (**5.5**) and $(L^1)Sc\{N\{B(NAr'CH)_2\}C(Me)C(Ph)\}$ (**5.6**) from $(L^1)Sc(Me)\{NHB(NAr'CH)_2\}$ (**5.1**).

Monitoring of the two reactions of **5.1** with HCCTol and MeCCPh, which form **5.5** and **5.6**, by ^1H NMR arrays at 343 K showed first order for both reactions. The observed first order rate constants (k_{obs}) for the two reactions are similar (16.96(10) x 10^{-5} s^{-1} and 17.40(9) x 10^{-5} s^{-1} for HCCTol and 16.60(5) x 10^{-5} s^{-1} and 18.44(4) x 10^{-5} s^{-1} for MeCCPh, values obtained by two independent runs for each substrate), and are also comparable to those previously listed in Table **1.30**. This confirms that the formation of **5.5** and **5.6** proceed *via* the same RDS as those previous reactions: initial α-hydrogen abstraction releases methane to leave the transient borylimide **5.1'**, which then gives a rapid C–H bond activation with HCCTol or [2+2] cycloaddition with MeCCPh. A competition reaction of **5.1** with HCCTol and MeCCPh (1:5:5) at 60 °C in C_6D_6 was reported to give 100% conversion to the acetylido complex **5.5**, showing that the C–H bond activation of HCCTol is considerably faster than [2+2] cycloaddition of MeCCPh. Mechanistic details of these reactions will be presented in the next Section.

5.5 Computational studies of the thermolysis reactions of $(L^1)Sc(Me)\{NHB(NAr'CH)_2\}$ (5.1)

In analogy with the DFT calculations reported in Chapter Four for half-sandwich model borylimido and imido compounds, a set of QTAIM calculations[31,32] and a FMOs analysis was performed to elucidate the nature of the bonding in the scandium imido and boryilmido complexes. In order to understand the electronic interactions and to discard any contribution from steric effects, small model systems were used, namely $\{(Ph)NC(Me)CHC(Me)NCH_2CH_2NMe_2\}Sc(NR)(py)$ (**6Q_R**; R = Me, Ph, $B(NHCH)_2$) where the Ar' group of the L^1 ligand in **1.31** and **5.3'** was modelled as a phenyl group, and the boryl moiety of **5.3'** was modelled as the much simpler $B(NHCH)_2$ group. Being representative of an alkylimide, an arylimide and a borylimide, respectively, the FMOs of the three models **6Q_R** are reported in Figure 5.3. Beginning first with the FMOs of the model methylimide **6Q_Me**, Figure 5.3 (top) shows the two orthogonal π components that make up the formal Sc–N triple bond, these being the HOMO and HOMO–1. These are almost isoenergetic (–3.93 and –3.94 eV respectively) as the two π-symmetry lone pairs of the $[NMe]^{2-}$ fragment are degenerate (C_{3v} symmetry) although they have different symmetries and mix with different acceptor orbitals at the metal centre.

Turning now to **6Q_Ph**, the HOMO and HOMO–1 again represent the two orthogonal π components of the Sc–N multiple bond (Figure **5.3**, middle). The HOMO is the π_v orbital which features an anti-bonding interaction between the Sc–N π bond and a filled π MO of the phenyl ring, and is destabilised relative to the HOMO of **6Q_Me** (–3.88 *vs* –3.93 eV). In contrast, the HOMO–1, is the π_h which is stabilised compared to that in **6Q_Me** (–4.56 *vs* –3.94 eV) due to the electron-withdrawing nature of a phenyl group relative to methyl. Additionally, the HOMO–5 (–6.82 eV) is a counterpart of the HOMO which shows backbonding from a Sc–N π bond into an unfilled π orbital of the phenyl ring.

The FMOs of **6Q_B(NHCH)$_2$** featured in Figure 5.3 (bottom) are all comparable in form to those of **6Q_Ph**, and all higher in energy due to the electropositive nature of boron. The HOMO is the π_v orbital, which is destabilised by an antibonding interaction between the Sc–N π bond and a filled π orbital of the boryl ring, while the HOMO–3 in this case is its counterpart in which electron density is donated from a Sc–N π bond to an unoccupied π orbital of the boryl ring.

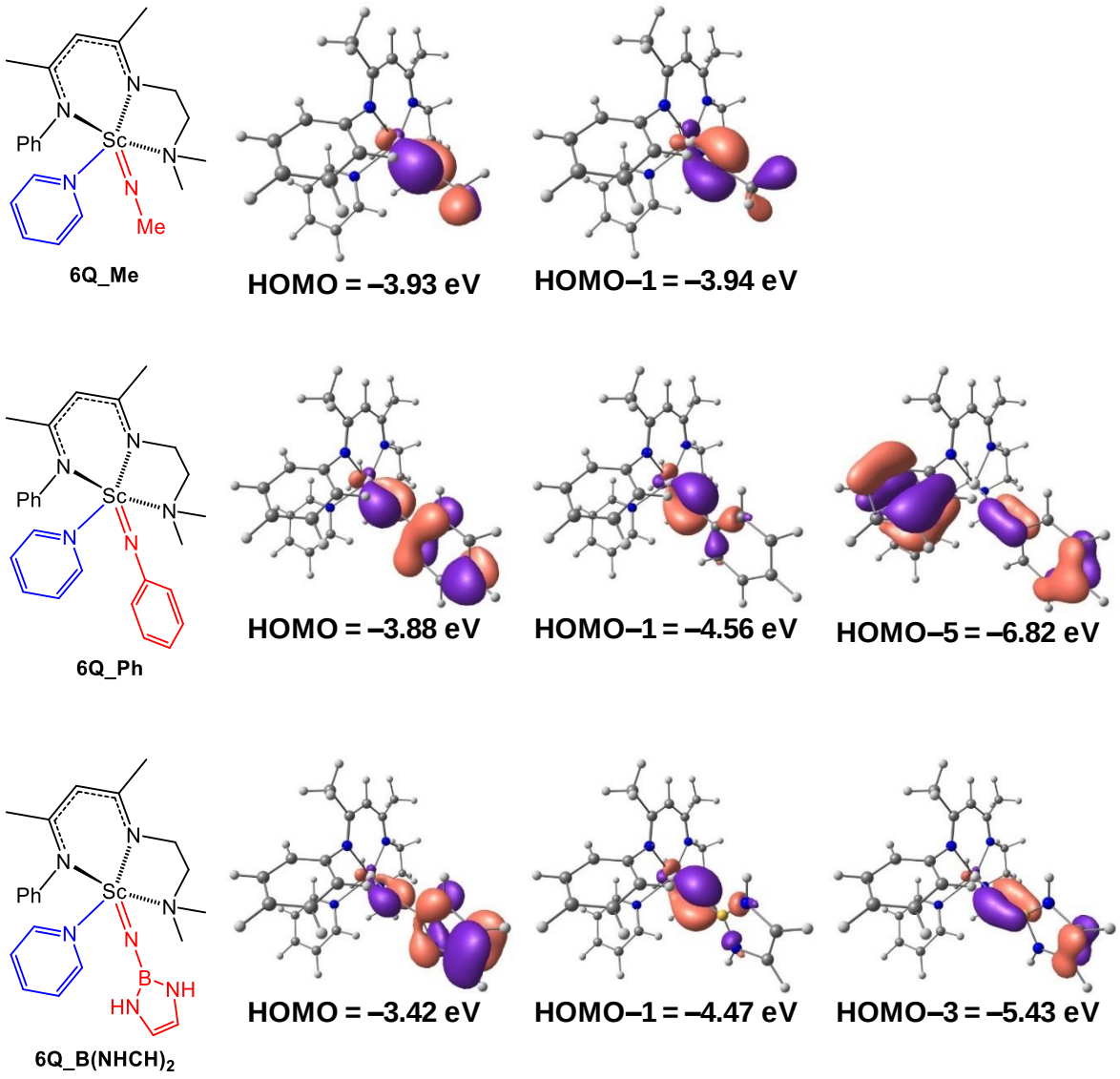

Figure 5.3. DFT model compounds {(Ph)NC(Me)CHC(Me)NCH$_2$CH$_2$NMe$_2$}Sc(NR)(py) (**6Q_R**; R = Me, Ph, B(NHCH)$_2$), and associated isosurfaces and energies of the π components of the Ti–N linkages.

A QTAIM study was then performed on the three model complexes **6Q_R**, and on a variant of these model complexes (denoted **6Q_R_fixed**) in which the Sc-N_{im} bond distance was fixed at 1.824 Å, which is the average of the three optimized distances found in **6Q_R**. This was done to see more clearly the relationship between the QTAIM parameters and the Sc-N_{im} bond dissociation energies. To test for the reliability of this approximation, the Sc–N_{im} bond of **6Q_Me** was extended from its value of 1.809 Å in its optimised structure to 1.850 Å. This resulted in the electronic SCF energy of the model complex increasing by only 0.3 kcal mol^{-1}, implying again that the strength of the bond is not strongly dependent on the bond distance over this short range. Indeed, the Sc–N_{im} bond dissociation energies of **6Q_R** (to relaxed fragments) were calculated to be 99.1 (R = Me), 106.0 (R = Ph) and 116.7 kcal mol^{-1} (R = $B(NHCH)_2$), which do not show a clear relationship to the trend in Sc–N_{im} bond distances across the three models. QTAIM data obtained for the model complexes **6Q_R** are shown in Table 5.2**,** along with the Sc–N_{im} bond distances in the optimised structures. In these model complexes, the δ(Sc–N_{im}) values are consistently smaller than δ(Ti–N_{im}) in the model titanium complexes **1Q_R** (Chapter 4), indicating a smaller degree of covalency in the more polar Sc–N_{im} bonds. **6Q_Me** has the largest δ(Sc–N_{im}) value, which corresponds to the shortest Sc–N_{im} bond distance, indicating a stronger bond, while **6Q_Ph** has the smallest δ(Sc–N_{im}) value and the longest Sc–N_{im} bond distance, as the multiple bond is disrupted by π interactions with the phenyl ring. **6Q_B(NHCH)$_2$** has an intermediate δ value and Sc–N_{im} bond distance as there is less orbital mixing with the heteroaromatic ring. Similarly, the electron densities (ρ) at the BCPs of the Sc–N_{im} bonds in **6Q_R** are consistently smaller than the ρ values of the Ti–N_{im} bonds in **1Q_R**, this again indicating reduced covalency for the more polar Sc–N_{im} bonds. However, no clear trend is found in the variation of ρ among the three models **6Q_R** themselves. Moving on to the complexes **6Q_R_fixed** (Table 5.3), it was shown that the electron density values, ρ of **6Q_Me_fixed** and **6Q_Ph_fixed** are now similar, whilst that of **6Q_B(NHCH)$_2$_fixed** is significantly more positive, reflecting increased covalency of the bond with the σ-electron-releasing nature of the electropositive boryl group. Similarly, the energy density values, *H*, of **6Q_Me_fixed** and **6Q_Ph_fixed** are also of similar magnitude, with that of **6Q_B(NHCH)$_2$_fixed** being significantly more negative, again reflecting the trend in σ-donor ability. The *H* value is in fact reported to be negative for covalent interactions, with its increasing magnitude reflecting a greater degree of covalency as explained in Chapter Four. A corresponding relationship is found with the Sc–N_{im} bond dissociation energies (ΔE_{BD}) in **6Q_R** (to relaxed fragments), which were found to increase moving from **6Q_Me** to **6Q_Ph** and to **6Q_B(NHCH)$_2$**. In summary,

6Q_B(NHCH)$_2$_fixed has the most covalent, and therefore strongest, Sc–N_{im} bond (most positive ρ and most negative H), while the model imides have less covalent linkages (least for **6Q_Me_fixed**) giving lower bond dissociation energies.

Table 5.2. Selected QTAIM data (atomic units) for the Sc–N_{im} bond in model complexes of the type {(Ph)NC(Me)CHC(Me)$NCH_2CH_2NMe_2$}Sc(NR)(py) (**6Q_R**; R = Me, Ph, $B(NHCH)_2$), Sc–N_{im} bond distances (*d*, Å) in the optimised structures, and charges (*Q*, units of *e*) of the model fragments (L is the model tridentate supporting ligand). Values for ρ (electron density), $\nabla^2\rho$ (electron density Laplacian), *H* (energy density) and ε (ellipticity) were obtained at the bond critical point. δ is the delocalisation index of the Sc–N_{im} bond.

	δ	ρ	$\nabla^2\rho$	ε	*H*	*d*(Sc–N_{im}) / Å	*Q*(L)	*Q*(Sc)	*Q*(py)	*Q*(NR)
6Q_Me	1.220	0.148	0.653	0.017	–0.052	1.809	–0.755	1.855	0.031	–1.131
6Q_Ph	1.083	0.141	0.613	0.074	–0.045	1.835	–0.706	1.894	0.041	–1.229
6Q_B(NHCH)$_2$	1.173	0.152	0.560	0.022	–0.056	1.829	–0.735	1.885	0.035	–1.186

Table 5.3. Selected QTAIM data (atomic units) for the Sc–N_{im} bond (fixed at 1.824 Å) in model complexes of the type {(Ph)NC(Me)CHC(Me)$NCH_2CH_2NMe_2$}Sc(NR)(py) (**6Q_R_fixed**; R = Me, Ph, $B(NHCH)_2$). All other bond metrics remain unchanged from the optimised structures. The bond dissociation energy (ΔE_{BD}, kcal mol^{-1}) is for Sc–N_{im} in **6Q_R** (to relaxed fragments).

	δ	ρ	$\nabla^2\rho$	*E*	*H*	ΔE_{BD}	*Q*(L)	*Q*(Sc)	*Q*(py)	*Q*(NR)
6Q_Me_fixed	1.206	0.143	0.635	0.018	–0.047	99.1	–0.755	1.858	0.030	–1.133
6Q_Ph_fixed	1.093	0.144	0.627	0.073	–0.049	106.0	–0.707	1.892	0.041	–1.226
6Q_B(NHCH)$_2$_fixed	1.178	0.154	0.565	0.022	–0.058	116.7	–0.735	1.885	0.035	–1.185

Three sets of different DFT calculations were next performed in order to better understand the mechanism of the three thermolysis reactions described in Section 5.4. The computational details are explained in Chapter 7. A first set involved the mechanistic calculations, including solvent and dispersion corrections, of the reactions of $(L^1)Sc(Me)\{NHB(NAr'CH)_2\}$ (**5.1**) as well as models of their analogues derived from the anilide $(L^1)Sc(Me)(NHAr')$ (**1.30**). The Ar' group was modelled as the smaller Xyl group in the imido- and amido-type ligands, giving $–B(NXylCH)_2$ as the model boryl moiety. However, given the role of an isopropyl group of the L^1 supporting ligand in the base-free tuck-in reaction, it was necessary to include L^1 in full. In the following scheme and discussion, the label **7Q** corresponds to borylamido and borylimido models, and **8Q** corresponds to the anilido and imido models incorporating a Xyl substituent. These models should give a good compromise between the full systems and very small systems which do not incorporate the steric bulk, while being computationally feasible.

Scheme 5.7 shows the set of hypothetical reactions originating from the model methyl-borylamide $(L^1)Sc(Me)\{NHB(NXylCH)_2\}$ (**7Q_A**) and the analogous reactions originating from the model methyl-anilide $(L^1)Sc(Me)(NHXyl)$ (**8Q_A**), along with relative Gibbs free energy values (G_{rel}) at 298 K for each of the model complexes (those for **7Q** in black, and those for **8Q** in red) as well as the G_{rel} values of selected transition states (shown in bold). G_{rel} values calculated at 343 K are shown in parentheses. In both systems, the G_{rel} values were referenced to the model methyl-amido complexes **A**, which were set at 0.0 kcal mol^{-1}.

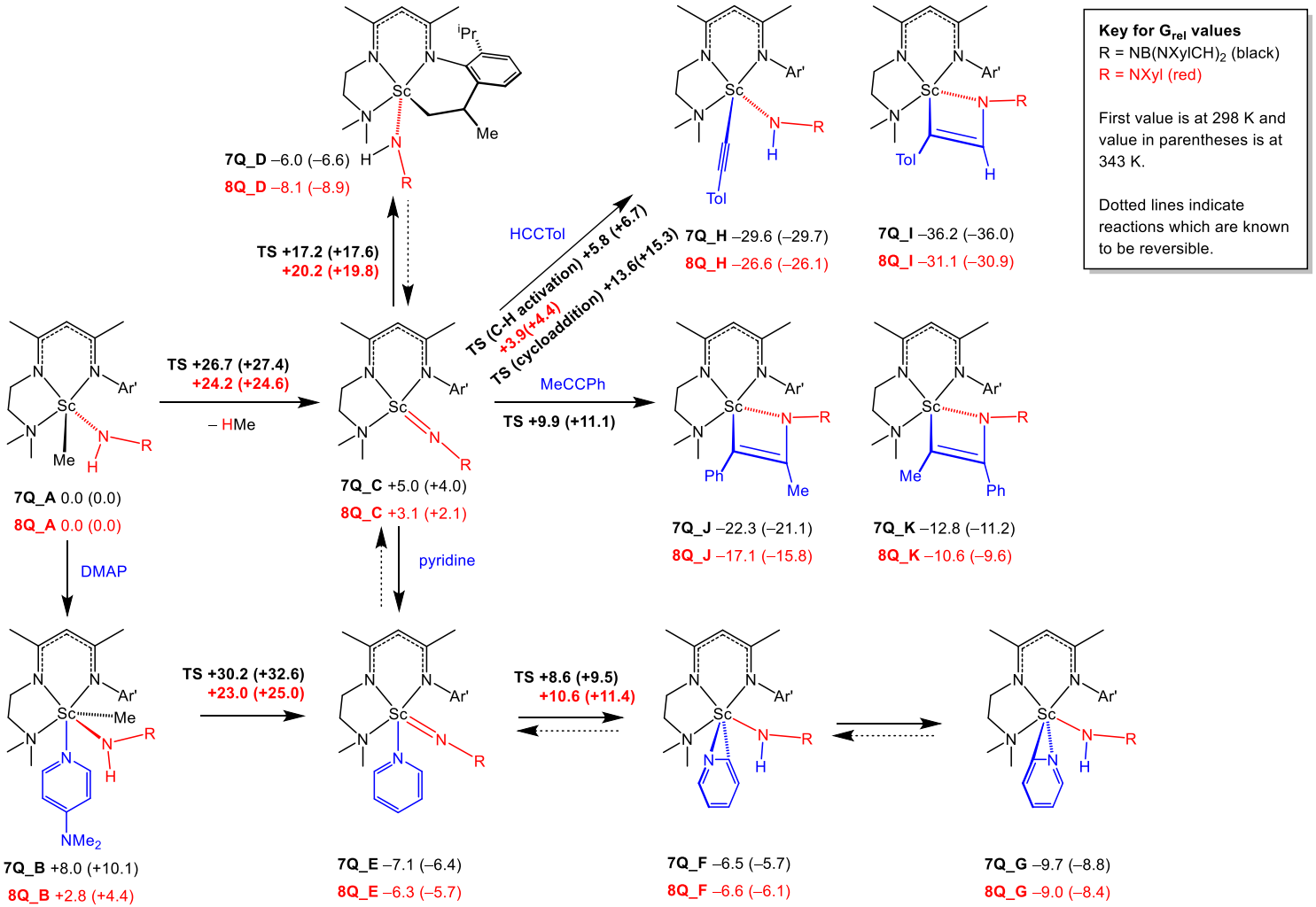

Scheme 5.7. Hypothetical reactions of model borylamide **7Q_A** and a model methyl-anilide **8Q_A** with G_{rel} values (kcal mol^{-1}) at 298 K (black for **7Q** and red for **8Q**). G_{rel} values calculated at 343 K are shown in parentheses. Transition state (TS) G_{rel} values are in bold.

The reaction starts with the α-abstraction step which forms the base-free (boryl)imido complexes 7Q_**C** and **8Q_C** from 7Q_**A** and **8Q_A** respectively. This reaction is calculated more endergonic for the borylimido system compared with the imido system (the relative Gibbs free energies of **7Q_C** and **8Q_C** are +5.0 and +3.1 kcal mol^{-1} respectively). This is attributed to the higher N–H bond strength in the borylamido ligand of **7Q_A** which was extensively discussed in Chapter Four and could be explained by the strong σ-donor ability of the borylimido fragment which arises from the electropositive nature of boron. The TS between **7Q_A** and **7Q_C**, namely a α-H elimination which proceeds via a four-membered TS, is also calculated to be higher in energy than that between **8Q_A** and **8Q_C** (by 2.5 kcal mol^{-1} at 298 K and 2.8 kcal mol^{-1} at 343 K). In Section 5.4, the first order rate constant of the α-abstraction of the methyl-borylamide **5.1** was measured as 16.20(3) × 10^{-5} s^{-1} which results in an experimental measurement of $\Delta G_{343}^{\ddagger}$ of 26.1 kcal mol^{-1}. The computational $\Delta G_{343}^{\ddagger}$ is calculated to be 27.4 kcal mol^{-1} at 343 K in line with the experimental results. In Chen's chemistry (system modelled by **8Q_A** etc.), a DMAP adduct with the starting complex **1.30**, was observed, namely **1.30'**. The model compound **8Q_B** was computationally found to have a relative Gibbs free energy of 2.8 kcal mol^{-1} at RT. Despite this adduct lying above the starting methyl-amido complex in energy, the transition state associated with methane release (namely to go from **8Q_B** to **8Q_E** + CH_4) is lower in energy than the corresponding TS to give **8Q_C** starting from the DMAP free complex **8Q_A** ($\Delta G_{298}^{\ddagger}$ = 23.0 kcal mol^{-1} *vs.* $\Delta G_{298}^{\ddagger}$ = 24.2 kcal mol^{-1}). This can be explained by steric hindrance of **8Q_B** which facilitates the release of CH_4. Moving on to the borylamido analogue, the DMAP adduct **7Q_B,** was higher in energy (G_{rel} of 8.0 kcal mol^{-1} at RT) than the amido analogue **8Q_B**. The TS to release methane from **7Q_B** is lower than the corresponding TS to eliminate methane from **7Q_A** (**$\Delta G_{298}^{\ddagger}$** = 30.2 kcal mol^{-1} *vs.* $\Delta G_{298}^{\ddagger}$ = 26.7 kcal mol^{-1}), but the high relative Gibbs free energy of **7Q_B** suggests that this intermediate is inaccessible in line with the experimental results.

Moving on to the tuck-in product formation, the conversion of **7Q_C** to the complex **7Q_D** proceeds with a comparable change in Gibbs free energy to its imido counterpart, the two processes having $\Delta_r G$ values of –11.0 and –11.2 kcal mol^{-1}, respectively, at 298 K. Thus, the gain of a stronger N–H bond for the borylimido compound in this case does not appear to give a more favourable reaction. Entropic and enthalpic contributions to these reactions will be considered later through calculations on full systems (*vide infra*).

Next, the C–H bond activation of pyridine was analysed. Experimentally, C–H bond activation of the putative pyridine-coordinated borylimide **5.3'** to give the η^2-pyridyl complex **5.3** is rapid, so **5.3'** cannot be observed, while Chen and co-workers found that the analogous reaction does not take place with the DMAP-stabilised arylimide (L^1)Sc(NAr')(DMAP) (**1.31**), which is thermally stable up to 90 °C. The calculations in Scheme 5.7 give $\Delta_r G$ values of –2.6 kcal mol^{-1} at 298 K for the model borylimide **7Q_E** forming the most stable isomer of the pyridyl complex (**7Q_G**) and –2.7 kcal mol^{-1} for the analogous reaction in the imido system, in disagreement with the reported experimental results. The experimental differences in the imido and borylimido systems will therefore be probed further through calculations on systems with full steric bulk later in this Section.

Finally, the calculated reactions of **7Q_C** and **8Q_C** with the alkynes HCCTol and MeCCPh are discussed. For HCCTol, the metallacyclic complex **I** is calculated to be more stable than the acetylide complex **H** in both the imido and borylimido cases, by 4.5 and 6.6 kcal mol^{-1}, respectively, at 298 K. The barrier associated with the N-H bond cleavage to yield the acetylide complex **H** is $\Delta G_{298}^{\ddagger}$ = 0.8 kcal mol^{-1} for both **7Q_H** and **8Q_H**, indicating that these products can be easily accessed. This is consistent with reactions of titanium borylimides with terminal alkynes previously reported in our research group,[24] in which the thermodynamic product was shown to be the metallacyclic complex, although an acetylide formed by C–H bond activation could be isolated in some cases as a kinetic product. These calculations therefore imply that the experimental formation of the acetylide **5.5** from thermolysis of **5.1** in the presence of HCCTol is under kinetic control. It was proved experimentally that, strong heating of **5.5** (up to 100 °C), however, did not result in conversion to a metallacyclic product. This is due to the high barrier of returning from **5.5** to the transient boryimide **5.1'**, namely $\Delta G_{298}^{\ddagger}$ = 35.4 kcal mol^{-1}. Interestingly, the barrier to form the cycloaddition product, **7Q_I** starting from the the transient borylimido compound **7Q_C** is $\Delta G_{298}^{\ddagger}$ = 8.6 kcal mol^{-1}, still easily accessible but higher than the corresponding C-H activation barrier. The calculated Gibbs free energies of the two alternative regioisomers of cycloadditions with MeCCPh show that the anti-Markovnikov isomer (**J**) is consistently lower in energy than the Markovnikov isomer (**K**), with a relative stabilisation, in the borylimido case of **7Q_J** *vs* **7Q_K**, of 9.5 kcal mol^{-1}. Experimentally, only the anti-Markovnikov metallacycle **5.6** was observed from the thermolysis of the methyl-borylamide **5.1**. It has been established, in titanium imido and hydrazido chemistry, that the anti-Markovnikov regioisomer is the electronically preferred isomer of alkyne cycloaddition.[33]

Furthermore, the positioning of the phenyl group adjacent to the R substituent in the Markovnikov isomer models **K** is also sterically disfavoured, especially in the case of the large boryl moiety in **7Q_K**.

In conclusion, these calculations gave a good agreement with the experimental results for the thermolysis reactions in presence of the alkynes and confirm that in all cases the rate determining step is associated with the CH_4 release, but a clear picture of the C-H bond activation of bound pyridine and of the nature of the intramolecular C-H activation of the supporting ligand was not obtained. For this reason, two additional sets of calculation were performed. The first set aimed at understanding the steric contribution of the full system in the reaction pathway and to give the most accurate description of ground state thermodynamic preferences (no TS was evaluated). Calculations were indeed performed on the same system although including the full steric bulk of both the supporting ligand L^1, and the boryl and Ar' moieties of the imido- and amido-type ligands. These calculations included solvent and dispersion corrections, and also explicitly analysed the enthalpic contribution (H_{rel}) to G_{rel} in each complex. Scheme 5.8 depicts this set of reactions in three cases. G_{rel} values (calculated at 298 K; H_{rel} in parentheses) typed in black denote the borylimido system **9Q** with R = $B(NAr'CH)_2$ and involving pyridine where relevant, those in blue denote the borylimido system **10Q** with R = $B(NAr'CH)_2$ and involving DMAP where relevant, and those in red denote the imido system **11Q** with R = Ar' and involving DMAP where relevant. G_{rel} values are also provided at 343 K (in square brackets). For clarity, those species which are observed experimentally have their G_{rel} and H_{rel} values in bold. In the discussion below, all G_{rel} and H_{rel} values described, and changes (Δ_r) between them, are those calculated at 298 K, unless stated otherwise.

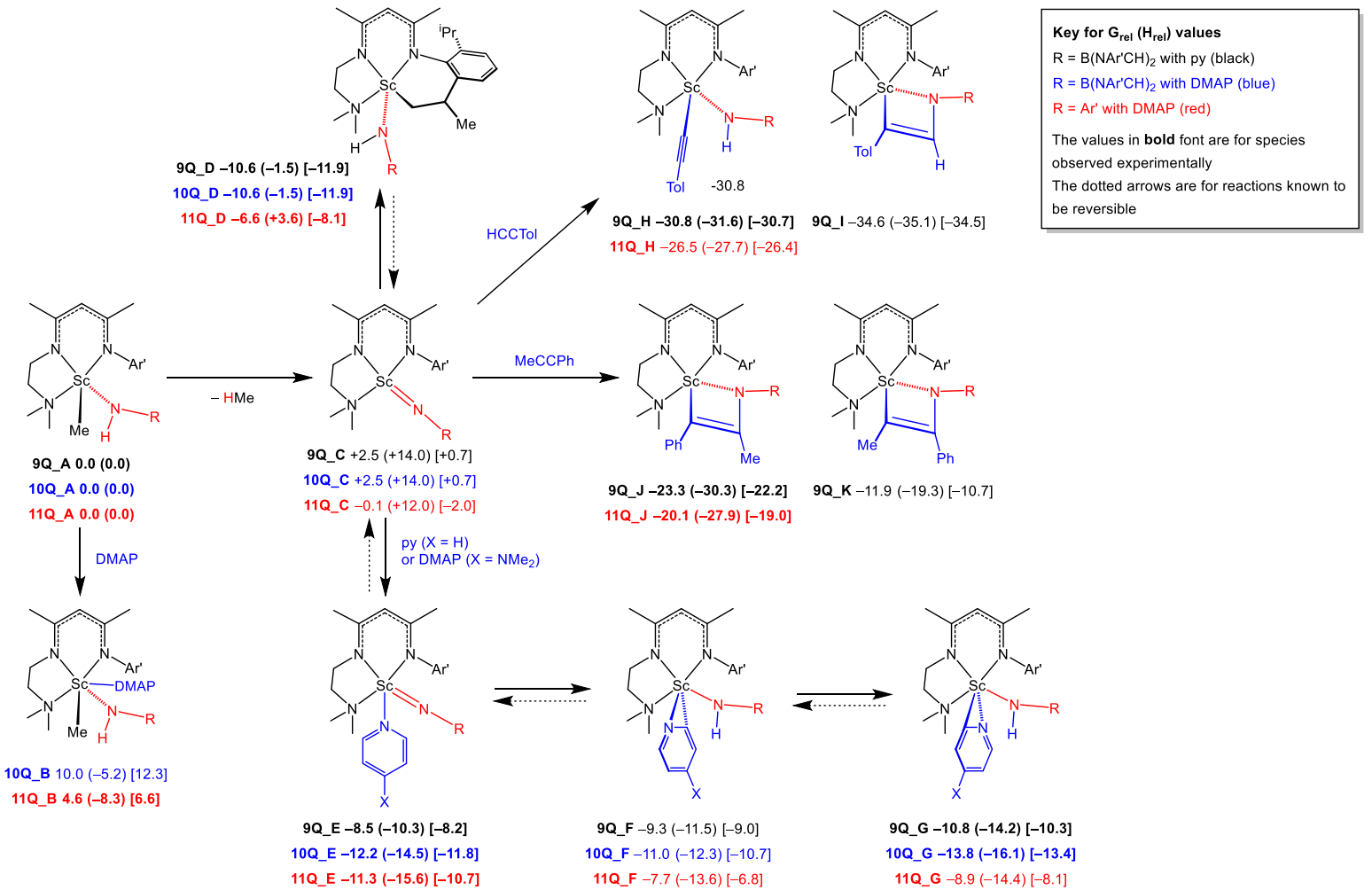

Scheme 5.8. Hypothetical reactions of methyl-borylamide **9Q_A (10Q_A)** and methyl-anilide **11Q_A** with G_{rel} values (and H_{rel} values in parentheses; both kcal mol^{-1}) calculated at 298 K. G_{rel} values calculated at 343 K are shown in square brackets. Refer to the key for colour coding.

The reactions with pyridine and DMAP will now be discussed. As explained before, both procced via an initial CH_4 release to form species **9Q_C** and **10Q_C** followed by pyridine or DMAP coordination and H abstraction to yield the final complexes **9Q_G** and **10Q_G**. Overall C–H bond activation process for DMAP and pyridine are both exergonic with Δ_rG = –10.8 kcal mol^{-1} for pyridine and Δ_rG = –13.8 kcal mol^{-1} for DMAP. However, some differences arise in the single steps described above. The addition of DMAP to **10Q_C** to give **10Q_E** is more favourable than the corresponding addition of pyridine to **9Q_C** to give **9Q_E** (Δ_rG = –14.7 *vs* –11.0 kcal mol^{-1}), arising from the stronger basicity of DMAP compared with pyridine. Moving on to the next step, which yields the first-formed η^2-pyridyl-type complexes **F**, this is found to be exergonic for pyridine in the system **9Q** (Δ_rG = –0.8 kcal mol^{-1} and Δ_rH = –1.2 kcal mol^{-1} from **9Q_E** to **9Q_F**) and endergonic for DMAP in the system **10Q** (Δ_rG = +1.2 kcal mol^{-1} and Δ_rH = +2.2 kcal mol^{-1} from **10Q_E** to **10Q_F**). This presumably arises as DMAP has a higher η^1-binding strength than pyridine in **E**, so has a relatively more unfavourable enthalpic contribution upon forming the η^2-pyridyl-type complexes **F**. Rotation of the η^2-pyridyl-ring gives the final most stable isomer, **10Q_G**.

Experimentally, the steps between complexes **C**, **E**, **F** and **G** are found to be reversible at 60 °C in the borylimido system and the exchange reactions suggested that **5.5** and **5.6** are similar in energy to give equilibrium mixtures close to equality. These DFT calculations showed the activated DMAP complex **10Q_G** to be 3.0 kcal mol^{-1} more stable than its pyridine counterpart. In enthalpy terms, however, the difference is less than 2 kcal mol^{-1} and within DFT accuracy for these large models. It is proposed that the interplay of opposing equilibria is responsible for the observed experimental outcome. In the first step, coordination of DMAP is favoured over that of pyridine in the equilibrium between complexes of the type **C** and **E**, due to the stronger donor ability, whilst the C–H bond activation of bound DMAP is disfavoured compared with that of pyridine in the equilibrium between complexes of the type **E** and **G**. This could result in an approximately equal mixture of C–H bond activation products derived from pyridine and DMAP. In the imido system, the conversion of the DMAP adduct **11Q_E** to the first-formed C–H bond activation product **11Q_F** is more endergonic than the corresponding activation of DMAP in the borylimido system **10Q** (Δ_rG = +3.6 *vs* +1.2 kcal mol^{-1}), reflecting that a less strong N–H bond is formed in the anilido case than the borylimido. This is consistent with experimental results in which the DMAP-stabilised arylimide **1.31** is thermally stable and does not undergo an intramolecular C–H bond activation.

The addition of DMAP to the methyl complexes **A** to form the respective adducts (**B**) is also considered. The DFT results match the previous set of calculations performed on the model system and reported above. Both reactions are found to be endergonic, though more so for the reaction in the borylamido system **10Q** (by 5.4 kcal mol^{-1}) due to the particularly unfavourable steric interactions in this six-coordinate complex containing the very bulky $B(NAr'CH)_2$ group. Although the experimentally successful formation of the anilide **11Q_B** would be expected to be exergonic, the large difference in Δ_rG between that reaction and the formation of **10Q_B** is consistent with the latter reaction not taking place in practice while the former reaction does.

Next, the formation of the tuck-in complexes is discussed. The formation of tuck-in complexes **D** from the base-free multiply bonded complexes **C**, is found to be more favourable for the borylimido system than the imido system (Δ_rG = –13.1 *vs* –6.5 kcal mol^{-1}). This difference in term of G primarily arises from a much greater negative enthalpic contribution in the former case (Δ_rH = –15.5 *vs* –8.4 kcal mol^{-1}) due to the stronger N–H bond which is formed in the borylamido ligand of **9Q_D**. Note that, the calculations performed on the system with less steric bulk were not able to fully describe this difference, and the two processes to form the tuck-in complexes, namely from **7Q_C** to **7Q_D** and from **8Q_C** to **8Q_D**, were found to have Δ_rG values of –11.0 and –11.2 kcal mol^{-1}, respectively, at 298 K. The calculated G_{rel} values of the compounds **G** at 298 K show that, of the three, only the pyridyl-borylamido complex **9Q_G** is comparable in energy to its respective tuck-in complex **D** (–10.8 *vs* –10.6 kcal mol^{-1}) and that at 343 K, **9Q_D** becomes even lower in energy than **9Q_G** (–11.9 *vs* –10.3 kcal mol^{-1}), This is now evidence to support the experimental conversion of **5.3** to **5.2** as a thermodynamic product at 90 °C, which does not happen for the conversion of the DMAP analogue, **5.4**, to the tuck-in complex **5.2**. The steric bulk helped to highlight these differences.

Finally, the calculated Δ_rG values for reactions with HCCTol and MeCCPh confirm those trends that were seen in the smaller model systems. In particular, the experimentally observed anti-Markovnikov isomer of cycloaddition with MeCCPh (**9Q_J**) is 11.4 kcal mol^{-1} more stable than the Markovnikov isomer **9Q_K**, with the similar enthalpic difference of –11.0 kcal mol^{-1} confirming that this is dominated by Δ_rH and is little affected by entropic considerations. Additionally, the experimentally observed acetylide complex **9Q_H** is 3.8 kcal mol^{-1} less stable than the HCCTol metallacycle **9Q_I**, with again a similar difference in H_{rel} (+3.5 kcal mol^{-1}). Furthermore, the reactions leading to the the anilido complexes

11Q_H and **11Q_J** are less exergonic than those of their borylamido counterparts, presumably due to the weaker bonds formed to the NAr' fragment compared with those to the $NB(NAr'CH)_2$ fragment.

Overall, the single point calculations performed on the full system were necessary to fully understand the single thermodynamic contributions to the energetics of the reaction and to clearly show that the steric bulk plays a key role in the reactivity of these systems toward C-H activation reactions.

The third set of complementary DFT calculations were performed on gas-phase systems having minimal steric bulk, and not including solvent or dispersion corrections. The modelling of ligands was the same as used in **6Q_R** at the beginning of this Section, replacing the Ar' groups of the L^1 supporting ligand and the arylimido ligand with phenyl groups, and using $NB(NHCH)_2$ as the model borylimido ligand. These calculations were performed to evaluate the underlying electronic preferences of reactivity without contributions from sterics or attractive dispersive effects. Scheme 5.9 summarises these hypothetical reactions for the model borylimido system denoted **12Q** and the model phenylimido system denoted **13Q**. The G_{rel} and H_{rel} values are here expressed relative to the base-free (boryl)imido complexes **C** which was set at 0.0 kcal mol^{-1}. It is noted that the pyridine-stabilised models **D** are identical to **6Q_Ph** and **6Q_B(NHCH)$_2$** shown earlier in this Section, though will be referred to here using the **D** notation for consistent comparison with the other species in Scheme 5.9.

Starting from the methane release, the results show that the α-abstraction of the methyl complexes to give the transient borylimides **C**, is more endergonic for the methyl-borylamide system. Because the entropic contribution of these two systems is comparable, this clearly explains that the difference arises from enthalpic contributions. This could be explained again by the different strengths of N-H bonds in borylamido and amido systems, as explained before. Moving on to the thermolysis reactions with pyridine and DMAP, as found for the two previous sets of calculations, the DFT results predict that C-H activation of bound pyridine and DMAP should both be favourable, whereas experimentally this occurs for the transient borylimide only **5.1'** but not for the DMAP-stabilized arylimide **1.31**.

The first step is the formation of the pyridine adducts **D** from **C** which is found to be more favourable in the imido system **13Q** than the borylimido system **12Q** (by 1.4 kcal mol^{-1}). This probably reflects the fact that the borylimido ligand has a greater σ-donor ability than

the phenylimido ligand (as discussed for the models **6Q_R**), thus reducing the ability of the Sc centre to accept electron density from the pyridine ligand. This results in a weaker Sc–N_{py} bond, and a less favourable enthalpic contribution, in the borylimido system. The subsequent C–H bond activations of complexes **D** is more favourable in the borylimido system **12Q** than the imido system **13Q** with an enthalpic contribution $\Delta_r H$ of –13.8 and –9.7 kcal mol^{-1} respectively, which is a further confirmation of the higher relative strength of N–H bonds to borylimido fragments. As in the calculations on the full system described above, coordination of DMAP to the base-free complexes **C** is more favourable than coordination of pyridine (by 2.7 kcal mol^{-1} in the borylimides **12Q** and by 3.1 kcal mol^{-1} in the imides **13Q)** while the C–H bond activation of coordinated DMAP is found to be less favourable than that of pyridine, for the same reasons described previously. It is noted, however, that both the model imido and borylimido systems predict that C–H bond activation of bound pyridine and DMAP should be favourable, whereas experimentally this occurs for the transient borylimide **5.1'** but not for the DMAP-stabilised arylimide **1.30'**. These calculations on small models, and the full system calculations above, suggest that the experimental differences in these systems arise from a combination of the electronic favouring of borylamido N–H bonds and the increased stability of η^1-coordination of DMAP relative to its η^2-pyridyl derivative compared with pyridine relative to an η^2-pyridyl ligand.

Moving on to the addition of pyridine to the methyl-amido complexes **A**, it was found that the overall $\Delta_r G$ from **12Q_A** to **12Q_B** for the borylamido system (13.3 kcal mol^{-1}) is very similar to the anilido system (from **13Q_A** to **13Q_B**, $\Delta_r G$ = 13.5 kcal mol^{-1}). As expected, these processes are dominated by entropic factors which are absent here. Finally, the formation of the metallacycle products **F** from **C** is favoured for the borylimido system **12Q**, with a $\Delta_r G$ = -18.6 kcal mol^{-1} from **12Q_C** to **12Q_F** as compared to a $\Delta_r G$ = -12.9 kcal mol^{-1} for the imido system (from **13Q_C** to **13Q_F**), and similarly, the formation of the model acetylide-borylamide **12G** is more exergonic than its anilido counterpart. The enthalpic contributions to these differences again highlight the higher strength of bonds formed to borylimido fragments relative to arylimido fragments.

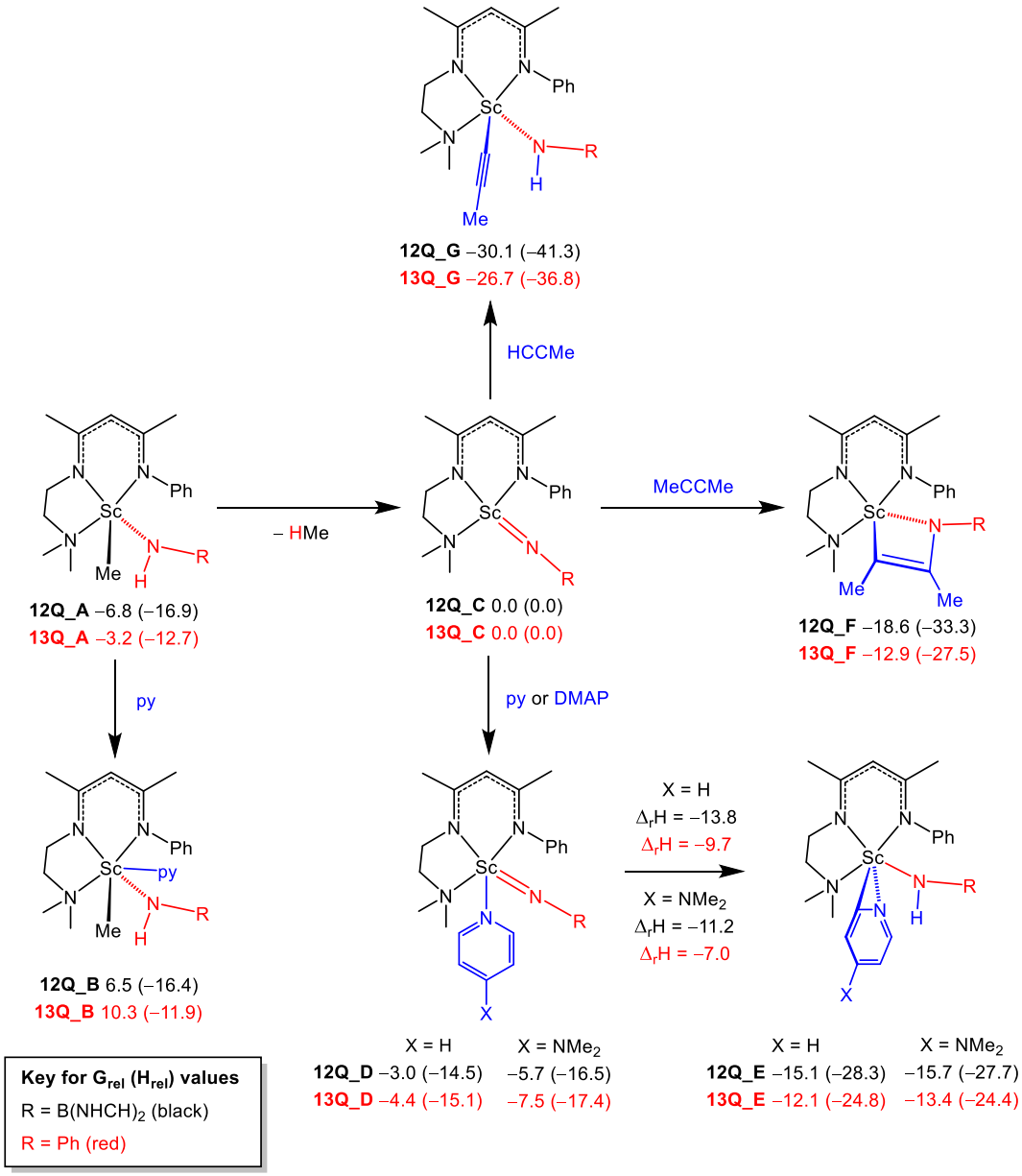

Scheme 5.9. Hypothetical reactions of model borylamide **12Q_A** and methyl-anilide **13Q_A** with G_{rel} values (and H_{rel} values in parentheses; both kcal mol^{-1}) calculated at 298 K. Those values for **12Q** are in black, and those for **13Q** are in red, and all are expressed relative to the base-free (boryl)imido complexes **C**.

5.6 Conclusions

This Chapter has described the reactions to form the first borylimido complexes of a rare earth metal, namely scandium, attempted by Dr. Ben Clough, former DPhil student in our group and the DFT calculations performed to better explain the reasoning behind the outcomes of these attempts.

In particular, the reactivity of the methyl-borylamide (L^1)Sc(Me){NHB(NAr'CH)$_2$} (**5.1**) was described. Thermolysis reactions of this complex with or without an external base, were reported to give respectively the tuck-in complex {MeC(NC$_6$H$_3$^{i}PrCH(Me)CH$_2$)CHC(Me)NCH$_2$CH$_2$NMe$_2$}Sc{NHB(NAr'CH)$_2$} (**5.2**) and, in the presence of pyridine or DMAP, the pyridyl-type complexes (L^1)Sc{NHB(NAr'CH)$_2$}(η^2-4-NC$_5$H$_3$R) (R = H (**5.3**), NMe$_2$ (**5.4**)). The mechanism is an intramolecular sp^3 C–H bond activation of an isopropyl group on the supporting ligand and the (sp^2) C–H bond activation at the 2-position of coordinated pyridine or DMAP, respectively. Kinetic analysis showed that all of these reactions proceed with comparable first order rate constants and that they share a common rate-determining step: initial α-abstraction to release methane and generate the transient borylimido complex (L^1)Sc{NB(NAr'CH)$_2$} (**5.1'**). This was confirmed by DFT studies which found the TS associated with methane release to be the highest in energy. Following this step, the respective C–H bond activations are rapid.

Thermolysis reactions of **5.1** in the presence of HCCTol and MeCCPh were experimentally tested to trap the transient borylimido compound **5.1'** and were reported to produce the acetylido complex (L^1)Sc{NHB(NAr'CH)$_2$}(CCTol) (**5.5**) *via* C–H bond activation at the sp centre and the azascandacyclobutene complex (L^1)Sc{N{B(NAr'CH)$_2$}C(Me)C(Ph)} (**5.6**) obtained by [2+2] cycloaddition across the multiple bond of **5.1'**, respectively.

DFT and QTAIM studies were first performed on model scandium alkylimides, arylimides and borylimides to better understand the bonding features of these complexes. QTAIM calculations confirmed that borylimides are expected to be comparable to arylimides structurally, due to the similar π effects arising from the aryl ring and aromatic boryl ring. Scandium borylimides are calculated to have stronger scandium–nitrogen multiple bonds than their imido counterparts due to the strong σ-donating nature of the boryl moiety. Mechanistic studies were then performed on the reaction products of a model base-free borylimide, and its arylimido counterpart, with a number of substrates to analyse the relative energetics of these processes. In particular, the three thermolysis reactions, without an

external base, with pyridine and with DMAP were explored. The reactions with the two different alkynes were also studied. Three different sets of calculations on small model systems and the full system were performed in order to better understand the electronic and steric contributions to the reaction mechanism.

It was shown that C–H bond activations are more favourable in the borylimido case, due to the higher strength of the N–H bond formed in a borylamido ligand compared with that in an anilido ligand. Other bonds formed to a borylimido fragment, such as the C–N bond in the metallacyclic product of a [2+2] cycloaddition, are also found to be stronger than those to arylimido fragments, as shown by the more favourable enthalpic contribution to free energy of the process in which it is formed. The addition of DMAP or pyridine to the methyl complexes **1.30** and **5.1** to form the respective adducts, **1.31** and **5.3'**, was instead driven by steric factors, which make the pyridine-coordinated boryilamide experimentally inaccessible.

DFT calculations highlighted that, the transient boryilimide **5.1'** is prone to undergoing C-H activation reactions, which results in the impossibility to experimentally isolate the compound. Undesired intramolecular activation of the ligand is also likely to happen. This provides a starting point in the choice of a new, robust supporting ligand or any future attempts to form an isolable scandium borylimide.

5.7 References

1 O. T. Summerscales and J. C. Gordon, *RSC Adv.*, 2013, **3**, 6682–6692.

2 G. R. Giesbrecht and J. C. Gordon, *Dalton Trans.*, 2004, 2387–2393.

3 D. Schädle, C. Schädle, K. W. Törnroos and R. Anwander, *Organometallics*, 2012, **31**, 5101–5107.

4 D. Schädle, C. Schädle, D. Schneider, C. Maichle-Mössmer and R. Anwander, *Organometallics*, 2015, **34**, 4994–5008.

5 K. D. Conroy, W. E. Piers and M. Parvez, *Organometallics*, 2009, **28**, 6228–6233.

6 A. A. Trifonov, M. N. Bochkarev, H. Schumann and J. Loebel, *Angew. Chemie Int. Ed.*, 1991, **30**, 1149–1151.

7 Z. Xie, S. Wang, Q. Yang and T. C. W. Mak, *Organometallics*, 1999, **18**, 1578–1579.

8 S. Wang, Q. Yang, T. C. W. Mak and Z. Xie, *Organometallics*, 1999, **18**, 5511–5517.

9 H. Chan, H. Li and Z. Xie, *Chem. Commun.*, 2002, 652–653.

10 J. C. Gordon, G. R. Giesbrecht, D. L. Clark, P. J. Hay, D. W. Keogh, R. Poli, B. L. Scott and J. G. Watkin, *Organometallics*, 2002, **21**, 4726–4734.

11 D. J. Beetstra, A. Meetsma, B. Hessen and J. H. Teuben, *Organometallics*, 2003, **22**, 4372–4374.

12 A. G. Avent, P. B. Hitchcock, A. V Khvostov, M. F. Lappert and A. V Protchenko, *Dalton Trans.*, 2004, 2272–2280.

13 D. Cui, M. Nishiura and Z. Hou, *Angew. Chemie - Int. Ed.*, 2005, **44**, 959–962.

14 C.-L. Pan, W. Chen, S. Song, H. Zhang and X. Li, *Inorg. Chem.*, 2009, **48**, 6344–6346.

15 E. Lu, Y. Li and Y. Chen, *Chem. Commun.*, 2010, **46**, 4469–4471.

16 T. Chu, W. E. Piers, J. L. Dutton and M. Parvez, *Organometallics*, 2013, **32**, 1159–1165.

17 W. Rong, J. Cheng, Z. Mou, H. Xie and D. Cui, *Organometallics*, 2013, **32**, 5523–5529.

18 E. Lu, J. Chu, Y. Chen, M. V Borzov and G. Li, *Chem. Commun.*, 2011, **47**, 743–745.

19 J. Chu, E. Lu, Z. Liu, Y. Chen, X. Leng and H. Song, *Angew. Chemie - Int. Ed.*, 2011, **50**, 7677–7680.

20 E. Lu, Q. Zhou, Y. Li, J. Chu, Y. Chen, X. Leng and J. Sun, *Chem. Commun.*, 2012, **48**, 3403–3405.

21 J. Chu, C. E. Kefalidis, L. Maron, X. Leng and Y. Chen, *J. Am. Chem. Soc.*, 2013, **135**, 8165–8168.

22 J. Chu, E. Lu, Y. Chen and X. Leng, *Organometallics*, 2013, **32**, 1137–1140.

23 J. Chu, X. Han, C. E. Kefalidis, J. Zhou, L. Maron, X. Leng and Y. Chen, *J. Am. Chem. Soc.*, 2014, **136**, 10894–10897.

24 B. Clough, DPhil Thesis, University of Oxford, 2016.

25 F. Brotzel, B. Kempf, T. Singer, H. Zipse and H. Mayr, *Chem. - A Eur. J.*, 2007, **13**, 336–345.

26 J. L. Bennett and P. T. Wolczanski, *J. Am. Chem. Soc.*, 1997, **119**, 10696–10719.

27 C. C. Cummins, S. M. Baxter and P. T. Wolczanski, *J. Am. Chem. Soc.*, 1988, **110**, 8731–8733.

28 C. C. Cummins, C. P. Schaller, G. D. Van Duyne, P. T. Wolczanski, A. W. E. Chan and R. Hoffmann, *J. Am. Chem. Soc.*, 1991, **113**, 2985–2994.

29 C. P. Schaller, C. C. Cummins, P. T. Wolczanski and N. York, *J. Am. Chem. Soc.*, 1996, **118**, 591–611.

30 L. M. Slaughter, P. T. Wolczanski, T. R. Klinckman and T. R. Cundari, *J. Am. Chem. Soc.*, 2000, **122**, 7953–7975.

31 R. F. W. Bader, *Atoms in Molecules: A Quantum Theory*, Oxford University Press, Oxford, 1990.

32 X. Fradera, M. A. Austen and R. F. W. Bader, *J. Phys. Chem. A*, 1999, **103**, 304–314.

33 A. D. Schofield, A. Nova, J. D. Selby, C. D. Manley, A. D. Schwarz, E. Clot and P. Mountford, *J. Am. Chem. Soc.*, 2010, **132**, 10484–10497.

6.1 General methods and implementation

All manipulations were carried out using standard Schlenk line or glove box techniques under an atmosphere of argon or dinitrogen. Solvents were either degassed by sparging with dinitrogen and dried by passing through a column of the appropriate drying agent[1] or refluxed over sodium (toluene), potassium (THF), Na/K alloy (Et_2O) or CaH_2 (pyridine) and distilled. Deuterated solvents were dried over sodium (toluene-d_8), potassium (C_6D_6) or CaH_2 (pyridine-d_5), distilled under reduced pressure and stored under argon in Teflon valve ampoules. NMR samples were prepared under dinitrogen in 5 mm Wilmad 507-PP tubes fitted with J. Young Teflon valves. ^1H, $^{13}C\{^1H\}$, $^{11}B\{^1H\}$, $^{19}F\{^1H\}$ and ^2H spectra were recorded on a Bruker Ascend 400 NMR spectrometer, a Bruker Advance III 500 NMR spectrometer or on a Bruker AVC 500 spectrometer fitted with a ^{13}C cryoprobe. Unless otherwise stated, all NMR spectra were recorded at 298 K. ^1H and $^{13}C\{^1H\}$ and spectra were referenced internally to residual protio-solvent (^1H) or solvent (^{13}C) resonances, and are reported relative to tetramethylsilane (δ = 0 ppm). ^2H NMR spectra were referenced to the natural abundance deuterium resonance of the protio solvent. ^{19}F and ^{11}B NMR spectra were referenced externally to $CFCl_3$ and $Et_2O{\cdot}BF_3$ respectively. Assignments were confirmed as necessary with the use of two dimensional ^1H–^1H, ^{13}C–^1H, ^1H–^{19}F and ^{19}F–^{19}F correlation experiments. Chemical shifts are quoted in δ (ppm) and coupling constants in Hz. Unless otherwise stated, IR spectra were recorded on a Thermo Scientific Nicolet iS5 FTIR spectrometer and samples prepared in a dry-box using NaCl plates as a Nujol mull or as a thin film. The data are quoted in wavenumbers (cm^{-1}). Mass spectra were recorded by the mass spectrometry service of Oxford University's Department of Chemistry. Elemental analyses were carried out by the Elemental Analysis Service at the London Metropolitan University.

6.2 Literature preparations

Cp*Ti(N^{t}Bu)Cl(py),[2] Cp*Ti{MeC(N^{i}Pr)$_2$}(N^{t}Bu),[3] Cp*Ti{MeC(N^{i}Pr)$_2$}(NTol),[3] Cp*Ti{MeC(N^{i}Pr)$_2$}(NNR$_2$) (R$_2$ = Me$_2$ (**1.39**), Ph$_2$ (**1.38**) or CPh$_2$ (**1.40**))[4], Cp*Ti{PhC(N^{i}Pr)$_2$}(N^{t}Bu),[5] Li[MeC(N^{i}Pr)$_2$],[6] Li[PhC(N^{i}Pr)$_2$],[5] Li[MeC(NCy$_2$)$_2$],[7] Li[PhC(NCy$_2$)$_2$],[8] HBCy$_2$,[9] H$_2$BTex,[10] HB(C$_6$F$_5$)$_2$,[11] (μ-H$_2$N)$_2$(BC$_8$H$_{14}$)$_2$,[12] Me$_2$NNCPh$_2$,[13] HB(N^{i}PrCH$_2$)$_2$[14] were synthesised according to literature procedures. HBMes$_2$[15] and Cp*Ti{MeC(N^{i}Pr)$_2$}(NXyl)[3] were provided by Dr Laura Stevenson; HB(NAr'CH)$_2$ (Ar' = Dipp)[16] was provided by Dr Andrey Protchenko.

H_2N^tBu was dried over CaH_2 and distilled before use. H_2NTol and DMAP were sublimed under dynamic vacuum at 100 °C and transferred to the dry-box. 1,1-diphenylhydrazine was obtained from Sigma-Aldrich as the hydrogen chloride salt, from which the free hydrazine was obtained by basification with NaOH, drying over Na_2SO_4 and removal of residual solvent, followed by distillation under inert atmospheric conditions. All other reagents were purchased from commercial suppliers, and (for liquid reagents) degassed before use.

6.3 X-ray data collection and processing parameters

Crystals were mounted on glass fibres using perfluoropolyether oil and cooled rapidly in a stream of cold N_2 using an Oxford Cryosystems Cryostream unit. Diffraction data were measured using either an Enraf-Nonius KappaCCD or Agilent Technologies Supernova diffractometer using Mo-K_α or Cu-K_α radiation, respectively. As appropriate, absorption and decay corrections were applied to the data and equivalent reflections merged.[17] The structures were solved with SIR92[18] or Superflip,[19] and further refinements and all other crystallographic calculations were performed using the CRYSTALS program suite.[20] Other details of the structure solutions and refinements are given in the individual CIFs contained in the CD Appendix.

6.4 Experimental details and characterising data for Chapter Three

Cp*Ti{MeC(N^{i}Pr)$_2$}(NBC$_8$H$_{14}$) (1) from Cp*Ti{MeC(N^{i}Pr)$_2$}(NNMe$_2$) (1.39) . To a stirred solution of Cp*Ti{MeC(N^{i}Pr)$_2$}(NNMe$_2$) (**1.39**, 0.338 g, 0.884 mmol) in benzene (10 mL) was added 9-BBN dimer (0.216 g, 0.884 mmol) all at RT. The solution was left to stir at RT for 12 h, filtered and volatiles removed under reduced pressure to afford Cp*Ti{MeC(N^{i}Pr)$_2$}(NBC$_8$H$_{14}$) (**1**) and Me$_2$NBC$_8$H$_{14}$ quantitatively in a 1:1 ratio as a sticky brown oil. Me$_2$NBC$_8$H$_{14}$ (**1**)[21] was sublimed (90 ^{0}C, 1 x 10^{-2} mbar, 2 h) onto a dry ice/acetone cold finger leaving **1** as a green powder. Yield: 0.150 g (37%). The ^{1}H NMR spectrum indicated that the solid contained less than 4% Me$_2$NBC$_8$H$_{14}$. Diffraction-quality crystals were grown from a concentrated hexane solution at -30 °C.

^{1}H NMR (C$_6$D$_6$, 400.1 MHz, 298K): δ 3.53 (2 H, app. sept., app. ^3J = 6.5 Hz, C<u>H</u>Me$_2$), 2.15 (15 H, s, C$_5$Me$_5$), 1.65 (3 H, s, MeCN$_2$), 2.30-1.0 (14 H, overlapping 3 x m, BCH, BCCH and BCCCH), 1.00 (6 H, d, ^3J = 6.5 Hz, CH<u>Me</u>$_2$), 0.91 (6 H, d, ^3J = 6.5 Hz, CH<u>Me</u>$_2$) ppm. ^{13}C{^{1}H} NMR (C$_6$D$_6$, 100.6 MHz, 298 K): δ 167.2 (Me<u>C</u>N$_2$), 121.96

($\underline{C}_5Me_5$), 49.4 ($\underline{C}HMe_2$), 34.7 (BC$\underline{C}$H), 26.1 (CH$\underline{Me}_2$), 24.7 (CH$\underline{Me}_2$), 24.4 (BCC$\underline{C}$H), 12.3 (B$\underline{C}$H), 13.0 ($C_5\underline{Me}_5$), 11.6 ($\underline{Me}CN_2$) ppm. ^{11}B NMR (C_6D_6, 128.4 MHz, 298K): 52.8 (s) ppm. IR (NaCl plates, Nujol mull, cm^{-1}): 1601 (w), 1337 (w), 1313 (w), 1280 (s), 1212 (w), 1093 (s), 1018 (s), 800 (s). EI-MS: *m/z* = 459 $[M]^+$ (2%). Anal. found (calcd. for $C_{26}H_{46}BN_3Ti$): C, 67.98 (67.95); H, 10.09 (9.84); N, 9.15 (8.82)%.

Cp*Ti{MeC(N^{i}Pr)$_2$}(NBC$_8$H$_{14}$) (1) from Cp*Ti{MeC(N^{i}Pr)$_2$}(NNPh$_2$) (1.38) . To a stirred solution of Cp*Ti{MeC(N^{i}Pr)$_2$}(NNPh$_2$) (**1.38**, 0.448 g, 0.884 mmol) in benzene (10 mL) was added 9-BBN dimer (0.216 g, 0.884 mmol) all at RT. The solution was left to stir at RT for 12 h at 60 ^{0}C, filtered and volatiles removed under reduced pressure to afford Cp*Ti{MeC(N^{i}Pr)$_2$}(NBC$_8$H$_{14}$) (**1**) and Ph$_2$NBC$_8$H$_{14}$ quantitatively in a 1:1 ratio as a sticky brown oil, which could not be separated. The mixture was fully characterized on the NMR scale.

NMR tube scale synthesis of Cp*Ti(H){MeC(N^{i}Pr)$_2$}(NBC$_8$H$_{14}$(NMe$_2$)) (1_Int1). To a solution of Cp*Ti{MeC(N^{i}Pr)$_2$}(NNMe$_2$) (**1.39**, 0.020 mg, 0.053 mmol) in C_6D_6 (0.3 mL) in an NMR tube equipped with a J. Young Teflon valve was added 9-BBN dimer (0.064 mg, 0.053 mmol) in toluene-d_8 (0.3 mL). The reaction was monitored by ^{1}H and ^{11}B NMR spectroscopy. After 1 h at 0 ^{0}C, the ^{1}H NMR spectrum showed complete conversion to the product, Cp*Ti(H){MeC(N^{i}Pr)$_2$}(N(NMe$_2$)BC$_8$H$_{14}$ and 0.5 equiv of 9-BBN dimer. Cp*Ti(H){MeC(N^{i}Pr)$_2$}(N(NMe$_2$)BC$_8$H$_{14}$) was fully characterized on the NMR tube scale.

^{1}H NMR (C_6D_6, 400.1 MHz, 298 K): δ 6.30 (1 H, s, Ti-H), 3.51 (1 H, app. sept., app. ^3J = 6.5 Hz, C$\underline{H}_a$MeMe), 3.34 (2 H, app. sept., app. ^3J = 6.5 Hz, C$\underline{H}_b$MeMe), 2.75 (3 H, broad s, NN$\underline{Me}$Me), 2.65 (3 H, broad s, NNMe$\underline{Me}$) 2.23 (15 H, s, $C_5\underline{Me}_5$), 1.81 (3 H, s, $\underline{Me}CN_2$), 2.30 - 1.0 (14 H, overlapping 3 x m, BC$\underline{H}$, BCC$\underline{H}$ and BCCC$\underline{H}$), 1.23 (6 H, d, ^3J = 6.5 Hz, CH$\underline{Me}_2$), 1.17 (6 H, d, ^3J = 6.5 Hz, CH$\underline{Me}_2$) ppm. ^{13}C{^{1}H} NMR (C_6D_6, 100.6 MHz, 298 K): δ 160.9 (Me$\underline{C}N_2$), 122.6 ($\underline{C}_5Me_5$), 56.7 (NN$\underline{Me}$Me), 51.5 (NNMe$\underline{Me}$), 48.1 (N$\underline{C}$H$_a$MeMe), 47.6 (N$\underline{C}$H$_b$MeMe), 33.5 (BC$\underline{C}$H), 25.9 – 24.4 (overlapping NCH$_a$$\underline{Me}Me, NCH_aMe\underline{Me}$, NCH$_b$$\underline{Me}$Me and NCH$_bMe\underline{Me}$), 24.4 (BCC$\underline{C}$H), 14.3 (B$\underline{C}$H), 13.4 ($C_5\underline{Me}_5$), 11.1 ($\underline{Me}CN_2$) ppm. ^{11}B{^{1}H} NMR (C_6D_6, 128.4 MHz, 298K): 28 (s) ppm.

Cp*Ti{MeC(N^{i}Pr)$_2$}{N(Tol)BH(C$_6$F$_5$)$_2$} (2). To a stirred solution of Cp*Ti{MeC(N^{i}Pr)$_2$}(NTol) (**3.1**, 0.300 g, 0.669 mmol) in benzene (10 mL) was added

$HB(C_6F_5)_2$ (0.231 g, 0.669 mmol) at RT. The solution was stirred at RT for 12 h, filtered and the volatiles removed under reduced pressure to afford brown oil. This was triturated with pentane to give a brown solid which was washed with cold pentane (3 x 10 mL) and dried *in vacuo*. Yield: 0.306 g (60%). Diffraction-quality crystals were grown from pentane at RT.

^{1}H NMR (C_6D_6, 400.1 MHz, 298 K): δ 6.94 (2 H, d, ^3J = 8.5 Hz, *m*-$C_6\underline{H}_4$Me), 6.67 (2 H, d, ^3J = 8.5 Hz, *o*-$C_6\underline{H}_4$Me), δ 3.04 (2 H, br. s, C$\underline{H}$Me$_2$), 2.11 (3 H, s, $C_6H_4\underline{Me}$), 1.78 (15 H, s, $C_5\underline{Me}_5$), 1.37 (3 H, s, $\underline{Me}CN_2$), 1.09 (6 H, d, ^3J = 6.7 Hz, CH$\underline{Me}_2$), 0.80 (6 H, d, ^3J = 6.7 Hz, CH$\underline{Me}_2$) ppm. ^{13}C{^{1}H} NMR (C_6D_6, 100.6 MHz, 298 K): δ 163.6 (Me$\underline{C}N_2$), 156.01 (*i*-$\underline{C}_6H_4$Me), 148.5 (br. d, ^1J = 236.4 Hz, *o*-$\underline{C}_6F_5$), 140.3 – 138.2 (overlapping br. d, *p*-$\underline{C}_6F_5$ and *m*-$\underline{C}_6F_5$), 132.5 (br, *i*-$\underline{C}_6F_4$), 133.3 (*p*-$\underline{C}_6H_4$Me), 128.2 (*m*-$\underline{C}_6H_4$Me), 122.2 (*o*-$\underline{C}_6H_4$Me), 126.6 ($\underline{C}_5Me_5$), 49.4 (N$\underline{C}$HMe$_2$), 26.8 (NCH$\underline{Me}$Me), 24.3 (NCHMe$\underline{Me}$), 19.6 ($C_6H_4\underline{Me}$), 14.6 ($\underline{Me}CN_2$), 12.4 ($C_5\underline{Me}_5$) ppm. ^{11}B NMR (C_6D_6, 128.4 MHz, 298 K): -7.68 (d, ^1J(B,H) = 59.8 Hz) ppm. ^{19}F{^{1}H} NMR (470.1 MHz, 298 K): -133.4 (*o*-$C_6\underline{F}_5$), -158.2 (*m*-$C_6\underline{F}_5$), -164.4 (*p*-$C_6\underline{F}_5$). IR (NaCl plates, Nujol mull, cm^{-1}): 1939 (s, ν(B–H)), 1530 (s), 1410 (m), 1094 (s), 1083 (s), 1015 (s), 971 (w), 833 (w), 813 (w), 662 (w). EI-MS: *m/z* = 775 $[M]^+$ (50%). Anal. found (calcd. for $C_{37}H_{40}BF_{10}N_3Ti$): C, 57.32 (57.93); H, 5.20 (5.53); N, 5.42 (5.37) %.

Cp*Ti{MeC(N^{i}Pr)$_2$}{NTol(H$_2$BTex)} (3) . To a stirred solution of Cp*Ti{MeC(N^{i}Pr)$_2$}(NTol) (**3.1**, 0.300 g, 0.669 mmol) in benzene (10 mL) was added H_2BTex (0.065 g, 0.669 mmol) at RT. The solution was left to stir at RT for 12 h, filtered and volatiles removed under reduced pressure to afford the adduct as a yellow oil. This was triturated with pentane to give a yellow/brown solid which was washed with cold pentane (3 x 10 mL) and dried *in vacuo*. Yield 0.263 g (75%). Diffraction-quality crystals were grown from pentane at RT.

^{1}H NMR (C_6D_6, 400.1 MHz, 298 K): δ 7.02 (4 H, overlapping *m*-$C_6\underline{H}_4$Me and *o*-$C_6\underline{H}_4$Me), 3.73 (1 H, broad , C$\underline{H}_a$Me$_2$), 3.51 (1 H, broad , C$\underline{H}_b$Me$_2$) 2.23 (3 H, s, $C_6H_4\underline{Me}$), 2.03 (1H, m, BCMe$_2$C$\underline{H}$Me$_2$), 1.85 (15 H, s, $C_5\underline{Me}_5$), 1.66 (3 H, s, $\underline{Me}CN_2$), 1.34 (3 H, d, ^3J = 6.5 Hz, NCH$_a\underline{Me}$Me), 1.30 (6H, d, BCMe$_2$CH$\underline{Me}_2$), 1.26 (3 H, d, ^3J = 6.5 Hz, NCH$_a$Me$\underline{Me}$), 1.21 (3 H, d, ^3J = 6.5 Hz, NCH$_b$Me$\underline{Me}$), 1.15 (3 H, d, ^3J = 6.5 Hz, NCH$_b$Me$\underline{Me}$), 1.01 - 0.96 (6H, overlapping, BC$\underline{Me}_2$CHMe$_2$). ^{13}C{^{1}H} NMR (C_6D_6, 100.6 MHz, 298 K): δ 164.7 (Me$\underline{C}N_2$), 154.6 (*i*-$\underline{C}_6H_4$Me), 132.4 (*p*-$\underline{C}_6H_4$Me), 130.4 (*m*-

$\underline{C}_6H_4Me$), 122.8 (*o*-$\underline{C}_6H_4Me$), 121.8 ($\underline{C}_5Me_5$), 50.7 ($N\underline{C}H_aMe_2$), 48.7 ($N\underline{C}H_bMe_2$), 37.1 ($BCMe_2\underline{C}HMe_2$), 26.0 ($BC\underline{Me}MeCH\underline{Me}_2$), 25.3 ($BCMe\underline{Me}CHMe_2$), 23.9 ($NCH_bMe\underline{Me}$), 23.0 ($NCH_b\underline{Me}Me$), 24.31 ($NCH_a\underline{Me}Me$), 19.5 ($NCH_aMe\underline{Me}$), 18.7 ($BCMe_2CH\underline{Me}_2$), 21.02 ($C_6H_4\underline{Me}$), 14.9 ($\underline{Me}CN_2$), 11.7 ($C_5\underline{Me}_5$) ppm. $^{11}B\{^1H\}$ NMR (C_6D_6, 128.4 MHz, 298 K): 1.46 (s) ppm. IR (NaCl plates, Nujol mull, cm^{-1}): 2327 (s, terminal ν(B–H)), 1908 (m, bridging ν(B–H)), 1599 (w), 1455 (s), 1378 (s), 1303 (s), 1130 (s), 1110 (s), 1079 (m), 1044 (m), 924 (w), 847 (w), 835 (w), 818 (w), 607 (w). EI-MS: *m/z* = 527 $[M\text{-}H]^+$ (20%), 324 $[M\text{-}\{N(Tol)BH_2Tex\}]^+$ (80%). Anal. found (calcd. for $C_{31}H_{54}BN_3Ti$): C 70.59 (67.72), N 7.97 (7.32), H 10.32 (10.50). The sample gave persistently high %C analysis, even of crystalline samples.

Cp*Ti{MeC(N^{i}Pr)$_2$}{N(Tol)HBC$_8$H$_{14}$} (4) . To a stirred solution of Cp*Ti{MeC(N^{i}Pr)$_2$}(NTol) (**3.1**, 0.300 g, 0.669 mmol) in benzene (10 mL) was added 9-BBN dimer (0.085 g, 0.669 mmol) at RT. The solution was left to stir at RT for 12 h, filtered and volatiles removed under reduced pressure to afford **4** as a sticky brown oil, which could not be crystallised and was washed with cold pentane (3 x 10 mL) and dried *in vacuo*. Yield: 0.184 g (50%).

^1H NMR (C_6D_6, 400.1 MHz, 298 K): δ 6.98 (2 H, d, ^3J = 8.5 Hz, *m*-$C_6\underline{H}_4Me$), 6.87 (2 H, d, ^3J = 8.5 Hz, *o*-$C_6\underline{H}_4Me$), δ 3.55 (2 H, br. s, $C\underline{H}Me_2$), 2.10 (3 H, s, $C_6H_4\underline{Me}$), 1.95 (15 H, s, $C_5\underline{Me}_5$), 1.66 (3 H, s, $\underline{Me}CN_2$), 2.30 - 1.0 (14 H, overlapping 3 x m, BC$\underline{H}$, BCC$\underline{H}$ and BCCC$\underline{H}$), 1.14 (6 H, d, ^3J = 6.7 Hz, $CH\underline{Me}_2$), 1.01 (6 H, d, ^3J = 6.7 Hz, $CH\underline{Me}_2$) ppm. $^{13}C\{^1H\}$ NMR (C_6D_6, 100.6 MHz, 298 K): δ 163.5 ($Me\underline{C}N_2$), 158.6 (*i*-$\underline{C}_6H_4Me$), 130.8 (*p*-$\underline{C}_6H_4Me$), 128.3 (overlapping *o*-$\underline{C}_6H_4Me$ and *m*-$\underline{C}_6H_4Me$), 125.4 ($\underline{C}_5Me_5$), 120.2 (4-$\underline{C}_6H_4Me$), 49.4 ($N\underline{C}HMe_2$), 33.7 (BC$\underline{C}$H), 25.9 (NCHMe$\underline{Me}$), 25.1 (NCH$\underline{Me}$Me), 24.4 (BCC$\underline{C}$H), 20.6 ($C_6H_4\underline{Me}$), 11.2 (B$\underline{C}$H), 13.6 ($\underline{Me}CN_2$), 12.5 ($C_5\underline{Me}_5$) ppm. $^{11}B\{^1H\}$ NMR (C_6D_6, 128.4 MHz, 298 K): 10.4 (s) ppm. IR (NaCl plates, Nujol mull, cm^{-1}): 1651 (s, ν(B–H)), 1517 (w), 1376 (w), 1260 (s), 1092 (s), 1093 (s), 1019 (s), 800 (s). EI-MS: *m/z* = 551 $[M]^+$ (2%). A satisfactory elemental analysis could not be obtained.

NMR tube scale synthesis of Cp*Ti{MeC(N^{i}Pr)$_2$}{N(Tol)BHCy$_2$} (5) . To a solution of Cp*Ti{MeC(N^{i}Pr)$_2$}(NTol) (**3.1**, 0.020 mg, 0.046 mmol) in C_6D_6 (0.3 mL) in an NMR tube equipped with a J. Young Teflon valve was added $HBCy_2$ (0.057 mg, 0.046 mmol) in C_6D_6 (0.3 mL). The reaction was monitored by ^1H and ^{11}B NMR spectroscopy. After 12 h at RT the ^1H NMR spectrum showed 82% conversion to **5**.

^{1}H NMR (C_6D_6, 400.1 MHz, 298 K): δ 6.94 (2H, d, , ^{3}J = 7.3 Hz, *m*-$C_6\underline{H}_4$Me), 6.81 (2H, d, ^{3}J = 7.3 Hz , *o*-$C_6\underline{H}_4$Me), 3.54 (2 H, br. s, C$\underline{H}Me_2$), 2.19 (3 H, s, $C_6H_4\underline{Me}$), 1.94 (15 H, s, $C_5\underline{Me}_5$), 1.80 – 1.30 (2 x 11, broad, BC$\underline{H}$, BCC$\underline{H}$, BCCC$\underline{H}$, BCCCC$\underline{H}$), 1.90 (3 H, s, $\underline{Me}CN_2$), 1.12 (6 H, d, ^{3}J = 6.5 Hz, NCH$\underline{Me}$Me), 1.00 (6 H, d, ^{3}J = 6.5 Hz, NCHMe$\underline{Me}$). ^{13}C{^{1}H} NMR (C_6D_6, 100.6 MHz, 298 K): δ 162.0 (Me$\underline{C}N_2$), 153.0 (*i*-$\underline{C}$6H4Me), 129.8 (*p*-$\underline{C}$6H4Me), 128.7 (*m*-$\underline{C}$6H4Me), 123.7 (*o*-$\underline{C}$6H4Me), 122.7 ($\underline{C}_5Me_5$), 48.99 (N$\underline{C}$HMe_2), 28.2 (2,6 – B$\underline{C}_6H_{11}$), 26.9 (3,5 – B$\underline{C}_6H_{11}$), 27.3 (NCHMe$\underline{Me}$), 26.5 (NCH$\underline{Me}$Me), 25.8 (4 – B$\underline{C}_6H_{11}$), 24.9 (1 – B$\underline{C}_6H_{11}$), 20.4 ($C_6H_4\underline{Me}$), 14.8 ($\underline{Me}CN_2$), 12.7 ($C_5\underline{Me}_5$) ppm. ^{11}B{^{1}H} NMR (C_6D_6, 128.4 MHz, 298 K): 7.99 (s) ppm.

Cp*Ti{MeC(N^{i}Pr)$_2$}{NN(BHTex)CHPh$_2$} (6). To a stirred solution of Cp*Ti{MeC(N^{i}Pr)$_2$}(NNCPh$_2$) (**1.40**, 0.300 g, 0.579 mmol) in benzene (10 mL) was added H_2BTex (0.057 g, 0.579 mmol) at RT. The solution was stirred for 12 h at RT, filtered and volatiles were removed under reduced pressure. The product was washed with cold pentane and dried *in vacuo* to afford a viscous yellow oil which could not be crystallised. Yield: 0.260 g (70%).

^{1}H NMR (C_6D_6, 400.0 MHz, 298 K): δ 7.47 (4 H, d, ^{3}J = 8.0 Hz, *o*-C_6H_5), 7.14 (4 H, m, *m*-C_6H_5), 7.09 (2 H, m, *p*-C_6H_5), 5.74 (1 H, s, C$\underline{H}Ph_2$), 3.52 (2 H, app. sept., ^{3}J = 7.0 Hz, NC$\underline{H}$MeMe), 2.05 (15 H, s, C_5Me_5), 1.75 (3 H, s, $\underline{Me}CN_2$), 1.03 (6 H, d, ^{3}J = 7.0 Hz, NCH$\underline{Me}_2$), 0.88 (7 H, overlapping BHC$\underline{Me}_2$CHMe$_2$ and BHCMe$_2$C$\underline{H}$Me$_2$), 0.79 (6 H, BHCMe$_2$CH$\underline{Me}_2$) 0.78 (6 H, d, ^{3}J = 7.0 Hz, NCH$\underline{Me}_2$). ^{13}C{^{1}H} NMR (C_6D_6, 100.0 MHz, 298 K): δ 161.2 (Me$\underline{C}N_2$), 142.4 (*i*-$\underline{C}_6H_5$), 129.4 (*o*-$\underline{C}_6H_5$), 127.4 (*p*-$\underline{C}_6H_5$), 126.4 (*m*-$\underline{C}_6H_5$), 119.3 ($\underline{C}_5Me_5$), 66.6 (C$\underline{H}Ph_2$), 49.1 (N$\underline{C}$HMe_2), 25.2 (NCH$\underline{Me}_2$), 26.0 (BHCMe$_2\underline{C}$HMe$_2$), 23.7 (BH$\underline{C}$Me$_2$CHMe$_2$), 23.4 (BCH$\underline{Me}_2$CHMe$_2$), 18.7 (BCHMe$_2$CH$\underline{Me}_2$), 18.6 (NCH$\underline{Me}_2$), 11.7 ($C_5\underline{Me}_5$), ^{11}B{^{1}H} NMR (C_6D_6, 128.4 MHz, 298 K): 46.4 (s) ppm. IR (NaCl cell, toluene, ν(B-H), cm^{-1}): 1601 (s). Anal. found (calcd. for $C_{37}H_{47}BN_4Ti$): C, 72.84 (72.08); H, 9.32 (9.38); N, 9.09 (9.60) %. The poor agreement between the found and the calcd. values may reflect retention of residual solvent in the viscous oil.

Cp*Ti{MeC(N^{i}Pr)$_2$}{NN(BCy$_2$)CHPh$_2$} (7) . To a stirred solution of Cp*Ti{MeC(N^{i}Pr)$_2$}(NNCPh$_2$) (**1.40**, 0.300 g, 0.579 mmol) in benzene (10 mL) was added HBCy$_2$ (0.103 g, 0.579 mmol) at RT. The solution was stirred for 12 h at RT, filtered and volatiles were removed under reduced pressure to afford a yellow oil which

could not be crystallised and was washed with cold pentane and dried *in vacuo*. Yield: 0.280 g (70%). ^{1}H NMR (C_6D_6, 400.0 MHz, 298 K): δ 7.54 (4 H, d, ^{3}J = 6.3 Hz, *o*-$C_6\underline{H}_5$), 7.19 (4 H, m, *m*-$C_6\underline{H}_5$), 7.09 (2 H, m, *p*-$C_6\underline{H}_5$), 5.98 (1 H, s, C$\underline{H}Ph_2$), 3.51 (2 H, broad app. sept., NC$\underline{H}$MeMe), 2.00 (15 H, s, $C_5\underline{Me}_5$), 1.72 (3 H, s, $MeCN_2$), 1.98 - 1.17 (20 H, m, overlapping CH_2 of the BCy_2), 1.59 (1H, s, 1-$BC_6\underline{H}_{11}$), 1.05 (6 H, d, NCH$\underline{Me}$Me), 0.90 (6 H, d, NCHMe$\underline{Me}$).^{13}C{^{1}H} NMR (C_6D_6, 100.0 MHz, 298 K): δ 164.2 ($Me\underline{C}N_2$), 142.4 (*i*-$\underline{C}_6H_5$), 129.4 (*o*-$\underline{C}_6H_5$), 127.4 (*p*-$\underline{C}_6H_5$), 126.4 (*m*-$\underline{C}_6H_5$), 126.1 ($\underline{C}_5Me_5$), 68.2 (C$\underline{H}Ph_2$), 48.2 (N$\underline{C}$HMeMe), 28.1 (NCH$\underline{Me}$Me), 25.0 (NCHMe$\underline{Me}$), 29.6 – 25.4 (overlapping BC_6H_{11}), 13.9 ($C_5\underline{Me}_5$), 12.3 (*i*-$B\underline{C}_6H_{11}$). ^{11}B{^{1}H} NMR (C_6D_6, 128.4 MHz, 298 K): δ 53.0 ppm. IR (NaCl plates, Nujol mull, cm^{-1}): 1653 (m), 1460 (s), 1280 (m), 1213 (w), 1198 (w), 1026 (m), 1019 (w), 800 (w), 721 (w), 696 (w), 647 (w). A satisfactory elemental analysis could not be obtained.

Cp*Ti{MeC(N^{i}Pr)$_2$}{NN(Bpin)CHPh$_2$} (8). To a stirred solution of Cp*Ti{MeC(N^{i}Pr)$_2$}(NNCPh$_2$) (**1.40**, 0.210 g, 0.549 mmol) in benzene (10 mL) was added HBpin (0.079 mL, 0.549 mmol) at RT. An immediate colour change from dark brown to dark green was observed after 30 min. The solution was filtered and volatiles removed under reduced pressure to give a brown solid which was washed with cold pentane (3 x 10 mL) a dried *in vacuo*. Yield: 0.177 g (50%). Diffraction-quality crystals were grown from a concentrated benzene solution at RT.

^{1}H NMR (C_6D_6, 400.0 MHz, 298 K): δ 7.49 (4 H, dd, ^{3}J = 7.4 Hz, *o*-$C_6\underline{H}_5$), 7.19 (4 H, m, *m*-$C_6\underline{H}_5$), 7.11 (2 H, t, *p*-$C_6\underline{H}_5$), 5.55 (1 H, s, C$\underline{H}Ph_2$), 3.62 (2 H, app. sept., ^{3}J = 6.1 Hz, NC$\underline{H}$MeMe), 2.13 (15 H, s, $C_5\underline{Me}_5$), 1.81 (3 H, s, $\underline{Me}CN_2$), 1.14 (6 H, d, ^{3}J = 6.5 Hz, BOC$\underline{Me}_2$), 1.07 (6 H, d, ^{3}J = 6.1 Hz, NCH$\underline{Me}_2$), 0.80 (6 H, d, ^{3}J = 6.1 Hz, NCH$\underline{Me}_2$). ^{13}C{^{1}H} NMR (C_6D_6, 100.0 MHz, 298 K): δ 161.4 ($Me\underline{C}N_2$), 143.7 (*i*-$\underline{C}_6H_5$), 130.0 (*o*-$\underline{C}_6H_5$), 127.9 (*p*-$\underline{C}_6H_5$), 127.7 (*m*-$\underline{C}_6H_5$), 119.4 ($\underline{C}_5Me_5$), 82.9 (BO$\underline{C}Me_2$), 66.1 (C$\underline{H}Ph_2$), 49.5 (N$\underline{C}$HMe$_2$), 26.7 (NCHMe$\underline{Me}$), 25.5 (NCH$\underline{Me}$Me), 24.9 (-BOC$\underline{Me}_2$), 12.5 ($C_5\underline{Me}_5$), 12.0 ($\underline{Me}CN_2$).^{11}B{^{1}H} NMR (C_6D_6, 128.4 MHz, 298 K): δ 44.9 ppm. IR (NaCl plates, Nujol mull, cm^{-1}): 1599 (m), 1462 (s), 1352 (m), 1309 (w), 1260 (m), 1145 (w), 1133 (m), 1083 (m), 1065 (m), 1018 (m), 971 (w), 799 (s), 740 (w) 700 (w), 649 (w). Anal. found (calcd. for $C_{37}H_{55}BN_4O_2Ti$): C, 68.70 (68.57); H, 8.57 (8.59); N, 8.67 (8.49) %.

Cp*Ti{MeC(N^{i}Pr)$_2$}{NN(BC$_8$H$_{14}$)CHPh$_2$} (9). To a stirred solution of Cp*Ti{MeC(N^{i}Pr)$_2$}(NNCPh$_2$) (**1.40**, 0.338 g, 0.652 mmol) in benzene (10 mL) was

added 9-BBN monomer (0.080 g, 0.652 mmol) at RT. The solution was stirred for 12h at RT, filtered and volatiles were removed under reduced pressure to afford a brown powder. The product was washed with cold pentane (3 x 10 mL) and dried *in vacuo*. Yield: 0.280g (67%). Diffraction-quality crystals were grown from a concentrated benzene solution at RT.

^{1}H NMR (C_6D_6, 400.0 MHz, 298 K): δ 7.42 (4 H, dd, ^{3}J = 8.1 MHz, *o*-$C_6\underline{H}_5$), 7.14 (4 H, m, *m*-$C_6\underline{H}_5$), 7.06 (2 H, m, *p*-$C_6\underline{H}_5$), 5.96 (1 H, s, C$\underline{H}$Ph$_2$), 3.52 (2 H, app. sept.,^{3}J = 6.3 Hz, NC$\underline{H}$MeMe), 2.30 - 1.0 (14 H, overlapping 3 x m, BC$\underline{H}$, BCC$\underline{H}$ and BCCC$\underline{H}$), 1.95 (15 H, s, $C_5\underline{Me}_5$), 1.73 (3 H, s, $\underline{Me}CN_2$), 0.96 (6 H, d, ^{3}J = 6.3 Hz, NCH$\underline{Me}_2$), 0.83 (6 H, d, ^{3}J = 6.3 Hz, NCH$\underline{Me}_2$). ^{13}C{^{1}H} NMR (C_6D_6, 100.0 MHz, 298 K): δ 161.4 (Me$\underline{C}N_2$), 142.4 (*i*-$\underline{C}_6H_5$), 129.4 (*o*-$\underline{C}_6H_5$), 127.4 (*p*-$\underline{C}_6H_5$), 126.4 (*m*-$\underline{C}_6H_5$), 119.7 ($\underline{C}_5Me_5$), 68.5 (C$\underline{H}$Ph$_2$), 48.8 (N$\underline{C}$HMe$_2$), 33.4 (B$\underline{C}$H) , 25.9 (NCH$\underline{Me}_2$), 25.3 (NCH$\underline{Me}_2$), 23.4, 22.7 (BCC$\underline{C}$H, BC$\underline{C}$H), 12.2 ($C_5\underline{Me}_5$), ^{11}B {^{1}H} NMR (C_6D_6, 128.4 MHz, 298K): 52.5 (s) ppm. IR (NaCl plates, Nujol mull, cm^{-1}): 1489 (w), 1418 (m), 1325 (w), 1308 (w), 1260 (s), 1214 (w), 1092 (s), 1020 (s) 800 (s), 695 (w), 668 (m). Anal. found (calcd. for $C_{39}H_{57}BN_4Ti$): C, 73.12 (72.88); H, 8.97 (9.15); N, 8.75 (8.62) %.

NMR tube scale synthesis of Cp*Ti{MeC(N^{i}Pr)$_2$}{N(HB(C$_6$F$_5$)$_2$)NCPh$_2$} (10a). In a glove box, to a solution of Cp*Ti{MeC(N^{i}Pr)$_2$}(NNCPh$_2$) (**1.40**, 20 mg, 0.036 mmol) in toluene-d_8 (0.3 mL) in an NMR tube equipped with a J. Young Teflon valve was added HB(C$_6$F$_5$)$_2$ (12.1 mg, 0.036 mmol) in toluene-d_8 (0.3 mL). The solution was immediately cooled to *ca*. 0 °C and transferred to the pre-cooled (internal temperature *ca*. 0 °C) probe of an NMR instrument. The NMR spectra showed quantitative conversion to **10a** which was characterised in situ.

^{1}H NMR (toluene-d_8, 400.0 MHz, 273 K): δ 7.54 (4 H, dd, ^{3}J = 6.6 Hz *o*-$C_6\underline{H}_5$), 6.94 (4 H, m, *m*-$C_6\underline{H}_5$), 6.71 (2 H, m, *p*-$C_6\underline{H}_5$), 3.05 (2 H, app. sept., ^{3}J = 6.3 Hz, NC$\underline{H}$MeMe), 1.89 (15 H, s, C_5Me_5), 1.70 (3 H, s, $MeCN_2$), 0.86 (6 H, d, ^{3}J = 6.3 Hz, NCH$\underline{Me}$Me), 0.75 (6 H, d, ^{3}J = 6.3 Hz, NCHMe$\underline{Me}$). ^{13}C{^{1}H} NMR (toluene-d_8, 100.0 MHz, 273 K): δ 164.5 (Me$\underline{C}N_2$), 137.1 (*i*-$\underline{C}_6H_5$), 128.7 (*o*-$\underline{C}_6H_5$), 126.6 (*p*-$\underline{C}_6H_5$), 124.6 (*m*-$\underline{C}_6H_5$), 123.1 ($\underline{C}_5Me_5$), 49.4 (N$\underline{C}$HMeMe), 25.9 - 25.4 (overlapping NCHMe$\underline{Me}$ and NCH$\underline{Me}$Me), 12.1 ($C_5\underline{Me}_5$), ^{11}B{^{1}H} (toluene-d_8, 128.4 MHz, 293 K) NMR -8.54 (s) ppm. IR (NaCl cell, toluene, ν(B-H), cm^{-1}): 2591 (s).

Cp*Ti{MeC(N^{i}Pr)$_2$}{NN(HB(C$_6$F$_5$)$_2$)CPh$_2$} (10b) . To a stirred solution of Cp*Ti{MeC(N^{i}Pr)$_2$}(NNCPh$_2$) (**1.40**, 0.338 g, 0.652 mmol) in benzene (10 mL) was added HB(C$_6$F$_5$)$_2$ (0.080 g, 0.652 mmol) at RT. The solution changed colour immediately from dark brown to red. After stirring for 12 h at RT, compound Cp*Ti{MeC(N^{i}Pr)$_2$}{NN(HB(C$_6$F$_5$)$_2$)CPh$_2$} (**10b**) was isolated, volatiles were removed under reduced pressure and the product was washed with cold pentane and dried *in vacuo*, to yield an orange oil. Yield: 0.346 g (62%).

Over several days at RT, solutions of Cp*Ti{MeC(N^{i}Pr)$_2$}{NBH(C$_6$F$_5$)$_2$NCPh$_2$} in toluene or benzene convert to Cp*Ti{MeC(N^{i}Pr)$_2$}{NNB(C$_6$F$_5$)$_2$CHPh$_2$} along with a number of unidentified side-products which could not be separated on the preparative scale. Compound Cp*Ti{MeC(N^{i}Pr)$_2$}{NNB(C$_6$F$_5$)$_2$CHPh$_2$} was therefore characterised by NMR spectroscopy in comparison with the fully-characterised analogues Cp*Ti{MeC(N^{i}Pr)$_2$}{NNB(HTex)CHPh$_2$}, Cp*Ti{MeC(N^{i}Pr)$_2$}{NN(BC$_8$H$_{14}$)CHPh$_2$} and Cp*Ti{MeC(N^{i}Pr)$_2$}{NN(Bpin)CHPh$_2$}.

^{1}H NMR (C$_6$D$_6$, 400.0 MHz, 298 K): δ 7.09 (4 H, dd, ^3J = 6.5 Hz, *o*-C$_6$H$_5$), 6.99 (4 H, m, *m*-C$_6$H$_5$), 6.89 (2 H, m, *p*-C$_6$H$_5$), 3.14 (2 H, app. sept., ^3J = 6.5 Hz, NCHMeMe), 1.71 (15 H, s, C$_5$Me$_5$), 1.57 (3 H, s, MeCN$_2$), 1.04 (6 H, d, ^3J = 6.5 Hz, NCHMeMe), 0.99 (6 H, d, ^3J = 6.5 Hz, NCHMeMe). ^{13}C{^{1}H} NMR (C$_6$D$_6$, 100.0 MHz, 298 K): δ 168.8 (MeCN$_2$), 145.7 (3,5-C$_6$F$_5$), 141.8 (4-C$_6$F$_5$), 137.6 (2,6-C$_6$F$_5$), 129.8 (*i*-C$_6$H$_5$), 129.5 (*o*-C$_6$H$_5$), 126.6 (*p*-C$_6$H$_5$), 124.6 (*m*-C$_6$H$_5$), 121.4 (C$_5$Me$_5$), 49.2 (NCHMeMe), 23.9 (NCHMeMe), 24.3 (NCHMeMe), 16.4 (MeCN), 11.2 (C$_5$Me$_5$). ^{11}B{^{1}H} NMR (C$_6$D$_6$, 128.4 MHz, 298 K): δ -9.72 ppm.^{19}F{^{1}H} NMR -130.7 (2 F, 2,6-C$_6$F$_5$), -162.0 (1 F, 4-C$_6$F$_5$), -166.1 (2 F, 3,5-C$_6$F$_5$). IR (NaCl cell, toluene, cm^{-1}): 1945 (s, ν(B-H)), 1795, 1803 (w), 1640 (s) 1509 (s), 1321 (m), 1086 (m), 892 (m), 766 (m), 697 (s), 621 (m). Anal. found (calcd. for C$_{43}$H$_{43}$BF$_{10}$N$_4$Ti): C, 59.74 (59.62); H, 5.01 (5.01); N, 6.48 (6.54) %.

The NMR assignments were confirmed using HOESY (^{1}H-^{19}F) spectroscopy.

NMR tube scale synthesis of Cp*Ti{MeC(N^{i}Pr)$_2$}{NN(B(C$_6$F$_5$)$_2$)CHPh$_2$} (10c) .

In a glove box, to a solution of Cp*Ti{MeC(N^{i}Pr)$_2$}(NNCPh$_2$) (**1.40**, 20 mg, 0.036 mmol) in toluene-*d*$_8$ (0.3 mL) in an NMR tube equipped with a J. Young Teflon valve was added HB(C$_6$F$_5$)$_2$ (12.1 mg, 0.036 mmol) in toluene-*d*$_8$ (0.3 mL). After several days at RT the NMR spectra showed conversion to **10c** which was characterised in situ and undefined decomposition products.

^{1}H NMR (C_6D_6, 400.0 MHz, 298 K): δ 7.31 (4 H, dd, ^3J = 6.7 Hz, *o*-$C_6\underline{H}_5$), 7.03 (4 H, m, *m*-$C_6\underline{H}_5$), 6.83 (2 H, m, *p*-$C_6\underline{H}_5$), 6.15 (1 H, s, $C\underline{H}Ph_2$), 3.24 (2 H, broad, $NC\underline{H}MeMe$), 1.85 (15 H, s, $C_5\underline{Me}_5$), 1.71 (3 H, s, $\underline{Me}CN_2$), 0.79 (6 H, d, $NCHMe\underline{Me}$), 0.66 (6 H, d, $NCH\underline{Me}Me$). ^{13}C{^{1}H} NMR (C_6D_6, 100.0 MHz, 298 K): δ 161.4 ($Me\underline{C}N_2$), 142.4 (*i*-$\underline{C}_6H_5$), 129.4 - 127.4 (overlapping *o*-$\underline{C}_6H_5$, *p*-$\underline{C}_6H_5$ and *m*-$\underline{C}_6H_5$), 121.4 ($\underline{C}_5Me_5$), 77.1 ($C\underline{H}Ph_2$), 48.5 ($N\underline{C}HMeMe$), 25.5 ($NCH\underline{Me}Me$), 24.5 ($NCHMe\underline{Me}$), 12.5 (MeCN), 11.8 ($C_5\underline{Me}_5$), ^{11}B{^{1}H} NMR (C_6D_6, 128.4 MHz, 298 K) 33.5 ppm.

Cp*Ti{MeC(N^{i}Pr)$_2$}{NHB(C$_6$F$_5$)$_2$)NMe$_2$} (11) . To a stirred solution of Cp*Ti{MeC(N^{i}Pr)$_2$}(NNMe$_2$) (**1.39**, 0.300 g, 0.750 mmol) in benzene (10 mL) was added $HB(C_6F_5)_2$ (0.260 g, 0.750 mmol) at RT. An immediate colour change from dark brown to dark red was observed. The solution was then filtered; volatiles were removed under reduced pressure to afford a red oil which could not be cristallized. This was washed with cold pentane (3 x 10 mL) and dried *in vacuo*. Yield: 0.367 g (80%).

^{1}H NMR (C_6D_6, 400.0 MHz, 298 K): δ 3.31 (1 H, app. sept., ^3J = 6.5 Hz, $NC\underline{H}Me_2$), 2.75 (6 H, s, $NN\underline{Me}_2$), 1.85 (15 H, s, $C_5\underline{Me}_5$), 1.63 (3 H, s, $\underline{Me}CN_2$), 0.89 (6 H, d, ^3J = 6.5 Hz, $NCH\underline{Me}Me$), 0.81 (6 H, d, ^3J = 6.5 Hz, $NCHMe\underline{Me}$). ^{13}C{^{1}H} NMR (C_6D_6, 100 MHz, 293 K): δ 161.9 ($Me\underline{C}N_2$), 149.1 (br d, ^1J = 236.4 Hz, *o*-$\underline{C}_6F_5$), 140.5 (overlapping br. d, *p*-$\underline{C}_6F_5$ and *m*-$\underline{C}_6F_5$), 132.5 (br, *i*-$\underline{C}_6F_5$), 120.2 ($\underline{C}_5Me_5$), 55.4 ($NN\underline{Me}_2$), 49.1 ($N\underline{C}HMe_2$), 26.3 ($NCH\underline{Me}Me$), 24.3 ($NCHMe\underline{Me}$), 13.9 ($C_5\underline{Me}_5$), 12.7 ($\underline{Me}CN_2$) ^{11}B{^{1}H} NMR (C_6D_6, 128.4 MHz, 293 K): -6.75 ppm. ^{19}F{^{1}H} NMR (470.1 MHz, 298 K): -128.4 (*o*-$C_6\underline{F}_5$), -158.7 (*m*-$C_6\underline{F}_5$), -164.2 (*p*-$C_6\underline{F}_5$). IR (NaCl plates, Nujol mull, cm^{-1}): 1990 (s, *v*(B-H)), 2185 (w), 1990 (s), 1857 (m), 1802 (m), 1648 (s) 1264 (w), 1120 (m). Anal. found (calcd. for $C_{32}H_{40}BF_{10}N_4Ti$): C, 52.39 (52.70); H, 5.30 (5.53); N, 7.49 (7.68) %.

Cp*Ti(H){MeC(N^{i}Pr)$_2$}{N(BPin)NMe$_2$} (12) . To a stirred solution of Cp*Ti{MeC(N^{i}Pr)$_2$}(NNMe$_2$) (**1.39**, 0.300 g, 0.785 mmol) in benzene (10 mL) was added HBpin (0.112 mL, 0.785 mmol) at RT. An immediate color change from dark brown to dark green was observed. After 4 h the solution was then filtered, the volatiles removed under reduced pressure and the resultant green powder washed with cold pentane (3 x 10 mL) and dried *in vacu*o. Yield: 0.200 g (50%). Diffraction-quality crystals were grown from a concentrated benzene solution at room RT.

^{1}H NMR (C_6D_6, 400.1 MHz, 298 K): δ 5.57 (1 H, s, Ti-H), 3.54 (1 H, app. sept., app. ^3J = 6.4 Hz, $C\underline{H}_aMeMe$), 3.16 (1 H, app. sept., app. ^3J = 6.4 Hz, $C\underline{H}_bMeMe$), 3.01 (3 H, s,

NNMeMe), 2.81 (3 H, s, NNMeMe), 2.27 (15 H, s, C_5Me_5), 1.67 (3 H, s, $MeCN_2$), 1.24 (3 H, d, ^3J = 6.5 Hz, NCH_aMeMe), 1.15 (3 H, d, ^3J = 6.5 Hz, NCH_aMeMe), 1.11 (6 H, s, $BOCMe_2$), 1.10 (3 H, d, ^3J = 6.5 Hz, NCH_bMeMe), 1.09 (6 H, s, $BOCMe_2$ of Bpin), 1.04 (3 H, d, ^3J = 6.5 Hz, NCH_bMeMe) ppm. $^{13}C\{^1H\}$ NMR (C_6D_6, 100.6 MHz, 298 K): δ 172.5 ($MeCN_2$), 120.1 (C_5Me_5), 81.5 ($BOCMe_2$), 59.9 (NNMeMe), 49.8 (NNMeMe), 48.8 (NCH_aMeMe), 47.8 (NCH_bMeMe), 27.4 (NCH_bMeMe), 26.8 (NCH_aMeMe), 25.7 (NCH_aMeMe), 24.9 ($BOCMe_2$) 24.7 (NCH_bMeMe), 13.9 (C_5Me_5), 12.7 ($MeCN_2$) ppm. $^{11}B\{^1H\}$ NMR (C_6D_6, 128.4 MHz, 298 K): δ 23.7 (s) ppm. IR (NaCl plates, Nujol mull, cm^{-1}): 1504 (s, ν(Ti-H)), 1336 (w), 1261 (m), 1201 (s) 1147 (s), 1107 (m), 1020 (m), 967 (m), 858 (m), 793 (s), 664 (m). EI-MS: *m/z* = 510 $[M]^+$ (2%). Anal. found (calcd. for $C_{26}H_{51}BN_4O_2Ti$): C, 61.18 (61.00); H, 10.07 (10.18); N, 10.98 (10.73)%.

Cp*Ti{PhC(N^{i}Pr)$_2$}(NNPh$_2$) (13) . To a solution of Cp*Ti{PhC(N^{i}Pr)$_2$}(N^{t}Bu) (0.500g, 1.36 mmol) in benzene (10 mL) was added a solution of Ph_2NNH_2 (0.285 g, 1.36 mmol) in benzene (10 mL) at RT. After 1 h the volatiles were removed under reduced pressure to afford Cp*Ti{PhC(N^{i}Pr)$_2$}(NNPh$_2$) (**13**) as a waxy oil which was triturated and washed with cold pentane (3 x 5 mL). The volatiles were removed under reduced pressure and the resultant brown solid dried *in vacuo*. Diffraction-quality crystals were grown from benzene at RT. Yield 0.580 g (75%).

^1H NMR (C_6D_6, 400.0 MHz, 298 K): δ 7.32 (4 H, m, *o*-NN(C_6H_5)$_2$), 7.27 - 7.07 (9 H, m, overlapping *m*-NN(C_6H_5)$_2$, *p*-NNCH(C_6H_5), *m*-NNCH(C_6H_5), *o*-NNCH(C_6H_5)), 6.86 (2 H, t, ^3J = 7.5 Hz, *p*-NN(C_6H_5)$_2$), 3.62 (2 H, sept., ^{3}J = 6.3 Hz, NCHMeMe), 2.08 (15 H, s, C_5Me_5), 1.05 (6 H, d, ^{3}J = 6.3 Hz, NCHMeMe), 0.92 (6 H, d, ^{3}J = 6.3 Hz, NCHMeMe) ppm. $^{13}C\{^1H\}$ NMR (C_6D_6, 100.0 MHz, 298 K): δ 161.7 ($MeCN_2$), 146.4 (*i*-NN(C_6H_5)$_2$), 134.4 (*i*-NNCH(C_6H_5)), 128.3 – 127.8 (*m*-NN(C_6H_5)$_2$, *p*-NNCH(C_6H_5), *m*-NNCH(C_6H_5), *o*-NNCH(C_6H_5)), 121.7 (*p*-NN(C_6H_5)$_2$), 120.0 (C_5Me_5), 119.4 (*o*-NN(C_6H_5)$_2$), 49.4 (NCHMeMe), 27.5 (NCHMeMe), 26.1 (NCHMeMe), 13.2 (C_5Me_5) ppm. IR (NaCl plates, Nujol mull, cm^{-1}): 1585 (s), 1337 (w), 1260 (m), 1092 (s) 1016 (m), 799 (m), 721 (m), 701 (m). EI-MS: *m/z* = 568 $[M]^+$ (90%). Anal. found (calcd. for $C_{35}H_{44}N_4Ti$): C, 73.50 (73.90); H, 7.90 (7.80); N, 10.85 (10.05)%.

Cp*Ti{MeC(NCy)$_2$}(NNPh$_2$) (14) . To a solution of Cp*Ti{MeC(NCy)$_2$}(N^{t}Bu) (0.400g, 0.853 mmol) in benzene (10 mL) was added a solution of Ph_2NNH_2 (0.157 g, 0.853 mmol) in benzene (10 mL) at RT. After 1 h the volatiles were removed under

reduced pressure to afford Cp*Ti{MeC(NCy)$_2$}(NNPh$_2$) (**14**) as a waxy oil which was triturated and washed with cold pentane (3 x 5 mL). The volatiles were removed under reduced pressure and the resultant green solid dried *in vacuo*. Diffraction-quality crystals were grown from pentane at RT. Yield 0.40 g (80%).

^{1}H NMR (C$_6$D$_6$, 400.0 MHz, 298 K): δ 7.76 (4 H, dd, overlapping o_a-C$_6$H$_5$ and o_b-C$_6$H$_5$), 7.13 (4 H, m, overlapping m_a- and m_b-C$_6$H$_5$), 6.84 (2 H, app. t, app. ^3J=7.5 Hz, overlapping p_a - and p_b - C$_6$H$_5$), 3.26 (2 H, broad sept., NC<u>H</u>Cy$_2$), 2.06 (15 H, s, C$_5$<u>Me</u>$_5$), 1.75 (<u>Me</u>CN), 1.89 – 1.15 (20 H, broad, overlapping Cy -CH$_2$ protons), 11.72 (1 H, broad, 1-C$_6$<u>H</u>$_{11}$ Cy ring). ^{13}C{^{1}H} NMR (C$_6$D$_6$, 100.0 MHz, 298 K): δ 160.7 (Me<u>C</u>N$_2$), 146.7 (*i*-C$_6$H$_5$), 128.3 (overlapping m_a- and m_b-<u>C</u>$_6$H$_5$), 121.2 (p_a-<u>C</u>$_6$H$_5$), 127.3 (p_b-<u>C</u>$_6$H$_5$), 119.6 (overlapping, o_a- and o_b- <u>C</u>$_6$H$_5$), 119.4 (<u>C</u>$_5$Me$_5$), 58.3 (N<u>C</u>HCy$_2$), 36.8 (-NCHC<u>C</u>H$_a$), 35.8 (-NCHC<u>C</u>H$_b$), 26.1 – 25.8 (overlapping -NCHCC<u>C</u>H and -NCHCCC<u>C</u>H), 12.7 (C$_5$<u>Me</u>$_5$) ppm, 12.2 (<u>Me</u>CN). IR (NaCl plates, Nujol mull, cm^{-1}): 1593 (s), 1583 (s), 1488 (s), 1356 (m), 1290 (m), 1276 (m), 1204 (m), 1178 (m), 1144 (w), 1078 (m), 1025 (w), 825 (w), 744 (w), 694 (w), 630 (w). EI-MS: *m/z* = 581 [Cp*Ti{MeC(NCy)$_2$}]$^+$ (80%). Anal. found (calcd. for C$_{36}$H$_{50}$N$_4$Ti): C, 72.19 (72.70); H, 8.64 (8.59); N, 9.68 (9.55)%.

Cp*Ti{PhC(N^{i}Pr)$_2$}(NBC$_8$H$_{14}$) (15). To a stirred solution of Cp*Ti{PhC(N^{i}Pr)$_2$}(NNPh$_2$) (0.338 g, 0.884 mmol) in benzene (10 mL) was added 9-BBN dimer (0.216 g, 0.884 mmol) all at RT. The solution was left to stir at 60 °C for 16 h, filtered and volatiles removed under reduced pressure to afford the products Cp*Ti{PhC(N^{i}Pr)$_2$}(NBC$_8$H$_{14}$) (**15**) and Ph$_2$NBC$_8$H$_{14}$ quantitatively in a 1:1 ratio as a sticky brown oil which could not be separated. The mixture was fully characterized on the NMR scale. ^{1}H NMR (C$_6$D$_6$, 400.1 MHz, 298K): δ 7.20 – 6.90 (overlapping *o*-, *m*-, *p*-BNPh$_2$ and *o*-, *m*-, *p*- NNCPh$_2$), 3.51 (2 H, app. sept., app. ^3J = 6.5 Hz, C<u>H</u>Me$_2$), 2.21 (15 H, s, C$_5$Me$_5$), 1.65 (3 H, s, MeCN$_2$), 2.30 - 1.0 (14 H, overlapping 3 x m, BCH, BCCH and BCCCH), 0.91 (6 H, d, ^3J = 6.5 Hz, CH<u>Me</u>$_2$), 0.81 (6 H, d, ^3J = 6.5 Hz, CH<u>Me</u>$_2$) ppm. ^{13}C{^{1}H} NMR (C$_6$D$_6$, 100.6 MHz, 298 K): δ 148.8 (overlapping *i*-NNCPh$_2$ and *i*-BNPh$_2$), 133.8, 129.0, 127.5, 125.2, 122.2 (*o*-, *m*-, *p*- BNPh$_2$ and *o*-, *m*-, *p*- NNCPh$_2$), (121.98 (<u>C</u>$_5$Me$_5$), 50.0 (<u>C</u>HMe$_2$), 34.4 (BC<u>C</u>H of Cp*Ti{PhC(N^{i}Pr)$_2$}(NBC$_8$H$_{14}$), 33.8 (BC<u>C</u>H of Ph$_2$NBC$_8$H$_{14}$), 26.1 (CH<u>Me</u>$_2$), 23.6 (CH<u>Me</u>$_2$), 24.7, 24.6, 24.4, 23.8 (BCC<u>C</u>H, B<u>C</u>H of the two products), 12.51 (C$_5$<u>Me</u>$_5$). ^{11}B NMR (C$_6$D$_6$, 128.4 MHz, 298K): 53.0 (broad) ppm

Cp*Ti{MeC(NCy)$_2$}(NBC$_8$H$_{14}$) (16). To a stirred solution of Cp*Ti{MeC(NCy)$_2$}(NNPh$_2$) (**14**, 0.300 g, 0.512 mmol) in benzene (10 mL) was added 9-BBN dimer (0.125 g, 0.512 mmol) all at RT. The solution was left to stir at 60 °C for 16 h, filtered and volatiles removed under reduced pressure to afford the products Cp*Ti{MeC(NCy)$_2$}(NBC$_8$H$_{14}$) (**16**) and Ph$_2$NBC$_8$H$_{14}$ quantitatively in a 1:1 ratio as a sticky brown oil which could not be separated. The mixture was fully characterized on the NMR scale. ^{1}H NMR (C$_6$D$_6$, 400.1 MHz, 298K): δ 7.20 – 6.90 (overlapping *o*-, *m*-, *p*-BNPh$_2$), 3.51 (2 H, broad, NC<u>H</u> of Cy ring), 2.19 (15 H, s, C$_5$Me$_5$), 1.78 (3 H, s, MeCN$_2$), 2.30 - 1.1 (34 H, overlapping 3 x m, BCH, BCCH and BCCCH of the two products) ppm. ^{13}C{^{1}H} NMR (C$_6$D$_6$, 100.6 MHz, 298 K): δ 167.7 (Me<u>C</u>N$_2$), 148.2 (*i*-BNPh$_2$), 129.0, 127.5, 125.2, 122.2 (*o*-, *m*-, *p*- BNPh$_2$), 121.95 (<u>C</u>$_5$Me$_5$), 50.0 (<u>C</u>HMe$_2$), 37.4 (BC<u>C</u>H of Cp*Ti{MeC(NCy)$_2$}(NBC$_8$H$_{14}$), 37.04 ((Cy)<u>C</u>H), 33.8 (BC<u>C</u>H of Ph$_2$NBC$_8$H$_{14}$), 26.9, 26.3, 26.2, 24.7, 24.6, 24.4, 23.8 (BCC<u>C</u>H, B<u>C</u>H of the two products, (Cy)CC<u>C</u>H and (Cy)CCC<u>C</u>H), 13.58 (C$_5$<u>Me</u>$_5$), 12.56 (<u>Me</u>CN). ^{11}B NMR (C$_6$D$_6$, 128.4 MHz, 298K): 53.0 (broad) ppm. An elemental analysis was not obtained..

NMR tube scale synthesis of Cp*Ti{MeC(N^{i}Pr)$_2$}(NNPh$_2$) (1.38) starting from Cp*Ti{MeC(N^{i}Pr)$_2$}{NBC$_8$H$_{14}$} (1) . To a solution of Cp*Ti{MeC(N^{i}Pr)$_2$}(NBC$_8$H$_{14}$) (**1**, 0.020 mg, 0.039 mmol, generated in situ) Ph$_2$NNH$_2$ (0.076 mg, 0.039 mmol) was added and the reaction monitored by ^{1}H and ^{11}B NMR spectroscopy. The ^{1}H NMR spectrum showed complete conversion to Cp*Ti{MeC(N^{i}Pr)$_2$(NNPh$_2$) (**1.38**) and H$_2$NBC$_8$H$_{14}$ after 10 mins. Compound **1.38** was identified by comparison to literature values[4] and H$_2$NBC$_8$H$_{14}$ was identified by comparison of its NMR data to that of an authentic sample.[12]

Kinetic measurements for the reaction of Cp*Ti{MeC(N^{i}Pr)$_2$}(NNMe$_2$) (1.39) with 9-BBN.

The general procedure is as follows, using the initial rates method. In a glove box, Cp*Ti{MeC(N^{i}Pr)$_2$}(NNMe$_2$) (**1.39**) was weighed into a vial and dissolved in C$_6$D$_6$ (0.3 mL). In a separate vial, 9-BNN dissolved in C$_6$D$_6$ (0.3 mL) and the solutions combined, agitated quickly and transferred to a J. Young valve NMR tube. A blank C$_6$D$_6$ sample was added to the NMR probe before being locked and shimmed. The experimental sample then replaced the blank sample (and allowed to thermally equilibrate where necessary), the shimming checked and an array set up recording a spectrum of 4 scans every 30 or

120 s. The conversion of the starting materials to product was calculated by measuring the integrals of $CH\underline{Me}_2$ groups of Cp*Ti{MeC(N^iPr)$_2$}($NNMe_2$) (**1.39**). Initial rates (t = 0) were obtained by analysis of plots of [Cp*Ti{MeC(N^iPr)$_2$}($NNMe_2$)]$_t$ *vs* time (t) using Origin.[22]

Low temperature NMR experiments. The general procedure is as follows. In a glove box, compound Cp*Ti{MeC(N^iPr)$_2$}(NTol) (**3.1**) or Cp*Ti{MeC(N^iPr)$_2$}($NNCPh_2$) **(1.38**) (0.0120 mmol) was weighed into a vial and dissolved in toluene-d_8 (0.3 mL) and cooled to -45 °C. In a separate vial, 9-BBN or any other borane reported in Chapter 3 was weighed and dissolved in toluene-d_8 (0.3 mL) and also cooled to -45 °C. The two vials were placed on a pre-cooled tile and the solutions combined using a pre-cooled pipette, agitated quickly and transferred to a pre-cooled J. Young NMR tube. The NMR tube was taken out of the glove box and placed in a dry ice/acetone cold bath. The NMR probe was cooled to -78 °C (other reaction temperatures were used as noted in Chapter 3) and a blank toluene-d_8 sample added before being locked and shimmed. The experimental sample then replaced the blank sample and allowed to thermally equilibrate, the shimming was then checked and an array set up recording a spectrum of 4 scans every 120 s. The ratios of the species were calculated by measuring the integrals of the $CH\underline{Me}_2$ groups of the starting material. Initial rate constants were obtained from plots of [**3.1** or **1.39**] *vs* time. Equilibrium constants were extracted from the measured integrals at the relevant temperatures.

6.5 References

1 A. B. Pangborn, M. A. Giardello, R. H. Grubbs, R. K. Rosen and F. J. Timmers, *Organometallics*, 1996, **15**, 1518–1520.

2 S. C. Dunn, P. Mountford and D. A. Robson, *J. Chem. Soc. Dalt. Trans.*, 1997, **2**, 293–304.

3 A. E. Guiducci, C. L. Boyd and P. Mountford, *Organometallics*, 2006, **25**, 1167–1187.

4 J. D. Selby, C. D. Manley, M. Feliz, A. D. Schwarz, E. Clot and P. Mountford, *Chem. Commun.*, 2007, **733**, 4937–4939.

5 L. R. Groom, University of Oxford, 2014.

6 M. P. Coles, D. C. Swenson, R. F. Jordan and V. G. Young, *Organometallics*, 1997, **16**, 5183–5194.

7 J. Sun, S. Chen, Y. Duan, Y. Li and X. Chen, *Organometallics*, 2009, **2**, 3088–3092.

8 Y. Yamaguchi and H. Nagashima, *Organometallics*, 2000, **19**, 725–727.

9 A. Zhdanko and M. E. Maier, *Eur. J. Org. Chem.*, 2014, 3411–3422.

10 J. R. Schwierl and H. C. Brown, *J. Org. Chem.*, 1993, **58**, 1546–1552.

11 A. M. Fuller, D. L. Hughes, S. J. Lancaster and C. M. White, *Organometallics*, 2010, **29**, 2194–2197.

12 R. Köster and G. Seidel, *J. Lieb. Ann. der Chemie*, 1977, **1977**, 1837–1846.

13 S. C. Chuang, P. Gandeepan and C. H. Cheng, *Org. Lett.*, 2013, **15**, 5750–5753.

14 C. J. Wallis, H. Dyer, L. Vendier, G. Alcaraz and S. Sabo-Etienne, *Angew. Chem. Int. Ed.*, 2012, **51**, 3646–3648.

15 K. S. and H. C. B. A. Pelter, *Borane Reagents*, 1988.

16 T. J. Hadlington, J. A. B. Abdalla, R. Tirfoin, S. Aldridge and C. Jones, *Chem. Commun.*, 2016, **52**, 1717–1720.

17 Z. Otwinowski and W. Minor, *Processing of X-ray Diffraction Data Collected in Oscillation Mode*, Academic press, New York, 1997.

18 A. Altomare, G. Cascarano, G. Giacovazzo, A. Guagliardi, M. C. Burla, G. Polidori and M. Camalli, *J. Appl. Cryst.*, 1994, **27**, 435.

19 L. Palatinus and G. Chapuis, *J. Appl. Cryst.*, 2007, **40**, 786–790.

20 P. W. Betteridge, J. R. Cooper, R. I. Cooper, K. Prout and D. J. Watkin, *J. Appl. Cryst.*, 2003, **36**, 1487.

21 A. G. M. Barrett, M. R. Crimmin, M. S. Hill, P. B. Hitchcock and P. A. Procopiou, *Organometallics*, 2007, **26**, 4076–4079.

22 Origin, Origin LAB, Northampton MA.

7.1 Density Functional Theory (DFT)

Density Functional Theory (DFT) has become very widely used to study the electronic structure and related properties of transition metal complexes. The development of DFT has led to a huge change in the field of transition metal chemistry.[1] Such development in the late 1980s and early 1990s of new, more accurate functionals and of efficient, user friendly computer codes led to DFT computations to become a widespread tool for analyzing structure, bonding, reactivity and properties. The reason of this remarkable development is that DFT is both relatively cheap and relatively accurate. This means that useful results can be obtained in a routine way for realistic models of the target molecule, or indeed for the molecule itself. The basic idea of DFT is that the energy of a system composed of fixed nuclei (Born Oppenheimer approximation) and electrons can be expressed as a functional $E[\rho]$ of the electron density function.[2] The electronic density function only depends on three variables. The foundations of DFT are the two Hohenberg-Kohn theorems,[3] which state that the external potential associated to the mutual position of the nuclei defines the density of the ground state of the system (in other words that the external potential is a unique functional of the density), and that the density can be derived from a variational procedure. However, the form of the exact functional is not clearly defined. The energy is usually written as a sum of three well defined terms and the exchange correlation term, in which the uncertainties concerning the form of the functional are collected (Equation 7.1).

$$E[\rho] = T_0[\rho] + J[\rho] + \int v(r)\rho(r)dr + E_{XC}[\rho] \qquad (7.1)$$

$T_0[\rho]$ is an approximation to the electronic kinetic energy. $J[\rho]$ is the Coulomb energy, and represents the repulsion between the electron density and itself. This term is non-zero even for one-electron systems because it includes electron self-interaction. The $\int v(r)\rho(r)dr$ term represents the electromagnetic interaction of the electron density with the external potential, in most cases this simply corresponds to the Coulombic interactions between electrons and nuclei. The $E_{XC}[\rho]$ term, the exchange correlation functional, corrects the first three terms. The energy expression given in Equation 7.1, leads to a set of equations defining the shape of the orbitals defined to expand the density, called the Kohn-Sham equations. In the Kohn-Sham approach, it is necessary to solve iteratively a set of self-consistent equations, called the Kohn-Sham equations (Equation 7.2):

$$h^{KS} = [-\frac{1}{2}\nabla^2 + V_{KS}(r)]\,\phi_i = \varepsilon_i\phi_i \qquad (7.2)$$

Where h^{KS} is the mono-electronic Kohn-Sham operator and $V_{KS}(r)$ is the external potential in which the particles move. The DFT theory is an exact theory, the only approximation stands from the choice of the approximated form for the exchange-correlation potentials. LDA, local density approximation, takes as reference the homogeneous electron gas, in which the exchange energy density is known in an analytic form and the correlation energy density is estimated in different ways. It was originally derived by Block and Dirac in the late 1920's. A simple approximation is the correlation functional due to Slater.[4]

A reasonable description of the molecular electronic structure and thermochemistry is not provided in the LDA method. The second one is the generalized-gradient approximation (GGA) which adds the gradient of the local spin densities. There are other classes of commonly used functionals. Meta-GGA is a semi-local functional that uses the Laplacian of the density or the kinetic energy density in addition to the density and the magnitude of the gradient of the density. Hybrid and meta-hybrid functionals are a class of approximations that incorporates a portion of exact exchange from Hartree Fock theory with exchange and correlation from other sources (ab initio or empirical). One of the most commonly used is B3LYP (B3PW91 is used in this Thesis). B3LYP was based on an earlier three-parameters functional in which the exchange correlation energy was expressed as a combination of the local exchange correlation energy, the HF exchange energy and the gradient corrections to the exchange and correlation energies as shown in Equation 7.3.

$$E_{XC} = E_{XC}^{LSDA} + a_0(E_X^{HF} - E_X^{LSDA}) + a_X\Delta E_X^{B88} + a_C\Delta E_C^{PW} \qquad (7.3)$$

semi-empirical coefficients a_0, a_X and a_C were fitted to reproduce as well as possible a set of ca. 100 atomization energies, ionization energies, proton affinities and atomic energies.[5] Climbing up the ladder of functionals, the approximations become more complicated, more sophisticated, and typically more accurate.

7.2 Basis sets

There are two types of basis functions commonly used in electronic structure calculations: Slater Type Orbitals (STO) and Gaussian Type Orbitals (GTO).[6] Slater type orbitals have the functional form shown in Equation 7.4.

$$\chi_{\zeta,n,l,m}(r,\theta,\varphi) = NY_{l,m}(\theta,\varphi)r^{n-1}e^{-\zeta r} \tag{7.4}$$

Here N is a normalization constant and $Y_{l,m}$ are spherical harmonic functions. The exponential dependence on the distance between the nucleus and electron mirrors the exact orbitals for the hydrogen atom. However, the STOs do not have any radial nodes; nodes in the radial part are introduced by making linear combinations of STOs. Gaussian type orbitals can be written in terms of polar or Cartesian coordinates as shown in Equation 7.5 (in terms of Cartesian coordinates):

$$\chi_{\zeta,lx,ly,lz}(x,y,z) = Nx^{lx}y^{ly}z^{lz}e^{-\zeta r^2} \tag{7.5}$$

The sum of l_x, l_y, l_z determines the type of orbital. The r^2 dependence in the exponential makes the GTOs inferior to the STOs in two respects. At the nucleus a GTO has a zero slope, in contrast to a STO which has a "cusp" (discontinuous derivative), and GTOs consequently have problems representing the proper behaviour near the nucleus. The other problem is that the GTO falls off too rapidly far from the nucleus compared with an STO, and the "tail" of the wave function is consequently represented poorly. Both STOs and GTOs can be chosen to form a complete basis, but the above considerations indicate that more GTOs are necessary for achieving a certain accuracy compared with STOs. Having decided on the type of function (STO/GTO) and the location (nuclei), the most important factor is the number of functions to be used. The smallest number of functions possible is a minimum basis set. Only enough functions are employed to contain all the electrons of the neutral atom, for example for hydrogen (and helium) this means a single s-function.

The next improvement of the basis set is doubling of all basis functions, producing a *Double Zeta* (DZ) basis set. In most of the cases higher angular momentum functions are important in describing the bond, and these are denoted as *polarization functions* (e.g. DZP, *Double Zeta plus Polarization*). Another common addition to basis sets is the addition of *diffuse functions*. These are Gaussian basis functions with a small exponent.

Diffuse basis functions are important for describing anions or dipole moments, but they can also be important for accurate modelling of intra- and intermolecular bonding.

One disadvantage of all energy-optimized basis set is the fact that they primarily depend on the wave function in the region of the inner-shell electrons. In practice, during most molecular bonding, it is the valence electrons which principally take part in the bonding. In recognition of this fact, it is common to represent valence orbitals by more than one basis function (each of which can in turn be composed of a fixed linear combination of primitive Gaussian functions). Since the different orbitals of the split have different spatial extents, the combination allows the electron density to adjust its spatial extent appropriate to the particular molecular environment. One example of this is the *split-valence* basis sets arising from the group of J. Pople and denoted as *X-YZG*.[7] In this case, *X* represents the number of primitive Gaussians comprising each core atomic orbital basis function. The *Y* and *Z* indicate that the valence orbitals are composed of two basis functions each, the first one composed of a linear combination of *Y* primitive Gaussian functions, the other composed of a linear combination of *Z* primitive Gaussian functions.

Combining the full set of basis functions, known as the primitive GTOs (PGTOs), into a smaller set of functions by forming fixed linear combinations is known as basis set *contraction*, and the resulting functions are called contracted GTOs (CGTOs). The degree of contraction is the number of PGTOs entering the CGTO, typically varying between one and ten.

7.3 Dispersion interactions

Dispersion interactions play an important role in organometallic chemistry. Dispersion interactions are generally described as the interactions between instantaneous dipole moments within the electron distributions of two atoms or molecules. The dispersion energy, E_{disp} between two atoms or molecules at large separation takes the form of a series expansion (Equation 7.6):

$$E_{\text{disp}} = -\frac{C_6}{R_6} - \frac{C_8}{R_8} - \frac{C_{10}}{R_{10}} .. \qquad (7.6)$$

In the wavefunction approach of quantum chemistry, dispersion is a dynamical correlation effect. The Hartree-Fock method, which is the simplest wavefunction approach, does not include dynamical correlation. Therefore, the HF method cannot model dispersion interactions and produces entirely repulsive potential energy surface (PESs) for dispersion-bound complexes. All standard DFT methods predict repulsive

interactions between nominally dispersion bound complexes at large separation, rather than the $-C_6/R_6$ behaviour that is characteristic of dispersion attraction. from a DFT perspective, dispersive interactions are a long-range correlation phenomenon that is very difficult to account for accurately. A simple and intuitive approach for correcting conventional DFT methods for dispersion is to add explicit, attractive $-C_6/R_6$ terms between all atomic pairs. The use of $-C_6/R_6$ terms to correct DFT is termed DFT-D. Within the general set of DFT-D methods, several approaches have been used to obtain the empirical dispersion coefficients, including use of the Slater-Kirkwood[8] model and London-type approximations.[9]

DFT-D methods, particularly the approaches of Grimme[9,10] has been successfully used in many applications. The general form for the dispersion energy, simply added to the Kohn Sham energy is the following:

$$E_{disp}^{DFT-D} = -\sum_{AB}\cdot\sum_{n=6,8,..} S_n \frac{C_n^{AB}}{R_{AB}^n} f_{damp}\, R(AB) \qquad (7.7)$$

where, the sum is over all atom pairs (A,B) in the system, C_n^{AB} denotes the averaged (isotropic) n^{th}-order dispersion coefficient for atom pair AB, and R_{AB} is the internuclear distance. S_n are scaling factors used to adjust the correction to the repulsive behaviour of the chosen parametrized functional. In order to avoid near singularities for small R, and double counting effect of correlations at intermediate distances, damping functions f_{damp} are used, which determinate the range of the dispersion correction. Over the years, several versions have been developed, in particular the one used in this thesis is DFT-d3(bj), where are geometry-dependent as they are adjusted on the basis of local geometry (coordination number) around atoms A and B. bj stands for Becke-Jonson, which determines the form of the damping function to be used.[10]

7.4 Solvation models

An important aspect of computational chemistry is to evaluate the effect of the environment, such as a solvent. Methods for evaluating the solvent effect may broadly be divided into two types: those describing the individual solvent molecules and those that treat the solvent as a continuous medium. Combinations are also possible, for example by explicitly considering the first solvation shell and treating the rest by a continuum model. The effects of solvation can be partitioned into two main groups: non-specific (long-range) solvation (e.g. polarization, dipole orientation) and specific (short-range) solvation such as hydrogen bonds, charge transfer effects etc. Continuum models[11] consider the

solvent as a uniform polarizable medium with a dielectric constant of ε, and with the solute is placed in a suitably shaped hole in the medium. Creation of a hole in the medium costs energy, while dispersion interactions between the solvent and the solute add stabilization. The electric charge distribution of the solute molecule will polarize the medium, which in turn acts back on the molecule, producing an electrostatic polarization. The solvation free energy might be written as in Equation 7.8:

$$\Delta G_{\text{solvation}} = \Delta G_{\text{cavity}} + \Delta G_{\text{dispersion}} + \Delta G_{\text{elect}} \qquad (7.8)$$

Reaction field models differ in different aspects: How the size and shape of the hole are defined, how the cavity/dispersion contribution is calculated, how the charge distribution of the solute is represented and how the solute and the dielectric medium are described.

A classical description of the solute molecule can be a force field with (partial) atomic charges, while a quantum description involves calculation of the electronic wave function. When a quantum description of the solute molecule is employed, the calculated electric moments induce charges in the dielectric medium, which in turn acts back on the molecule, causing the wave function to respond and thereby changing the electric moments, etc. The interaction with the solvent model must thus be calculated by an iterative procedure, leading to various *Self-Consistent Reaction Field* (SCRF) models. In connection with the electronic structure methods (i.e. quantum description of the solute molecule) the term SCRF is generic and it does not by itself relate to a specific model. For example, the *Polarizable Continuum* Model (PCM) employs a van der Waals cavity formed by interlocking atomic van der Waals radii scaled by an empirical factor, a detailed description of the electrostatic potential, and parameterizes the cavity/dispersion contributions based on the surface area.[12] The *COnductor-like Screening Model* (COSMO) also employs molecular shaped cavities, and represents the electrostatic potential by partial atomic charges.[13] The SMD solvation model, was developed by Truhlar and co-workers in 2009, where the "D" stands for "density" to denote that the full solute electron density is used without defining partial atomic charges. SMD[14] is a universal solvation model, where "universal" denotes its applicability to any charged or uncharged solute in any solvent or liquid medium for which a few key descriptors are known. The model has been parametrized for more than 100 solvents. The model separates the observable solvation free energy into two main components. The first component is the bulk electrostatic contribution arising from a self-consistent reaction field treatment. The second component is called the cavity-dispersion-solvent-structure

term and is the contribution arising from short-range interactions between the solute and solvent molecules in the first solvation shell.

7.5 Natural bond orbitals (NBO) analysis

NBO are an useful tool to create effective atomic orbitals for each atom in the molecule environment and examine the bonding from a "Lewis-like" perspective. The delocalization of NBOs creates Natural Localized Molecular Orbitals (NLMOs), which are defined as the least delocalized orbitals in the molecule, unitary equivalent to Canonical Molecular Orbitals. As originally introduced by Lowdin, natural orbitals $\{\theta_k\}$ are the eigenfunctions of the one electron density operator, $D^{(1)}$, derived by averaging the N electron space-spin coordinates (Equation 7.9):

$$D^{(1)} = N \int |\psi(1,2 \ldots, N)^2 \, dr_1 dr_2 \ldots dr_N \tag{7.9}$$

The key distinguishing feature of NBOs is their formulation in terms of natural atomic orbitals (NAOs), a complete orthonormal set for optimally describing the effective atom-like constituents within the molecule environment.[15] These NAOs $\{\chi^{(A)}\}$ of atom A are obtained by diagonalizing the matrix representing $D^{(1)}$ on the AO centered on A. Lewis-type NBOs of highest occupancy can be directly associated with the localized electron pairs of the chemists Lewis-structure diagram. Each Lewis type NBO can be decomposed into constituent natural hybrid orbitals (NHOs) h_A and h_B on atoms A and B as reported in Equation 7.10:

$$\theta_{AB} = c_A h_A + c_B h_B \tag{7.10}$$

with polarization coefficients c_A and c_B satisfying $|c_A|^2 + |c_B|^2 = 1$. The hybrid orbitals h_A and h_B are constructed from NAOs on atoms A and B in a manner that closely resembles the classical Pauling hybridization picture, but all details of NHO hybridization and polarization are numerically optimized to give the best possible description of electron density. The two valence hybrids h_A and h_B give rise to two valence-shell NBOs: an in-phase Lewis-type NBO (Equation 7.10) and a corresponding out-of-phase non-Lewis NBO. The localized wavefunction $\psi^{(L)}$ formed from N/2 doubly occupied Lewis-type NBOs, corresponds to an idealized natural Lewis-structure picture. The delocalization of Lewin NBOs into non-Lewis NBOs creates symmetric and antisymmetric combinations with small mixing coefficients. This mixing produces exactly doubly occupied Natural Localized Molecular Orbitals (NLMOs) that are unitarily equivalent to Canonical Molecular Orbitals (CMOs). NLMOs are equally valid to CMOs as descriptors of the

density and, thus, all computed observable properties. NLMOs are the least delocalized orbitals that are unitarily equivalent to CMOs.

7.6 Quantum Theory of Atoms in Molecules (QTAIM)

The Quantum Theory of Atoms in Molecules (QTAIM) is a model of molecular and condensed matter electronic systems in which the principal objects of molecular structure - atoms and bonds - are natural expressions of a system's observable electron density distribution function. An electron density distribution of a molecule is a probability distribution that describes the average manner in which the electronic charge is distributed throughout real space in the attractive field exerted by the nuclei. Bader and co-workers, showed that the topology of the electron density, $\rho(\mathrm{r})$, yields a mapping of the concepts of the molecular structure hypothesis, the concepts of atoms, bonds and structure.[16] The QTAIM approach presents two advantages; a more quantitative consistency, because $\rho(\mathbf{r})$ can be derived by accurate methods,[17] and a robust physical basis. Thorough QTAM analysis of many main group light atom molecules has led to the identification of a set of 'correspondence rules' between common chemical concepts and topological properties of the electron density. However, such an analogy cannot be easily extended to organometallic compounds, which have an inherently different 'physics' due to the presence of donor/acceptor bonds and to the character of the orbitals involved. Each topological feature of $\rho(\mathbf{r})$, whether it be a maximum, a minimum, or a saddle, has associated with it a critical point (abbreviated to CP), a point denoted by the coordinate rc where $\nabla \rho(\mathbf{r}_c) = 0$. The rank and the sign of the Hessian matrix will define the type of CP. For bonds between a given pair of atoms the value of the electron density at the bond CP, may be used to define a bond order. The topology of the Laplacian of the electron density, the quantity $\nabla^2\rho(\mathbf{r})$, does provide a physical basis for the Lewis model. The Laplacian of a scalar field such as $\rho(\mathbf{r})$ determines where the field is locally concentrated and depleted; if it is < 0, the value of $\rho(\mathbf{r})$ is greater than the average of its values in the immediate neighbourhood of the point **r** and $\rho(\mathbf{r})$ is locally concentrated at **r**, while if the Laplacian is > 0, the reverse is true and $\rho(\mathbf{r})$ is locally depleted at **r**. The delocalization index $\delta(\mathrm{A,B})$ is a measure of the number of electrons that are shared or exchanged between A and B independent of the nature of the interaction, but it determines the corresponding number of contributing bonded pairs only when the pairs are equally shared. The delocalization index is not identified with a bond order because, while determining the number of electrons that are shared between two atoms, it does not, with

the exception of equally shared pairs, determine the number of contributing Lewis electron pairs.

7.7 Frequency calculations in Gaussian

The determination of stationary points in Gaussian is done via a frequency calculation. This calculation computes force constants and the resulting vibrational frequencies. Intensities are also computed. By default, the force constants are determined analytically if possible, by single numerical differentiation for methods for which only first derivatives are available, and by double numerical differentiation for those methods for which only energies are available. Vibrational frequencies are computed by determining the second derivatives of the energy with respect to the Cartesian nuclear coordinates and then transforming to mass-weighted coordinates. Vibrational frequencies depend on the force constant and the reduced mass. Frequency calculations are useful to determine the nature of a stationary point on the potential energy surface. The number of imaginary frequencies indicates the sort of stationary point to which the given molecular structure corresponds. Vibrational frequencies calculated for equilibrium structures are positive real numbers, because the force constants are positive (second derivative is positive at a minimum of a function.) However, for saddle point (transition states) one force constant is negative, yielding an imaginary frequency. Imaginary frequencies (usually reported as negative values) are tell-tale signs of saddle points. By definition, a structure which has n-imaginary frequencies is an nth order saddle point. Thus, the minimum will have zero imaginary frequencies, and an ordinary transition structure will have one imaginary frequency since it is a first order saddle point. It is important to notice that in any transition state, the imaginary vibrational frequency must be associated with the motion over the saddle point. In other words, the final optimized transition state should exhibit one negative (imaginary) frequency that corresponds to the desired bond cleavage for example. In addition, transition state geometries may be connected to ground state geometries with an intrinsic reaction coordinate (IRC) calculation. In the process, one follows the path downhill from the transition state in either the *forward* or *reverse* direction, in order to find the reactant and the product.

7.8 Pseudopotential and relativistic effects

As discussed in Section 7.2, for many qualitative considerations the chemistry of an element is only determined by its valence electrons, which actively participate in chemical bonding. In this picture the core electrons remain essentially inert and at most play an indirect role, for example, by providing together with the nucleus somewhat modified effective potentials for the valence electrons of the elements within a group of the periodic table. The method of effective core potentials (ECPs) makes use of these ideas in first-principles electronic structure theory calculations. The main goals are a considerable reduction of the computational eff ort by avoiding the costly explicit treatment of the atomic cores in the calculations and at the same time an implicit treatment of the major relativistic effects for the valence electron system. The elimination of the atomic cores from the calculations allows to treat all elements of a group of the periodic table on equal footing. Since the same number of valence electrons has to be dealt with, one can expect that the same computational effort is required for all elements of a column of the periodic table and one may also hope that a similar accuracy is achieved.

Relativistic effects in chemistry can be considered to be perturbations, or small corrections, to the non-relativistic theory of chemistry, which is developed from the solutions of the Schrödinger equation. These corrections affect the electrons differently depending on the electron speed relative to the speed of light, *c*. The central theme of relativity is that the speed of light, *c*, is constant in all inertia frames. Augmented with the requirement that physical laws should be identical in such frames, this has a consequence that time and space coordinates become equivalent. One of the most important and familiar results of relativity is that the relativistic mass of the electron (which moves at a substantial fraction of *c*) increases over the rest mass m_0 (Equation 7.11):

$$m = m_0 \left(\sqrt{1 - \frac{v^2}{c^2}} \right).^{-1} \qquad (7.11)$$

The speed of light in atomic units is 137.036, and it is clear that relativistic effects cannot be neglected for the core electrons in heavy nuclei. For atoms with large Z, the 1s-electrons are relativistic and thus heavier, which has the effect that the 1s orbitals shrinks in size. In order to maintain orthogonality, the higher s-orbitals also contract. This

provides a more effective screening of the nuclear charge for the higher angular momentum orbitals, which consequently increase in size. For p-orbitals the spin–orbit interaction, which mixes s- and p-orbitals, counteracts the inflation. The net effect is that p-orbitals are relatively unaffected in size, while d- and f-orbitals become larger and more diffuse. In terms of total energy, the relativistic correction becomes comparable to the correlation energy already for Z~10, while it becomes comparable to the exchange energy for Z~50. Since the majority of the relativistic effects are concentrated in the core orbitals, there is a large error cancellation for molecular properties. Relativistic effects for geometries and energetics are normally negligible for the first three rows in the periodic table, the fourth row represents an intermediate case, while relativistic corrections are necessary for the fifth and sixth rows, and for lanthanide/actinide metals. Relativistic contributions, which become non-negligible quantitatively and sometimes even qualitatively for heavy elements and thus cannot be neglected for accurate investigations, require an additional computational effort. In this thesis, the titanium atom was represented by a relativistic effective core potential (RECP), although the relativistic effects on Ti could not be considered. The reason behind is to have comparable results across the Group 4 transition metals (Zr and Hf) where analogues calculations were performed by other students in our research group.

7.9 General Computational methodology

DFT calculations described in this Thesis were performed in collaboration with Prof. Philip Mountford at the University of Oxford and Dr Eric Clot at Université Montpellier. Geometry optimisations were performed with the Gaussian09 package[18] at the B3PW91 level of hybrid density functional theory,[5,19,20] with or without the inclusion of Grimme's d3(bj) correction[10,21] in the optimisation process. For systems with realistic steric bulk, single-point calculations took into account both solvent and dispersion effects. The solvent (benzene) influence was taken into consideration through single point calculations on the gas-phase optimized geometry with SCRF calculations within the SMD model.[14] Influence of the dispersion forces was also considered by computing the d3(bj) corrections. SCF energies reported in this work are for gas-phase model systems. For larger systems the Gibbs free energies and enthalpies were obtained by summing the SMD energy, the gas-phase Gibbs or enthalpy contribution at 298.15 K (or another temperature where specified) obtained from the geometry optimisations, and the d3(bj) correction. The NBO analyses were carried out using NBO 6.0,[22,15] on wavefunctions

computed with B3PW91 in the gas phase. Atoms-in-molecules analyses were performed using the AIMALL programme,[23] using Gaussian09 wavefunction (.wfx) files as input. The nature of the basis set used will be described in each Section. ^{11}B NMR calculations reported in Chapter 3 were performed with the Gauge-Independent Atomic Orbital (GIAO) method and a pcS-2 basis set, using BF_3OEt_2 as reference for ^{11}B NMR shifts. Structures used for NMR calculations should have been optimized at a good level of theory. In general, there are two factors that make the calculation of magnetic properties somewhat more complicated than the corresponding electric properties. First, the angular momentum operator is imaginary, implying that the wave function must be allowed to be complex. Second, the presence of the gauge origin in the operators means that the results may be origin dependent. An exact wave function will of course give origin independent results. In practice, as described in Section 7.2, a finite basis must be employed, and standard basis sets will yield results that depend on where the user has chosen the origin of the gauge. The gauge error depends on the distance between the wave function and the gauge origin, and some methods try to minimize the error by selecting separate gauges for each (localized) molecular orbital. However, a more recent and robust method, namely GIAO, eliminates the gauge dependence of properties, by making the basis functions explicitly dependent on the magnetic field by inclusion of a complex phase factor referring to the position of the basis function and was chosen as the methodology for NMR calculations in this Thesis.

7.10 Chapter 2

7.10.1 Reactions of Ti($N_2^{iPr}N^{Me}$)($NNPh_2$)(py) (1.70) with $PhSiH_3$

An initial screening of a variety of DFT functionals has been performed to establish the best one to be used in the reactions of Ti($N_2^{iPr}N^{Me}$)($NNPh_2$)(py) (**1.70**) with silanes and boranes. M06,[24] M06L,[24] PBE0,[25] TPSS,[26] TPSSh,[26] B3PW91[5] have been tested. Geometry optimizations have been performed with inclusion of Grimme's d3(bj) correction in the optimization process, for all the aforementioned functionals except M06 and M06L which already include dispersions, for the reaction of both isomers of Ti($N_2^{iPr}N^{Me}$)($NNPh_2$)(py) (**1.70**) with $PhSiH_3$. The titanium atom was represented by the relativistic effective core potential (RECP) from the Stuttgart group and the associated basis set,[27] augmented by an f polarization function. The remaining atoms were represented by a svp basis set.[28] The solvent (benzene) influence was taken into consideration through single point calculations on the gas-phase optimized geometry with

SCRF calculations within the SMD model. For the SCRF calculations the atoms were treated with a def2-tzvp basis set, and the respective functional. Influence of the dispersion forces was also considered by computing the d3(bj) correction as described by Grimme. B3PW91 was the functional of choice, due to the best agreement with the reported experimental results, in particular the experimental mixture of isomers observed and the values of the TS barriers were investigated. All the calculations performed in this Thesis have been subsequently performed at the B3PW91 level of hybrid density functional level. The same set of calculations have been also performed using the same methodology described above for the optimization process, but with SCRF calculations were all the atoms were treated with a def2-qzvpp basis set.

7.10.2 Reactions of Ti($N_2^{iPr}N^{Me}$)($NNPh_2$)(py) (1.70) with boranes and H_2

The same methodology for the optimization process described for the reaction of Ti($N_2^{iPr}N^{Me}$)($NNPh_2$)(py) (**1.70**) with $PhSiH_3$ has been used, while in the SCRF calculations the atoms were treated with a def2-qzvpp basis set for $HBMes_2$, HBBN and H_2.

Table 7.1. Total SCF Energies. Thermal corrections to Enthalpies, Thermal corrections to Gibbs Free Energies (in Hartree) and relative Gibbs Free Energies (in kcal mol^{-1}) for the reactions of $Ti(N_2^{iPr}N^{Me})(NNPh_2)(py)$ (**1.70**) with $PhSiH_3$ using a def2tzvp basis set for the SCRF calculations. All the reported values are computed at 298.15 K.

Entry	Total SCF Energy	Thermal correction to H	Thermal correction to G	G_{rel}
Pyridine	-248.301520728278	0.94245	0.061624	
$PhSiH_3$	-522.945644921435	0.122506	0.085094	
Trans-1.70	-2269.25964	0.681331	0.57595	**0.0**
Cis-1.70	-2269.257498	0.680201	0.577326	**2.2**
Int-1.70	-2020.905475	0.58368	0.491934	**19.7**
TS1	-2543.881863	0.708850	0.60303	**16.0**
Int2	-2543.88263	0.709790	0.599471	**13.3**
TS2	-2543.878013	0.707291	0.601058	**17.2**
Int3	-2543.908954	0.708943	0.60452	**-0.1**
Trans-1.71	-2544.002905	0.713316	0.604993	**-58.7**
Int1'	-2020.907678	0.582288	0.495342	**19.0**
Int2'	-2543.883288	0.711026	0.598867	**12.5**
TS1'	-2543.883029	0.709975	0.601337	**14.2**
Int3'	-2543.905066	0.710474	0.604812	**2.6**
TS2'	-2544.000929	0.707103	0.599869	**25.2**
Cis-1.71	-2543.864094	0.713113	0.603197	**-58.6**

Trans-TSA	-2543.95676	0.709180	0.599554	**-33.2**
Trans-1.71_IntA	-2543.96825	0.713793	0.6077	**-35.3**
IntA	-2025.23044	0.501576	0.414887	**-31.8**
Cis-1.71_IntA	-2543.97198	0.714318	0.604721	**-39.5**
Cis-TSA	-2543.94311	0.708502	0.59676	**-26.4**
Trans-TS_B	-2543.94334	0.708773	0.599137	**-25.0**
Trans-1.71_IntB	-2543.98835	0.715568	0.607599	**-47.9**
Trans-1.71_Int2	-3066.94764	0.841756	0.717256	**-41.1**
Cis-TSB	-2543.95275	0.708746	0.601605	**-29.4**
Cis1.71_IntB	-2543.98573	0.714908	0.605737	**-47.5**
Cis1.71_Int2	-3066.94933	0.842641	0.723094	**-47.8**

Table 7.2. Total SCF Energies, Thermal corrections to Enthalpies, Thermal corrections to Gibbs Free Energies (in Hartree) and relative Gibbs Free Energies (in kcal mol^{-1}) for the reactions of $Ti(N_2{}^{iPr}N^{Me})(NNPh_2)(py)$ (**1.70**) with $PhSiH_3$, 9-BBN, $HBMes_2$ and H_2 using a def2qzvpp basis set for the SCRF calculations. All the reported values are computed at 298.15 K.

Entry	Total SCF Energy	Thermal correction to H	Thermal correction to G	G_{rel}
Pyridine	-248.316503718	0.94245	0.061624	
DMAP	-382.3175167	0.171571	0.127784	
$PhSiH_3$	-522.970872491	0.122506	0.085094	
Trans-1.70	-2269.37160289	0.680201	0.681331	**0.0**

Trans-1.70_DMAP	-2403.377338	0.757792	0.643356	**0.0**
Cis-1.70	-2269.36978197	0.681331	0.57595	**2.0**
Cis-1.70_DMAP	-2403.375748	0.757694	0.645113	**2.1**
Int1	-2021.0083056	0.582288	0.491934	**17.5**
TS1	-2544.00439298	0.70885	0.60303	**15.8**
Int2	-2544.00466408	0.70979	0.599471	**13.4**
TS2	-2544.0005013	0.707291	0.601058	**17.0**
Int3	-2544.03187829	0.708943	0.60452	**-0.5**
Trans-1.71	-2544.12603059	0.713316	0.604993	**-59.3**
Int1'	-2021.00687589	0.58368	0.495342	**16.2**
Int2'	-2544.00637572	0.711026	0.598867	**11.9**
TS1'	-2544.00594905	0.709975	0.601337	**13.8**
Int3'	-2544.0262569	0.710474	0.604812	**4.3**
TS2'	-2543.98767623	0.707103	0.599869	**24.3**
Cis-1.71	-2544.1239532	0.713113	0.603197	**-59.1**
9-BBN$_{monomer}$	-338.797816206	0.187079	0.228888	
9-BBN$_{dimer}$	-677.656055735	0.402674	0.463271	
Int2_B	-2359.87595748	0.817438	0.711653	**2.0**
TS1_B	-2359.86245604	0.815479	0.708352	**8.4**
Int3_B	-2359.88683909	0.814596	0.706729	**-7.9**
TS2_B	-2359.85363088	0.810158	0.704749	**11.7**
Trans-1.73	-2359.9724184	0.81816	0.70704	**-61.4**

$HBMes_{2monomer}$	-724.7726529	0.382673	0.307924	
$HBMes_{2dimer}$	-1449.59460613	0.770798	0.650952	
Int2_B'	-2745.839265	0.973743	0.605737	**6.0**
TS1_B'	-2745.826722	0.97003	0.723094	**9.8**
Int3_B'	-2745.845776	0.972034	0.829508	**-1.2**
TS2_B'	-2745.811601	0.966084	0.829508	**14.7**
Trans-2.3	-2745.940406	0.972932	0.834248	**-63.2**
H_2	-1.17910790232	0.013447	-0.001553	
Int2_H	-2022.19636786	0.507887	0.600412	**20.7**
TS0_H	-2022.18102975	0.507168	0.598233	**29.9**
Int3_H	-2022.21333581	0.513499	0.603896	**13.6**
TS1_H	-2022.17690752	0.509059	0.600615	**33.6**
Trans-H	-2022.30484555	0.512792	0.606757	**-44.3**

7.11 Chapter 3

Geometry optimisations using the B3PW91 functional with the titanium atom represented by the relativistic effective core potential (RECP) from the Stuttgart group and the associated basis set,[27] augmented by an f polarization function and the remaining atoms represented by a def2-svp basis set.[29] The SCRF single point calculations were performed with a def2-qzvpp basis set for all atoms. Dispersion interactions were taken into account with the d3(bj) corrections in both the optimizations and the single point calculations. Calculations on sterically-pruned model systems were performed with the same methodology for the geometry optimizations without dispersion interactions in the optimization process. The SCRF single point calculations were performed with a def2-tzvp basis set[29] for all atoms with and without dispersion interactions.

Table 7.3. Total SCF Energies. Thermal corrections to Enthalpies, Thermal corrections to Gibbs Free Energies (in Hartree) and relative Gibbs Free Energies (in kcal mol^{-1}) for the reactions of the model system $CpTi\{MeC(NMe)_2\}(NNMe_2)$ (**1.39Q**) with $HBMe_2$ and $HB(OMe)_2$ shown in Figures 3.21 and 3.22 using a def2tzvp basis set for the SCRF calculations. All the reported values are computed at 298.15 K.

Entry	Total SCF Energy	Thermal correction to H	Thermal correction to G	G_{rel}
1.39Q	-1499.777038	0.324228	0.057758	**0.0**
$HBMe_2$	-105.2856087	0.091157	0.251288	
$HBOMe_2$	-255.8187567	0.106912	0.068987	
H_2	-1.178260307	0.013447	-0.001535	
Me_2NBMe_2	-239.3316388	0.171777	0.128853	
$Me_2NB(OMe)_2$	-389.8424497	0.185787	0.277566	
1.39Q_Int1	-1605.126407	0.419025	0.340776	**-20.1**
1.39Q_TS1	-1605.119629	0.417312	0.339708	**-16.5**
1.39Q_Int2	-1605.131074	0.418771	0.341588	**-22.5**
1.39Q_TS2	-1605.118324	0.41688	0.33964	**-15.7**
1Q_Int1	-1605.127366	0.418135	0.337915	**-22.5**
1.39Q_TS3	-1605.071566	0.413576	0.332773	**9.3**
1Q_Int2	-1605.191195	0.4201	0.336833	**-63.2**
1.39Q_Int4	-1710.426366	0.513385	0.425702	**-12.1**
1.39Q_TS4	-1710.395667	0.510701	0.422244	**5.0**
1.39Q_Int5	-1471.17409	0.341238	0.271762	**-77.6**

1.39Q_TS5	-1471.163938	0.338956	0.268533	**-73.3**
1.39Q_Int6	-1471.17409	0.340565	0.271547	**-77.7**
1.39Q_TS6	-1471.136438	0.341238	0.26054	**-61.0**
1Q	-1469.963693	0.320529	0.245252	**-75.0**
1.39Q_Int1'	-1755.623721	0.432531	0.348286	**0.1**
1.39Q_TS1'	-1755.620088	0.43131	0.347752	**2.0**
1.39Q_Int2'	-1755.632068	0.43277	0.350838	**-3.6**
1.39Q_TS2'	-1755.628955	0.431955	0.348977	**-2.8**
12Q	-1755.646606	0.432875	0.346764	**-15.3**
1.39Q_TS3'	-1755.588581	0.42821	0.341011	**17.5**
12Q_Int2	-1755.71029	0.434633	0.347635	**-54.7**

Table 7.4. Total SCF Energies. Thermal corrections to Enthalpies, Thermal corrections to Gibbs Free Energies (in Hartree) for the reactions of all of the full systems described in Chapter 3. All the reported values are computed at 298.15 K.

Entry	Total SCF Energy	Thermal correction to H	Thermal correction to G
$H_2BTex_{monomer}$	-262.5575712	0.20833	0.165037
H_2BTex_{dimer}	-525.1731636	0.422833	0.356024
$9\text{-}BBN_{monomer}$	-338.797816206	0.187079	0.228888
$9\text{-}BBN_{dimer}$	-677.656055735	0.402674	0.463271
HBPin	-411.939879	0.201840	0.158349

1	-2057.46875	0.72313	0.61977
1_Int1	-2192.631401	0.82356	0.71217
1_Int2	-2192.696349	0.82580	0.716072
1.39	-1853.771923	0.59053	0.496176
1.39_TS1	-2192.595696	0.82131	0.714229
1.39_Int1	-2192.624441	0.82397	0.715145
1.39_TS2	-2192.577376	0.81868	0.705786
1.39_Int1'	-2265.745248	0.796284	0.683235
1.39_Int2'	-2265.748931	0.796208	0.685464
1.39_TS1'	-2265.734677	0.793778	0.685624
1.39_TS2'	-2265.747391	0.793921	0.684348
1.39_TS3'	-2265.698527	0.791025	0.67405
1.40	-2275.437723	0.708620	0.594508
$HB(C_6F_5)_{2monomer}$	-1481.244532	0.13438	0.065055
$HB(C_6F_5)_{2dimer}$	-2962.537712	0.27346	0.156059
2	-3471.549426	0.76332	0.618621
3	-2252.860739	0.837888	0.718755
3.1	-1990.227752	0.625883	0.520117
4	-2329.08786	0.856275	0.738412
8	-2687.432597	0.912656	0.782521
9	-2614.309298	0.9413	0.808427
10a	-3756.743285	0.846373	0.692497
10b	-3756.744644	0.845828	0.693563
10c	-3756.760854	0.849093	0.694823

10a_9-BBN	-2614.273055	0.937962	0.812423
10b_9-BBN	-2614.289026	0.936785	0.816516
10a_HBPin	-2687.380135	0.909372	0.781091
10b_HBPin	-2687.401496	0.910963	-0.288814459
11	-3335.09082691	0.724955	0.587915
11_Nbeta	-3335.07349669	0.726612	0.588499
12_Nbeta	-2265.742779	0.794682	0.682207
12	-2265.768968	0.796162	0.685134
12_Int2	-2265.823958	0.796662	0.685061
TS5_memberred	-2531.40214	1.05289	0.932728

7.12 Chapter 4

Geometry optimisations were performed at the B3PW91 level of hybrid density functional theory. For geometry optimisations in the gas phase all atoms were represented by the def2-svp basis set.[28] For sterically-pruned model systems additional single-point calculations were carried out on the optimised geometry using the def2-tzvp basis set. For systems with realistic steric bulk, single-point calculations took into account both solvent and dispersion effects. The solvent (benzene) influence was taken into consideration through single point calculations on the gas-phase optimized geometry with SCRF calculations within the SMD model. For the SCRF calculations all the atoms were treated with a def2-tzvp basis set. Influence of the dispersion forces was also considered by computing the d3(bj) corrections. SCF energies reported in this work are for gas-phase model systems using the def2-tzvp basis set.[29] For larger systems the Gibbs free energies and enthalpies were obtained by summing the SMD energy, the gas-phase Gibbs or enthalpy contribution at 298 K (or another temperature where specified) obtained from the geometry optimisations, and the d3(bj) correction.[21]

Table 7.5. Total SCF Energies, Thermal corrections to Enthalpies, Thermal corrections to Gibbs Free Energies (in Hartree) for the reactions of all of the real systems described in Chapter 4 using a def2tzvp basis set for the SCRF calculations. All the reported values are computed at 298.15 K.

Entry	Total SCF Energy	Thermal correction to H	Thermal correction to G
$H_2NBC_8H_{14}$	-394.2066081	0.248739	0.204994
H_2NBMes_2	-780.1514491	0.40147	0.13970
H_2NNPh_2	-574.0214717	0.228272	0.177835
H_2NPh	-287.6348552	0.088255	0.124156
H_2N^tBu	-213.8378619	0.155932	0.119321
1	-2057.365111	0.719612	0.617172
1.90_O	-1752.18966255	0.89596	0.76463
1.90_S	-2075.09429489	0.89498	0.76230
1.37	-1877.005408	0.628021	0.531006
1.90_Odimer_trans	-3506.64295	0.89596	0.76463
1.90_Odimer_cis	-3506.62963	0.89498	0.77033
1.90_Sdimer_trans	-4152.53728	0.89363	0.76230
1.90_Sdimer_cis	-4152.53608	0.89400	0.76371
1.91	-2866.22307612	1.104227	0.957294

$H_2NB(NAr'CH)_2$	-1203.04531	0.63002	0.531325
$TiCl_2(HNMe_2)_2(NNPh_2)$	-2613.257709	0.414687	0.332878
$TiCl_2(HNMe_2)_2(NPh)$	-2326.857321	0.311764	0.238015
$TiCl_2(HNMe_2)_2(N^tBu)$	-2253.057441	0.343207	0.268778
$TiCl_2(NMe_2)_2$	-2039.184393	0.181653	0.123889
4.1	-3242.276235	0.817849	0.694858
4.1_BBN	-2433.41232	0.435933	0.353934
4.1_$BMes_2$	-2819.371089	0.586545	0.481500

Table 7.6. Total SCF Energies, Thermal corrections to Enthalpies, Thermal corrections to Gibbs Free Energies (in Hartree) for the reactions of all the optimised model systems and fragments described in Chapter 4 using a def2tzvp basis set. All the reported values are computed at 298.15 K.

Entry	Total SCF Energy	Thermal correction to H	Thermal correction to G
1.90Q_ $B(NMeCH)_2$	-1582.96964408	0.319863	0.248527
1.90Q_BMe_2	-1396.02041308	0.267677	0.204081
1.90Q_Me	-1331.19077980	0.223502	0.165754
1.90Q_O	-1556.55110	0.298730	0.239904
1.90Q_Odimer_cis	-3113.16272	0.601040	0.501414

1.90Q_Odimer_trans	-3113.16497	0.600084	0.502847
1.90Q_R_py	-1831.26523091	0.416910	0.335618
1.90Q_S	-1879.49101	0.298820	0.235389
1.90Q_Sdimer_cis	-3759.03174	0.599435	0.496636
1.90Q_Sdimer_trans	-3759.03170	0.599573	0.498599
1Q_B(NMeCH)$_2$	-1656.831293	0.371366	0.289413
1Q_BMe$_2$	-1469.874383	0.318918	0.243719
1Q_frag (T)	-1310.327865	0.229060	0.168436
1Q_Me	-1405.053365	0.275160	0.208337
1Q_O	-1385.658257	0.234619	0.173792
1Q_Ph	-1596.795361	0.331957	0.2573
1Q_S	-1708.597313	0.233675	0.171251
CO (S)	-113.3103121	0.008366	-0.014055
CO$_2$	-188.592047	0.015351	-0.008888
CS (S)	-436.1836316	0.006324	-0.017559
CS$_2$	-834.4451233	0.011063	-0.015871
H (D)	-270.2051357	0.002360	0.073088
H$_2$NB(NMeCH)$_2$	-347.6430762	0.162543	0.116655
H$_2$NBMe$_2$	-160.703523	0.111755	0.116655
H$_2$NMe	-95.86382766	0.068306	0.041002
H$_2$NPh	-287.6029569	0.123704	0.087782
H$_2$O	-76.43342302	0.025222	0.003787

$NB(NMeCH)_2$ (T)	-346.3128062	0.137820	0.094463
$NBMe_2$ (T)	-159.3356356	0.085000	0.048057
NMe (T)	-94.55073698	0.040720	0.013614
NPh (T)	-286.2951353	0.097404	0.061315
O (T)	-75.06543857	0.002360	-0.014952
$OCNB(NMeCH)_2$	-459.783067	0.151884	0.102976
OCNMe	-207.9931304	0.056351	0.023423
OCNPh	-399.7235435	0.110027	0.073172
PhC (S)	-270.2051357	0.108866	0.073088
PhC(NMe)H	-364.9956021	0.158617	0.116819
PhC(NPh)H	-556.728318	0.214556	0.164334
PhCHO	-345.5652542	0.116969	0.079104
S (T)	-398.0783587	0.002360	-0.015933
$SCNB(NMeCH)_2$	-782.7163368	0.149855	0.100531
SCNMe	-530.9264055	0.054125	0.018705
SCNPh	-722.651521221	0.108911	0.068830

Table 7.7. Total SCF Energies (in Hartree) for the unrelaxed fragments reported in Table 4.1 using a def2tzvp basis set. All the reported values are computed at 298.15 K.

Entry	Total SCF Energy
NMe (T)	-94.54881425
NPh (T)	-286.2915664
$NBMe_2$ (T)	-159.3262014
$NB(NMeCH)_2$ (T)	-346.3108515
1Q_frag (T)	-1310.315295

Table 7.8. Total SCF Energies (in Hartree) for the model complexes **1Q_R_fixed** reported in Table 4.5 using a def2tzvp basis set. All the reported values are computed at 298.15 K.

Entry	Total SCF Energy
1Q_BMe_2_fixed	-1469.8742489
1Q_$B(NMeCH)_2$_fixed	-1656.8313785
1Q_BMe_2NH_3_fixed	-1526.4413594
1Q_Me_fixed	-1405.0534912
1Q_4-$C_6H_4CF_3$_fixed	-1933.8667296
1Q_Ph_fixed	-1596.7953187
1Q_4-$C_6H_4NH_2$_fixed	-1652.1538687
1Q_NMe_2_fixed	-1499.6862986
1Q_NMe_2_planar_fixed	-1499.6806806

7.13 Chapter 5

The computational methodology is the same described in Section 7.4.

Table 7.9. Total SCF Energies, Thermal corrections to Enthalpies, Thermal corrections to Gibbs Free Energies (in Hartree, at 298.15 K and 343.0 K) and relative Gibbs Free Energies (in kcal mol^{-1}, at 298.15 K and 343.0 K) for the reactions of depicted in Scheme 5.7 (Chapter 5).

Entry	Total SCF Energy	Thermal correction to H (298.15 K)	Thermal correction to G (298.15 K)	Thermal correction to G (343.0 K)	G_{rel} (298.15 K)	G_{rel} (343.0 K)
Pyridine	-248.301097308	0.094253	0.06163	0.046795		
DMAP	-382.292523584	0.171569	0.127802	0.102741		
CH_4	-40.5222847824	0.048402	0.027246	0.019228		
MeCCPh	-347.745648262	0.147357	0.101065	0.078242		
TolCCH	-347.73760934	0.145445	0.145445	0.105223		
7Q_A	-2673.73273726	0.967389	0.829648	0.702186	**0.0**	**0.0**
7Q_B	-3056.04245314	1.141483	0.987436	0.838264	**8.0**	**10.1**
7Q_C	-2633.18652873	0.917995	0.786405	0.665365	**5.0**	**4.0**
7Q_D	-2633.20749401	0.917084	0.789837	0.669539	**-6.0**	**-6.6**
7Q_E	-2881.53165793	1.013727	0.872789	0.739733	**-7.1**	**-6.4**
7Q_F	-2881.53133867	1.013788	0.873401	0.740417	**-6.5**	**-5.7**
7Q_G	-2881.53650908	1.013851	0.873584	0.74061	**-9.7**	**-8.8**
7Q_H	-2981.00035874	1.068095	0.912819	0.771501	**-29.6**	**-29.7**
7Q_I	-2981.01436835	1.068733	0.916308	0.775396	**-36.2**	**-36.0**
7Q_J	-2981.00833654	1.069013	0.920205	0.779809	**-22.3**	**-21.1**

7Q_K	-2980.99478298	1.067517	0.921829	0.782089	**-12.8**	**-11.2**
7TS_A_C	-2673.6894446	0.962368	0.828825	0.702594	**26.7**	**27.4**
7TS_C_D	-2633.16304831	0.912652	0.783092	0.662947	**17.6**	**17.2**
7TS_C_H	-2980.94349265	1.06162	0.912259	0.772622	**5.8**	**6.7**
7TS_C_I	-2980.94982361	1.065359	0.918872	0.779233	**9.9**	**11.1**
7TS_C_J	-2980.95378455	1.066823	0.91695	0.776619	**13.6**	**15.3**
7TS_B_E	-3056.00220476	1.137057	0.982512	0.833768	**30.2**	**32.6**
7TS_E_F	-2881.49913101	1.008888	0.865346	0.732395	**8.6**	**9.5**
8Q_A	-2151.52081695	0.75744	0.645385	0.545122	**0.0**	**0.0**
8Q_B	-2533.83320547	0.93178	0.797588	0.674673	**2.8**	**4.4**
8Q_C	-2110.97577569	0.707094	0.600397	0.506528	**3.1**	**2.1**
8Q_D	-2110.9952706	0.706438	0.601945	0.508473	**8.1**	**8.9**
8Q_E	-2359.31739392	0.804501	0.687516	0.581291	**6.3**	**5.7**
8Q_F	-2359.317618	0.804517	0.687263	0.580986	**6.6**	**6.1**
8Q_G	-2359.32170636	0.804605	0.687561	0.581306	**9.0**	**8.4**
8Q_H	-2458.78647021	0.85614	0.73128	0.618155	**-26.6**	**-26.1**
8Q_I	-2458.79458936	0.858515	0.732184	0.618565	**-31.1**	**-30.9**
8Q_J	-2458.77415487	0.858027	0.732237	0.618746	**-17.1**	**-15.8**
8Q_K	-2458.78824171	0.858355	0.73609	0.623098	**-10.6**	**-9.6**
8TS_A_C	-2151.47877722	0.752759	0.641902	0.54235	**24.2**	**24.6**
8TS_C_D	-2110.94636498	0.702064	0.59819	0.50531	**20.2**	**19.8**
8TS_C_H	-2458.73125951	0.852072	0.794855	0.672693	**3.9**	**4.4**
8TS_B_E	-2533.79840363	0.927384	0.724622	0.611499	**23.0**	**25.0**
8TS_E_F	-2359.28341296	0.798567	0.680391	0.574627	**10.6**	**11.4**

Table 7.10. Total SCF Energies, Thermal corrections to Enthalpies, Thermal corrections to Gibbs Free Energies (in Hartree, at 298.15 K and 343.0 K) and relative Gibbs Free Energies (in kcal mol^{-1}, at 298.15 K and 343.0 K) for the reactions of depicted in Scheme 5.8 (Chapter 5). The values for the organic substrates (Pyridine, CH_4, DMAP, TolCCH, MeCCH) are the same reported in Table xx.

Entry	Total SCF Energy	Thermal correction to H (298.15 K)	Thermal correction to G (298.15 K)	Thermal correction to G (343.0 K)	G_{rel} (298.15 K)	G_{rel} (343.0 K)
9Q_A (and 10Q_A)	-2985.83243705	1.20506	1.05105005	1.026576	**0.0**	**0.0**
9Q_C (and 10Q_C)	-2945.32239	1.155298	1.003988	0.979980	**2.5**	**0.7**
9Q_D (and 10Q_D)	-2945.35454	1.153972	1.006668	0.983261	**-10.6**	**-11.9**
9Q_E	-3193.41284	1.253220	1.090675	1.064853	**-8.5**	**-8.2**
9Q_F	-3193.41370	1.251837	1.089827	1.064092	**-9.3**	**-9.0**
9Q_G	-3193.41869	1.252221	1.092197	1.066762	**-10.8**	**-10.3**
9Q_H	-3292.77555	1.305274	1.133340	1.106039	**-30.8**	**-30.7**
9Q_I	-3292.78765	1.306370	1.134125	1.106779	**-34.6**	**-34.5**
9Q_J	-3292.78877	1.307959	1.141535	1.115071	**-23.3**	**-22.2**
9Q_K	-3292.77437	1.307465	1.141657		**-11.9**	**-10.7**
10Q_B	-3367.73003	1.3801377	1.2066697		**10.0**	**12.3**
10Q_E	-3327.26698	1.330638	1.157780	1.130325	**-12.2**	**-11.8**
10Q_F	-3327.26558	1.330349	1.155882	1.128183	**-7.7**	**-6.8**

10Q_G	-3327.26967	1.330220	1.155235	1.127457	**-13.8**	**-13.4**
11Q_A	-2307.05669	0.876286	0.754987	0.735789	**0.0**	**0.0**
11Q_B	-2688.95769	1.050846	0.906387	0.883509	**4.6**	**6.6**
11Q_C	-2266.55195	0.825707	0.706281		**-0.1**	**-2.0**
11Q_D	-2266.56995	0.825598	0.709271	0.843835	**-6.6**	**-8.1**
11Q_E	-2648.48999	1.000802	0.863725	0.842018	**--11.3**	**-10.7**
11Q_F	-2648.48878	1.000073	0.865696	0.844404	**-7.7**	**-6.8**
11Q_G	-2648.49061	1.000385	0.865243		**--8.9**	**-8.1**
11Q_H	-2613.99170	0.975714	0.837241	0.815338	**-26.5**	**-26.4**
11Q_J	-2614.00423	0.976584	0.844017	0.823018	**-20.1**	**-19.0**

Table 7.11. Total SCF Energies, Thermal corrections to Enthalpies, Thermal corrections to Gibbs Free Energies (in Hartree, at 298.15 K and 343.0 K) and relative Gibbs Free Energies (in kcal mol^{-1}, at 298.15 K) for the reactions of depicted in Scheme 5.9 (Chapter 5).

Entry	Total SCF Energy	Thermal correction to H	Thermal correction to G	G_{rel}
Pyridine	-248.27671	0.09398	0.061356	
CH_4	-40.52077	0.04845	0.027320	
DMAP	-382.24923	0.17017	0.128660	
MeCCMe	-155.97715	0.09066	0.057226	
MeCCH	-116.65272	0.06045	0.031390	
12Q_A	-1818.20228	0.50095	0.409570	**-6.8**

12Q_B	-2085.05244	0.61738	0.513474	**6.5**
12Q_C	-1777.65382	0.45173	0.365366	**0.0**
12Q_D (X = H)	-2025.95623	0.54830	0.447662	**-3.0**
12Q_D (X = NMe_2)	-2159.93305	0.62566	0.514916	**-5.7**
12Q_E (X = H)	-2025.97788	0.54801	0.449961	**-15.1**
12Q_E (X = NMe_2)	-2159.95049	0.62514	0.516490	**-15.7**
12Q_F	-1933.68718	0.54550	0.449212	**-18.6**
12Q_G	-1894.37584	0.51563	0.418092	**-30.1**
13Q_A	-1836.77390	0.52037	0.428803	**-3.2**
13Q_B	-2066.48084	0.59759	0.493880	**10.3**
13Q_C	-1796.23185	0.47088	0.385305	**0.0**
13Q_D (X = H)	-2044.53522	0.56743	0.466273	**-4.4**
13Q_D (X = NMe_2)	-2178.51252	0.64472	0.533402	**-7.5**
13Q_E (X = H)	-2044.55079	0.56758	0.469643	**-12.1**
13Q_E (X = NMe_2)	-2178.52361	0.64472	0.535209	**-13.4**
13Q_F	-1952.25573	0.56449	0.468658	**-12.9**
13Q_G	-1912.94699	0.53505	0.436560	**-26.7**

7.14 References

1 J. Harvey, *J. Annu. Rep. Prog. Chem. - Sect C*, 2006, **102**, 203.

2 C. Cramer, *Essential of Computational Chemistry - Theories and Models;* Wiley, 2004.

3 P. Hohenberg and W. Kohn, *Phys. Rev. B*, 1964, **136**, B864.

4 J. Slater, *Phys. Rev. A.*, 1951, **81**, 385–390.

5 A. D. Becke, *J. Chem. Phys.*, 1993, **98**, 5648–5652.

6 F. Jensen, *J. Chem. Theory Comput.*, 2008, **4**, 719–727.

7 R. Ditchfield, W. J. Hehre and J. Pople, *J. Chem. Phys.*, 1971, **54**, 724–728.

8 Q. Wu and W. Yang, *J. Chem. Phys.*, 2002, **116**, 515–524.

9 S. Grimme, *J. Comput. Chem.*, 2006, **27**, 1787–1799.

10 S. Grimme, S. Ehrlich and L. Goerigk, *J. Comput. Chem.*, 2011, **32**, 1456–1465.

11 B. Roux and T. Simonson, *Biophys. Chem.*, 1999, **78**, 1–20.

12 M. Cossi, V. Barone, R. Cammi and J. Tomasi, *Chem. Phys. Lett.*, 1996, **255**, 327–335.

13 A. Klamt, *J. Phys. Chem.*, 195AD, **99**, 2224–2235.

14 A. V Marenich, C. J. Cramer and D. G. Truhlar, *J. Phys. Chem. B*, 2009, **113**, 6378–6396.

15 F. Weinhold and C. R. Landis, *Chem. Educ. Res. Pr.*, 2001, **2**, 91–104.

16 C. F. Matta and R. J. Boyd, *The Quantum Theory of Atoms in Molecules*, Wiley-VCH, Weinheim, 2007.

17 P. Macchi and A. Sironi, *Coord. Chem. Rev.*, 2003, **238**–**239**, 383–412.

18 M. J. Frisch, G. W. Trucks, H. B. Schlegel, G. E. Scuseria, M. A. Robb, J. R. Cheeseman, G. Scalmani, V. Barone, B. Mennucci, G. A. Petersson, H. Nakatsuji, M. Caricato, X. Li, H. P. Hratchian, A. F. Izmaylov, J. Bloino, G. Zheng, J. L. Sonnenberg, M. Hada, M. Ehara, K. Toyota, R. Fukuda, J. Hasegawa, M. Ishida, T. Nakajima, Y. Honda, O. Kitao, H. Nakai, T. Vreven, J. A. Montgomery Jr., J. E. Peralta, F. Ogliaro, M. J. Bearpark, J. Heyd, E. N. Brothers, K. N. Kudin, V. N. Staroverov, R. Kobayashi, J. Normand, K. Raghavachari, A. P. Rendell, J. C. Burant, S. S. Iyengar, J. Tomasi, M. Cossi, N. Rega, N. J. Millam, M. Klene, J. E. Knox, J. B. Cross, V. Bakken, C. Adamo, J. Jaramillo, R. Gomperts, R. E. Stratmann, O. Yazyev, A. J. Austin, R. Cammi, C. Pomelli, J. W. Ochterski, R. L. Martin, K. Morokuma, V. G. Zakrzewski, G. A. Voth, P. Salvador, J. J.

Dannenberg, S. Dapprich, A. D. Daniels, Ö. Farkas, J. B. Foresman, J. V Ortiz, J. Cioslowski and D. J. Fox, *Gaussian 09, Revis. D.01, Gaussian Inc., Wallingford CT*, 2013.

19 S. H. Oakley, M. P. Coles and P. B. Hitchcock, *Inorg. Chem.*, 2003, **42**, 3154–3156.

20 J. P. Perdew and Y. Wang, *Phys. Rev. B*, 1992, **45**, 13244–13249.

21 S. Grimme, J. Antony, S. Ehrlich and H. Krieg, *J. Chem. Phys.*, 2010, **132**, 154104–154119.

22 E. D. Glendening, J. K. Badenhoop, A. E. Reed, J. Carpenter, J. A. Bohmann, C. M. Morales, C. R. Landis and F. Weinhold, *NBO 6.0, Theor. Chem. Institute, Univ. Wisconsin, Madison*.

23 T. A. Keith, *AIMAll (Version 16.10.31), TK Gristmill Software, Overl. Park KS, USA,*.

24 Y. Zhao and D. G. Truhlar, *Theor. Chem. Acc.*, 2008, **120**, 215–241.

25 C. Adamo and V. Barone, *J. Chem. Phys.*, 1999, **110**, 6158.

26 V. N. Staroverov, G. E. Scuseria, J. Tao and J. P. Perdew, *J. Chem. Phys.*, 2003, **119**, 12129–12137.

27 S. Doye, *Synlett*, 2004, **2004**, 1653–1672.

28 A. Schäfer, H. Horn and R. Ahlrichs, *J. Chem. Phys.*, 1992, **97**, 2571–2577.

29 F. Weigend and R. Ahlrichs, *Phys. Chem. Chem. Phys.*, 2005, **7**, 3297–3305.

Figure A1. Plots o ([**1_Int**]) *vs.* time plotted in Origin. Top: half equivalent of 9-BBN dimer, the best-fit line (R^2 = 0.9964) shown gave A_1 = -0.0531(4) and B_1 = 2568(36) giving an initial rate of 2.6(1) x 10^{-5} mol dm^{-3} s^{-1}. Second: one equivalents of 9-BBN dimer, the best-fit line (R^2 = 0.9820) shown gave A_1 = -0.0785(4) and B_1 = 1591(12), giving an initial rate of 3.1(1) x 10^{-5} mol dm^{-3} s^{-1}. Third: one and an half equivalents of 9-BBN dimer, the best-fit line (R^2 = 0.9941) shown gave A_1 = -0.0785(3) and B_1 = 1591(12), giving an initial rate of 4.9(4) x 10^{-5} mol dm^{-3} s^{-1}. Fourth: two equivalents of 9-BBN dimer, the best-fit line (R^2 = 0.9927) shown gave A_1 = -0.0601(2) and B_1 = 803(75), giving an initial rate of 7.4(4) x 10^{-4} mol dm^{-3} s^{-1}.

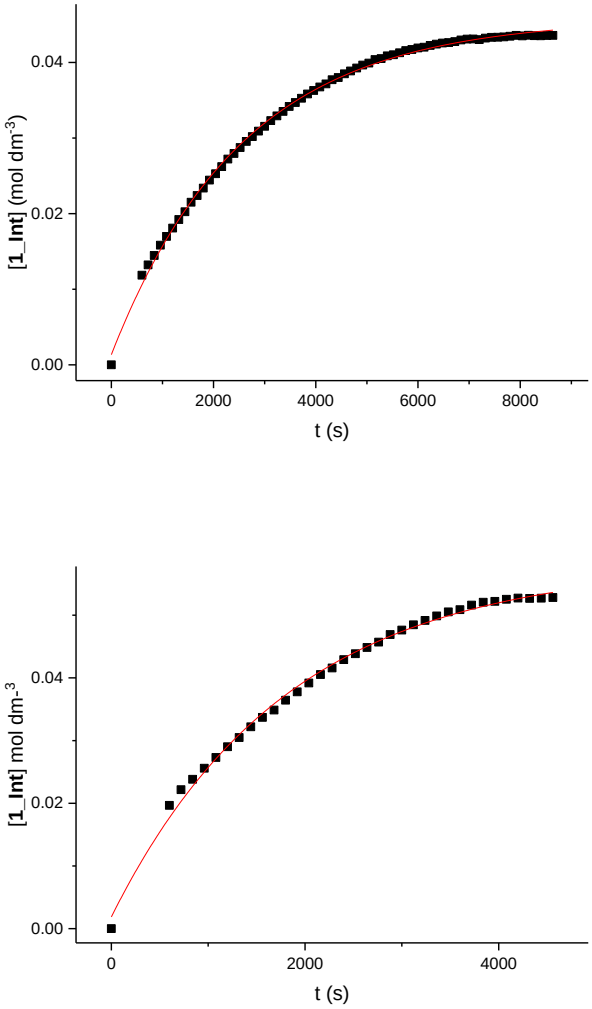

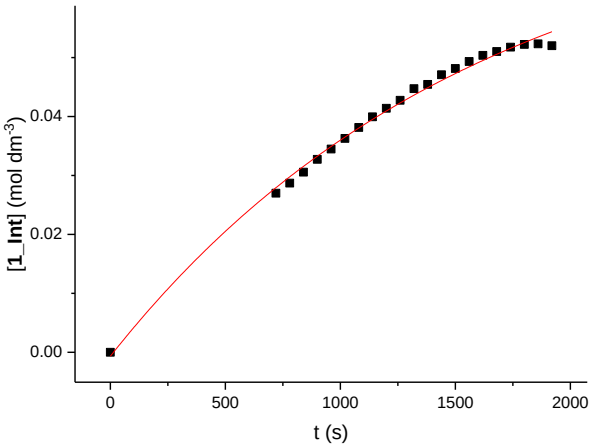
[1_Int] (mol dm-3)
0.00
0.02
0.04
0
500
1000
1500
2000
t (s)

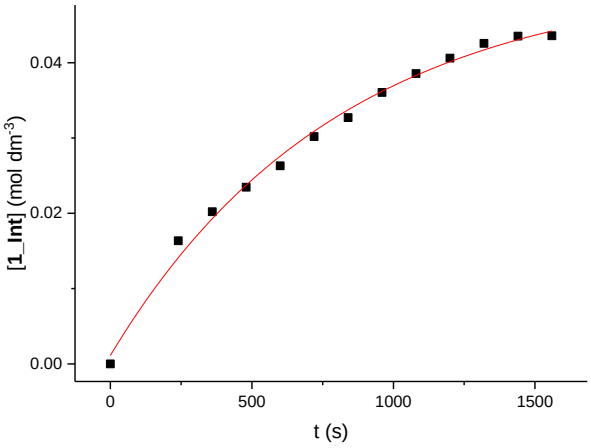
[1_Int] (mol dm-3)
0.00
0.02
0.04
0
500
1000
1500
t (s)

Figure A2. Full derivation of Equations 3.10 - 3.12 described in Chapter Three.

$$\frac{d[\mathbf{1_Int}]}{dt} = k_2[\mathbf{1.39}][\text{9-BBN}]$$

$$\frac{d[\text{9-BBN}]}{dt} = k_1[\text{9-BBN dimer}] - k_{-1}[\text{9-BBN}]^2 - 0.5\, k_2[\mathbf{1.39}][\text{9-BBN}] = 0$$

$$[\text{9-BBN}] = \frac{k_1[\text{9-BBN dimer}]}{k_{-1}[\text{9-BBN}] + 0.5\, k_2[\mathbf{1.39}]}$$

$$\text{Rate} = \frac{k_1 k_2[\mathbf{1.39}][\text{9-BBN dimer}]}{k_{-1}[\text{9-BBN}] + 0.5\, k_2[\mathbf{1.39}]} \qquad (3.10)$$

if $k_{-1}[\text{9-BBN}] << k_2[\mathbf{1.39}]$

$$\text{Rate} = 0.5\, k_1[\text{9-BBN dimer}] \qquad (3.11)$$

if $k_{-1}[\text{9-BBN}] >> k_2[\mathbf{1.39}]$

$$K_{eq} = \frac{k_1}{k_{-1}} = \frac{[\text{9-BBN}]^2}{[\text{9-BBN dimer}]}$$

$$[\text{9-BBN}] = \left[\frac{k_1}{k_{-1}}\right]^{1/2} [\text{9-BBN dimer}]^{1/2}$$

$$\text{Rate} = \left[\frac{k_1}{k_{-1}}\right]^{1/2} k_2[\mathbf{1.39}][\text{9-BBN dimer}]^{1/2} \qquad (3.12)$$